FINAL REPORT

Energy Sustainable Wastewater Treatment Systems for Forward Operating Bases Based on Microbial Fuel Cells

SERDP Project ER-2216

JANUARY 2017

Bruce E. Logan, Ph.D.
Kyoung-Yeol Kim, Ph.D.
The Pennsylvania State University

Patrick J. Evans, Ph.D.
CDM Smith

Distribution Statement A
This document has been cleared for public release

SERDP
DOD ▪ EPA ▪ DOE

Page Intentionally Left Blank

This report was prepared under contract to the Department of Defense Strategic Environmental Research and Development Program (SERDP). The publication of this report does not indicate endorsement by the Department of Defense, nor should the contents be construed as reflecting the official policy or position of the Department of Defense. Reference herein to any specific commercial product, process, or service by trade name, trademark, manufacturer, or otherwise, does not necessarily constitute or imply its endorsement, recommendation, or favoring by the Department of Defense.

Page Intentionally Left Blank

REPORT DOCUMENTATION PAGE

Form Approved
OMB No. 0704-0188

Public reporting burden for this collection of information is estimated to average 1 hour per response, including the time for reviewing instructions, searching existing data sources, gathering and maintaining the data needed, and completing and reviewing this collection of information. Send comments regarding this burden estimate or any other aspect of this collection of information, including suggestions for reducing this burden to Department of Defense, Washington Headquarters Services, Directorate for Information Operations and Reports (0704-0188), 1215 Jefferson Davis Highway, Suite 1204, Arlington, VA 22202-4302. Respondents should be aware that notwithstanding any other provision of law, no person shall be subject to any penalty for failing to comply with a collection of information if it does not display a currently valid OMB control number. **PLEASE DO NOT RETURN YOUR FORM TO THE ABOVE ADDRESS.**

1. REPORT DATE *(DD-MM-YYYY)*
31-01-2017

2. REPORT TYPE
Final

3. DATES COVERED *(From - To)*
July 2012 – January 2017

4. TITLE AND SUBTITLE
Energy Sustainable Wastewater Treatment Systems for Operating Bases Based on Microbial Fuel Cells

5a. CONTRACT NUMBER
W912HQ-12-C-0044

5b. GRANT NUMBER

5c. PROGRAM ELEMENT NUMBER

6. AUTHOR(S)
Bruce E. Logan, Kyoung-Yeol Kim, Patrick J. Evans

5d. PROJECT NUMBER
W74RDV20056578

5e. TASK NUMBER

5f. WORK UNIT NUMBER

7. PERFORMING ORGANIZATION NAME(S) AND ADDRESS(ES)
The Pennsylvania State University
University Park, PA 16802

8. PERFORMING ORGANIZATION REPORT
7A720

9. SPONSORING / MONITORING AGENCY NAME(S) AND ADDRESS(ES)
Strategic Environmental Research & Development Program
901 North Stuart St, Suite 200
Arlington, VA 22203

10. SPONSOR/MONITOR'S ACRONYM(S)
USACE

11. SPONSOR/MONITOR'S REPORT NUMBER(S)

12. DISTRIBUTION / AVAILABILITY STATEMENT
Publically available

13. SUPPLEMENTARY NOTES

14. ABSTRACT
A microbial fuel cell (MFC) is an innovative method using exoelectrogenic bacteria to oxidize organic and inorganic matter in wastewater, accomplishing at the same time both wastewater treatment and electrical power generation. The objective of this project was to examine materials that would improve reactor performance, and enable the use of MFCs for treatment of wastewater at forward operating bases. Novel electrodes (anode and cathode), separators (insulation between the electrodes) and spacers (air flow to the cathode) were examined and tests for impacts on power and organics removal based on wastewater chemical oxygen demand (COD). Optimal aspects of the MFC were: using graphite fiber brush electrodes, activated carbon cathodes, cloth separators, wire spacers, and a continuous flow design based on combined treatment of graywater and blackwater. The results of this work was the development of engineering design plans and drawings for a pilot-scale MFCs that could be demonstrated and validated in the field.

15. SUBJECT TERMS
Bioelectricity; Forward operating bases; microbial fuel cells; wastewater treatment; water resuse.

16. SECURITY CLASSIFICATION OF:
Unclassified

a. REPORT	b. ABSTRACT	c. THIS PAGE
Unclassified	Unclassified	Unclassified

17. LIMITATION OF ABSTRACT
SAR

18. NUMBER OF PAGES

19a. NAME OF RESPONSIBLE PERSON

19b. TELEPHONE NUMBER *(include area code)*
814-863-7908

Page Intentionally Left Blank

Abstract

Objectives

The two main wastewaters produced at forward operating bases (FOBs) are graywater, which contains organic matter at concentrations of 300-500 mg/L based on chemical oxygen demand (COD), and black water, which has 7,000–10,000 mg COD/L. The purpose of this project was to investigate methods to treat these wastewaters (individually, or combined) using an energy neutral or energy positive process, in order to avoid the need to consume fuel for wastewater treatment. A microbial fuel cell (MFC) was examined here to serve as a net energy-producing technology to recover electrical energy from the organics in the wastewater. The specific goals of the project were to: develop novel materials for the electrodes and other components; examine configurations that could be used to scale up the system; and produce plans for a prototype reactor that could be installed at a Department of Defense (DoD) facility or a FOB to treat the gray and black wastewaters.

Technical Approach

Anode electrode materials are needed to be electrically conductive, inexpensive, and have high surface areas for the exoelectrogenic bacteria. Different designs, numbers, sizes, and orientations were investigated as a part of this task to understand how these properties influence the performance of the MFCs (**Task 1**). The separator is an important component of the MFCs as it is used to insulate the electrodes and prevent electrode short circuiting, it can mitigate contamination of the cathode surface, and it reduces oxygen diffusion from the air-cathode into the anode chamber. A new separator material, poly(vinyl alcohol) (PVA), was tested to see if it could work well as existing materials, with the PVA used as either a separate membrane or as a cathode coating (**Task 2**). Spacers are needed to prevent the collapse of electrodes due to water pressure, but they must also allow oxygen in air to reach the cathode surface. Various types of spacers (wired, plastic, mesh frame) were tested to identify the material and configuration that enabled the highest power densities. Selected spacers were then used in larger-scale MFC stacks that were operated with domestic wastewater (**Task 3**). The cathode can be the most expensive component of the system, especially if expensive precious metal catalysts such as Pt are used for oxygen reduction, and expensive binders are used such as Nafion to hold the catalyst. **Task 4** was aimed at developing novel cathode electrode materials that could be effective alternatives to more expensive Pt catalysts. The wastewater treatment in terms of COD removal by the MFCs which is developed through this project was evaluated on the basis of achieving 80% COD removal (**Task 5**). In order to maximize the efficiencies for power generation and wastewater treatment, MFCs need to be operated under continuous flow conditions. All of the optimized materials developed in Tasks 1 through 4 were tested under various operational conditions using actual wastewaters under continuous flow conditions (**Task 6**). For **Task 7**, we developed process flow diagrams and conducted material and energy balances for various treatment scenarios at different FOB scales. The scenarios included both disposal of treated water and treatment for non-potable reuse. The life cycle assessment (LCA) focused on conventional metrics (e.g., fossil fuel depletion, climate change, etc.) as well as potential reduction in casualties, which was of specific interest to the DoD.

Results

The importance of the brush anodes to fully cover the cathode was shown by reducing the number of brushes (either by disconnecting or removing them) as this reduced power. Performance was

improved by using smaller brushes (0.8 cm) placed close to the cathode with acetate solutions, but stable performance with wastewater required brushes that were more than a centimeter in diameter, and so further tests were conducted using brushes 2.5 cm in diameter. PVA separators increased the coulombic efficiency and produced minimal power losses due to little impact on the internal resistance. PVA separators prepared using a simple spray-on application method produced more power in a low conductivity solution, but power was eventually reduced due to PVA degradation. It was concluded that cloth separators provided the best material properties for use in MFCs. Several cathode spacers were examined, with the wire spacers producing the best performance as they minimized blockage of the cathode surface and allowed good air flow to the cathode, resulting in a reactor design that produced the highest power densities yet obtained in larger reactors using domestic wastewater. Blending carbon black (CB) into the activated carbon (AC) when making the cathode was found to be a simple and effective strategy to enhance AC cathode performance in MFCs. Cathodes made using a phase inversion process with a polyvinylidene fluoride (PVDF) binder, placed onto a stainless steel mesh current collector, produced a structure that did not require a separate diffusion layer to prevent water leakage. However, adding an additional hydrophobic PVDF membrane to the air side of the cathode further improved resistance to water leakage and did not adversely affect performance. Under continuous flow conditions, MFCs with full brush anodes (three total) and two cathodes produced more power than MFCs with a half-sized brush anodes placed closer to a single cathode in tests using domestic wastewater. Slightly higher COD removals were obtained using the single cathode system due to the slightly lower measured hydraulic retention times (HRTs) anodes. Experiments with diluted swine wastewater, used to simulate FOB black water, showed low rates of treatment, and thus it was concluded that black water should be mixed with gray water for treatment rather than being treated separately in MFCs.

A modular MFC design that had multiple anodes in a module (two modules) (1.4 L, 29 m^2/m^3) produced 250±20 mW/m^2 of maximum power density using domestic wastewater under continuous flow conditions, with an average COD removal of 57±5% (HRT of 8 h). A larger (6.1 L) MFC stack made in the same scalable configuration (constructed with four alternating anode and three two-sided cathode modules) produced the total volumetric power density of 4.8 W/m^3. Design plans and drawings were prepared based on these experimental data for a pilot-scale MFC comprised of 44 removable cathode modules and 45 anode modules, set in a tank measuring 8.1 ft long by 3.8 ft wide by 3 feet high. Power harvesting from the MFC was based on use of commercially available off the shelf (COTS) boost converters. The LCA developed for MFCs as a part of this project was conducted in collaboration with SERDP project ER-2239, and therefore the LCA results were presented in the report for that project.

Benefits

Transport of water, wastewater, fuel, and treatment chemicals to and from FOBs are major security risks. MFCs can minimize this risk by treating combined gray water and black water in a near energy-neutral configuration. Wastewater aeration, which is the primary major energy consumer for conventional wastewater treatment processes is avoided by using MFCs. While MFCs eliminate the need for active aeration and produce net energy, an additional process, such as an anaerobic fluidized membrane bioreactor or biofilters, which are being investigated as a part of the ESTCP program, must be used to produce water suitable for reuse. The combined effluent can be of sufficient quality for reuse applications that include vehicle coolants, aircraft washing, pest control, laundry, centralized hygiene (field showers), personnel decontamination, retrograde cargo washing, and heat casualty body cooling.

Table of Contents

Table of Contents.....i

List of Tables.....iv

List of Figures.....v

List of Appendices.....xi

List of Acronyms.....xii

Keywords.....xv

Acknowledgements.....xvi

1. Objectives.....1

2. Background.....2

3. Materials and Methods.....5

3.1. Anode Testing (Task 1).....5

3.1.1. Examination of Brush Anode Sizes and Packing Densities (28 mL reactor).....5

3.1.2. Examination of Brush Anode Sizes and Packing Densities in Larger MFCs.....7

3.1.3. Nutrient Removal Test Using Larger Scale MFCs (130 mL).....8

3.2. Separator Testing (Task 2).....9

3.2.1. PVA Separator Tests with Acetate Buffer Solution.....9

3.3. Spacer Testing (Task 3).....11

3.3.1. Spacer Tests with Acetate.....11

3.3.2. MFC Module Design.....13

3.4. Cathode Testing (Task 4).....15

3.4.1. Enhanced AC cathode by Blending Carbon Black.....15

3.4.2. Long-term Operation of AC based Cathodes.....16

3.4.3. Cathode Preparation using a PVDF Phase Inversion Method.....17

3.4.4. New Cathode Preparation Method: Carbon free diffusion layer AC cathode.....18

3.4.5. Impaired Cathode Performance by Adsorption of Humic Acids.....19

3.5. Continuous Flow Tests (Task 6).....20
3.5.1. Test with Different Anode Configurations and Cathode Surface Area.....20
3.5.2. Test with a Larger, multiple-module MFC (5.7 L).....21
3.5.3. Black Water Test using MFCs.....23
4. Results and Discussion.....25
4.1. Anode Testing (Task 1).....25
4.1.1. Power Generation Using Different Anode Sizes in Smaller MFCs (28 mL).....25
4.1.2. Examination of Brush Anode Sizes and Packing Densities in Larger MFCs.....27
4.1.3. Performance of Larger Scale MFCs (130 mL) with Domestic Wastewater.....30
4.1.4. Nutrient Removal Test Using Larger Scale MFCs (130 mL).....31
4.2. Separator Testing (Task 2).....32
4.2.1. PVA Separator Tests with Acetate Buffer Solution.....32
4.2.2. Separator Tests with Domestic Wastewater.....34
4.3. Spacer Testing (Task 3).....34
4.3.1. Spacer Tests with Acetate.....34
4.3.2. Spacer Tests with Domestic Wastewater.....36
4.3.3. MFC Module Design.....37
4.4. Cathode Testing (Task 4).....37
4.4.1. Enhanced AC cathode by Blending Carbon Black.....37
4.4.2. Long-term Operation of AC based Cathodes.....39
4.4.3. Testing PVDF Phase Inversion AC Cathode.....40
4.4.4. Testing Carbon Free Diffusion Layer AC Cathode.....43
4.4.5. Impaired Cathode Performance by Adsorption of Humic Acids.....46
4.5. Tests Demonstrating 80 % COD Removal with Wastewater.....46
4.6. Continuous Flow Tests (Task 6).....47
4.6.1. Test with Different Anode Configurations and Cathode Surface Area.....47
4.6.2. Test with Stacked MFC Reactor (1. 5 L).....49

4.6.3. Test with a Larger, multiple-module MFC (5.7 L).....51

4.6.4. Black Water Test using MFCs.....56

4.7. Engineering and Economic Analysis (Task 7).....58

4.7.1. Engineering Design of a Pilot-Scale MFC.....58

4.7.2. Life Cycle Assessment.....89

5. Conclusion and Implications for Future Research/Implementation.....92

6. Literature Cited.....95

List of Tables

Table 1. Monitoring of nutrients concentrations in the larger scale MFC during operation.

Table 2. Operational conditions.

Table 3. Wastewater flow rates for different scale FOBs.

Table 4. Gray water and black water composition documented in a selection of the literature.

Table 5. Wastewater composition basis.

Table 6. MFC design basis summary.

Table 7. Voltage boosting options for MFCs.

Table 8. Estimated boost converter efficiencies.

Table 9. Power loss calculation for current transmission.

Table 10. Assumed wastewater composition used for the LCA.

Table 11. Scenarios evaluated in the LCA.

List of Figures

Figure 1. Four MFC configurations without air-cathode: (A) C1-thick, (B) C1, (C) C3, and (D) C6 (left). Carbon fiber brushes used as cubic MFC anode electrodes in configurations.

Figure 2. (A) Power density (solid symbols) and polarization curves (white symbols) for the four configurations, obtained through multi-cycle method. (B) Electrode potential curves (A = anode; and C = cathode) measured against a reference electrode (Ag/AgCl) for the four configurations.

Figure 3. (A) COD removal, and (B) CE percentages vs. external resistance.

Figure 4. Average power density and charge of the successive brush disconnection and removal for (A) C3, and (B) C6. Values for C1-thick and C1 are included in (A) for comparison purposes.

Figure 5. Three vertical rectangular MFC configurations showing the different brushes used as anodes: (A) R3 has three brush anodes, (B) R5 has five brush anodes, and (C) R8 has eight brush anodes.

Figure 6. (A and C) Power density (solid symbols) and polarization curves (white symbols) for MFCs obtained using the single-cycle method with three configurations. The curves were obtained in fed-batch (A, B) and continuous flow (C, D) operation.

Figure 7. COD removal (A,C) and Coulombic efficiency (B,D) in fed-batch (A,B) and continuous flow (C, D).

Figure 8. (A and C) Power density (solid symbols) and polarization curves (white symbols) obtained through the single-cycle method for the two configurations: R8 and R8C. The curves were obtained in fed-batch (A, B) and continuous flow (C, D) operation.

Figure 9. Polarization and power curves obtained from the larger scale MFC fed with a domestic wastewater.

Figure 10. COD monitoring during current generation in the larger scale MFC fed with domestic wastewater (left). First-order fitting data for COD removal (right).

Figure 11. (A) Configuration for spaced electrode (SPA) and separator electrode assembly (SEA) testing. (B) Photos of PVA separator (up) and PVA separator on the cathode electrode (down).

Figure 12. Comparison of SEA (closed symbols) and SPA (open symbols) power density curves in (A) 5 mM, (B) 50 mM and (C) 100 mM PBS.

Figure 13. Test data for cast (closed symbols) and spray-on (open symbols) PVA separators in SEA on Pt and AC cathodes showing: (A) power density curves, (B) cell voltages, and (C) electrode potentials (cathodes: solid lines; anodes; dashed lines).

Figure 14. The photograph (a), the schematic diagram of the air cathode modular MFC (b) and the isometric view (c) of a dual-side cathode cassette, and the mesh spacer (d), column spacer (e) and wire spacer (f) for the cathode cassette.

Figure 15. The polarization curve (a) and electrode potential (b) of the mesh, column and wire spacers. The error bars ± SD were calculation based on averages data from the chamber A and B of the MFC stack.

Figure 16. Internal resistance distribution for the anodes (An) and cathodes (Ca) using mesh (MS), column (CS), or wire (WS) spacers. The error bars are ±SD based on averages from the A and B sides of the MFC.

Figure 17. (a) Polarization curves and (b) anode (An) and cathode (Ca) potentials of the MFC operated in fed-batch mode using raw domestic wastewater: solid lines, results after one month (1M); dashed lines, results after 3 months (3M); P=potential, V=voltage. Average and error bars (± SD) based on individual measurements for 6 brush anodes in compartments A or B.

Figure 18. Anode resistances analyzed in terms of ohmic and non-ohmic resistances, using raw wastewater in fed-batch tests. The error bars are ±SD based on averages from the A and B sides of the MFC. T1 – T6: Time intervals, obtained by dividing one complete cycle of MFC operation (8 h) into six equal parts (80 min each).

Figure 19. The schematic of multi-module plug-in MFC reactor (left: the isometric view of the MFC stack; right: the isometric view of the inter configuration).

Figure 20. The dimension (left, top view, unit: mm) and electrode arrays (right, top view) of multi-module plug-in MFC.

Figure 21. (A) (B) (C) Power densities and (D) (E) (F) electrode potentials as a function of current density in MFCs using different cathodes after 1-week, 3.5-month and 5-month operation.

Figure 22. Current-potential curves of different cathodes in electrochemical cells.

Figure 23. Current-potential curves of different cathodes in electrochemical cells.

Figure 24. Fabrication procedures for AC cathode by phase inversion method.

Figure 25. (A) Power density curves for a PVDF cathode, reversed-side PVDF cathode, and a PTFE cathode; (B) electrode potentials (solid symbols, and potentials; open symbols, cathode potentials).

Figure 26. Water pressure resistance of PVDF cathodes with different polymer loadings (8.8, 6.6 and 4.4 mg/cm^2) with the polymer layer facing the air, compared to the reversed orientation of a PVDF cathode (8.8 mg/cm^2), and a PTFE cathode.

Figure 27. Synthesis of PVDF membrane via phase inversion method and solvent exchange process.

Figure 28. (A) Polymer loadings in PDMS wipe, 15%, 20%, 25% (w/v) PVDF membrane diffusion layers (B) Water pressure resistance of PDMS wipe and PVDF membrane diffusion layers with and without nylon spacer support.

Figure 29. (A) Power density curve for AC cathodes with PDMS wipe, 15%, 20% and 25% (w/v) PVDF membrane diffusion layers (B) Electrode potentials (solid symbols for anode potentials and open symbols for cathode potentials)

Figure 30. (A) Power density curves for AC cathodes filtrated with 0, 100 and 1000 mg/L HA solutions. (B) Electrode potentials (solid symbols, anode potentials; open symbols, cathode potentials). (C) Nyquist plots of EIS spectra of AC cathodes filtrated with 0, 100 and 1000 mg/L HA solutions at polarized conditions of 0.1 V vs. SHE. (D) Component analysis of internal resistance of the AC cathodes.

Figure 31. (A) Power density curves for AC cathodes filtrated with 1000 mg/L HA solution with and without backwashing. (B) Electrode potentials (solid symbols, anode potentials; open symbols, cathode potentials).

Figure 32. (A) Full brush anodes spaced evenly between two cathodes (S2C) and trimmed brush anodes near a single cathode (N1C), not drawn to scale. (B) Experimental set-up used in this study. Pairs of S2Cs and N1Cs were arranged in a series, and domestic wastewater was continuously provided through the inlet channel to each of the paired reactors.

Figure 33. Power generation (external resistor of 200 Ω for each MFC) produced by S2Cs and N1Cs (U = upstream, D = downstream) during continuous operation under different theoretical HRTs (8.8, 4.4 and 2.2 h).

Figure 34. COD concentrations in the influent and effluent of the S2Cs and N1Cs (U = upstream, D = downstream) and percentage of COD removal at theoretical HRTs of 8.8, 4.4 and 2.2 h.

Figure 35. COD removals (%) by S2C and N1C MFCs based on the theoretical and measured HRTs. The regression line (black dashed) was drawn to fit the COD removals based on the measured HRTs of both MFC configurations.

Figure 36. The polarization curve of the anode brushes of the MFC stack in continuous mode (HRT = 8 h) by using original domestic wastewater. The current data are the current generated from each anode; the power density were calculated based on the total cathode surface area (200 cm^2) divided by the number of anodes (6).

Figure 37. (a) Influent and effluent total COD and (b) SCOD for MFCs operated under continuous flow conditions using raw wastewater. Arrows above the x axis indicate data taken under different conditions: during reactor acclimation; operation at a fixed resistance (30 Ω); during polarization tests (Test*); or under open circuit conditions (OCV). (c) Average removals (error bars ± SD) of

the two sides (A or B) in terms of COD or sCOD. (d) COD removal rate and current density measured with under OCV (no current) conditions, or with larger (OCV; 2000, 1000, 500, 200 and 120 Ω) or smaller (90, 60, 30, or 20 Ω) resistances. Two different wastewater samples were used, as shown by the solid or dashed lines.

Figure 38. (A) Flow mode regulation controlled by baffles in the parallel flow path with alternating direction, and (B) flow in the serial flow path with alternating direction.

Figure 39. The COD and SCOD removal with different flow mode. (In-COD/SCOD: the influent COD/SCOD; Eff-COD/SCOD: the effluent COD/SCOD. Start: startup period; S-P: flow direction switch parallel flow mode; S-S: flow direction switch serial flow mode, N-P: parallel flow mode with fixed flow direction, N-S: serial flow mode with fixed flow direction)

Figure 40. Power density curves for the power generation of multi-module MFC following operation under various continuous flow modes: (a) alternating direction, parallel flow, A-P, Phase 3; (b) alternating direction, serial flow, A-S, Phase 4; (c) fixed direction, parallel flow, F-P, Phase 5b; (d) fixed direction, serial flow, F-S, Phase 6. (All tests under fed-batch conditions.)

Figure 41. Current (mA) and energy production (kWh/m^3) of swine wastewater-fed MFCs (SMFCs) under different external resistances during 27 days operation.

Figure 42. Influent and effluent COD (left side), COD removal and Coulombic efficiencies (right side) of swine wastewater-fed MFCs (SMFCs) under different external resistances (U: upstream; D: downstream).

Figure 43. Conceptual design of the pilot-scale MFC. The number of anodes and cathode modules are for concept illustration only and do not reflect the actual pilot-scale MFC design.

Figure 44. Process flow diagram concept of a process train for wastewater treatment and reuse based on the MFC. Eq. tank: equalization tank. GAC-BF: granular activated carbon biological filtration.

Figure 45. GAC-BAF system developed by ERDC-CERL that can be used to polish MFC effluent. A) isometric design illustrating two GAC vessels. B) pilot-scale system.

Figure 46. Ft. Riley Camp Funston wastewater composition for data reported from June 1, 2012 through May 31, 2013.

Figure 47. Trends of COD concentration and current density for acetate (A-D) and wastewater (E-F) at high (A,C,E), and low (B,D,F) cell resistance.

Figure 48. Current density relationship to COD concentration at high (A) and low (B) cell resistance.

Figure 49. (A) Current density, soluble (sCOD) and total COD (tCOD) changes with time in the MFCs fed with raw domestic wastewater; (B) first-order model fits for the two phases.

Figure 50. Comparison of COD removal in continuous-flow MFCs to theoretical COD removals based on first-order kinetics. Solids lines: model. Symbols: data based on measured HRTs taken from Figure 35.

Figure 51. Energy harvesting from arrays of MFCs at boosted voltages without voltage reversal: (A) whole electric circuit diagram, (B) simplified diagram without unnecessary lines which are used in the alternating charging and discharging time period. While 4 MFCs and 8 capacitors are shown in this figure, various numbers of MFCs and capacitors can be used. (C: capacitor; R: external resistance; +: MFC cathode; –: MFC anode).

Figure 52. Power harvesting systems.

Figure 53. Two-stage voltage boost converter system with optional third-stage inverter.

Figure 54: Reactor plan view showing serpentine flow through the anodes in the 45 anode modules and around the 44 cathode modules.

Figure 55. Reactor detail showing individual anode and cathode modules.

Figure 56. Tank cutaway showing angle iron brackets used to support both anode and cathode modules.

Figure 57. Section view of the reactor showing liquid distributor piping, anode and cathode modules, angle iron supports, and rectangular box channel supports.

Figure 58. Anode module and air scour system. Note holes in rectangular channel adjacent to anodes.

Figure 59. Cathode module details (yellow module bracket on left removed for clarity).

Figure 60. Cathode assembly plan view.

Figure 61. Spacer photographs.

Figure 62. Cathode module assembly. A) Plastic module frame with rubber seal on sides and bottom. B) Spacer inserted into frame. C) Cathodes with current collector rod (top in red) mounted on both sides of spacer. D) Separators laid on top of cathode sheets and held in place with securement brackets that are bolted to the plastic module frame.

Figure 63. Reactor tank dimensional drawings showing plan view (a), inlet section (b), and outlet section (c).

Figure 64. System for harvesting energy from the MFC anode/cathode modules.

Figure 65. Process and instrumentation diagram for the MFC system.

Figure 66. Process and instrumentation diagram for the MFC system.

Figure 67. System boundary for the LCA.

List of Appendices

Appendix A: Process-Mechanical Engineering Calculations and Details

Appendix B: Electrical Design Details

Appendix C: Instrumentation Design Details

Appendix D: List of Scientific/Technical Publications

List of Acronyms

AC	activated carbon
AEM	anion exchange membrane
AFMBR	anaerobic fluidized membrane biofilm reactor
BOD_5	5-day biochemical oxygen demand
BW	black water
CB	carbon black
CE	coulombic efficiency
CERL	Construction Engineering Research Laboratory
CL	catalyst layer
COD	chemical oxygen demand
COD_{in}	chemical oxygen demand in the influent
COTS	commercially available off the shelf
CS	column spacer
C_{th}	coulombic efficiency, theoretical
CV	cyclic voltammetry
DC	direct current
DI	deionized
DL	diffusion layer
DMAc	N, N-dimethylacetamide
DoD	Department of Defense
EIS	electrical impedance spectroscopy
ER	Environmental Restoration
ERDC	Engineering Research and Development Center
ESTCP	Environmental Security Technology Certification Program
FOB	forward operating base
FRP	fiberglass reinforced plastic
GAC	granular activated carbon
GAC-BF	granular activated carbon biofilter
GF	glass fiber
GW	gray water
HA	humic acid
HFC	hydrogen fuel cell
HMI	human-machine interface
HRT	hydraulic residence time

IC	ion chromatography
I/O	input/output
ISO	International Organization for Standardization
LCA	life cycle assessment
LCI	life cycle inventory
LCIA	life cycle impact assessment
LSV	linear sweep voltammetry
MEC	microbial electrolysis cell
MFC	microbial fuel cell
MS	mesh spacer (plastic)
N1C	near spacing, one cathode
NEMA	National Electrical Manufacturers Association
NOM	natural organic matter
NS	no separator
OCP	open-cell potential
OCV	open-cell voltage
O&M	operations and maintenance
ORR	oxygen reduction reaction
PBS	phosphate buffer nutrient solution
PDMS	poly(dimethylsiloxane)
PFD	process flow diagram
P&ID	process and instrumentation diagram
PLC	programmable logic controller
PSU	Pennsylvania State University
PTFE	polytetrafluoroethylene
PVA	poly(vinyl alcohol)
PVDF	polyvinylidene fluoride
RDE	rotating disc electrode
S2C	spaced electrode, two cathodes
SCOD	soluble COD
SEA	separator electrode configuration
SERDP	Strategic Environmental Research and Development Program
SHE	standard hydrogen electrode
SMFCs	swine wastewater fed MFCs
SPA	spaced electrode configuration
tCOD	total COD
TOC	total organic carbon
TSS	total suspended solids

UPS	uninterruptable power supply
USEPA	United States Environmental Protection Agency
VDC	volts DC
WS	wire spacer (steel)

Keywords

Activated carbon
Air cathode
Alternating flow
Anode configuration
Bioelectricity
Black water
Carbon black
Carbon brush anode
Catalytic activity
Cathode diffusion layer
Chemical oxygen demand (COD) removal rate
Continuous flow
Coulombic efficiency
Current collector
Domestic wastewater treatment
Electrode combinations
Electrode distance
Energy sustainable
Exoelectricigens
First-order reaction
Forward operating bases
Gray water
Humic acid
Hydraulic retention time (HRT)
Long-term performance
Membranes
Microbial fuel cell
Modular design
Multi-module reactor
Phase inversion method
Poly(vinylidene fluoride) (PVDF)
Polyvinyl alcohol
Separators
Spacers
Wastewater treatment

Acknowledgements

This project spanned many years and involved a number of individuals at Penn State and CDM Smith. We especially thank the students and researchers that work on this project at Penn State or with the research team during these studies: Yongtae Ahn, Weihua He, Michael A. Hickner, Peiying Hong, Daniel L. Hoskins, Ivan Ivanov, Nicole LaBarge, Vanessa A. Lanas, Jia Liu, Lijiao Ren, Pascal Saikaly, Jennifer Stager, Max J. Wallack, Xue Xia, Wulin Yang, Fang Zhang, Xiaoyuan Zhang, and Xiuping Zhu. We also gratefully acknowledge the work of several CDM Smith staff including: Michaela Bogosh, Marco DeLiso, Oscar Del Olmo, Josh Goldman, Taha Mohammed, Eva Opitz and Matt Schultz.

1. OBJECTIVES

The Department of Defense's Forward Operating Bases (FOBs) need innovative systems that can provide energy sustainable wastewater treatment systems. These systems should be capable of on-site treatment of graywater (including water with low levels of microbial contamination from laundries, wash racks, and showers) and blackwater (from toilet facilities). The systems should be scalable in size and able to handle flows from 500 to thousands of personnel. The delivery of fuel to FOBs places many people at risk for injury or death, and therefore the operation of these systems that produce energy or are nearly energy neutral will help to protect he welfare of all troops and personnel involved in operation of FOBs. It is also desirable that these systems treat water to a level suitable for reuse for some operations, such as use in vehicle coolants, aircraft washing, pest control, laundry, centralized hygiene (field showers), personnel decontamination, retrograde cargo washing, and heat casualty body cooling. The systems should need only minor maintenance when used at these sites.

In order to meet these objectives we examined the use of microbial fuel cells (MFCs) to treat gray and black water (separately or combined). An MFC is an innovative treatment method that uses exoelectrogenic bacteria that can oxidize organic and inorganic matter in wastewater and produce electricity, accomplishing at the same time both wastewater treatment and electrical power generation. In this project, we tested several different materials and MFC reactor configurations in order to develop a final design suitable for modular scale-up to sizes applicable to FOBs. Specifically, the research objectives were to:

- Evaluate several materials in small-scale reactors in order to improve system performance including: optimization of brush anode surface area and mass including fiber length reduction; development of mesh cathodes that do not use precious metals and/or expensive binders; and minimization of electrode spacing using innovative separator materials;
- Build continuous flow MFCs based on units containing multiple high surface area graphite fiber brush anodes and high-performance cathodes;
- Characterize electrochemical performance of MFCs using various techniques such as electrochemical impedance, polarization data, and linear sweep voltammetry;
- Evaluate operation schemes that could either maximize treatment rates or electricity production; and
- Obtain operational data using actual wastewaters, including both gray water (domestic wastewater from a local treatment plant) and blackwater (diluted swine wastewater).

2. BACKGROUND

The operation of FOBs can incur significant costs in terms of both the cost to setup, operate and maintain these sites, as well protect as the health and lives of personnel at the site. FOBs can range from smaller platoon-sized sites to larger division sized sites. Sufficient water and sanitation is essential for the operation of these sites. By reducing water consumption, through water recycling and reuse, and treatment, FOBs can become more self-sufficient. Potable water treatment and used water treatment have unique challenges at these sites, as energy use must be minimized due to the hazards associated with bringing fuel to the sites. Thus, they have a unique need for energy neutral used water treatment compared to systems typically employed in the US. Therefore, the goal here was to develop a deployable and easy-to-use wastewater treatment system that would minimize or produce net energy to improve the security of personnel at FOBs, and reduce associated costs by minimizing the need for fresh water and fuel from off-base sources.

MFCs are being developed as a method to both treat used water and produce electricity. In an MFC, organic matter is directly converted to electricity by certain bacteria abundant in the environment and in wastewater that are able to exogenously transfer electrons outside the cell, called *exoelectrogens* [1]. These bacteria oxidize organic matter in wastewater (treating the wastewater) and release electrons to an electrode (the anode) where they flow through a circuit to the counter electrode (cathode), producing treated water. The electrons are released from the cathode to the terminal electron acceptor oxygen. The energy produced by an MFC makes it is possible to achieve energy-neutral wastewater treatment and even generate useful electricity [1-4]. Researchers have been working on methods to eliminate the use of precious metals [5, 6] and expensive membranes and binders, and the development of materials that reduce costs and increase power densities.

The design of an MFC is dependent on the use of high performance, and low cost materials that can be packaged into a compact size reactor. For these reasons, MFCs must be designed to use high surface area electrodes that can fit into compact compartments in order to maximize electrode specific surface area (m^2 of electrode per volume of reactor; m^2/m^3). We review below the background on the materials used for point in this project, and summarize operational information needed to produce MFCs suitable for treatment of gray water and black water (separately or combined) at FOBs.

2.1. Anodes

High surface area electrodes are needed for bacteria to grow on, and they must be electrically conductive, low in cost, and able to function when placed close to the cathode which can leak oxygen and reduce power. Many materials have been examined including carbon cloth, paper, foam, felt, reticulated vitreous carbon, and others [7, 8]. The best performance (highest power densities) has been obtained using graphite fiber brush anodes [9]. These electrodes are made by winding thin graphite fibers into a metal core, using the same technology used to make bottle brushes. Many of these anode brushes are currently hand made, but this process could easily be automated using commercially off the shelf (COTS) equipment making manufacture of the brushes relatively inexpensive. The brushes have very high surface areas and porosities, and are easily cleaned using air-sparging *in situ*. Similar cleaning methods are used for full-scale ultrafiltration membranes used for wastewater and drinking water treatment. Several papers have been published on flat anodes, but flat anode configurations have so far proven to be less effective than the brush anodes [10-13].

2.2. Cathodes

The cathode is the most complex part of the MFC: poor design can limit power production and affect coulombic efficiencies (current generation from substrate). The cathode includes three major components: a current collector, a catalyst, and a catalyst binder. The cathode can be the most expensive component of the system if precious metal catalysts such as Pt are used for oxygen reduction, and expensive binders such as Nafion are used to hold the catalyst against the current collector. Larger cathodes needed for scaled up reactors will require current collectors based on highly conductive thin metals wires and metal mesh instead of graphite. The most useful cathodes have been developed by constructing an active carbon catalyst layer on top of a stainless steel mesh current collector, with inexpensive diffusion layers of polymers such as poly(dimethylsiloxane) (PDMS) to avoid water leakage [14, 15]. These activated carbon cathodes can perform as well as those made from much more expensive carbon cloth [16]. The incorporated current collector allows the size of the electrode to be increased without large increases in electrical resistance. Thus, this stainless steel current collector-based cathode allows for high current densities and low resistances. The stainless steel is protected from corrosion when used as a part of the cathode as electrons from the circuit are released at a potential that does not result in metal corrosion (i.e., cathodic protection).

2.3. Separators

Membranes are often used between electrodes creating two-chamber systems, but a membrane that accomplishes selective separation should be avoided as they result in large pH gradients in MFCs [17-19]. A separator, rather than a membrane can be used to insulate the electrodes and prevent short circuiting, and allow close spacing of the electrodes [20-22]. J-cloth (commonly used as a kitchen wipe material for cleaning) has been shown to work the best to date, but glass fiber separators work almost as well [21, 23]. Existing disadvantages of these separators is that J-cloth is biologically degraded over time (due to cellulose degradation), while the glass fiber mat can unravel [21]. New approaches to separators are needed, and these separators should be evaluated in terms of electrochemical performance and longevity.

2.4. Using MFCs for Wastewater Treatment

It has been estimated that wastewater contains 9.3 times as much energy as is consumed for its treatment using conventional technologies [24]. Recent studies also suggest there is more energy in wastewater than previously thought due to the loss of volatiles during wastewater preparation for testing in bomb calorimeters [25]. A treatment system based on MFCs therefore should be able to recover more energy than needed to treat the wastewater, and at least can achieve treatment without power input [8].

The power produced in an MFC varies with the strength and type of wastewater, and MFC architecture is the most important factor affecting treatment efficiency for a given wastewater. The highest power densities have been obtained using graphite fiber brush anodes and cathodes made using an activated carbon catalyst [16]. Electrodes should be closely spaced to minimize internal resistance, and insulated against short circuiting using a separator.

Another useful characteristic of the MFC process is low solids production compared to aerobic processes. While an aerobic activated sludge process converts ~50% of the carbonaceous COD into biosolids, the MFC processes have lower biosolids production due to anaerobic conditions. It was shown using bench-scale MFCs in continuous flow studies that a two-stage MFC process produced effluent with <13 mg/L particulate COD over a six-month period [26]. This result implies

that treated wastewater would meet National Secondary Effluent Standards for suspended solids (<30 mg/L) without the need for a clarifier. This finding needs to be further investigated in MFCs optimized for more complete COD removal than that achieved in this earlier study. MFCs have no moving parts and have been operated for periods over one year. Thus these systems have the potential to be robust wastewater treatment systems that are simple to operate and maintain.

MFCs can be used for gray water and also perhaps for black water treatment based on results using domestic and animal wastewaters. Tests using semi-continuous (fed-batch) operation of small, bench-scale MFCs has shown good COD removal from domestic wastewater, and thus effective wastewater treatment. These results have shown that it is possible to achieve 84±2% (range of 72 to 98%) COD removal with domestic wastewater (Penn State University Wastewater Treatment Plant) [27]. However, continuous flow tests were not conducted for this type of wastewater. For every gram per of COD removed, it is possible in theory to generate 125 moles of electrons at approximately 0.2 to 0.5 Volts. As wastewater treatment efficiency (e.g., BOD or COD removal) is increased, power generation can decrease, making it necessary to balance energy generation and treatment efficiency.

Research has shown much different results are obtained using optimized solutions such as acetate or other so-called “synthetic” wastewaters compared to actual wastewaters. Similarly, amending domestic wastewater with acetate to simple organics to increase COD does not realistically predict possible performance with wastewater. Current and power densities are much higher using well buffered solutions and synthetic substrates than with actual wastewaters [2, 28-30]. It was therefore critical for this project to conduct tests with actual wastewaters to properly evaluate final performance.

3. MATERIALS AND METHODS

3.1. Anode Testing (Task 1)

3.1.1. Examination of Brush Anode Sizes and Packing Densities (28 mL reactor)

Many materials have been tested as anodes, but for this project we determined that the graphite fiber brush anodes were the optimal material because they have very high surface areas and porosities, and produce the highest power densities compared to other materials that are cost effective. However, the optimal design using brush anodes, in terms of brush sizes and packing density or relative position to the cathode, were not known. Therefore we examined using brush anodes in reactors containing different numbers, sizes, and orientations of the anodes in order to identify how these properties influenced performance (power generation and COD removal). The tests were initially conducted with acetate substrate to identify an optimized brush anode design, and then tested with domestic wastewater.

Reactor construction. Single-chamber, air-cathode MFCs were made from a 4 cm cube of Lexan (polycarbonate), and contained a cylindrical anode chamber of approximately 28 mL (Figure 1) [31]. Anodes (manufactured by Mill-Rose) were made from carbon fibers (PANEX 35 50K, Zoltek) wound into two twisted titanium wires. The anodes were heat treated at 450 °C for 30 min before being placed horizontally in the cylindrical chamber. The electrode spacing was set at 5 mm, measured from the front end of the brush anode to the inner face of the cathode. Four different reactor configurations (C1-thick, C1, C3, and C6) were used for comparison of power densities and overall performance with different anode conditions. The C1-thick configuration (Figure 1A) was identical to previous studies, consisting of a single anode brush 25 mm in diameter made using two thick titanium wires (length = 60 mm, diameter = 1.5 mm, 15 gauge, #2 grade; carbon fiber coverage length = 25 mm). The other three anodes all used a thinner titanium wire (~73% less metal in weight) with a diameter of 0.8 mm (20 gauge) (Figure 1), which was selected based on availability by a commercial supplier (Titanium Industries). The C1 configuration (Figure 1B) was therefore identical to the C1-thick anode except for the wire size. Multiple anode configurations were also tested using three brush anodes, each with diameter of 12 mm (C3, Figure 1C), or six brushes each with diameter of 8 mm (C6, Figure 1D). The C3 and C6 anodes were connected externally by a single copper wire [31].

The surface areas of brush anodes were calculated for all configurations using several different approaches in order to allow assessment of brush geometry in the reactor. The cylindrical area was calculated as $2\pi rn(r+h)$, where h is the length, r is the radius and n is the number of brushes. The specific bristle area was estimated as the surface area of each carbon fiber multiplied by the total number of fibers in a brush and by the number of brushes. Each of these areas was normalized by dividing it by the cathode surface or the anolyte volume. The projected area of the brushes was calculated as a coverage percentage: the circular side closer to the cathode (πr^2) multiplied by the total number of brushes and divided by the cathode surface.

Air-cathodes (projected surface area of 7 cm^2, cathode-specific surface area of 25 m^2/m^3) were constructed in our laboratory from wet-proofed (30%) carbon cloth (Type B-1B, E-TEK), coated with carbon black and platinum (0.5 mg Pt/cm^2) using a Nafion binder on the electrolyte-facing side, and a carbon black base layer and four PTFE diffusion layers on the air-facing side. Reactors were equipped with an Ag/AgCl (+0.211 V vs. standard hydrogen electrode, SHE) reference electrode (RE-5B, BASi) in contact with the electrolyte to obtain electrode potential measurements.

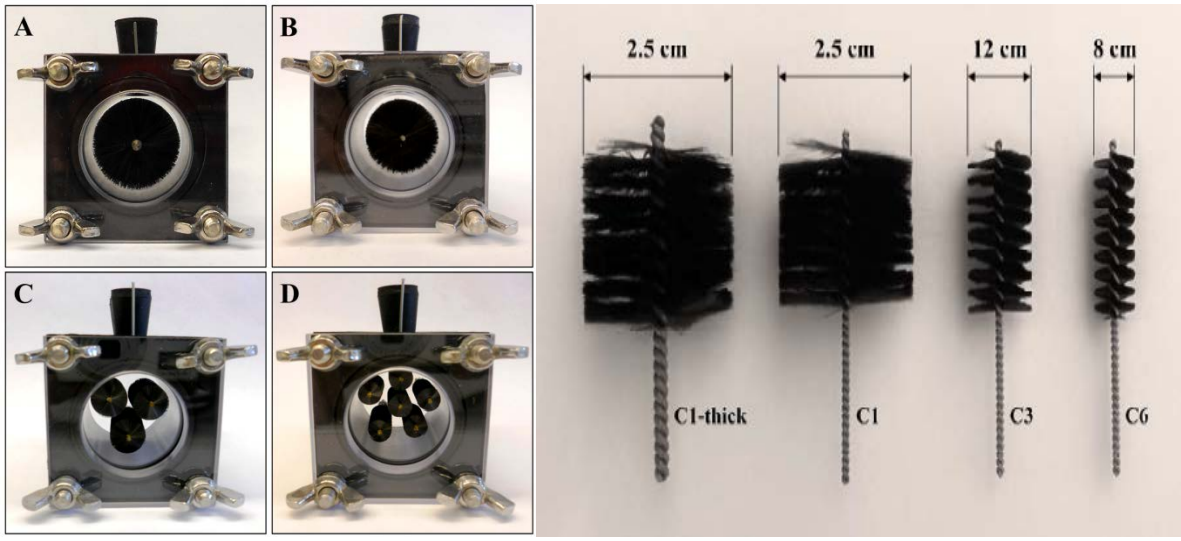

Figure 1. Four MFC configurations without air-cathode: (A) C1-thick, (B) C1, (C) C3, and (D) C6 (left). Carbon fiber brushes used as cubic MFC anode electrodes in configurations.

Inoculation and operation. The electrolyte was prepared with sodium acetate as the carbon source and electron donor (1.0 g/L) in a 50 mM phosphate buffer nutrient solution (PBS) containing Na_2HPO_4 (4.58 g/L), $NaH_2PO_4 \cdot H_2O$ (2.45 g/L), NH_4Cl (0.31 g/L), KCl (0.13 g/L), trace minerals (12.5 mL/L), and vitamins (5 mL/L). The medium conductivity was 7.8 mS/cm with a pH = 7. For the first seven days, eight MFCs (four configurations, tested in duplicate) were inoculated with a 50% (v/v) effluent from reactors that had been operated for over a year, and 50% PBS plus acetate. The MFCs were considered to have reached steady state and to be ready for experiments once they achieved a repeatable peak potential difference for three consecutive batch cycles (8 to 9 days for all configurations). Following acclimation, only PBS plus acetate was added over subsequent fed-batch cycles. The medium was replaced when the potential decreased below ~ 20 mV. All MFCs were operated in a temperature-controlled room at 30 °C. The external resistor was 1000 Ω (except as otherwise noted for polarization tests and brush disconnection/removal experiments), as it helps to shorten the development period of an exoelectrogenic biofilm relative to lower resistances. The potential difference across the resistor was measured at 20 minutes intervals using a multimeter (Keithley Instruments, model 2700) and recorded on a computer.

Two types of experiments were conducted following the initial polarization tests: brush anode disconnection, and brush anode removal. All reactors were switched to 100 Ω for these tests since this resistance produced the highest maximum power in polarization tests. For the brush disconnection experiment, anode brushes were successively disconnected (one by one), until only one brush was connected through the external circuit. For the brush removal experiment, all the brushes were connected together in parallel again and then brushes were disconnected and removed from the reactor one at the time until the final test with only a single remaining brush connected through the external circuit. Other changes that may have occurred to the reactor over time were a concern in evaluating the outcome of brush removal. Also, there can be disturbances to the anode biofilms when opening the reactor to remove a brush and exposing the anode to air. To account for these factors, the first set-up (all brushes connected) was repeated after the reactors were opened for five minutes (approximately the time that it took to open a reactor, remove one

brush, close it and seal the brush hole with epoxy) to establish a comparable point for the following set of electrode removal experiments.

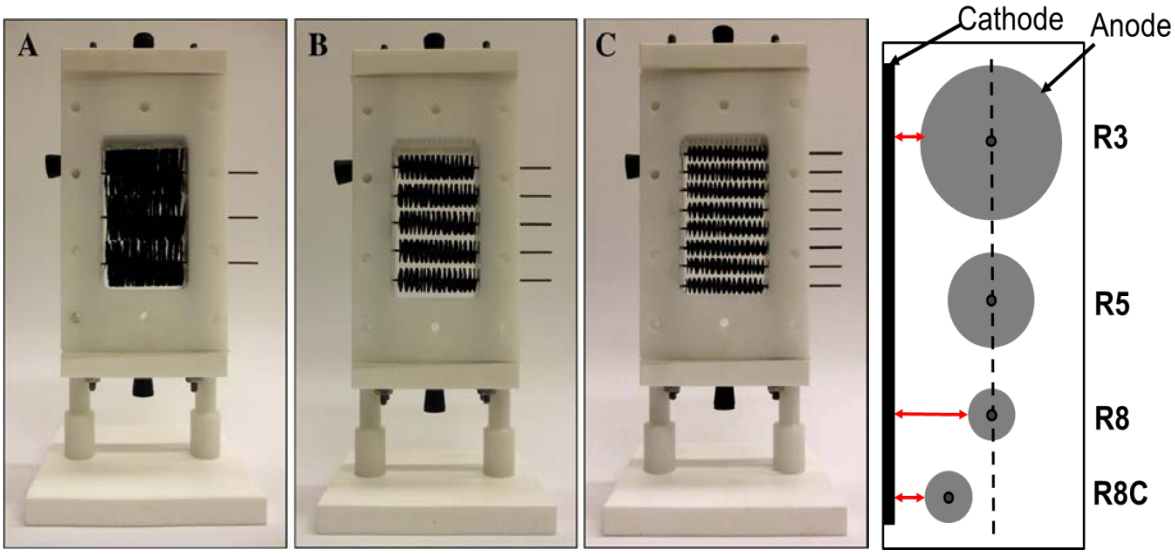

Figure 2. Three vertical rectangular MFC configurations showing the different brushes used as anodes: (A) R3 has three brush anodes, (B) R5 has five brush anodes, and (C) R8 has eight brush anodes.

3.1.2. Examination of Brush Anode Sizes and Packing Densities in Larger MFCs

Reactor construction. A rectangular shape single chamber, air-cathode MFC was designed with an anode chamber volume of 130 mL (Figure 2) [32]. The main reactor body of the MFC was made of high density polyethylene, but no separator was used, and the anode sizes and placement were varied (Figure 2). The brush anodes were designed to fully span the width of the anode chamber, with the brushes placed parallel to the cathode, in the middle of the anode chamber (95 × 142 × 38 mm, 174 ± 3 mL), except as noted. The anodes were connected externally in parallel by a single copper wire. Three different sized anodes were made using carbon fibers (PANEX 35 50K, Zoltek) wound into two twisted titanium wires (length ¼ 95 mm, diameter ¼ 0.8 mm, gauge 20) (made by Mill-Rose). In order to examine if the anode size and the distance between electrodes affected power generation. The anode sizes were: 3 brushes each 25 mm in diameter, with an electrode space (between the brush edge and the cathode) of 4 mm (R3; Figure 2A); 5 brushes each 12 mm in diameter with an electrode space of 10 mm (R5; Figure 2B); and 8 brushes each 8 mm in diameter, with an electrode space of 12 mm (R8; Fig. 2C). The R8 configuration was modified in a subsequent experiment by moving the anodes closer to the cathode (R8C), so that the gap between the anode edge and the cathode was the same as that of the R3 configuration (4 mm). All anodes were heat treated for 30 min at 450 °C before inoculation. Anode specific surface areas varied due to the differences in geometries. Surface areas were calculated in several different ways. The cylinder-equivalent projected area, that includes the ends and the main cylinder surface, was calculated as $(2\pi r^2 + 2\pi rh)n$. The percentage of the cathode covered by the projected area of the brushes was calculated from the two dimensional area of the brush (rh) multiplied by the number of brushes, and divided by the cathode surface area. A single air-cathode 35 cm^2 in projected area (5 × 7 cm) was used, producing a cathode-specific surface area of 20 m^2/m^3. Air-cathodes were made from wet-proofed (30%) carbon cloth (Type B-1B, E-TEK), coated with

carbon black, platinum (0.5 mg Pt/cm^2) and Nafion binder on the electrolyte-facing side, and carbon black base layer and four PTFE diffusion layers on the air-facing side. A titanium shim pressed against the cathode was used as cathode current collector. An Ag/AgCl reference electrode (RE-5B, BASi) was placed laterally in each reactor in contact with the electrolyte to measure electrode potentials. There was no separator as the distance between the brushes and the cathode prevented electrical contact.

Inoculation and operation. The electrolyte was prepared with sodium acetate as the carbon source and electron donor (1.0 g/L) in a 50 mM PBS. For continuous flow tests, the hydraulic retention time (HRT) was set at 8 h, with flow (0.36 mL/min) from the bottom to the top of the reactor set using a peristaltic pump (Masterflex, Cole-Parmer). For tests with domestic wastewater, the wastewater was collected from the primary clarifier of the Penn State University Wastewater Treatment plant.

Analytical methods. Polarization and power density curves were obtained using the multi-cycle method by changing the external resistance (from 1000 Ω to 10 Ω), and operating the reactors for at least three fed-batch cycles at each resistance to allow the biofilm to adapt and ensure reproducible power output. At each cycle, the voltages were measured for 2 h after the MFC produced the peak voltage and were averaged for the final reported value. Current (I, mA) was calculated according to Ohm's Law, $I = U/R_{ex}$, where U is the voltage (mV), and R_{ext} the applied external resistance. Current was normalized by the projected cathode surface area to obtain current density (mA/cm^2). Power, (P, mW), was calculated as $P = IU$, and power density was reported based on the projected cathode surface area or the total electrolyte volume.

COD (mg/L) was measured using standard methods (Standard Method 5220, APHA 1995, high range 20 - 1,500 mg/L, low range 3 - 150 mg/L; HACH COD System, HACH Company). COD removal (%) was calculated based on influent and effluent COD of a single batch cycle. The coulombic efficiency (CE, %) was calculated using CE = $(C_{ex}/C_{th}) \times 100$, where C_{ex} is the actual charge (C) transferred to the anode during one fed batch cycle (obtained integrating the current over time) and C_{th} is the theoretical amount of coulombs available from the substrate, and it is calculated as $C_{th} = (F\ b\ \mathrm{COD}_{in}\ v)/M$, where F is the Faraday's constant (96,485 C/mol e$^-$), b the number of moles of electrons exchanged per mole of oxygen (4 mol e$^-$/mol O_2), COD_{in} is the influent COD (g/L), v is the volume of liquid in the anode chamber (0.028 L), and M is the molecular weight of oxygen (32 g/mol).

3.1.3. Nutrient Removal Test Using Larger Scale MFCs (130 mL)

Batch mode test. For nutrient removal tests, the larger-scale 130 mL MFC was used (Figure 2) with the R8C configuration. Changes in nutrient concentrations in domestic wastewater were monitored using MFCs using a poly(vinyl alcohol) **(**PVA) separator and platinum catalyst cathode (external resistance of 50 Ω). PVA was prepared in water (8% w/w) with a porogen (5.6% of tetrabutylammonium chloride by weight) [33].

Continuous mode test. Two types of reactors were tested: N1C MFCs (3 half-cut brush anodes near the 1 cathode, 100 mL each) and S2C MFCs (3 full-size brush anodes between 2 cathodes, 140 mL each). Four MFCs (2 N1C and 2 S2C MFCs) were arranged in two separate flow lines, with two of the same types of reactors hydraulically connected in series. Effluent from the MFCs was collected together as total MFC effluent. Domestic wastewater was continuously provided to the MFC reactors by peristaltic pumps, with a set theoretical HRT of 8.8 h [34].

Analytical methods. Nutrient concentrations were determined using ion chromatography (IC), except for ammonia, which were measured using HACH ammonia test kits (Method 10031, HACH Company, Loveland, CO).

3.2. Separator Testing (Task 2)

3.2.1. PVA Separator Tests with Acetate Buffer Solution

A separator is used in MFCs to insulate the electrodes and prevent short circuiting, to minimize fouling of the cathode surface, and to reduce oxygen cross over from the air-cathode to the anode. In this task, we examined the use of PVA as a separator material, both as a separate membrane (cast separator) and applied directly to the cathode (sprayed on separators), using different types of cathodes.

Reactor construction and operation. MFCs were single-chamber, cubic-shaped reactors (2 cm long cylindrical chamber, 12 mL liquid volume). Anodes were heat-treated (450° C, 30 min), graphite fiber brushes twisted between two titanium wires. Cathodes with a Pt catalyst layer (5 mg/cm^2 10% Pt on Vulcan XC-72 with 33.3 $\mu L/cm^2$ of 5 wt % Nafion as binder) were constructed with a stainless steel mesh support and a PDMS diffusion layer, with the Pt catalyst layer facing the solution. AC cathodes were made using a nickel mesh (VITO, Belgium), with the AC between the mesh and a polytetrafluoroethylene (PTFE) diffusion layer, and used in the MFCs with the nickel mesh facing the solution. Electrodes were used in a spaced electrode configuration (SPA, 1.25 cm spacing), with the anode on the opposite side of the MFC chamber than the cathode, or in the separator electrode assembly (SEA) configuration (0.75 cm spacing) (Figure 3A) [33], with the anode and cathode on the same side of the MFC chamber, with a separator placed in between.

MFCs were inoculated with the effluent from MFCs operated for over one year. Solutions used for all tests contained 1 g/L sodium acetate and trace vitamins (5 mL/L) and minerals (12.5 mL/L). The concentration of the PBS was varied from a conductivity typical of wastewater, of 1 mS/cm (5 mM PBS; 458 mg Na_2HPO_4, 245 mg $NaH_2PO_4 \cdot H_2O$, 31 mg NH_4Cl, 13 mg KCl), to higher conductivities typical of laboratory tests: 7 mS/cm (50 mM PBS; 4.58 g Na_2HPO_4, 2.45 g $NaH_2PO_4 \cdot H_2O$, 0.31 g NH_4Cl, 0.13 mg KCl) and 13 mS/cm (100 mM PBS; 9.16 g Na_2HPO_4, 4.90 g $NaH_2PO_4 \cdot H_2O$, 0.62 g NH_4Cl, 0.26 g KCl). Reactors were fed in batch mode and operated at room temperature (19-27° C). MFCs were tested in duplicate for all testing, with the exception of the 50 mM testing on Pt, which occurred in 8 MFCs to ensure that all reactors were running in parallel.

PVA separator preparation. PVA was prepared in water (8% w/w) with a porogen (5.6% of tetrabutylammonium chloride by weight) (Figure 3B) [33]. Spray-on PVA separators were applied with an air brush in multiple layers (8-15 layers, depending on cathode type). Pt cathodes were made with a PVA loading of 10.0 ± 1.4 mg/cm^2, as determined by a gravimetric analysis before and after applying the PVA, with the PVA applied directly on top of the catalyst layer. AC cathodes were made with a higher loading of 19.5 ± 0.1 mg/cm^2 due to a different cathode structure which resulted in the nickel mesh current collector facing the solution in the MFC. A larger amount of PVA was needed to both fill the space between the nickel mesh pores, and produce a separator that was thick enough to provide insulation against short-circuiting of the electrodes.

Spray separators were compared to cast PVA separators (10.8 ± 0.4 mg PVA/cm^2) made using PTFE molds. Cast separators were dried for a minimum of 48 h at room temperature (19-27 °C) rather than the 36 hours drying at 50 °C used previously, to simplify the cast preparation. Preliminary experiments test results indicated that these two drying conditions yielded similar

power densities (data not shown). The dried separators were placed in the medium used in MFCs to allow the membranes to swell prior to insertion into the MFCs. All loadings reported here include water trapped in the PVA matrix, as the measurements were taken at ambient, non-desiccated conditions. All references to PVA separators are of the cast variety, unless otherwise noted. Cathodes containing PVA separators were also compared to cloth separators (Dupont Sontara, style 8864). These cloth separators are referred to as wipe separators as the material is sold as a wipe or cleaning cloth. All separators or plain cathodes were covered with a polypropylene mesh support (No.145872, Spectrum Medical Industries Inc., CA.). The mesh was needed to press the cloth and membrane separator onto the cathodes, and therefore it was used in other tests to maintain similar test conditions.

Analytical methods. Voltage was measured across an external resistor (1000 Ω) at 20 min intervals with a data acquisition system (34792A, Agilent LXI Data Acquisition/Switch Unit; Santa Clara, CA) connected to a personal computer, with current and power density normalized to the projected surface area of the cathode (7 cm^2). CE was calculated as the ratio of coulombs from the measured current compared to change in substrate based on COD. In tests using AC cathodes and spray-on or cast separators, MFCs were acclimated at 1000 Ω, and polarization data were obtained by varying external resistance from 1000 Ω to 25 Ω in decreasing order over separate cycles at each resistance (multiple cycle method). For tests of PVA in different salinity solutions, reactors were acclimated to 25 Ω, prior to polarization tests, to avoid power overshoot. Polarization curves were then obtained using a single-cycle method where the external resistance was decreased every 20 minutes at the beginning of a single cycle. Cycle times were defined as time from start of the fed batch cycle until the voltage was reduced to <50 mV (AC and spray-on/cast testing) or <20 mV (salinity testing). Components of the internal resistance were analyzed using electrochemical impedance spectroscopy (EIS) technique and a potentiostat (PC 4/750, Gamry Instruments Inc.; Warminster, PA). Ohmic and charge transfer resistances were obtained by EIS analysis with a set potential of –100 mV versus an Ag/AgCl reference electrode (+209 mV versus a standard hydrogen electrode, SHE) (RE-5B, Bioanalytical Systems, Inc., West Lafayette, IN) with the separator pressed against the working electrode. Working and counter electrodes were made of carbon cloth with a Pt catalyst (water side) and 4 PTFE diffusion layers (air side).

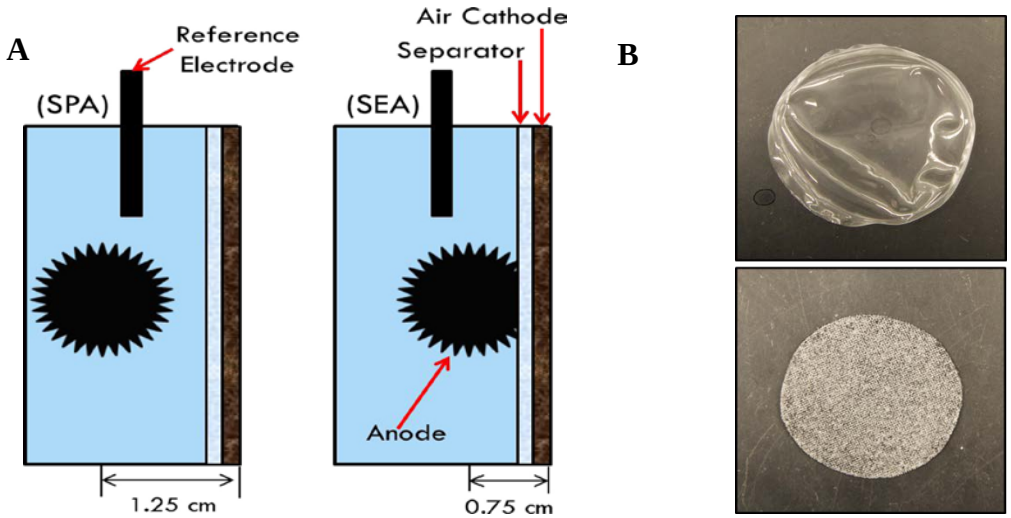

Figure 3. (A) Configuration for spaced electrode (SPA) and separator electrode assembly (SEA) testing. (B) Photos of PVA separator (up) and PVA separator on the cathode electrode (down).

3.3. Spacer Testing (Task 3)

3.3.1. Spacer Tests with Acetate

Spacers are used to prevent the collapse of the electrode chambers due to water pressure, but in the cathode chamber they must also allow oxygen in air to reach the cathode surface. Various types of spacers (wired, plastic, mesh frame) were tested to identify the material and configuration that enabled the highest power densities. Selected spacers were then used in larger-scale MFC stacks that were operated with domestic wastewater.

Reactor construction. The MFC tank was made of polycarbonate with a total empty bed volume (no electrodes or spacers) of 2 L (22 cm long, 7 cm wide, 13 cm high), with 1 cm of the width used for the spacer. Each cathode module had two cathodes joined by a single spacer, and it was placed between two anode modules (Figure 4) [35]. The two anode modules were individually connected to one of the cathodes, with designations A or B used to identify the two sides of the module. The anode module had an empty bed volume of 0.86 L and a working liquid volume of 0.7 L due to the space occupied by the anode brushes and cover plate. The working area of a single cathode was 200 cm^2 (10 cm × 20 cm), producing a total cathode specific surface area of 29 m^2/m^3 based on the total liquid volume (1.4 L), or 20 m^2/m^3 based on total reactor volume (2 L). Neither of these cathode surface areas included thickness of the container walls. The anodes were graphite fiber brushes (2.5 cm diameter, 12 cm long; Mill-Rose, USA) made from carbon fibers (PANEX 35 50K, Zoltek) held between two twisted titanium wires. Anodes were heat treated at 450ºC for 30 min prior to use. The air cathodes were made from an activated carbon catalyst on a stainless steel mesh (60 mesh type 304) manufactured using a rolling machine.

Preparation of spacers. Three different spacers were examined: a flexible plastic mesh spacer (MS) (Figure 4d); a rigid polycarbonate column spacer (CS) (Figure 4e); and a painted (corrosion-resistant) steel wire spacer (WS) (Figure 4f) [35]. A single plastic mesh spacer was previously reported to be suitable for maintaining power generation between two MFCs, but the cathode size was only 3 cm in diameter. Six flexible plastic mesh layers were used, each with a thickness of 1.5 mm (S1.5, 30PTFE50-625P, Dexmet Corp.), to provide a wide, porous spacer that filled the spacer compartment. Mesh spacers were equipped with six U-type gaskets, each with the same thickness, on three sides of the cathode to prevent leakage into the cathode compartment. The column spacer, which did not have a gasket, was constructed from five rigid polycarbonate columns to physically separate the cathodes. Ten holes (3 mm diameter) were drilled through the top of the polycarbonate bar that connected the columns as air diffusion holes to allow air flow into the spacer. Each column had another five lateral diffusion holes to allow air passage across the cathode compartment. The wire spacer was made from a tube rack wire (VWR, SCIENCEWARE, Poxygrid, 96-Place). The rigid wires supported the space between the cathodes using only one single open layer to support each cathode. The wire spacer was embedded into a rectangle frame with a thickness of ~ 4 mm. One layer of U-type gaskets (1.5 mm thick, in the middle of two rectangle frame) (Figure 4f) were used to seal the cathode compartment and allow open air circulation through the top. Two cover plates were fixed from the outside of the cathodes using nylon screws to hold together the assembled cathode module (Figure 4c). Cathodes were verified not to leak prior to their use. For each of these designs, a part of the cathode is covered by the air-impermeable spacer. The percentage of the cathode that was covered, called the "shadow effect" of the spacer, was estimated by the impression of the spacer on the cathode when it was assembled.

Inoculation and operation. Domestic wastewater, collected from the primary clarifier of the Pennsylvania State University Wastewater Treatment Plant, was used as the inoculum. In initial

comparisons of the three spacers, the wastewater was amended (90:10 mixture of domestic wastewater: medium) with additional sodium acetate (final concentration of 1.0 g/L) to produce a more consistent feed, a higher COD, and a biofilm that would be acclimated to wastewater in subsequent tests. The medium was a 500 mM phosphate buffer containing: Na_2HPO_4, 45.8 g/L; $NaH_2PHO_4 \cdot H_2O$, 24.5 g/L; NH_4Cl, 3.1 g/L; and KCl, 1.3 g/L. The final pH was ~7, the conductivity of the amended wastewater varied from 8.7 to 9.2 mS/cm, and the final total COD ranged from 1200~1300 mg/L. Two reference electrodes (Ag/AgCl, BASi, RE-5B, 210 mV versus a standard hydrogen electrode, SHE) were inserted through the top of the reactor into the anode compartments in order to measure anode potentials directly (cathode potential by difference from the whole cell potential), with all potentials reported here versus Ag/AgCl. The MFC was started up in batch mode using the acetate-amended wastewater and a mesh spacer, with the external resistance in the circuit gradually decreased for each cycle by using a different resistor (1000, 500, 200,100, 50, 20, 10, 8, 7, 6 and 5 Ω), in order to acclimate the reactor to higher current densities and to identify the point of maximum power.

Measurements and calculations. The voltage (U) was recorded using a data acquisition system (model 2700, Keithley Instruments) at 20 minute time intervals. The current ($I = U/R$) was calculated from the set external resistance (R), and power ($P = IU$) was normalized by the exposed projected area of the cathode (200 cm^2) or the liquid volume of the anode compartment (0.7 L). Polarization and power density curves were obtained by varying the external resistance over a single cycle in fed batch mode at 45 minute intervals, or for 2 HRTs (16 hours) in continuous flow mode. COD was measured using a standard method (HACH Co., Loveland, CO) in the high range (20 to 1500 mg/L). CE was as the ratio of the total coulombs transferred in the circuit divided by the theoretical amount of coulombs for the measured change in COD as previously described. The resistances of the anode and whole cell were obtained using EIS under working conditions of the maximum power output point. The impedance measurements were taken using a potentiostat (BioLogic, VMP3) by applying a sinusoidal voltage to the electrodes with signal amplitude of 10 mV around a potential of –450 mV for anode tests with acetate-amended wastewater, and –420 mV for raw (non-amended) domestic wastewater condition. The whole cell EIS tests were performed around a cell voltage of 300 mV for spacer comparison test. The frequency was varied from 100 kHz to 0.01 Hz. The ohmic resistance was determined by the intercept value on the real axis at the high-frequency; non-ohmic resistance, including the charge transfer and diffusion resistances, were determined by fitting the EIS spectra to a circuit. The cathode resistance was calculated as the difference between the whole cell and anode resistances.

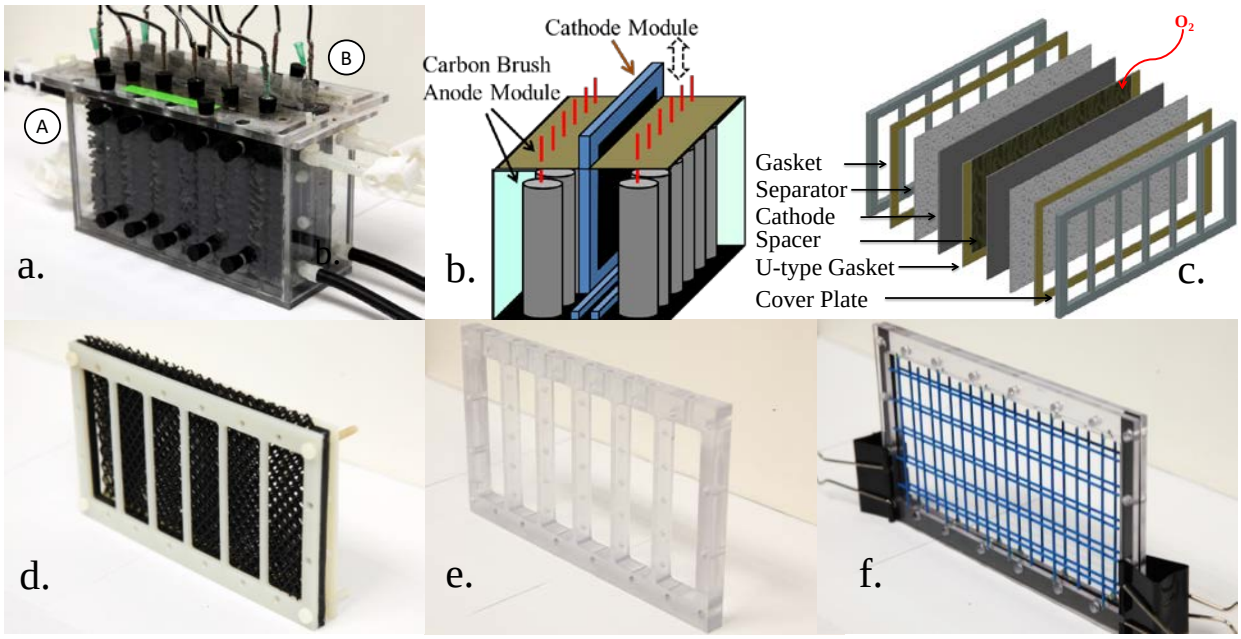

Figure 4. The photograph (a), the schematic diagram of the air cathode modular MFC (b) and the isometric view (c) of a dual-side cathode cassette, and the mesh spacer (d), column spacer (e) and wire spacer (f) for the cathode cassette.

3.3.2. MFC Module Design

MFC module construction and operation. The MFC module was made of clear polycarbonate with inner dimensions of 19.5 cm × 25 cm × 13 cm (width × length × height) (Figure 6) [36]. The influent flowed through porous diffusers made from four layers of soft mesh spacers, each with a thickness of 1.50 mm (S1.5, 30PTFE50-625P, Dexmet Corp.), and height of 3 cm, that were used to produce a more uniform cross-sectional flow into the inlet and outlet channels. The inlet/outlet channels had a width of 1.5 cm. The MFC contained four anode arrays each containing eight graphite fiber brushes (2.5 cm diameter, 12 cm long; Mill–Rose), and three dual-sided air cathode modules (22 cm × 13 cm × 2.5 cm) constructed with a gap of 1 cm between the cathodes that was maintained using rigid wire spacers (Figure 5) [36]. Each cathode (22 cm × 15 cm; effective area of 200 cm^2) was made using an activated carbon catalyst and stainless steel current collector using a rolling press method as previously described [37]. Two cloth separators (46% cellulose and 54% polyester, 0.3 mm thickness, Amplitude Prozorb, Contec Inc., Spartanburg, SC) covered the water side of the AC cathodes to prevent short-circuiting and reduce cathode fouling [37]. The first and last anode modules (1 and 4) were connected to only a single cathode, while the inner anode modules (2 and 3) were each connected to two adjacent cathodes (Figure 6). The fully assembled multi-module MFC reactor was filled with wastewater in batch mode for pre–inoculation of anode community. The wastewater was refilled every day. After about one week, the reactor was installed in wastewater treatment plant with external circuit and voltage acquisition system. After another 12 days, the reactor was started up by progressively reducing the external resistances from open circuit voltage (OCV) to 2 Ω and fed with domestic wastewater in HRT of 4 h.

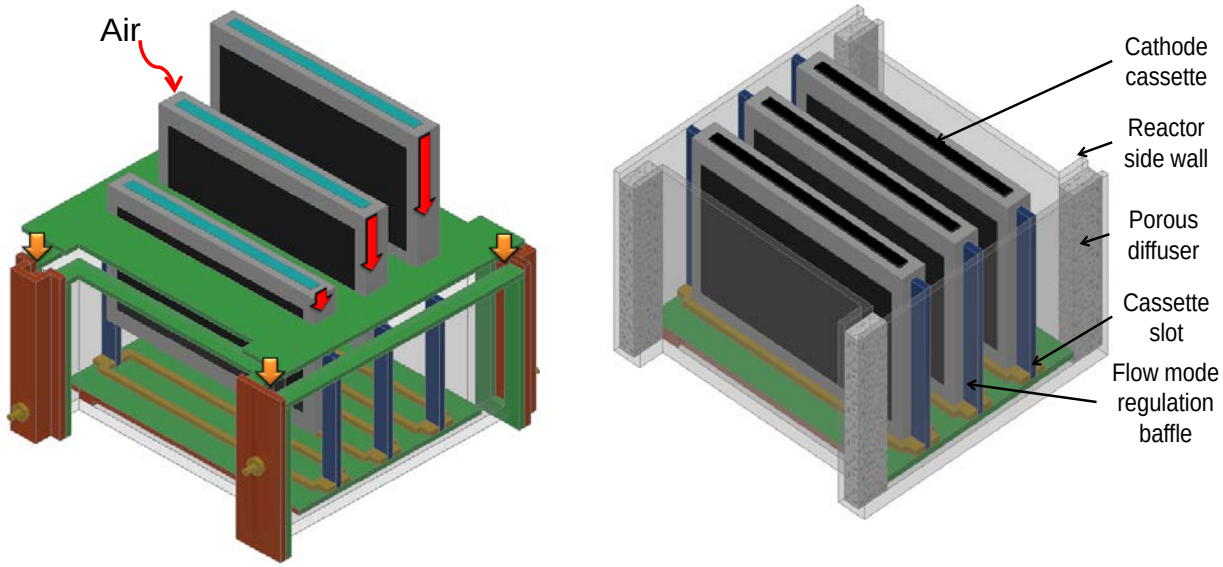

Figure 5. The schematic of multi-module plug-in MFC reactor (left: the isometric view of the MFC stack; right: the isometric view of the inter configuration).

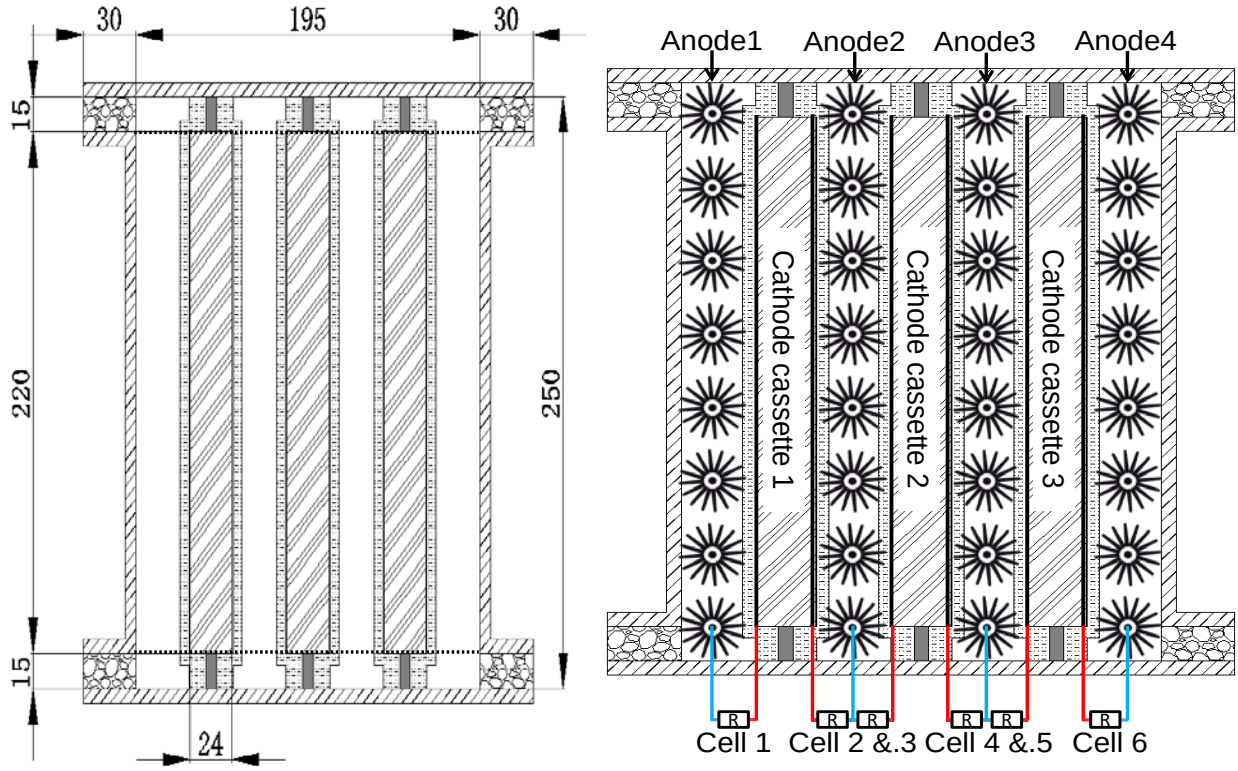

Figure 6. The dimension (left, top view, unit: mm) and electrode arrays (right, top view) of multi-module plug-in MFC.

3.4. Cathode Testing (Task 4)

3.4.1. Enhanced AC cathode by Blending Carbon Black

Preparation of AC cathodes with carbon black. AC (Norit SX plus, Norit Americas Inc., USA) was selected based on its better performance compared to other types of readily available carbons, and applied at a constant optimal loading of 0.43 kg/m^2 (300 mg for each 7 cm^2 cathode,). Carbon black (CB) powder (Vulcan XC-72, Cabot Corporation, USA) was added into AC and the content varied at weight ratios of CB:AC = 0% (pure AC control), 2%, 5%, 10% and 15%. Cathodes were fabricated using a batch, cold-press process. The AC (300 mg) and CB (0 to 45 mg) powders were added into a vial and mixed by vortexing for 0.5 min. The binder solution was prepared by adding 37.8 µL of 60% PTFE and 700 µL of DI water into a beaker, followed by ultrasonication for 1 min. Then the AC and CB powders were transferred into the beaker with the binder and mixed in a blender for 0.5 min to form a paste. The paste was then ultrasonicated for 1 min and spread using a spoon onto one side of a stainless steel mesh (50 × 50, type 304, McMaster-Carr, USA) that served as the support material and current collector. Diffusion layers were prepared by applying two layers of PDMS solution onto a textile material (Amplitude Prozorb, Contec Inc., USA), with the textile placed onto the cathode side facing the AC. Then, the cathode and the textile were pressed together at 40 MPa for 20 min (Model 4386, Carver Inc., USA) and dried at 80 °C in an oven overnight before use. Pt cathodes were also prepared to benchmark performance compared to the AC cathodes by applying a Pt catalyst layer (5 mg/cm^2 10% Pt on Vulcan XC-72 and Nafion binder) on one side of a stainless steel mesh, and two diffusion layers of PDMS on the other side of the mesh

MFC experiments. Cubic-shape single-chamber MFCs were constructed using a 4-cm length Lexan block with a 3-cm diameter inner cylindrical chamber. The anode was a graphite fiber brush (2.5 cm in both diameter and length) with a core of two twisted titanium wires that functioned as a current collector. The cathode was placed at the other side of the reactor, with the diffusion layers facing the air. All MFCs were inoculated with the effluent of MFCs which were operated for over one year. The medium was 1 g/L sodium acetate in 50 mM PBS. All the MFCs were operated in batch mode with a 1000 Ω external resistor (except as noted) in 30 ± 1 ºC room. Initially, a standard Pt/C carbon cloth cathode was used for all the MFCs during start-up to ensure that the anodes achieved the same performance during acclimation. After 1 week, a repeatable cycle of voltage was produced by the MFCs. To ensure all the anode biofilms were fully acclimated, the MFCs were operated for 1 month, and then the Pt/C cathodes were removed and replaced with the new AC based cathodes or new Pt/C stainless steel cathodes.

Analytical methods. Polarization tests were conducted after the MFCs had been operated after 1 week, 3.5 months and 5 months, by varying the external resistances from 1000 Ω to 20 Ω. Electrochemical tests were conducted using a potentiostat (VMP3 Multichannel Workstation, BioLogic Science Instruments, USA). Cathodes were examined in an abiotic and electrochemical reactor which was cubic shaped, with two 2-cm cylindrical chambers bolted together with an anion exchange membrane (AEM; AMI-7001, Membrane International Inc., USA) in the middle. A high purity platinum plate (99.99%, 1 cm^2) was placed in the middle of one chamber as a counter electrode, a cathode was placed on one side of the other chamber facing the air as a working electrode, and a Ag/AgCl reference electrode (3 M KCl, +0.21 V versus a standard hydrogen electrode; RE-5B; BASi, West Lafayette, USA) was placed close to the cathode. A 50 mM PBS was used as medium, and Chronoamperometry tests were carried out by setting a potential in a

stepwise manner after the reactor operated in open circuit condition for 3 h. Each potential (0.2 V, 0.1 V, 0 V, −0.1 V and −0.2 V versus Ag/AgCl) was applied for 2 h.

3.4.2. Long-term Operation of AC based Cathodes

Cathode preparation. The AC material used for all tests was a peat-based powder (Norit SX plus, Norit Americas Inc., USA) that was previously shown to have performance superior to several other types of AC. Three methods were used to modify the carbon: Fe, heat treatment, and blending CB. AC was combined with Fe at a weight ratio of FeEDTA:AC = 0.2:1 and pyrolyzed using argon gas at 800 °C for 1.5 h (AC-Fe). Heat treatment consisted of heating at 800 °C under argon gas for 1.5 h (AC-Heat). AC was blended with a previously-determined optimum weight of 10 wt % CB (AC-CB). These different treatment processes were compared to the original, unmodified (plain) AC for a baseline comparison. All AC based catalyst powders were applied at a constant loading of 0.5 kg/m^2, rather than keeping the loading of AC itself constant. AC cathodes were manufactured by a proprietary method (VITO CORE^{TM} electrodes) based on pressing at 150 bar using the mixtures of the different AC powders and a PTFE binder onto stainless steel mesh current collector (SS316, #53 mesh, 330 µm opening, 150 µm wire diameter). An additional PTFE layer (30% porosity, 0.13 kg/m^2) was added onto the catalyst layer on the air-facing side as a diffusion layer to avoid water leakage, and to help control oxygen transfer into the liquid solution. These cathodes were further benchmarked against a Pt cathode prepared in a similar manner. Briefly, the Pt catalyst layer (5 mg/cm^2 10% Pt on Vulcan XC-72 and 5 wt% Nafion binder) was applied to one side of a stainless steel mesh current collector (50 × 50, type 304, McMaster-Carr, USA), and two diffusion layers of PDMS and carbon black were added on the air-side of the mesh.

MFC experiments. MFCs were cube-shaped single-chamber reactors (4-cm length Lexan blocks with an inner cylindrical chamber of 3 cm in diameter) constructed. The anode was a graphite fiber brush (2.5 cm in both diameter and length) with a titanium wire core, and was placed horizontally in the middle of the chamber. The cathode was placed on the other side of the reactor, and the distance between the edges of the anode and the cathode was ~1 cm. All anodes were inoculated with the effluent of MFCs that were operated for over one year. The medium was 1 g/L sodium acetate amended with 12.5 mL/L minerals and 5 mL/L vitamins in 50 mM PBS. All the MFCs were operated in fed-batch mode with a 1000 Ω external resistor (except as noted) at 30 ºC.

Analytical methods. Polarization tests were conducted by using a multi-cycle method, by varying the external resistances from 1000 Ω to 30 Ω or 20 Ω, with each resistance applied for one complete cycle. Polarization tests were carried out after the MFCs had been operated for 1, 3.5, 5.5, 12, 16 and 17 months. Before the polarization tests after 5.5 months, biofilms on the cathodes were removed, and the diffusion layers were gently rinsed with distilled water to remove the precipitated salt. This was used to try to reduce electrode fouling, but it is known to not be completely effective with plain AC, but modified AC powders have not been previously tested. After 16-months operation and the polarization tests, the cathodes were soaked in a weak hydrochloric acid solution (60 mM) for 2 h. The salt was dissolved in the solution. After this 2-h weak acid treatment, the biofilm was gently removed and the cathodes were soaked in distilled water for 3 h. Then the cathodes were rinsed by distilled water for 3 times and placed back in the MFCs. Total resistances of the cathodes were calculated by Ohm's law using data from polarization tests with the Data Analysis Tools in Microsoft Excel (Professional Plus 2010). Chronoamperometry tests were conducted using a potentiostat (VMP3 Workstation, BioLogic Science Instruments, USA). The reactor was operated at open circuit condition for 3 h, and then

the cathode potential was set in a stepwise manner with each potential (0.2, 0.1, 0, −0.1 and −0.2 V versus Ag/AgCl) applied for 2 h.

3.4.3. Cathode Preparation using a PVDF Phase Inversion Method

Preparation of AC cathode using phase inversion method. PVDF solutions with different concentrations of 5%, 7.5% and 10% (w/v) were prepared by dissolving PVDF powder (~534,000 Da; Sigma Aldrich) in N, N-dimethylacetamide (DMAc), with vigorous stirring using a stir bar at room temperature (23 ± 1 °C) for over 8 h to completely dissolve the polymer. AC powder (Norit SX plus, Norit Americas Inc., TX) was applied at an optimum AC loading of 26.5 mg/cm^2, based on previous experiments. Catalyst mixtures were prepared with different PVDF loadings (all mass ratios) of: (1) 8.8 mg/cm^2, AC:CB (Vulcan XC-72, Cabot Corporation, USA):PVDF (10% as prepared) = 30:3:10; (2) 6.6 mg/cm^2, AC:CB:PVDF (7.5 %) = 30:3:7.5; (3) 4.4mg/cm^2, AC:CB:PVDF (7.5%) = 30:3:5. The mixtures were spread directly onto an 11.3 cm^2 circular section of stainless steel mesh (50 × 50, type 304, McMaster-Carr, USA) with a spatula (except as noted). The cathodes were then immersed into deionized (DI) water for 15 min at room temperature to induce phase inversion (Figure 7) [38]. Cathodes were then air dried in a fume hood for >6 h, and stored in DI water prior to testing. The performance of the PVDF cathodes was compared to controls made with an AC (26.5 mg/cm^2), CB, and a PTFE (60%) emulsion at a AC:CB:PTFE ratio of 9:1:0.9 (w/w) with a PDMS (12.1 mg/cm^2) wipe diffusion layer.

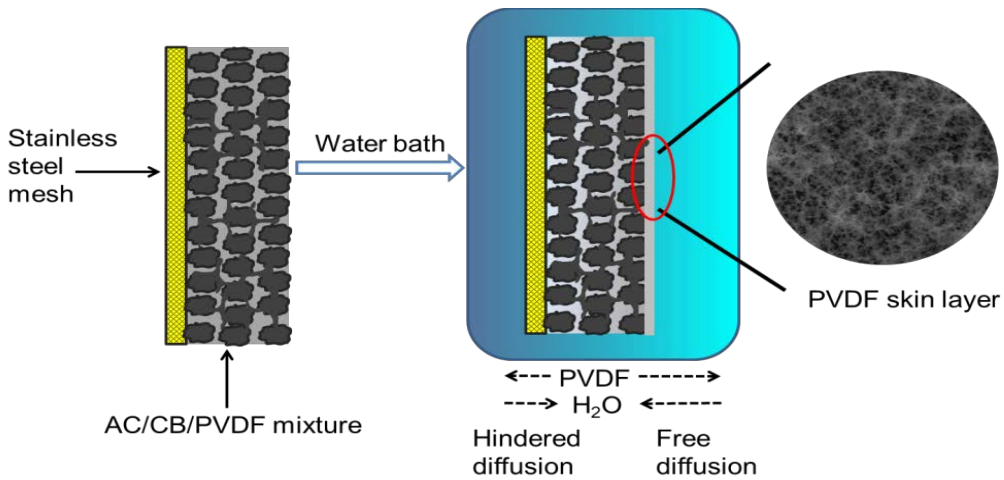

Figure 7. Fabrication procedures for AC cathode by phase inversion method.

MFC experiments. Cubic single-chamber MFCs were used in all tests (except as noted). They were constructed from a Lexan block 4 cm in length, with an inside diameter of 3 cm. The anodes were graphite fiber brushes (2.5 cm in both diameter and length, heat treated at 450 °C in air for 30 min) then placed horizontally in the middle of MFC chambers. Anodes were fully acclimated by operation for over one year at a constant temperature (30 °C) and fixed external resistance (1000 Ω). The medium contained 1 g/L sodium acetate dissolved in 50 mM PBS (except as noted). In larger-scale MFC tests, PVDF cathodes (7 cm × 10 cm, with 5 cm × 7 cm exposed to the air) were constructed and tested in a multi-brush anode reactor (130 mL) fed with domestic wastewater as previously described [39]. Carbon cloth-based cathodes with a platinum catalyst (ETEK C1-10 10% Pt on Vulcan XC-72) and a PTFE diffusion layer was prepared and used as a Pt catalyst control.

Analytical methods. MFC power curves were obtained by decreasing the external resistance from 1000 through 500, 200, 100, 75, 50 to 20 Ω at 20 min intervals. Coulombic efficiencies were calculated at a resistance of 1000 Ω based on changes in COD concentration, as previously described. Cathode polarization measurements were conducted with new cathodes in a two chamber electrochemical cell (2 cm length, 3 cm diameter, with a Nafion® membrane and Pt counter electrode) using a step current method, with a series of different set currents after the cell was acclimated under open circuit conditions for 1 h. The lower currents (1 mA, 2 mA, 3 mA and 4 mA) were applied for 1 h and the higher currents (5 mA, 6 mA, 7 mA, 8 mA, 9 mA and 10 mA) were applied for 30 min to obtain steady-state conditions. A fully assembled reactor was used to determine the maximum water pressure (in cm of static head) that would produce water leakage through the cathodes. A rubber ring covered with at least three layers of Teflon tape was used to seal the edge during the pressure test.

3.4.4. New Cathode Preparation Method: Carbon free diffusion layer AC cathode.

Cathode fabrication. The AC catalyst layer (CL) was prepared by mixing AC powder (Norit SX plus, Norit Americas Inc., TX) with PVDF (5% w/v) PVDF and carbon black (CB; Vulcan XC-72, Cabot Corporation, USA) powder at a mass ratio of AC:CB:PVDF = 30:3:5, with an AC catalyst loading of 26.5 mg/cm^2 as previously described.[9] The mixture was spread directly onto an 11.3 cm2 circular section of stainless steel mesh (50 × 50, type 304, McMaster-Carr, USA) with a spatula (except as noted). The mesh with the catalyst was then immersed into deionized (DI) water for 15 min at room temperature to leach out DMAc solvent, and air dried in a fume hood overnight prior to use. The final cathode was produced by attaching the diffusion layer (DL) onto the CL (fixed by rubber O ring) with the dense skin layer facing the CL. The cathode was positioned in the reactor with the DL facing the air side and CL towards the solution (Figure 8) side [40]. A PDMS/CB wipe DL [cloth coated with PDMS/CB mixture] was used as a control, and prepared as previously described [41].

Membrane fabrication. Membrane casting solutions of 15%, 20% and 25% (w/v) PVDF were prepared by dissolving PVDF powder (~534,000 Da; Sigma Aldrich) in DMAc (anhydrous, 99.8%, Sigma Aldrich) and vigorously stirring using a stir bar at 60 °C for over 6 h, until the solution became homogeneous and transparent. A slow stirring process was continued for another 2 h to remove bubbles in the solution. The solution was then cast onto a clean glass plate with a doctor blade (Microm II, Gardco, USA) set at a height of 200 µm, and exposed to air for 30 s. The glass plate was then immersed in a distilled water bath, in which the phase inversion process took place. After 10 min, the membrane was transferred to an ethanol/water (1:1, v/v) bath for 6 h and then to a pure ethanol bath for another 24 h (Figure 8). This solvent exchange procedure was adopted to prevent the shrinkage of the PVDF membranes. The PVDF membrane was then air dried in a fume hood for 10 min to restore hydrophobicity, and stored in sealed plastic bag at room temperature prior to use.

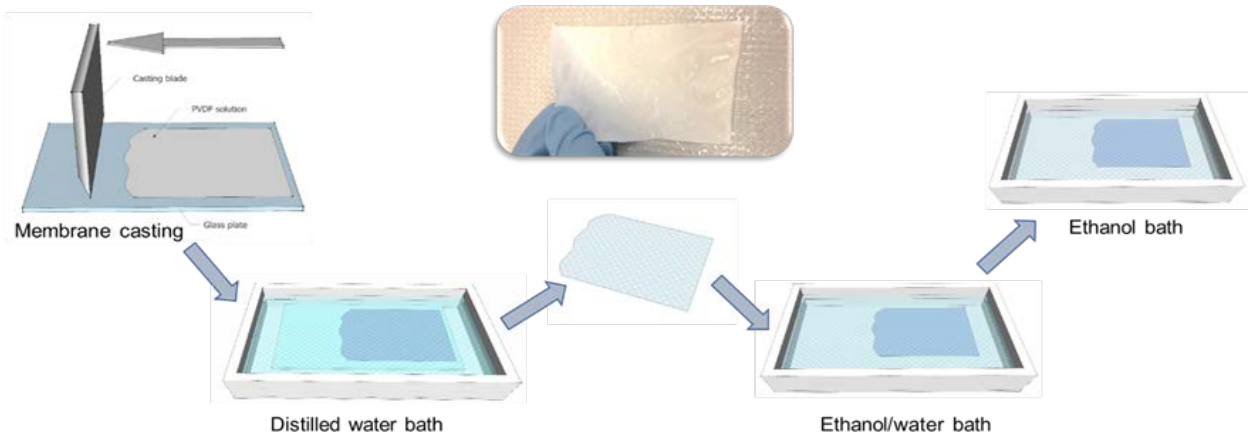

Figure 8. Synthesis of PVDF membrane via phase inversion method and solvent exchange process.

3.4.5. Impaired Cathode Performance by Adsorption of Humic Acids.

Humic acid adsorption test. Humic acid (HA) solutions with 100 and 1000 mg/L were prepared by dissolving a commercial humic acid sodium salt (Sigma-Aldrich) in DI water. The solutions were then filtered through 1.2 and 0.22 μm membrane filters (PVDF, 47 mm diameter, Millipore) to remove any solids, and stored at 4 °C prior to tests. The resulting 100 and 1000 mg/L HA solutions contained 33 ± 2 and 330 ± 20 mg-C/L of total organic carbon (TOC). The as prepared 100 and 1000 mg/L HA solutions had substantially higher concentrations of HA than ~2 mg/L of HA in typical wastewater effluent but were in a reasonable range compared to the TOC concentration in wastewater (~120 mg-C/L). The high concentrations of HA were needed to rapidly accumulate HA onto the cathode, before other factors would also contribute to the cathode fouling (such as biofouling) and preclude study of just the impact of the HA alone. HA adsorption onto the carbon was examined by dispersing 1 g of AC powder into 100 mL containing 0, 100, and 1000 mg/L HA solutions in sealed flasks, with continuous stirring for 24 h at 30 °C. The AC/HA slurries were then filtered through a 1.2 μm PVDF membrane and the filtered solutions were collected for analysis. The AC powders were further dried in a vacuum oven at 100 °C for 24 h. HA was adsorbed onto the cathodes by filtering solutions containing 0, 100, and 1000 mg/L of HAs directly through the AC cathodes to shorten the time of HA adsorption into AC cathodes. Prior to the filtration process, AC cathodes were sequentially wetted by ethanol and DI water each for 10 min. HA solutions (30 mL) were then pressure filtered through the cathodes and the filtrates were collected for analysis. The cathodes were dried in the fume hood for 12 h prior to testing. The control cathodes were also treated using this same ethanol and ethanol wetted process, but only DI water was filtered through these cathodes. The extent of HA desorption from the AC was examined by filtering 30 mL of DI water through AC cathodes (~5 min) following the previous procedures, and collecting the effluent for further analysis.

Analytical methods. A rotating disc electrode (RDE) was used to examine the catalytic activity of the AC in the absence of appreciable external mass transfer limitations. All RDE tests were conducted in 50 mM PBS (without nutrient addition) sparged with nitrogen and then air. Solutions were sparged with a gas for 30 min before conducting linear sweep voltammetry (LSV) tests and the gas was constantly streamed into the headspace during LSV runs. The potential of the disk electrode was scanned from 0.2 V to −1 V (vs Ag/AgCl) at 10 mV/s, at rotation rates of 100 to 2100 rpm. The current generated under nitrogen sparging was subtracted from that obtained

under air sparging to evaluate current generation due only to oxygen reduction. The electrochemical performance of AC cathodes were evaluated by LSV in an electrochemical cell (2 cm length, 3 cm diameter) containing two chambers separated by an anion exchange membrane (AEM; AMI-7001, Membrane International Inc.). The electrolyte was 50 mM PBS prepared without nutrient addition. A potentiostat (VMP3 Multichannel Workstation, Biologic Science Instruments) was used for all measurements in a constant temperature room (30 °C). The potentials on the cathodes were scanned from +0.509 V to −0.209 V versus SHE at a scan rate of 0.1 mV/s for 7 times to reach steady state. Impedance measurements of AC cathodes were conducted at 0.1 V vs SHE over a frequency range of 100 kHz to 0.02 Hz with a sinusoidal perturbation of 14.2 mV amplitude. The spectra were then fitted into an equivalent circuit to identify the solution resistance (R_s), charge transfer resistance (R_{ct}) and diffusion resistance (R_d).

3.5. Continuous Flow Tests (Task 6)

3.5.1. Test with Different Anode Configurations and Cathode Surface Area

Reactor construction and operation. We conducted continuous flow tests using domestic wastewater with two different types of MFC reactors, with two of each reactor types operated hydraulically in series. Anodes were graphite fiber brushes (Mill-Rose, Mentor, OH) with a titanium core (25 mm diameter by 35 mm length) heat treated at 450 °C for 30 min before use. Cathodes (40 cm^2, projected surface area) were made by a phase inversion technique using a PVDF binder and a mixture of AC (8.8 mg/cm^2) and CB (Vulcan XC-72, Cabot Corporation, USA) as previously described [38]. Four single-chamber, air-cathode MFCs were constructed using three graphite fiber brush anodes per reactor. Two of these reactors had the anodes placed directly next to a single cathode (N1C, Figure 9) [34]. The other two MFCs had the anodes placed in the middle of the anode chamber with a space between the edge of the anodes and two cathodes on either side of the brushes (S2C). The spaced electrode reactor design is different from previous spaced electrode designs as two cathodes each containing separators were used per anode array. Brushes used in the N1C reactor (100 mL empty bed volume) were trimmed along their length to form a half cylinder, with the flat side placed on the separator that was positioned against the air-cathode (0.5 cm distance from the cathode). Full brushes were used in the S2C reactors (140 mL empty bed volume) with an edge-cathode distance of 0.8 cm (Figure 9). The four MFC reactors (2 N1Cs, 2 S2Cs) were arranged with two flow paths, with the two similar types of MFCs hydraulically connected in series (Figure 9). The first MFC was the labeled the upstream (U) reactor, and the second one the downstream (D) reactor. The MFCs were inoculated and fed domestic wastewater from the primary clarifier of the Pennsylvania State University Wastewater Treatment Plant. The theoretical HRT was calculated from the set flow rate (Q, mL/h) and reactor volume (V, mL) as HRT = V/Q. Flow rates were chosen to obtain the same theoretical HRTs for the two reactors of: 8.8 h (31.8 mL/h, S2C; 22.8 mL/h, N1C); 4.4 h (63.6 mL/h, S2C; 45.6 mL/h, N1C); 2.2 h (127.2 mL/h, S2C; 91.2 mL/h, N1C). A salt tracer test was conducted to measure the actual residence time of solutes in the two pairs of MFCs during continuous mode operation. A NaCl solution (1 M) was injected into the flow line of the upstream flow line of the MFC for 36 min (8.8 h HRT), 18 min (4.4 h HRT), or 9 min (2.2 h HRT), with the effluent conductivity monitored using a meter (SB90M5, VWR International, USA). Measured HRTs were defined as the time to the peak of the tracer input. The HRT measured using this approach includes the entrance and exit volumes (not working area) of the reactors. Thus, the measured HRTs were adjusted by multiplying a ratio of working volume to total reactor volume.

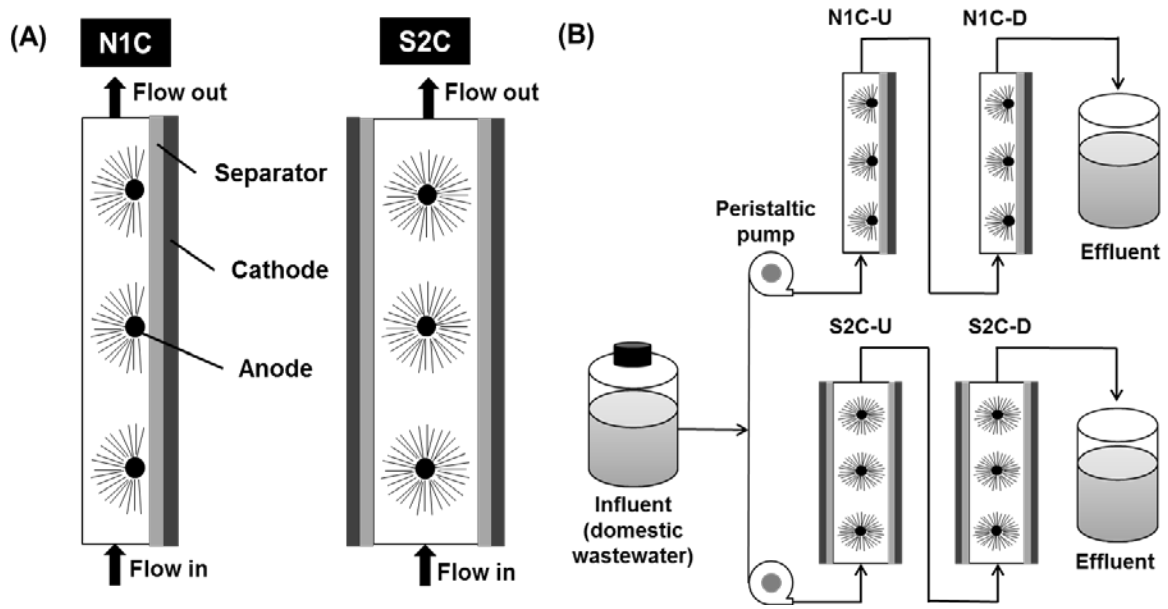

Figure 9. (A) Full brush anodes spaced evenly between two cathodes (S2C) and trimmed brush anodes near a single cathode (N1C), not drawn to scale. (B) Experimental set-up used in this study. Pairs of S2Cs and N1Cs were arranged in a series, and domestic wastewater was continuously provided through the inlet channel to each of the paired reactors.

3.5.2. Test with a Larger, multiple-module MFC (5.7 L)

Reactor construction and operation. A larger MFC, which contained four cathode modules and three anode modules each containing eight anode brushes, was assembled and operated using domestic wastewater (total reactor volume of 5.7 L) (Figure 5). (Reactor details are in Section 3.3.1. Materials and Methods.) The cathodes contained two sides, each made using a rolling AC process (22 × 15 cm) with an effective cathode area of 200 cm^2. This multi-modules MFC was examined for power production under either serial or parallel flow conditions, with the flow path controlled using baffles (Figure 10A, 10B) [36]. Serial and parallel flow modes were set by either inserting or removing the baffles, with the same net flow applied to the reactor so as to maintain the overall loading rate to the system. The reactor was installed at a municipal wastewater treatment plant and continuously fed domestic wastewater (effluent from a primary clarifier). The MFC was initially inoculated without cathode modules for 7 days, and refilled daily with fresh wastewater. The MFC stack was then operated in continuous parallel flow mode (Figure 10A) for 12 days (Phase 2, Startup period, Table 1) [36], with the direction of flow alternated in the opposite direction every day to avoid extended exposure of the anodes at the effluent side of the reactor to the lowest COD concentrations. During this period, the external resistance was progressively reduced from OCV to 2 Ω (OCV, 2000, 1000, 500, 200,100, 50, 20, 10, 5 and 2 Ω) to gradually acclimate the biofilms to continuous flow conditions and a low external resistance. After this Startup period, the flow direction was periodically alternated every 2 d (days 20-39, Phase 3, Table 1). Days without flow operation (for cathode maintenance, power tests or electrochemical measurements) were not included in this summation of operational days. The reactor was then operated with serial flow (Figure 10B) through the reactor, with alternating flow directions every 2 d (days 40-58, Phase 4). In the last two phases of testing, the flow was set in a fixed direction in parallel (days 59 to 100, Phase 5) or series (days 101-119, Phase 6) flow through the modules.

Flow during Phase 5 was separated into two phases (days 59-79, Phase 5 a; and days 80-100, Phase 5b) due to a significant (based on the Student's t-test) change in COD concentration (Table 1). Electrochemical tests (polarization, cyclic voltammetry and electrochemical impedance spectroscopy measurements) were only performed when COD concentrations were over 400 mg/L to ensure comparable results between tests (avoid differences due to changes in COD concentration during tests). After a series of electrochemical tests the reactor was operated under steady flow conditions for several days to ensure steady conditions for the next flow mode tests. The cathode was periodically cleaned to avoid changes in performance over time due to cathode fouling. The cathode modules were removed from the reactor and sprayed with a commercial bleaching liquid to disinfect the cathode biofilm. After 5 minutes, the cathodes were sprayed with dilute hydrochloric acid (0.01M HCl solution) to dissolve any salts that may have formed on the cathode, and then after 10 min the cathodes were rinsed with tap water before being re-inserted back into the MFC stack. Due to poor performance of the cathodes even with this cleaning procedure, new cathodes were installed for Phase 5 b and 6 starting at day 80.

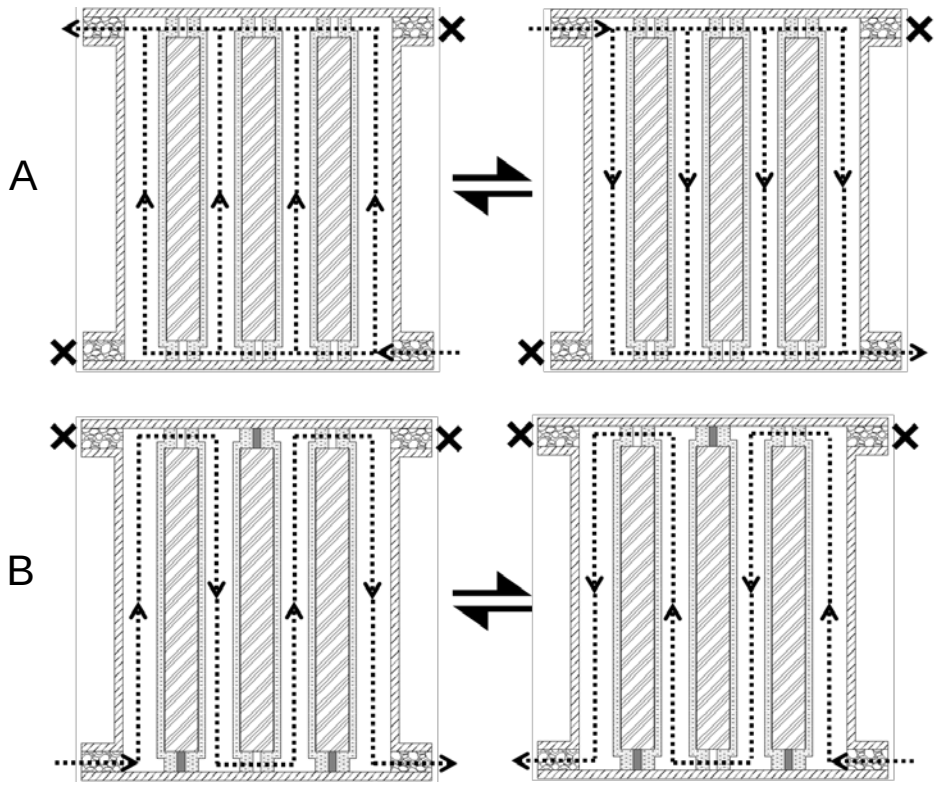

Figure 10. (A) Flow mode regulation controlled by baffles in the parallel flow path with alternating direction, and (B) flow in the serial flow path with alternating direction.

Table 1. Operational Conditions

Phase	Days*	Operational conditions	Flow direction	Hydraulic flow	COD (mg/L)
1	1-7	Inoculation	No flow	Fed-batch	450 ± 30
2	8-19	Startup	Alternating (1 d)	Parallel	490 ± 70
3	20-39	A-P	Alternating (2 d)	Parallel	480 ± 70
4	40-58	A-S	Alternating (2 d)	Serial	540 ± 85
5a	59-79	F-P	Fixed	Parallel	550 ± 100
5b	80-100	F-P	Fixed	Parallel	350 ± 95
6	101-119	F-S	Fixed	Serial	240 ± 80

* Days for cathode maintenance, power tests and electrochemical measurements were not included.

3.5.3. Black Water Tests using MFCs

A set of experiments were conducted to simulate COD removal with black water in an MFC, by using swine wastewater, as a high strength wastewater from a FOB was not readily available for transport to Penn State. Swine wastewater was collected from the Penn State Swine Center (total COD of 21,500 mg/L), a level similar to that of black water. The swine wastewater was initially screened through a stainless steel mesh (50 × 50 mesh, 0.23 mm wire) to remove large particles. The screened swine wastewater had 19 ± 2 g/L COD with conductivity of 17.8 ± 0.5 mS/cm. Without further modification or treatment, the screened swine wastewater was used as inoculum for bacteria acclimation of in MFCs. For the MFC operation in continuous flow mode, the COD of the screened swine wastewater was adjusted to a range of 7−8 g/L by settling and dilution. Each new wastewater sample was first stored in a plastic container (at 4°C) for at least one day without shaking, and solids that settled to the bottom of the container were discarded. If the COD after this step exceeded 8 g/L, the wastewater was diluted using deionized water to keep the COD in the desired range of 7−8 g/L, and then stored at 4°C.

Reactor construction and operation. Two identical air-cathode MFC reactors (working volume of 100 mL) were constructed as previously described in Section 3.5.1. The two swine wastewater fed MFCs (SMFCs) were initially filled with screened swine wastewater as both fuel and inoculum, and the anode and cathode were connected with a 1000 Ω resistor for each MFC. After 30 d of acclimation, two MFCs were hydraulically connected in series, and the swine wastewater adjusted to a COD of 7−8 g/L was pumped into the first MFC reactor using peristaltic pump (Model no. 7523-90, Masterflex, Vernon Hills, IL). The first MFC was labeled the upstream (U) reactor and the second one the downstream (D) reactor. The MFCs were initially operated in continuous flow mode for ~3 months at a flowrate of 0.05 mL/min (theoretical HRT of 2.8 d), and an external resistance R_{ext}=50 Ω. After 74 days of operation, the separators were replaced, the cathode surfaces (solution side) were cleaned using DI water. The flowrate was then increased after 74 d to 0.2 mL/min, for a total HRT of 16.7 h.

Analytical methods. Cell voltages (at each external resistance) were monitored using a multimeter (Model 2700, Keithley Instruments, USA) at 10 min intervals, with the current calculated using Ohm's law ($I = U/R$), where U is the measured voltage (V), and R the external resistance (Ω). The current was normalized by cathode surface area of MFCs (40 cm^2) to obtain the current density. Polarization and power curves were obtained by varying the external resistance from open circuit to 5 Ω. MFCs were first operated under open circuit conditions at least 4 h prior to each polarization test. Total COD was measured using a standard method (method 5220, HACH

Company, Loveland, CO). The student's *t*-test (Microsoft® Office Excel 2010) was used to evaluate whether effluent CODs were significantly different. Total suspended solids (TSS) were measured using standard methods (APHA, 1998). The removal rate (g/L-d) was calculated as $R = (COD_i - COD_t)/t$, where COD_i is the influent COD, and COD_t is the effluent COD at time t (the HRT of the reactor). For comparisons of these rates to previous studies, where the COD removal was found to be first order, a first order rate constant k (h^{-1}) was calculated based on the overall COD removal as $k = -\ln (COD_t/COD_i)/t$. CE was calculated as CE (%) = $C_t/C_{th} \times 100$, where C_t was the total coulombs calculated by integrating the current over time ($C_t = \sum I \Delta t$, where Δt is the time interval of one HRT), and C_{th} was the theoretical amount of coulombs available based on the COD removed in the MFC, calculated as $C_{th} = [Fb(COD_i - COD_t)Q\Delta t]/M$, where F is Faraday's constant, b=4 the number of electrons exchanged per mole of oxygen, Q the flow rate, and M=32 the molecular weight of oxygen.

4. RESULTS AND DISCUSSION

4.1. Anode Testing (Task 1)

4.1.1. Power Generation Using Different Anode Sizes in Smaller MFCs (28 mL)

Power generation. The maximum power densities were: 1150 ± 40 mW/m^2 (0.40 mA/cm^2), C1-thick; 1220 ± 50 mW/m^2 (0.42 mA/cm^2), C1; 1250 mW/m^2 ± 70 (0.42 mA/cm^2), C3; and 1190 ± 50 mW/m^2 (0.41 mA/cm^2), C6 (Figure 11) [31]. The lack of differences in power densities (based on similar values within a standard deviation) showed that all configurations, despite large differences in total brush anode areas, were able to produce the same power. The nearly flat slope of all anode potentials suggested that all configurations offer abundant surface area for the development of an exoelectrogenic biofilm and that the anode was not limiting power production under these conditions. This lack of an effect of anode type indicated that anode surface area could be reduced without affecting performance. The similar power production obtained using MFCs with a single anode but different wire gauges (C1-thick and C1) indicated that the current collector on the anode brush was not a limiting factor for current production, and reducing the wire had no effect on power generation.

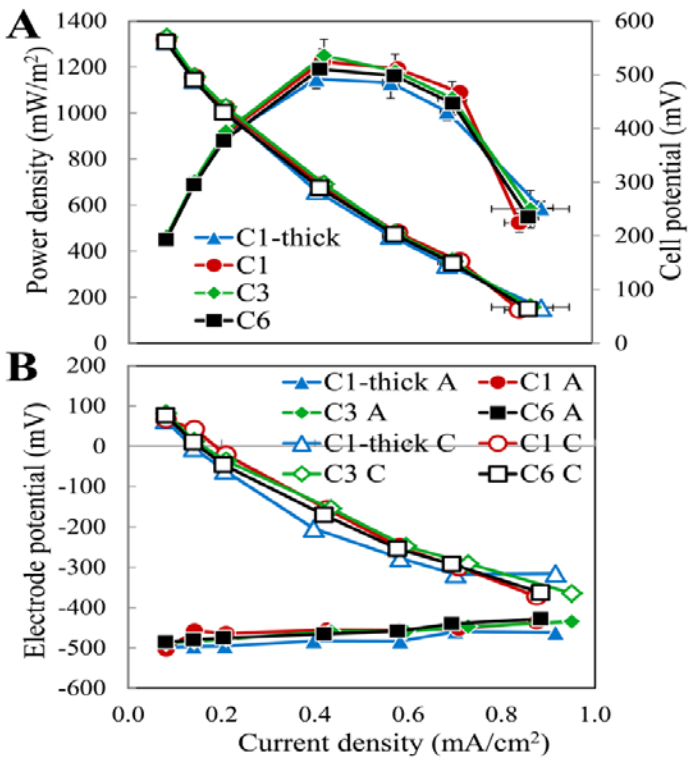

Figure 11. (A) Power density (solid symbols) and polarization curves (white symbols) for the four configurations, obtained through multi-cycle method. (B) Electrode potential curves (A = anode; and C = cathode) measured against a reference electrode (Ag/AgCl) for the four configurations.

COD removal. COD removals over an individual cycle were over 90% for all configurations and resistances. CEs ranged from 21 to 64% depending on the current density (Figure 12) [31]. As external resistance decreases, current density and CE increase due in part to reduced oxygen crossover as a result of shorter cycles. The highest CE (64%) was obtained with C1 at a current

density of 0.82 mA/m^2 (external resistance 10 Ω). At this same external load, CE was 50% for C1-thick and 56% for C3 and C6. Single brush anodes exhibited higher CEs than multi-brush systems, with the sole exception of the maximum external resistance (1000 Ω), although in this case the difference was quite small.

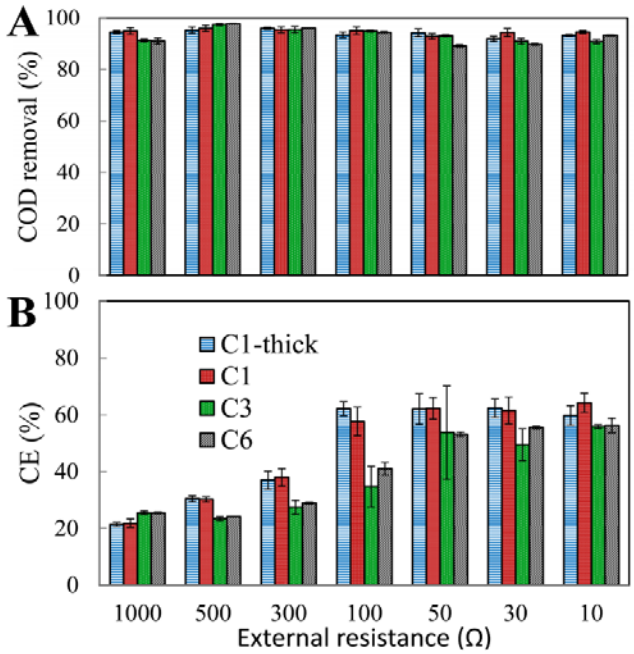

Figure 12. (A) COD removal, and (B) CE percentages vs. external resistance.

Brush disconnection or removal test. The effect of total anode surface area reduction on power production was evaluated in two ways: brush disconnection; and brush removal. For the brush disconnection experiment the power densities decreased by 21% (C3) and 40% (C6) as the brushes were disconnected (from 1330 to 1050 mW/m^2 for C3, and from 1170 to 700 mW/m^2 for C6) (Figure 13A) [31]. Peak power output is an important criterion to assess MFCs performance, but total charge recovery also provides relevant information on energy recovery. The total charge extracted remained stable at 155 ± 2 C for C3 and 152 ± 7 C for C6 even though the duration of the cycle increased from 18 h (all brushes connected) to 22 h (one brush connected) for C3, and from 18 h (all brushes connected) to 25 h (one brush connected) for C6 (Figure 13A). For the brush removal experiment, there were decreases of 21% (C3) and 32% (C6) in the power densities as the brushes were removed (from 1190 to 940 mW/m^2 for C3, and from 1000 to 680 mW/m^2 for C6) (Figure 13B). Thus, the change in power densities were larger for the C6 case than the C3 case, with the percent change equal to (C3) or slightly less (C6) with brush removal compared to disconnection of the brushes. Charge again remained constant for C3 (165 ± 1 C), but for C6 it fluctuated between 144 and 174 C. When brushes were disconnected, the decrease in power appeared to be associated with the limited capacity of fewer anodes to sustain the maximum current compared to that produced with all brushes connected. The use of the multi-brushes was likely a more important factor relative to power production than just the specific surface area of the brushes.

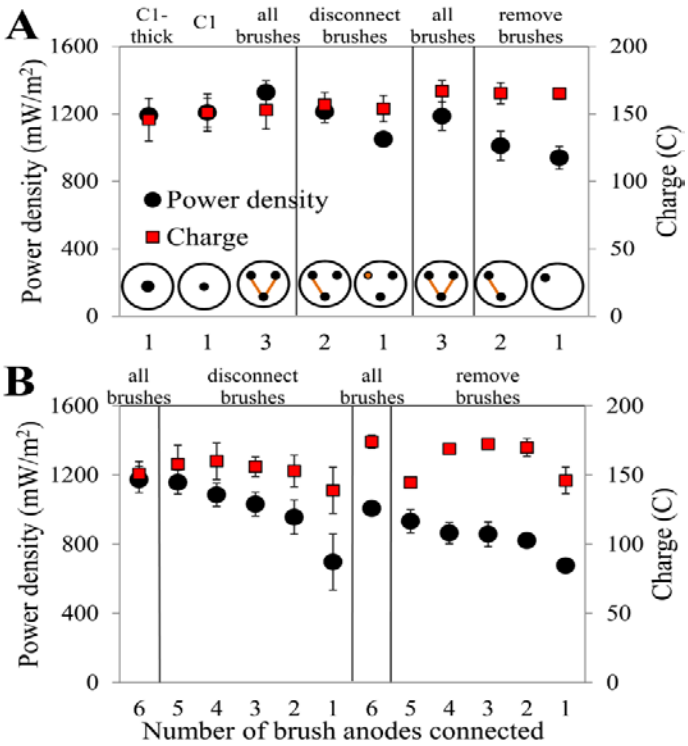

Figure 13. Average power density and charge of the successive brush disconnection and removal for (A) C3, and (B) C6. Values for C1-thick and C1 are included in (A) for comparison purposes.

4.1.2. Examination of Brush Anode Sizes and Packing Densities in Larger MFCs

Power generation. All anodes were initially tested in the same relative position, with the brush core set at the same distance from the cathode (17 mm). In fed-batch mode, the maximum power density was highest for the R3 configuration with 1240 mW/m^2. The maximum power produced decreased when more brushes were used, to 910 mW/m^2 for R5, and 600 mW/m^2 for R8 (Figure 14) [32]. When reactors were operated in continuous flow mode, the maximum power densities were all lower, with slightly different results in terms of which anode configuration was optimal. The R3 and R5 configurations produced about the same maximum power densities, with 560 mW/m^2 for R3 and 600 mW/m^2 for R5. The lowest power density of 280 mW/m^2 was again obtained by the R8 configuration. These power densities are lower than those obtained in fed-batch mode.

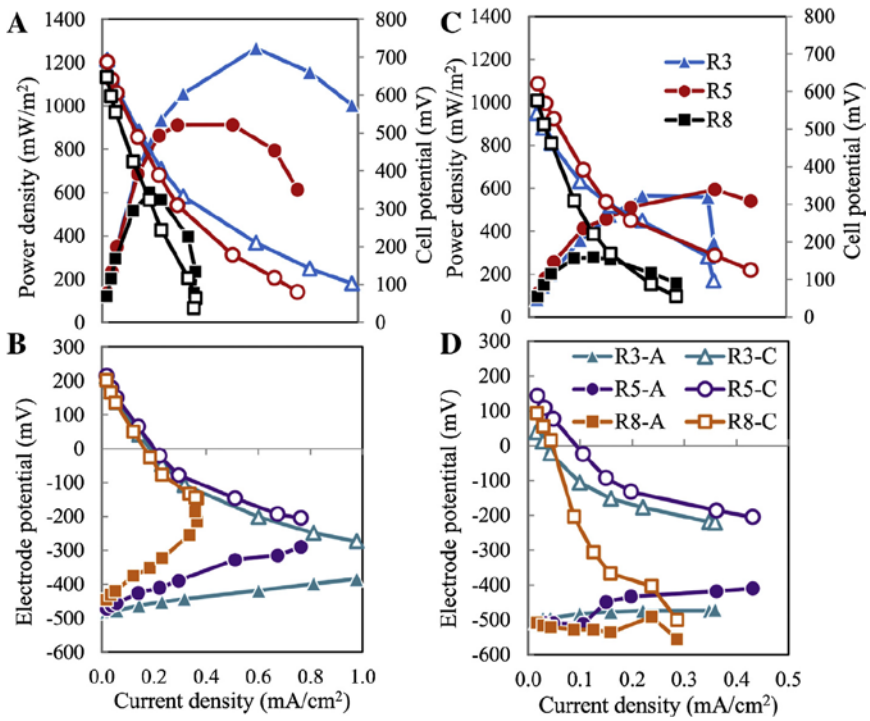

Figure 14. (A and C) Power density (solid symbols) and polarization curves (white symbols) for MFCs obtained using the single-cycle method with three configurations. The curves were obtained in fed-batch (A, B) and continuous flow (C, D) operation.

COD removal. COD removal was decreased in continuous mode (it was >85 % in batch mode compared to 14-45 % in continuous flow mode) due to the much longer cycle lengths in fed-batch mode (3 days) compared to a shorter HRT (8 h) in continuous flow. CEs ranged from 11 to 77 % in fed-batch mode, and from 4 to 82 % in continuous flow operation, depending on resistance used as this affected the current density (Figure 15) [32]. There was a general decrease in CE in continuous mode compared to fed-batch mode, likely due to oxygen diffusion in the anodic chamber. During continuous operation mode there was also a change in the leading CE performance. At the lowest external resistances R3 and R8 had the highest CE during fed-batch mode, whereas R5 was the best performer in continuous mode for this parameter.

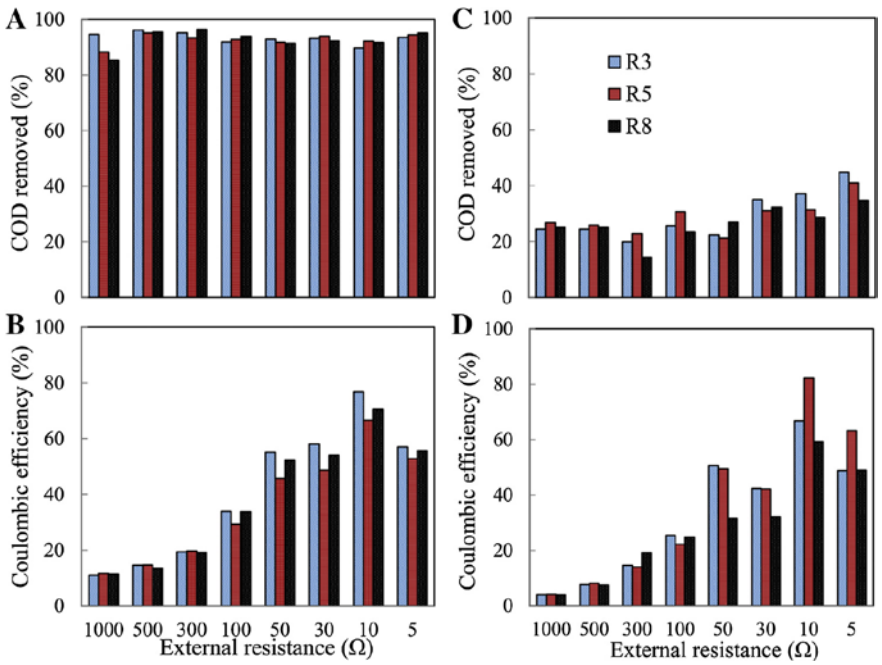

Figure 15. COD removal (A,C) and Coulombic efficiency (B,D) in fed-batch (A,B) and continuous flow (C, D).

Power generation with different electrode spacing. To demonstrate that the change in distances between the anodes and cathodes affected the power densities produced by the smaller and larger brushes (and not just the brush size), the brush anodes for R8 were moved closer to the cathode (from 12 to 4 mm) to produce the same spacing between the brush edges and the cathodes as R3. Power density substantially increased in both fed-batch and continuous mode, making this new smaller brushes configuration with closer spaced electrodes (R8C) the best performer. The maximum power in batch mode was 1030 mW/m^2 (R8C) compared to 600 mW/m^2 (R8) (Figure 16A) [32]. In continuous flow, the maximum power was 1020 mW/m^2 (R8C) compared to 280 mW/m^2 (R8) (Figure 16B). Electrode potential curves showed that cathode potentials were more stable in configuration R8C than R8. EIS and LSV analyses were consistent with this trend in increased power with the closer electrode spacing. There was a substantial decrease in all impedance components for R8C compared to R8, with the solution resistance (directly related to electrode spacing) having the largest decrease by 84%, followed by a large reduction in diffusion resistance (51%).

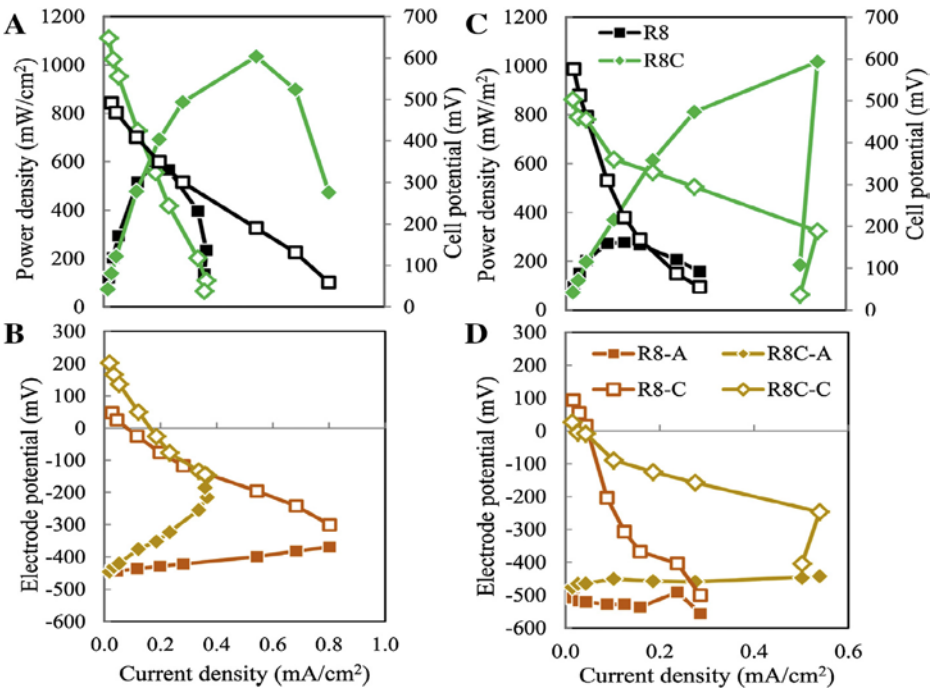

Figure 16. (A and C) Power density (solid symbols) and polarization curves (white symbols) obtained through the single-cycle method for the two configurations: R8 and R8C. The curves were obtained in fed-batch (A, B) and continuous flow (C, D) operation.

Conclusions relative to anode sizes with acetate solutions. The conclusion from these tests was that using a larger number of smaller anodes to cover the cathode surface provided superior performance. However, this conclusion was only validated using relatively high concentrations of acetate in well-buffered solutions. Thus, the next task was to examine performance of these small electrodes when using domestic wastewater, which is much lower in the initial concentration of organic matter, and it is not as well buffered against pH changes at the electrode surfaces.

4.1.3. Performance of Larger Scale MFCs (130 mL) with Domestic Wastewater

For wastewater tests, the larger-scale 130 mL MFC was used (Figure 2) [32] with the R8C configuration, with all experimental conditions the same except the solution (previously acetate buffer solution was used) and the separator.

Power generation. Three polarization tests were run to determine the maximum power density of the reactors. The first two tests used unfiltered primary clarifier effluent and resulted in power overshoot (a doubling back of the power curve). The maximum power density achieved in the first test was 315 ± 17 mW/m^2 at the current density of 0.9 A/m^2, and the second test achieved a maximum power density of 220 ± 7 mW/m^2 at 1.1 A/m^2 (Figure 17). To correct for power overshoot, sodium chloride (NaCl) was added to the wastewater to increase conductivity. Once acclimated, a third polarization test was conducted. The maximum power density achieved was 320 ± 9 mW/m^2 at the current density of 1.0 A/m^2 with less power overshoot than previous tests.

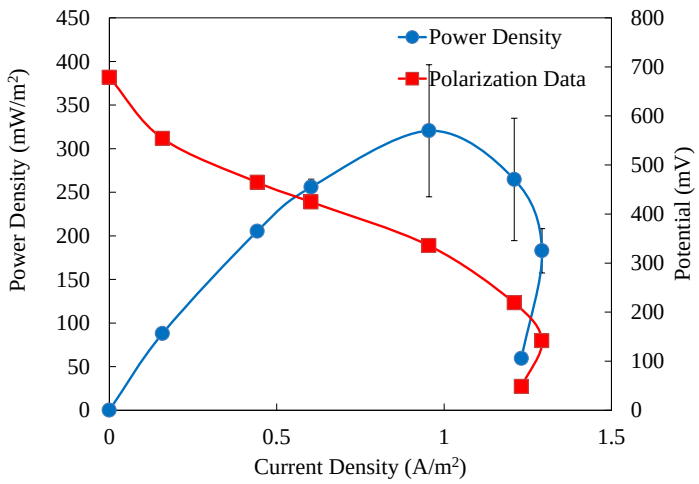

Figure 17. Polarization and power curves obtained from the larger scale MFC fed with a domestic wastewater.

COD removal. COD removal rates were characterized for wastewater under 100 Ω in fed-batch mode. Mid-cycle COD and soluble COD (SCOD readings were taken at various intervals to see COD removals over the course of the cycle (a batch cycle lasts 72 h). COD and sCOD removal follows first order kinetics, with a removal rate constant of 0.047 h^{-1} (COD) and 0.048 h^{-1} (SCOD) (Figure 18). Overall COD and SCOD removal during a fed batch cycle was 82% and 72%, respectively.

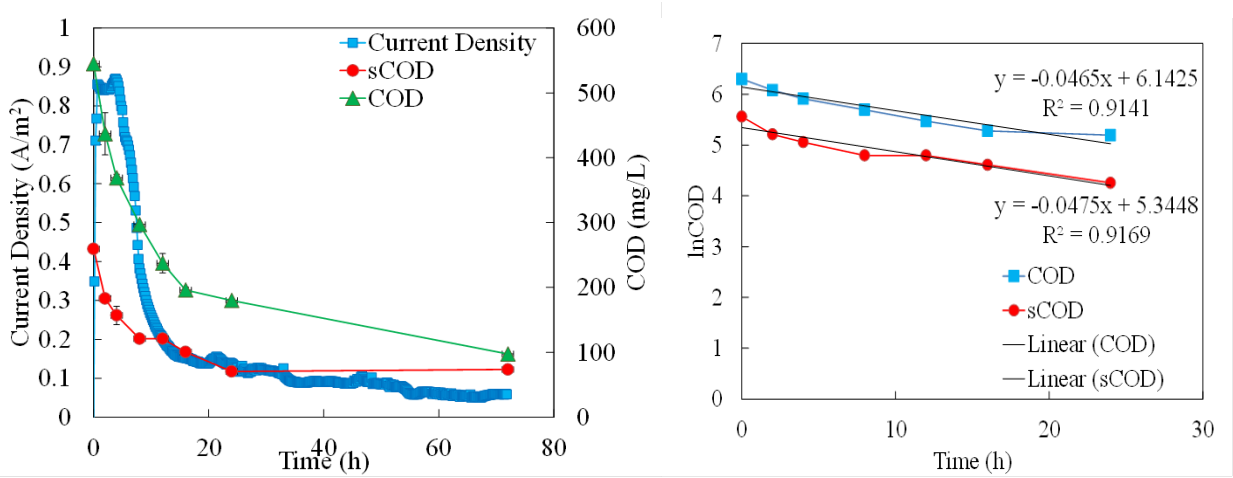

Figure 18. COD monitoring during current generation in the larger scale MFC fed with domestic wastewater (left). First-order fitting data for COD removal (right).

4.1.4. Nutrient Removal Test Using Larger Scale MFCs (130 mL)

Since the domestic wastewater contains nutrients as well organic matter that need to be removed, nutrient concentrations in the influent and effluent of the larger scale MFCs were examined.

Batch mode operation. Samples were collected at two points in a cycle where current started to drop from the maximum point (after about 9 h), and when current and nearly completely ceased (about 24 h). The ammonia concentrations decreased over the course of a fed batch cycle, from an initial concentration of 43.4 mg/L, to 35.4 mg/L after 9 h, and 23.9 mg/L after 24 h, for a total

overall reduction of 45% (Table 2). Chloride concentrations remained constant. Nitrate and phosphate concentrations increased slightly. Effluent sulfate concentrations decreased from, an initial 30.2 mg/L to 10.0 mg/L at the end, a 67% decrease. These results showed that there was ammonia removal and nitrification, and likely that there was organics removal using nitrate and sulfate.

Table 2. Monitoring of nutrients concentrations in the larger scale MFC during operation.

Sampling point	Chloride (mg/L)	Nitrite (mg/L)	Nitrate (mg/L)	Phosphate (mg/L)	Sulfate (mg/L)	Ammonia (mg/L)
Initial concentration (0 h)	164.0	48.6	1.8	2.5	30.2	43.4
After 9 h	151.7	41.8	2.2	3.7	4.64	35.4
After 24 h	170.0	48.7	2.3	4.2	9.96	23.9

Continuous flow mode. In tests with under continuous flow mode operation, the NH_3-N concentration in the effluent was 37.1 ± 1.3 mg/L, which indicated there was no significant change in NH_3-N concentrations due to similar concentrations in the MFC influent (37.4 ± 0.8 mg/L). Although ammonia removal was not observed for MFCs in continuous flow here, this does not preclude use of MFCs for wastewater treatment at FOBs. Additional processes could be used to remove nutrients, and ESTCP is funding research on downstream removal of nutrients that can be used at military installations and FOBs. Thus, it may be possible to use the MFC for removal of biodegradable organic removal and energy recovery, with residual nutrients being removed by other downstream processes such as ammonia volatilization or adsorption, or nitrification and denitrification, using established technologies. However, nutrient removal may not be needed as many water reuse applications do not require nutrient removal, such as dust suppression, vehicle washing, toilet flushing, and other applications. Nutrient removal is only required if the water will be discharged to a navigable water in the US, although other countries have different discharge requirements.

4.2. Separator Testing (Task 2)

4.2.1. PVA Separator Tests with Acetate Buffer Solution

Comparison of power densities with different separators. Moving from a spaced to an SEA configuration produced a 27% increase in power (740 ± 58 mW/m^2 vs. 942 ± 43 mW/m^2) in tests with stainless steel cathodes and Pt catalyst. PVA was compared against wipe separators (cellulose/polyester blend) and no separator (NS) in the spaced configuration, and against wipe separators and glass fiber (GF) separators in the SEA configuration. In the spaced configuration, PVA performed better than wipe separators (518 ± 6 mW/m^2 vs. 487 ± 6 mW/m^2), but not as well as the reactor without a separator (702 ± 29 mW/m^2). In the SEA configuration, wipe separators (700 ± 57 mW/m^2) performed better than PVA (635 ± 64 mW/m^2) or GF (610 ± 24 mW/m^2) separators. The SEA results were unexpected due to the PVA performing better in the spaced configuration. Coulombic efficiencies for all testing involving separators reached a maximum of 65-75% while the test with no separator produced 60%. Based on EIS measurements, ohmic

resistance 2.3 ± 0.1 Ω for PVA separators, and 10.1 ± 0.1 Ω for the wipe separators. Charge transfer resistance was measured in a single chamber cell at a set potential of –0.1V. Charge transfer resistance was 31.2 ± 16.6 Ω for PVA separators, and 12.4 ± 0.8 Ω for wipe separators.

Power generation using solutions with different conductivities. Tests of PVA in both SPA and SEA configurations was conducted using solutions with different PBS concentrations (5 mM, 50 mM and 100 mM) (Figure 19) [33]. With 5 mM PBS, there was no loss in power when the PVA separator was added to the reactor in the SPA format (336 ± 3 mW/m^2 for no separator, NS; 339 ± 29 mW/m^2 with PVA separator), but power was increased by 32% in the SEA format (444 ± 8 mW/m^2). With 50 mM PBS, there was a 28% loss in power with the addition of PVA into SPA format (1228 ± 55 mW/m^2, NS; 889 ± 0 mW/m^2 with PVA). Part of this loss was recovered by using the SEA configuration, as there was an increase in power of 8% vs SPA to 956 ± 51 mW/m^2, but this was still 22% lower than the NS tests. For the 100 mM PBS tests, there was a 50% decrease in power density with the addition of PVA into the SPA reactors (1848 ± 18 mW/m^2 for NS; 932 ± 76 mW/m^2 with PVA separator). Part of this loss was recovered when the electrodes were switched to operation with a separator (SEA mode) as there was an increase in power of 30% vs SPA to 1207 ± 110 mW/m^2, but this was still 35% lower than the NS tests.

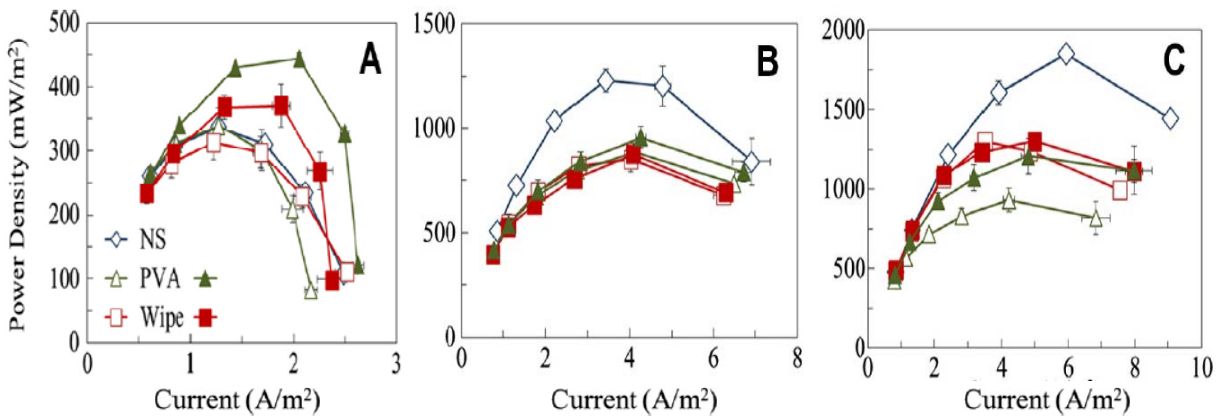

Figure 19. Comparison of SEA (closed symbols) and SPA (open symbols) power density curves in (A) 5 mM, (B) 50 mM and (C) 100 mM PBS.

Spray-on vs. cast PVA separators. With cast separators, power densities of 942 ± 43 mW/m^2 with Pt cathode catalysts were 7% higher than with spray-on separators (873 ± 33 mW/m^2) (Figure 20) [33]. Similarly, the power densities of 718 ± 74 mW/m^2 with cast separators were 8% higher than spray-on separators (664 ± 67 mW/m^2) on AC cathodes (19.5 ± 0.1 mg PVA/cm^2) was roughly twice as much as the loading on the Pt cathodes (10.0 ± 1.4 mg/cm^2) due to the cathode configuration that required the PVA to completely cover the metal mesh. The additional PVA loading had only a small impact on power production. PVA thickness was not compared between cast and spray-on separators, but the general trend was that a thicker separator yielded a higher CE, but resulted in a lower maximum power density. It is likely that the spray-on separators were thicker than the cast separators due to the inclusion of air bubbles in the application process but this only had a minimal effect on performance due to the greater porosity created by those air bubbles.

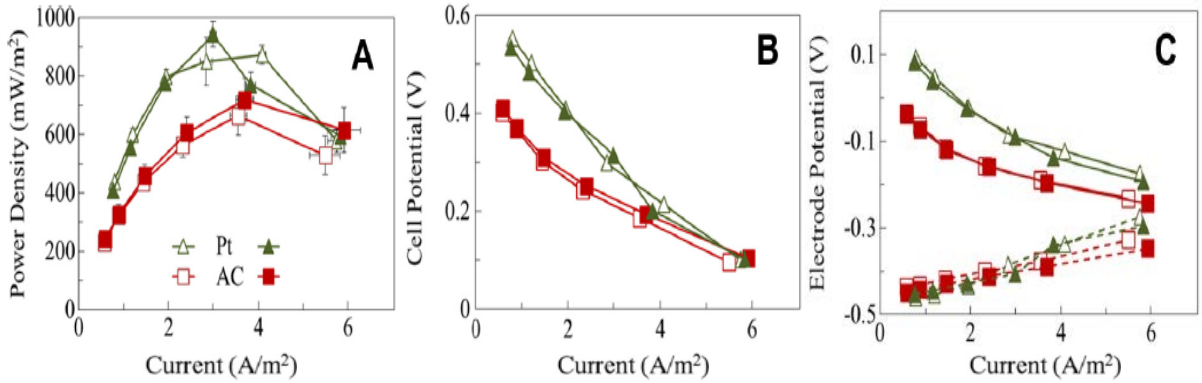

Figure 20. Test data for cast (closed symbols) and spray-on (open symbols) PVA separators in SEA on Pt and AC cathodes showing: (A) power density curves, (B) cell voltages, and (C) electrode potentials (cathodes: solid lines; anodes; dashed lines).

4.2.2. Separator Tests with Domestic Wastewater

Domestic wastewater (collected from Penn State Wastewater Treatment Plant) was used for tests to evaluate PVA separators in 28 mL reactors. Tests with cast PVA separators with domestic wastewater in the SPA configuration showed that power density was reduced by 12% with the addition of the separator versus the NS control (292 ± 5 mW/m^2 for NS vs 255 ± 7 mW/m^2 with PVA). This power loss was not that large, but a decrease was unexpected based on previous tests in a solution with similar conductivity (5 mM PBS) that showed no power loss with the addition of the PVA separator (337 ± 3 mW/m^2 for NS vs 339 ± 29 mW/m^2 with PVA separator). Maximum coulombic efficiencies were unchanged in the SPA testing with the addition of a PVA separator (26% with NS, 25% with PVA). Overall, it was found that cloth (wipe) separators had similar performance to PVA separators.

4.3. Spacer Testing (Task 3)

4.3.1. Spacer Tests with Acetate

Power generation with different types of spacers. The best performance was observed with the WS. The maximum power densities achieved with the WS were 1100 ± 10 mW/m^2 based the one effective cathode area, and 32 ± 0.2 W/m^3 based on the liquid volume of one anode compartment, using an eternal resistance of 2.5 Ω. The maximum power densities observed with CS were 1010 ± 10 mW/m^2 and 29 ± 0.2 W/m^3, which were slightly less than those obtained with the WS. The performance of MS was much lower than WS and CS, with power densities of 650 ± 20 mW/m^2 and 20 ± 0.2 W/m^3 (Figure 21a) [35]. The anode potentials with the different spacers were very similar to each other (Figure 21b). Thus, the cathode potential should have limited power production and determined the general shape of the whole cell potential curves. In the current density range from 0 to 1.2 ± 0.04 A/m^2, the cathode potential with MS was similar with that of CS and WS. At greater current densities, the cathode with MS had a more negative potential. The cathode potentials with CS were mostly similar to those with the WS. When the current density increased up to 4.0 ± 0.1 A/m^2, the cathode potential started to show a slight drop relative to the other tests.

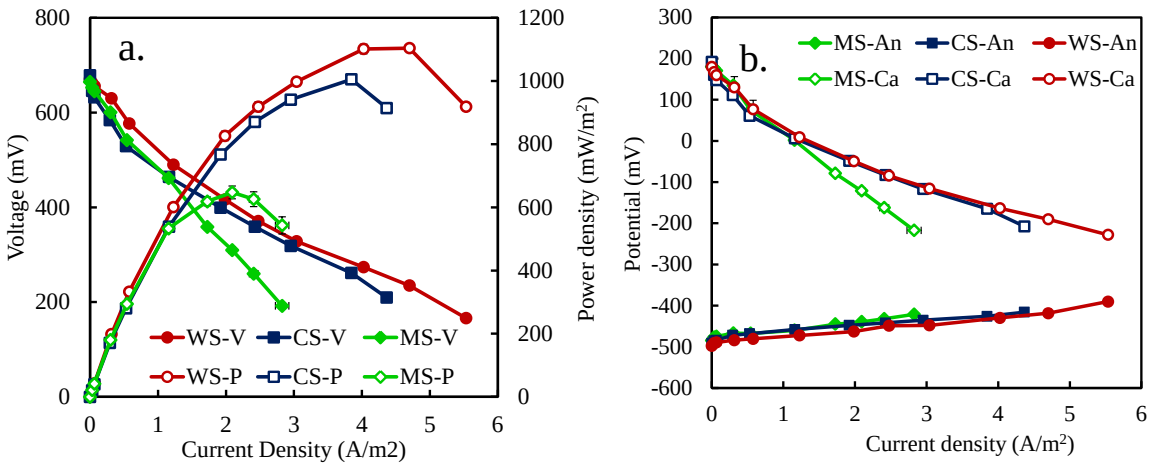

Figure 21. The polarization curve (a) and electrode potential (b) of the mesh, column and wire spacers. The error bars ± SD were calculation based on averages data from the chamber A and B of the MFC stack.

Internal resistance distributions with different types of spacers. In order to prove the differences in performance of the MFCs with the different spacers was due to the oxygen transfer limitations at the cathode, EIS tests were performed to analysis the internal resistance distribution in each condition. The EIS tests for each spacer were performance at conditions similar to that maximum power output point on the polarization curve. The anode resistances with MS (0.35 ± 0.08 Ω), CS (0.55 ± 0.08 Ω) and WS (0.40 ± 0.05 Ω) were similar and accounted for a small fraction in the total internal resistance (Figure 22) [35]. In the distribution of the cathode resistances, the ohmic resistance part of three spacers was similar. However, the non-ohmic resistance of the MFC with the MS spacer (1.40 ± 0.15 Ω) was more than two times larger than those with CS (0.63 ± 0.10 Ω) or WS (0.69 ± 0.08 Ω) spacers (Figure 22). The non-ohmic resistance refers to the sum of the charge transfer resistance and diffusion resistance.

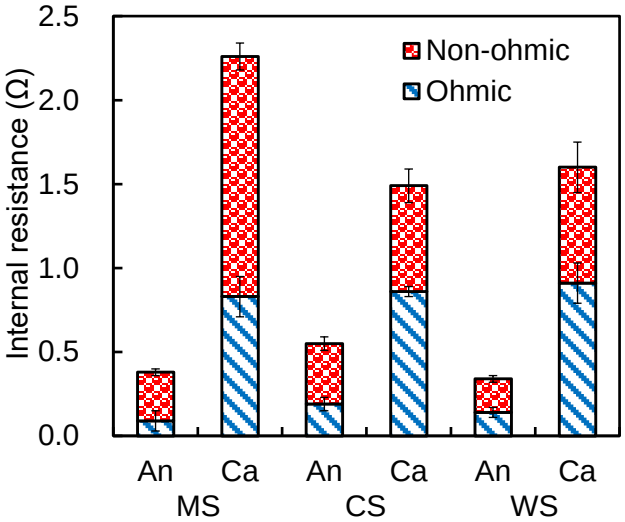

Figure 22. Internal resistance distribution for the anodes (An) and cathodes (Ca) using mesh (MS), column (CS), or wire (WS) spacers. The error bars are ±SD based on averages from the A and B sides of the MFC.

4.3.2. Spacer Tests with Domestic Wastewater

Additional tests were conducted with the same reactors in the above tests, but using domestic wastewater or wastewater amended with acetate. The wastewaters collected had a total COD in the range of 400-550 mg/L, and a soluble COD (SCOD) in the range of 200-300 mg/L. Polarization tests showed that there were similar maximum power densities of the two anode compartments of 400 ± 8 mW/m^2 (A side) and 400 ± 3 mW/m^2 (B side), with an average maximum empty bed volume power density of 7.9 ± 0.1 W/m^3 (11.2 ± 0.1 W/m^3 based on liquid volume) (Figure 23) [35]. After operation of the MFCs for 3 months, polarization data were again obtained to evaluate electrode performance. The maximum power densities had decreased to 300 ± 10 mW/m^2 (compartment A) and 275 ± 7 mW/m^2 (compartment B) (Figure 23). The anode potentials were the same in the original (1 month) and final (3 month) polarization tests, indicating that changes were due to cathode performance rather than changes in wastewater quality or composition. A decline in cathode performance was expected given previous long-term studies of MFCs with acetate that have shown reduced cathode performance over time.

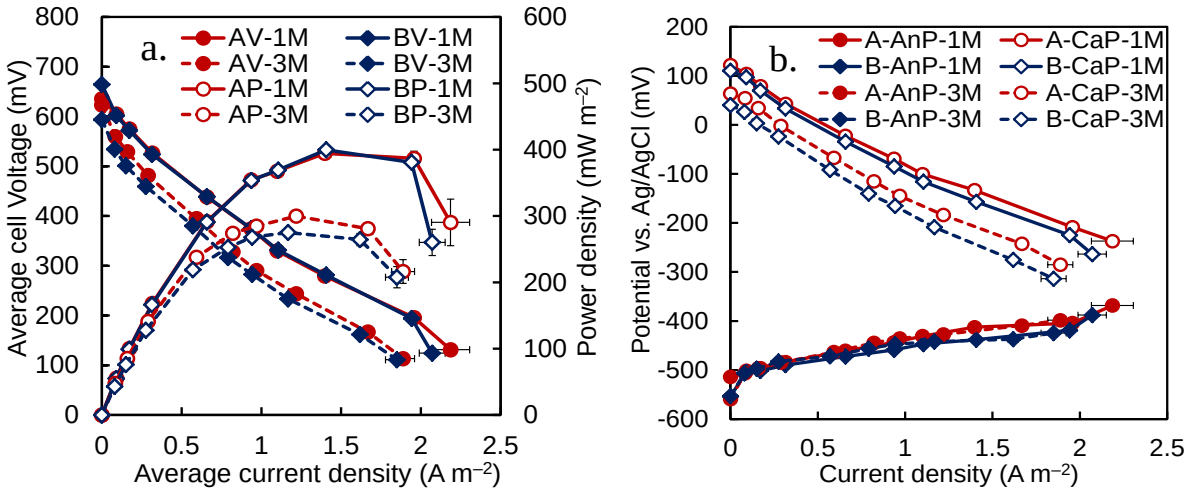

Figure 23. (a) Polarization curves and (b) anode (An) and cathode (Ca) potentials of the MFC operated in fed-batch mode using raw domestic wastewater: solid lines, results after one month (1M); dashed lines, results after 3 months (3M); P=potential, V=voltage. Average and error bars (± SD) based on individual measurements for 6 brush anodes in compartments A or B.

Impact of influent COD on current density. The current and power produced in an MFC can depend on the strength of the wastewater. To examine how the change in COD affected MFC performance here, current and COD concentrations were measured over the course of ~8 h during a fed-batch cycle, with measurements taken 6 times during this period. Thus, the six time intervals (T1–T6) were obtained with six sampling times separated by 80 min each. Current production was relatively stable at 2.0 ± 0.1 A/m^2 while the COD concentration decreased from 450 ± 10 mg/L to 288 ± 15 mg/L (T1 – T4) (Figure 24) [35]. However, current production sharply decreased to 1.3 ± 0.2 A/m^2 at 275 ± 15 mg-COD/L (T5) and 0.9 ± 0.1 A/m^2 at 250 ± 5 mg/L (T6). This decrease in performance was consistent with a previous study that showed that current production sharply decreased at COD concentrations lower than ~250 mg/L, using wastewater from the same treatment plant.

The changes in anode resistances during multiple fed batch cycles were monitored by briefly setting the anode potential at a set potential of –420 mV for 50 min, followed by an EIS test with

the same anode potential for another ~30 min (Figure 24). The non-ohmic resistance of the anodes paralleled observations of rapid decreases in current density as the COD was reduced. In the two last time intervals, with the COD of 275 mg/L or less, the non-ohmic anode resistance rose from 0.56 ± 0.09 Ω, to 0.77 ± 0.18 Ω (T5) and 1.62 ± 0.33 Ω (T6). The low current production by the MFC at these COD concentrations is a further example of the need for a secondary treatment process, such as an AFMBR, to reduce COD to levels suitable for wastewater discharge [42].

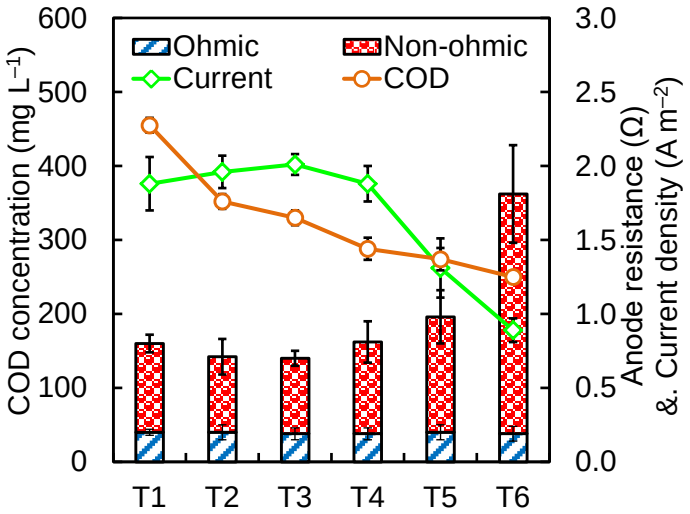

Figure 24. Anode resistances analyzed in terms of ohmic and non-ohmic resistances, using raw wastewater in fed-batch tests. The error bars are ±SD based on averages from the A and B sides of the MFC. T1 – T6: Time intervals, obtained by dividing one complete cycle of MFC operation (8 h) into six equal parts (80 min each).

4.3.3. MFC Module Design

Performance of MFC module (Batch mode). During the start-up period, the total COD and SCOD removal rate was 45 ± 4 % and 33 ± 3 % for each anode circuit. The maximum volume power density was 8.5 W/m^3, while in single cycle power test, the maximum volume power density after startup period reduced to 6.6 W/m^3. The reducing of power densities was due to the performance drop of the AC cathodes after initially immersed in wastewater. In the comparison between electrode configurations, based on the voltage output with various resistances, the power density based on cathode area for anode 1 and 4, which combined with one layer of cathode, was 370 ± 4 mW/m^2, while that of anode 2 and 3 was 290 ± 30 mW/m^2. After startup period, in single cycle power test, the anodes 2 and 3 generated an average power density of 225 ± 8 mW/m^2, while that of anodes 1 and 4 was 290 ± 8 mW/m^2. By doubling the cathode area matched for each anode array, about 78 ± 2 % of the maximum power densities was obtained based on cathode area, compared with 1An1Ca configuration.

4.4. Cathode Testing (Task 4)

4.4.1. Enhanced AC cathode by Blending Carbon Black

Power generation with different carbon black loading and durability. Power generation was enhanced in MFCs by adding CB into the AC, with the same optimum ratio of 10% as that obtained in abiotic tests. After one week of operation, the MFCs with cathodes prepared with a 10% ratio

produced the highest power density of 1560 ± 40 mW/m^2, followed by 5% (1510 ± 10 mW/m^2), 15% (1510 ± 10 mW/m^2), and 2% ratio cathodes (1460 ± 10 mW/m^2) (Figure 25A) [43]. The power density of the MFCs with the 10% ratio cathode was 16% higher than those with the plain AC cathodes (1340 ± 120 mW/m^2), and 7% higher than MFCs with a Pt cathode (1460 ± 10 mW/m^2). Anode potentials were essentially the same at the same current densities in all the MFCs, indicating that the cathode potentials were responsible for the differences in power generation.

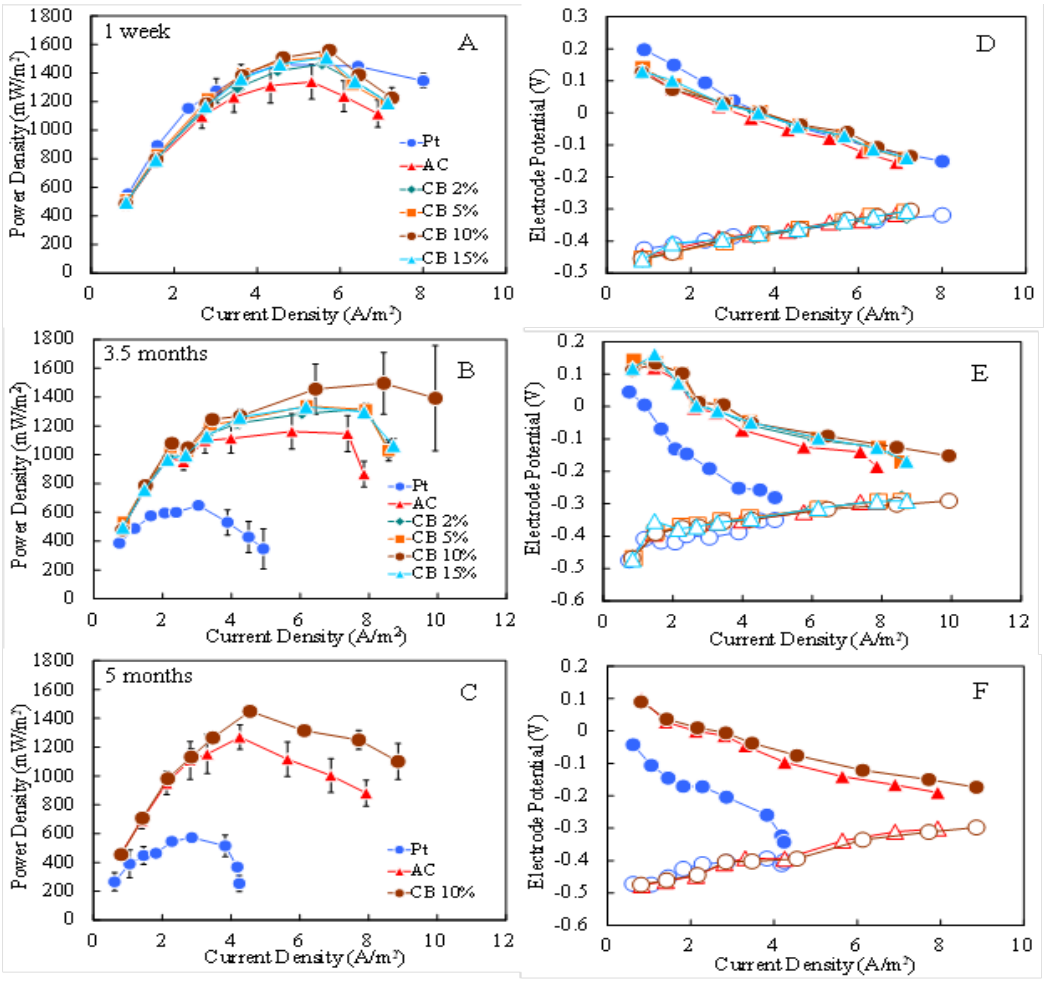

Figure 25. (A) (B) (C) Power densities and (D) (E) (F) electrode potentials as a function of current density in MFCs using different cathodes after 1-week, 3.5-month and 5-month operation.

After 3.5-months of operation, the MFCs with 10% CB still produced the highest maximum power density of 1500 ± 210 mW/m^2, which was 29% higher than the plain AC cathodes (1160 ± 120 mW/m^2) (Figure 25B) [43]. The cathodes with the 5% and 15% ratios still produced similar maximum power densities of 1340 ± 40 mW/m^2 (5% ratio) and 1330 ± 40 mW/m^2 (15% ratio). The MFCs with the Pt cathodes had greatly reduced power production, with a 55% reduction in maximum power to 650 ± 10 mW/m^2. The AC with a 10% CB:AC ratio had the lowest decrease in performance of 4% in the maximum power densities, compared to a 13% decrease for plain AC.

After 5 months, the MFCs with the 10% ratio continued to produce the highest power density of 1450 ± 10 mW/m^2, which was now 150% higher than Pt (570 ± 30 mW/m^2) and 14% higher than plain AC (1270 ± 80 mW/m^2) (Figure 25C) [43]. The maximum power densities for this 10%

ratio cathode were decreased by only 7% compared to the first week, demonstrating that AC based cathodes sustained high power generation. The slight decrease of AC cathode performance over time might be due to the clogging of micro pores in the AC.

Electrochemical performance with different CB loading. Chronoamperometry tests were conducted to examine the electrochemical activity of the AC cathodes blended with 0%, 2%, 5%, 10% and 15% CB powder (Figure 26) [43]. CB and AC ratio of 10% was optimal and it had an open circuit potential (OCP) of 0.25 V (vs Ag/AgCl, same as below), higher than the one without CB (0.20 V) and those with the other ratios (2%, 0.22 V; 5%, 0.23 V, 15%, 0.23 V). The cathode with the 10 % CB ratio generated current density of 8.7 A/m^2 in the chronoamperometry test, higher than the one without CB (7.1 A/m^2) and the other ratios (8.0-8.5 A/m^2), and even Pt (7.8 A/m^2). The plain AC cathode had a lower internal resistance (78 Ω) than that of Pt (112 Ω). The internal resistance of AC cathode was further reduced by adding CB (65-70 Ω). The cathode with CB and AC ratio of 10% obtained lowest internal resistance of 65 Ω. The chronoamperometry test results were consistent with the power generation results (the cathode with CB and AC ratio of 10% produced the highest power density).

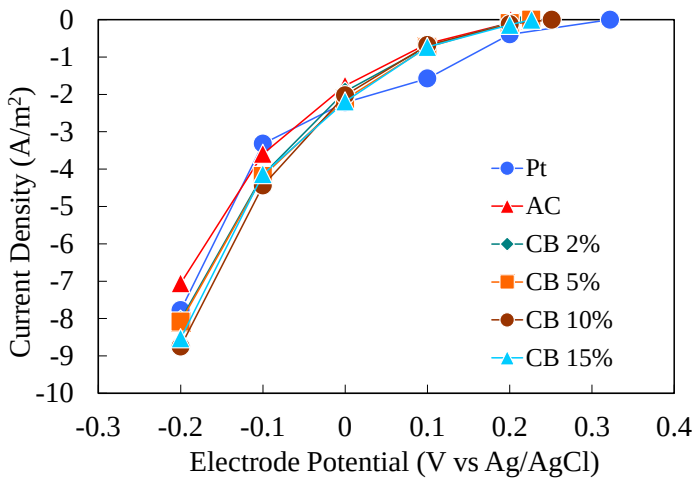

Figure 26. Current-potential curves of different cathodes in electrochemical cells.

4.4.2. Long-term Operation of AC based Cathodes

MFC performance and durability of AC based cathodes. Long-term tests (over 16 months) were performed to compare the longevity of Pt/C catalyst cathode and different AC-based cathodes made by our industrial partner. After 5.5-month operation, FeEDTA modified AC and heat treated AC cathodes still generated the highest maximum power densities of 1244 ± 60 and 1262 ± 2 mW/m^2, 14% higher than that of pure AC (1092 ± 15 mW/m^2). AC with CB produced maximum power density of 1199 ± 30 mW/m^2. Generally, AC-based cathode maintained high power generation after 5.5 months, with 1% to 12% reduction compared to those after 1 month operation. The maximum power density of Pt/C cathode was only 388 ± 63 mW/m^2, a decrease of 69% compared to that after 1 month (1266 ± 46 mW/m^2). After 12 and 16 months of operation, heat treated AC cathodes generated the highest maximum power densities of 1000 ± 20 mW/m^2, followed by AC with CB (970 ± 10 mW/m^2) and FeEDTA modified AC (960 ± 40 mW/m^2) (Figure 27) [44]. The maximum power densities of these modified AC cathodes were 8 to 12% higher than that with plain AC (890 ± 20 mW/m^2), and greater than twice than that with Pt (290 ± 50 mW/m^2). Therefore, these modified AC cathodes sustained higher performance for one year, much better

than the Pt cathodes. AC and 10% CB was concluded to be the most cost-effective catalyst material for air cathode MFCs.

After 17 months, biofilm and salt precipitation on the cathodes were removed by a weak acid (hydrochloric) cleaning procedure. The power densities were improved by 14% to 29% compared to the results after 16 months, and restored to >85% of the original (at 1 month) levels (Figure 27) [44]. All AC based cathodes had significantly improved power densities compared to Pt cathodes during long-term operation, which produced only 270 mW/m^2 after 17 months even after cleaning. Based on considerations of the performance, cost, and simplicity of cathode preparation, it is suggested that blending 10% CB into the AC material is the most useful and cost effective method to enhance AC catalytic performance.

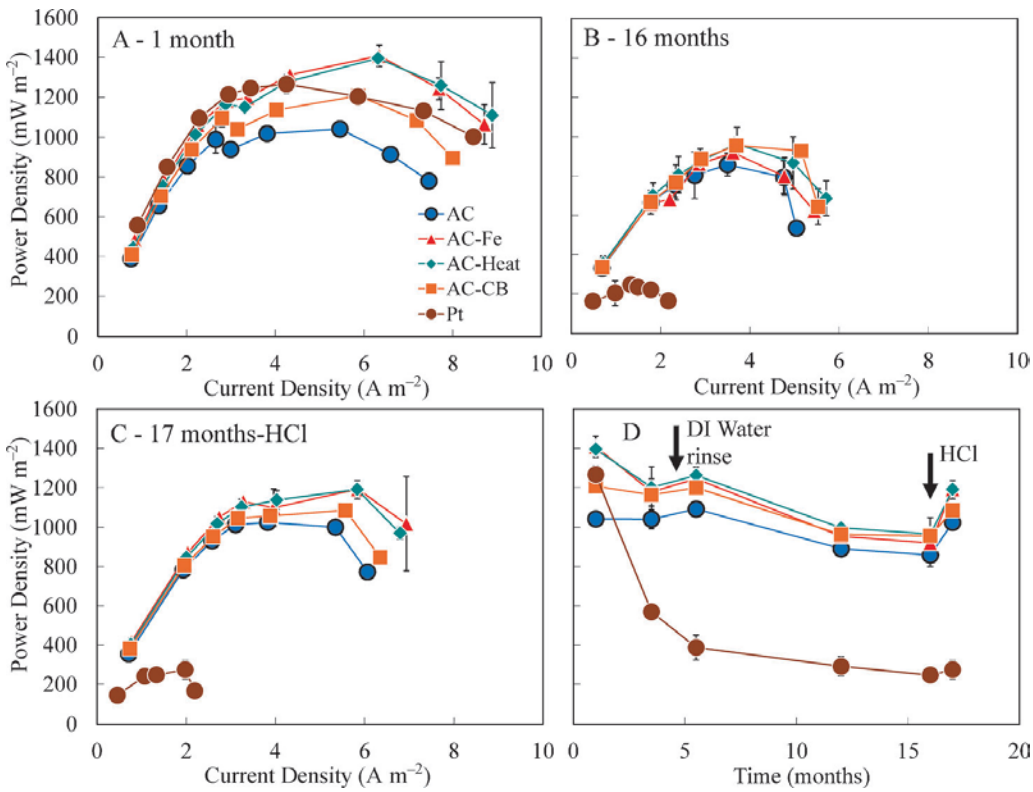

Figure 27. Current-potential curves of different cathodes in electrochemical cells.

4.4.3. Testing PVDF Phase Inversion AC Cathode

Cathode performance with acetate. A maximum power density of 1470 ± 50 mW/m^2 was produced by PVDF cathode with 8.8 mg/cm^2 loading. This power density was similar to that obtained using a wipe diffusion layer and AC/PTFE (1450 ± 10 mW/m^2) (Figure 28), but the new procedure was easier and the materials cost were reduced [38]. A high water pressure tolerance of 1.22 ± 0.04 m was achieved, which was six times higher compared to wipe-based AC/PTFE cathode. The porous PVDF structure formed via phase inversion process helped retain most surface area of AC catalyst and minimize the charge transfer resistance. Tests were also made using a larger 7 cm × 10 cm PVDF cathode. These results showed that the performance was similar to the more expensive PTFE cathodes made with Pt, in terms of the maximum power density (231 ± 10 mW/m^2). This AC cathode was made without separate fabrication of the diffusion layer. A

material and cost analysis was conducted to demonstrate that these PVDF cathodes can be made using materials that cost ~$13 /m^2, where the stainless steel mesh accounts for $10 /m^2.

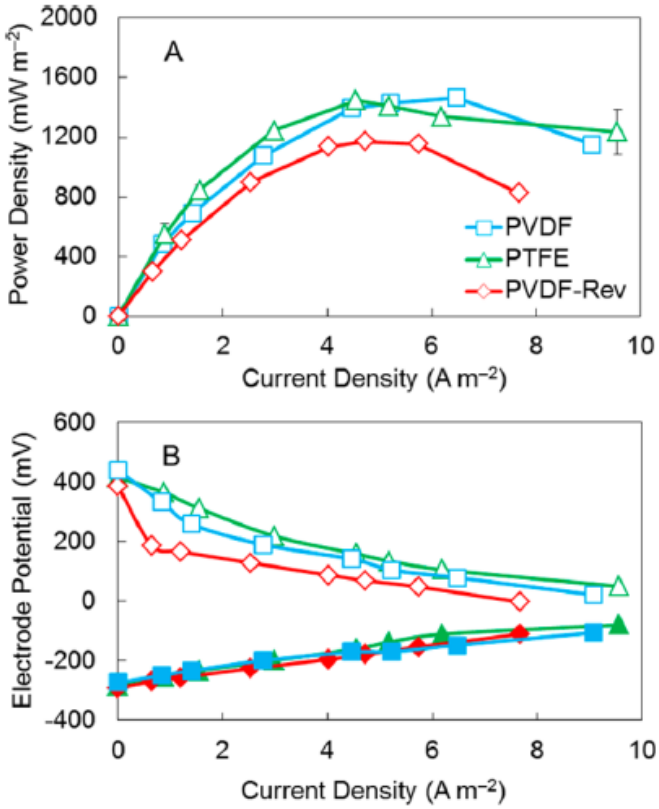

Figure 28. (A) Power density curves for a PVDF cathode, reversed-side PVDF cathode, and a PTFE cathode; (B) electrode potentials (solid symbols, and potentials; open symbols, cathode potentials).

Water pressure resistance. Different activated carbon loadings were tested relative to performance and water height (Figure 29). A vertical distribution of activated carbon loading (17.7, 26.5, 35.4, 44.2 mg/cm^2 from top to bottom) in PVDF cathodes had a better electrochemical performance under elevated water pressure compared to the reverse distribution (highest loading on top). With this new design of the PVDF cathode, dual goals could be achieved in both stronger water pressure resistance and higher catalytic efficiency [38]. This new cathode design demonstrated the existence of different cathode water profiles when cathodes were exposed to different water pressures.

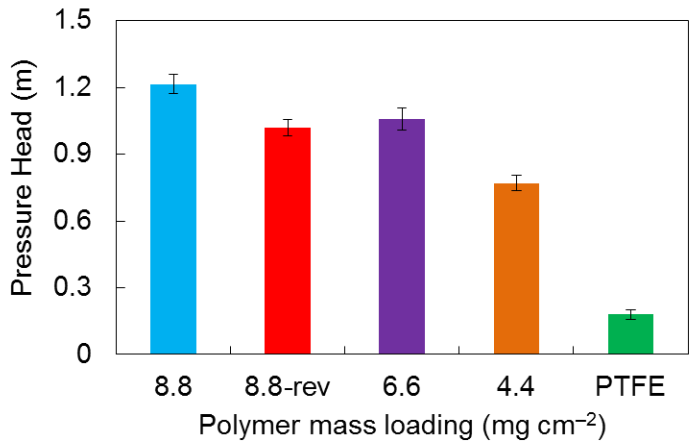

Figure 29. Water pressure resistance of PVDF cathodes with different polymer loadings (8.8, 6.6 and 4.4 mg/cm^2) with the polymer layer facing the air, compared to the reversed orientation of a PVDF cathode (8.8 mg/cm^2), and a PTFE cathode.

Performance with larger cathodes and domestic wastewater. Larger PVDF cathodes (35 cm^2) were prepared and installed in MFC reactors which were operated with domestic wastewater. After 1 month operation, a maximum power density of 104 ± 6 mW/m^2 was produced by the MFC with the PVDF cathode (current density 0.38 A/m^2 at R_{ext} = 200 Ω). The power density with the larger reactor was comparable with the previous test with Pt/C based cathode (89 ± 6 mW/m^2) [38].

Membrane stability test. The water pressure resistance of cathodes, examined at PVDF loadings of the DL of 29 ± 2 g/m^2 (15 % w/v), 36 ± 2 g/m^2 (20%) and 40 ± 2 g/m^2 (25%), increased with PVDF loading (Figure 30) [40]. The 25% PVDF membrane reached the maximum water pressure possible in our tests of 2.1 m, indicating good mechanical strength and water containment. Slightly lower water pressure resistances of 1.9 m were obtained with the 20 % PVDF membrane DL and 1.8 ± 0.1 m for the 15% PVDF membrane (Figure 30). The maximum water pressure of the PDMS wipe DL was 0.2 ± 0.05 m. There was noticeable deformation of the membranes at the higher water pressures. Using a plastic mesh support to minimize membrane deformation, all the PVDF membrane DLs reached the maximum testing water pressure of 2.1 m while the PDMS wipe DL still leaked at the same water pressure.

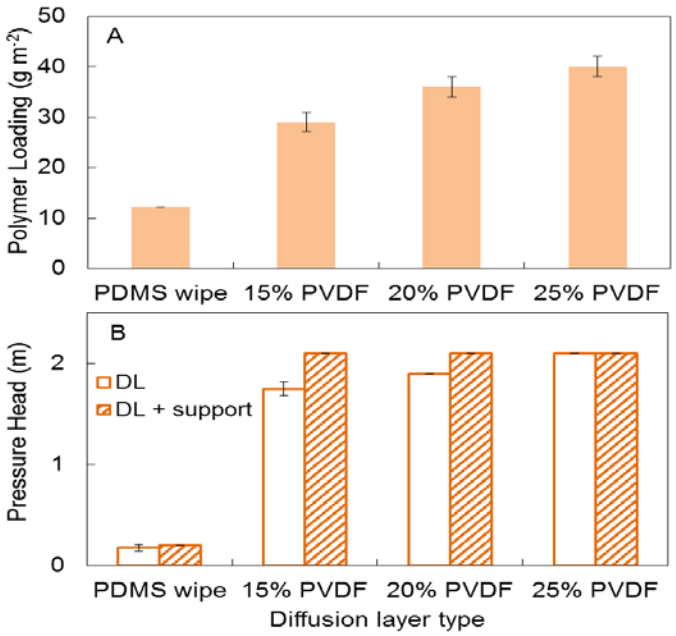

Figure 30. (A) Polymer loadings in PDMS wipe, 15%, 20%, 25% (w/v) PVDF membrane diffusion layers (B) Water pressure resistance of PDMS wipe and PVDF membrane diffusion layers with and without nylon spacer support.

4.4.4. Testing Carbon Free Diffusion Layer AC Cathode

Power generation of MFCs with membrane DLs. The power produced using AC cathodes with the different DLs in MFCs was evaluated based on single cycle polarization data. A maximum power density of 1400 ± 7 mW/m^2 was obtained with the 20% PVDF membrane DL, which was similar to 1450 ± 7 mW/m^2 achieved by the PDMS wipe DL (Figure 31) [40]. The 25% PVDF membrane DL produced a lower maximum power density of 1260 ± 80 mW/m^2, likely due to a denser polymer network in the DL which would reduce oxygen transport to the catalyst. The lowest power density of 1180 ± 120 mW/m^2 was obtained with the 15% PVDF membrane, with a large standard deviation among tests suggesting uneven PVDF content in the DL. The PDMS wipe DL and 20% PVDF membrane had similar cathode potentials (Figure 31), further supporting the similar electrochemical performance of these two types of DLs. Cathodes with 15% and 25% PVDF membrane DLs had the lowest potentials in the current density range of 3 to 7 A/m^2.

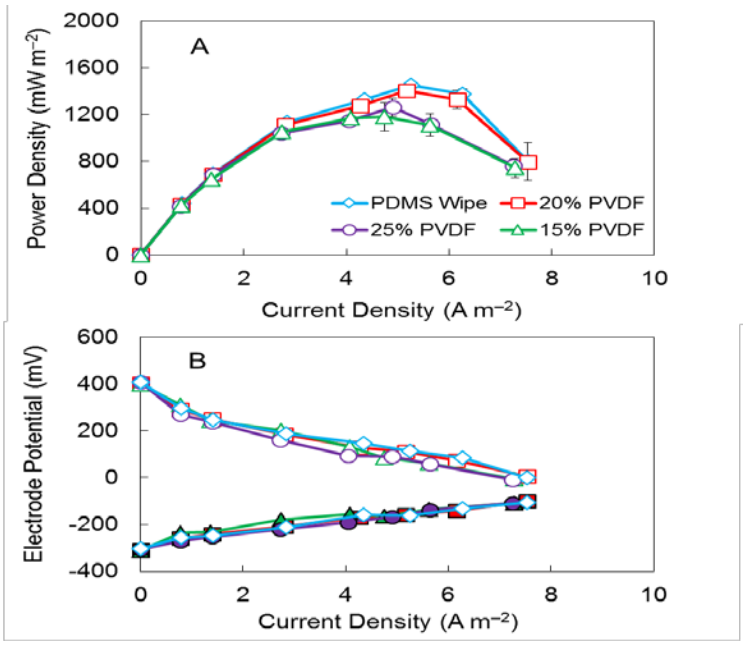

Figure 31. (A) Power density curve for AC cathodes with PDMS wipe, 15%, 20% and 25% (w/v) PVDF membrane diffusion layers (B) Electrode potentials (solid symbols for anode potentials and open symbols for cathode potentials).

4.4.5. Impaired Cathode Performance by Adsorption of Humic Acids

Effect of humic acid concentration on cathode performance. This test performed using same MFC reactors used in previous section. To test the role of humics (organics naturally present in water) on potential cathode fouling, water containing very high concentrations of humic acids were filtered through activated carbon air cathode (100 and 1000 mg/L and compared to a control (0 mg/L added). However, the maximum power density decreased from 1310 ± 60 mW/m^2 to 1130 ± 30 mW/m^2 by filtrating a very high concentration of 1000 mg/L humic solution, which is a 14 % power drop (Figure 32A,B) [45]. The impedance spectra showed that AC cathodes filtered with 1000 mg/L HA solution had a higher resistance of 74 Ω compared to 57 Ω for AC cathodes filtered with 0 mg/L HA solution and 59 Ω for AC cathodes filtered with 100 mg/L HA solution. The increased resistance mainly came from a larger diffusion resistance of 50 Ω for cathodes filtered with 1000 mg/L HA solution compared to just 32 and 34 Ω for cathodes filtered with 0 and 100 mg/L HA solutions (Figure 32C,D) [45].

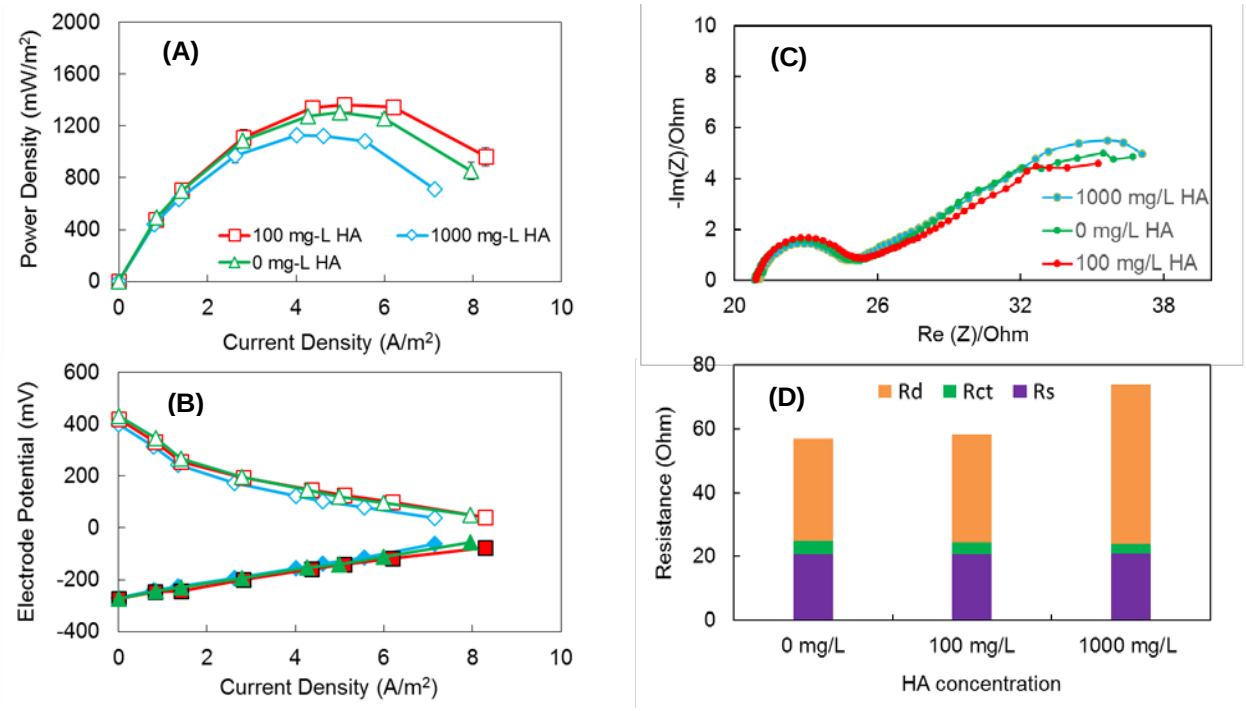

Figure 32. (A) Power density curves for AC cathodes filtrated with 0, 100 and 1000 mg/L HA solutions. (B) Electrode potentials (solid symbols, anode potentials; open symbols, cathode potentials). (C) Nyquist plots of EIS spectra of AC cathodes filtrated with 0, 100 and 1000 mg/L HA solutions at polarized conditions of 0.1 V vs. SHE. (D) Component analysis of internal resistance of the AC cathodes.

Recovery of cathode performance after backwashing. We tested whether cathode performance could be restored by backwashing using distilled water. The power density using the AC cathode filtered with 1000 mg/L HA solution was not improved even after backwashing using deionized water (Figure 33) [45]. This result suggested that an irreversible power decrease could occur by HA adsorption and that chemical cleaning (using acid or base) might be needed to recover the performance of AC cathodes fouled with humic acids.

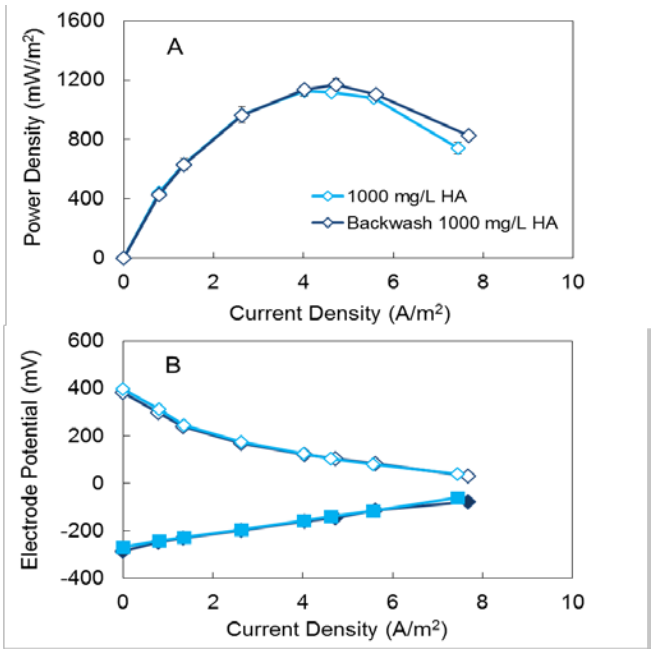

Figure 33. (A) Power density curves for AC cathodes filtrated with 1000 mg/L HA solution with and without backwashing. (B) Electrode potentials (solid symbols, anode potentials; open symbols, cathode potentials).

4.5. Tests Demonstrating 80 % COD Removal with Wastewater

By adding 1 g/L sodium acetate and 50 mM PBS into domestic wastewater (COD concentration of 1100 to 1200 mg/L, conductivity 8.3 ~ 8.7 mS/cm), artificial wastewater was made that had a higher COD and more consistent composition than normal domestic wastewater. This solution was fed into the scalable MFC reactor with modular design (having a multiple anode electrode array and cathode cassettes) for startup and testing of performance. During this process, the COD removal rate was 91 ± 1% in a complete cycle under all external resistances from 1K Ω to 5 Ω. After being changed to non-amended wastewater (COD concentration of 500 to 550 mg/L, conductivity 1.4 ~ 1.7 mS/cm), and operated in fed-batch mode, the MFC had a COD removal of 81 ± 1% over a 20 h cycle, with an external resistance of 5 Ω. Near the end of the cycle, as the COD was very low, the anode potential became more positive and the current production was very low. These tests demonstrated a project goal of >80% COD removal with wastewater.

4.6. Continuous Flow Tests (Task 6)

4.6.1. Test with Different Anode Configurations and Cathode Surface Area

Power generation as a function of theoretical HRT. When the MFCs (S2C and N1C MFCs, Figure 9) were started up at the longest HRT of 8.8 h (200 Ω external resistance), there was inconsistent power produced for the similar reactor configurations (Figure 34) [34]. For example, the S2C upstream MFC produced the most power, but the downstream S2C produced the least power. When operation was switched to shorter HRTs of 4.4 and 2.2 h, there was more consistent power production, with the S2C MFCs consistently producing more power (1.36 mW at 4.4 h, and 1.30 mW at 2.2 h) than the N1C MFCs (1.01 mW at 4.4 h, and 1.22 mW at 2.2 h). The upstream MFCs generally produced greater power than the downstream MFCs, likely due to the higher COD concentrations in the upstream MFCs. After these tests at the two shortest HRTs, the reactors were switched back to the longer 8.8 h HRT, and a fresh wastewater sample was used. This time at this longer HRT, the MFCs produced more consistent power densities based on reactor configuration, with power by the two-cathode MFCs (1.14 mW, S2C) larger than that produced by the single-cathode MFCs (0.85 mW, N1C).

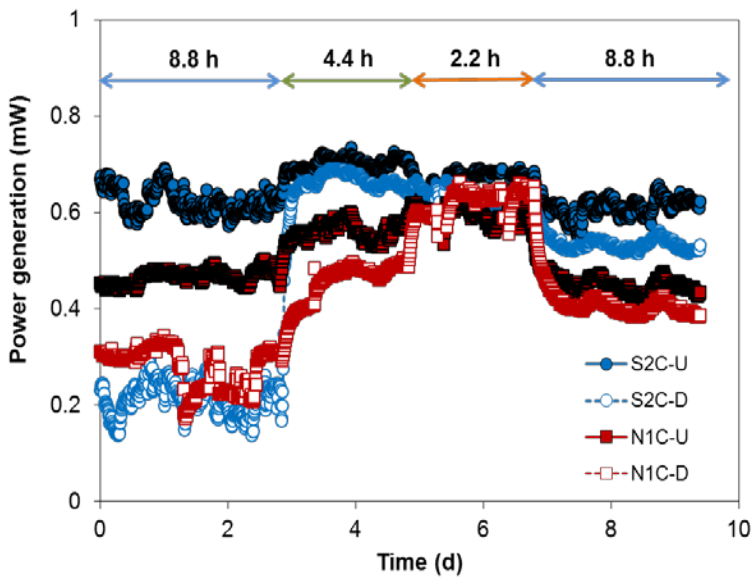

Figure 34. Power generation (external resistor of 200 Ω for each MFC) produced by S2Cs and N1Cs (U = upstream, D = downstream) during continuous operation under different theoretical HRTs (8.8, 4.4 and 2.2 h).

COD removals as a function of HRTs. COD removals with the two-cathode S2C MFCs decreased in proportion to HRTs, with removals of 64.8 ± 1.7 % at an HRT of 8.8 h, decreasing to 48.3 ± 1.0 % at 4.4 h, and 32.8 ± 1.9 % at 2.2 h (Figure 35) [34]. It was expected that the S2C MFC would have greater COD removal than the N1C MFC due to higher current densities [46] and greater cathode surface area per volume of reactor (which would allow more leakage of oxygen into the reactor) at the same set HRT. However, the COD removals with the single-cathode N1C MFC were higher than those of the S2C MFCs, with removals of 69.0 ± 0.4 % at 8.8 h, 54.2 ± 2.3 % at 4.4 h, and 40.7 ± 2.7% at 2.2 h. This is 6.4 to 24.4 % greater COD removal for the single cathode MFCs than the two-cathode MFCs at each of these set HRTs.

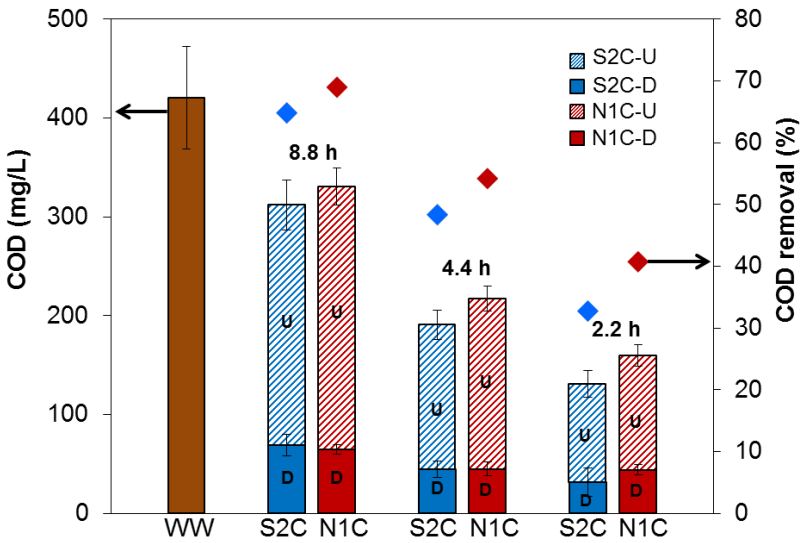

Figure 35. COD concentrations in the influent and effluent of the S2Cs and N1Cs (U = upstream, D = downstream) and percentage of COD removal at theoretical HRTs of 8.8, 4.4 and 2.2 h.

Effect of reactor configuration on HRTs in continuous flow mode MFCs. The unexpected results showing better COD removals for single cathode MFCs compared to the two-cathode suggested that configuration of the MFCs may have produced HRTs different than the theoretical ones (calculated from reactor empty bed volume and flow rate). Therefore, salt tracer tests were conducted to measure the actual residence time of solutes through the two types (S2C and N1C) of reactors. The results showed that the actual HRTs of S2C reactors were less than or equal to the theoretical HRTs, with actual:theoretical HRTs of 7.4:8.8 h, 3.8:4.4 h, and 2.2:2.2 h. A slight reduction in HRT due to short circuiting in these MFCs was likely a result of the reactor volume occupied by the brushes as there may not have been advective flow through the brushes. However, the HRTs of the two N1C reactors were longer than those measured for the S2C reactors by 39 % (7.4:10.3 h for S2C:N1C), 37 % (3.8:5.2 h), and 32 % (2.2:2.9 h) [34]. Thus, the greater removal by the N1C reactors was likely due to the much longer HRTs produced using this configuration compared to that obtained with the S2C configuration.

A comparison of the COD removals on the basis of the measured HRTs shows that there was generally good agreement with the observed COD removals and measured HRTs despite differences in the two reactor configurations (Figure 36) [34]. The COD removals for both types of reactors show good agreement with measured HRTs based on a non-linear regression. However, there was little agreement between the two configurations in terms of COD removal on the basis of the theoretical HRTs, with slightly better COD removals indicated to occur for the N1C MFC than the S2C MFC. These results suggest that the COD removal was more a function of the HRTs, and thus how the HRT was altered by the use of the two different brush configurations, rather other factors such as cathode surface area.

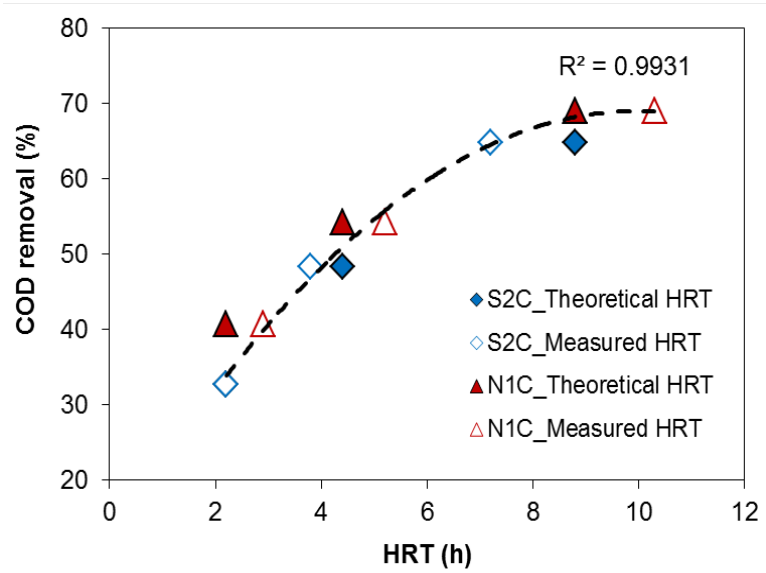

Figure 36. COD removals (%) by S2C and N1C MFCs based on the theoretical and measured HRTs. The regression line (black dashed) was drawn to fit the COD removals based on the measured HRTs of both MFC configurations.

4.6.2. Test with Stacked MFC Reactor (1. 5 L)

Power generation. After 1 month of operation in fed-batch mode, and continuous mode with various HRTs and external resistances, the MFC (Figure 4) was switched to continuous flow mode and acclimated at a single HRT of 8 h. Each brush in the anode array was connected to the cathode with a separate wire and resistor (30 Ω) to allow measurement of the voltage produced by each anode. A maximum power density of 250 ± 20 mW/m^2 was obtained using 60 Ω external resistors for each anode (Figure 37) [35]. Polarization data for the individual anodes showed a trend of increased power overshoot for the anodes near the reactor effluent (anodes 4, 5 and 6), where the COD concentration would be low and approaching the effluent concentration, compared to the anodes near the influent (anodes 1, 2 and 3), which would have been exposed to higher COD concentrations. Power overshoot can be seen in the polarization curves by first, a rapid decrease in voltage with increasing current, followed by a doubling back of the power curve at the highest currents as the external resistance is further reduced. Voltage overshoot was more apparent for the B compartment, which had a lower power density, than the A compartment. These results show the spacers are working well in the stacked module.

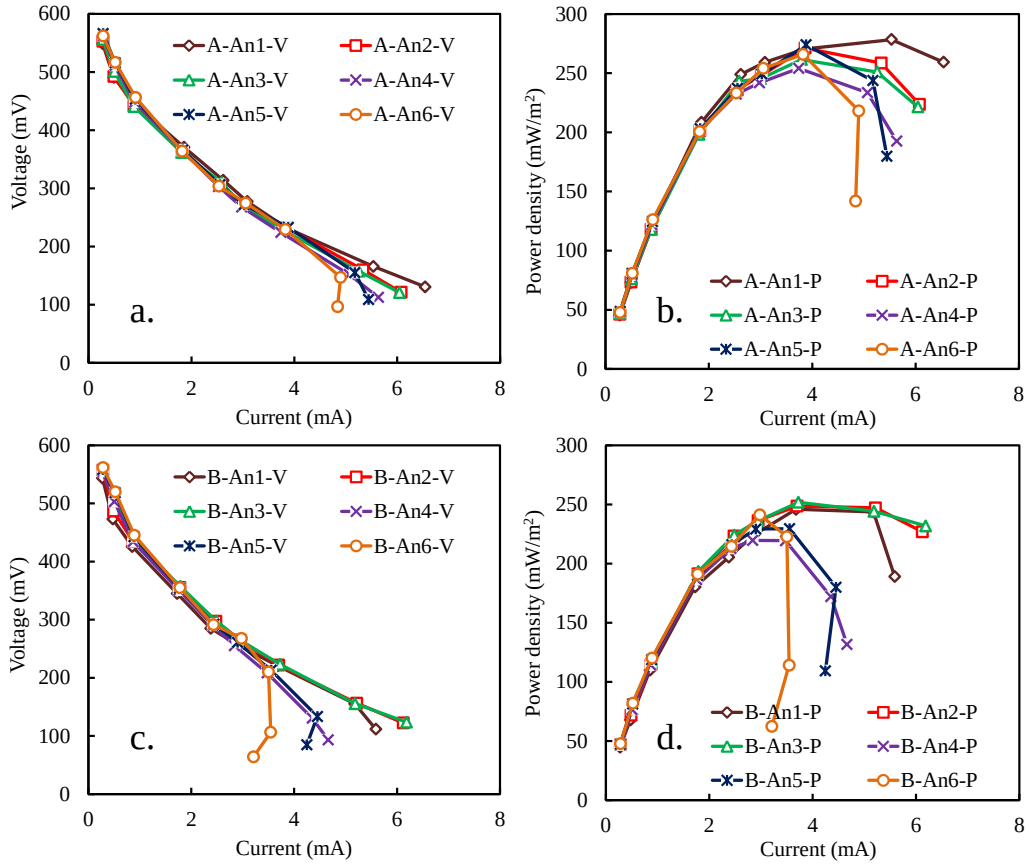

Figure 37. The polarization curve of the anode brushes of the MFC stack in continuous mode (HRT = 8 h) by using original domestic wastewater. The current data are the current generated from each anode; the power density were calculated based on the total cathode surface area (200 cm^2) divided by the number of anodes (6).

COD removal under different current densities. There were no obvious trends in the influent total or soluble COD concentrations over time, despite the use of two separate wastewater samples for these tests (one wastewater sample for days 1-4, and another sample for day 5-7) and sample storage over this period of time (Figure 38a and 38b) [35]. The average influent CODs were 480 ± 25 mg/L for total COD and 225 ± 12 mg/L for SCOD, with the same overall removals in the two anode compartments of 57 ± 5 % for total COD and 48 ± 7 % for SCOD (Figure 38c).

A reduction in the circuit resistance increased current density and also increased the rate of COD removal under continuous flow conditions (Figure 38d) [35]. The COD removal rate under open circuit conditions, supported primarily by oxygen leakage through the cathode [46], was 0.42 ± 0.01 kg-COD/d m^3. With separate external resistances ranging from 2000 Ω (0.08 ± 0.002 A/m^2) to 120 Ω (0.75 ± 0.03 A/m^2), the COD removal rate increased by 67 % to 0.70 ± 0.04 kg-COD/d m^3.

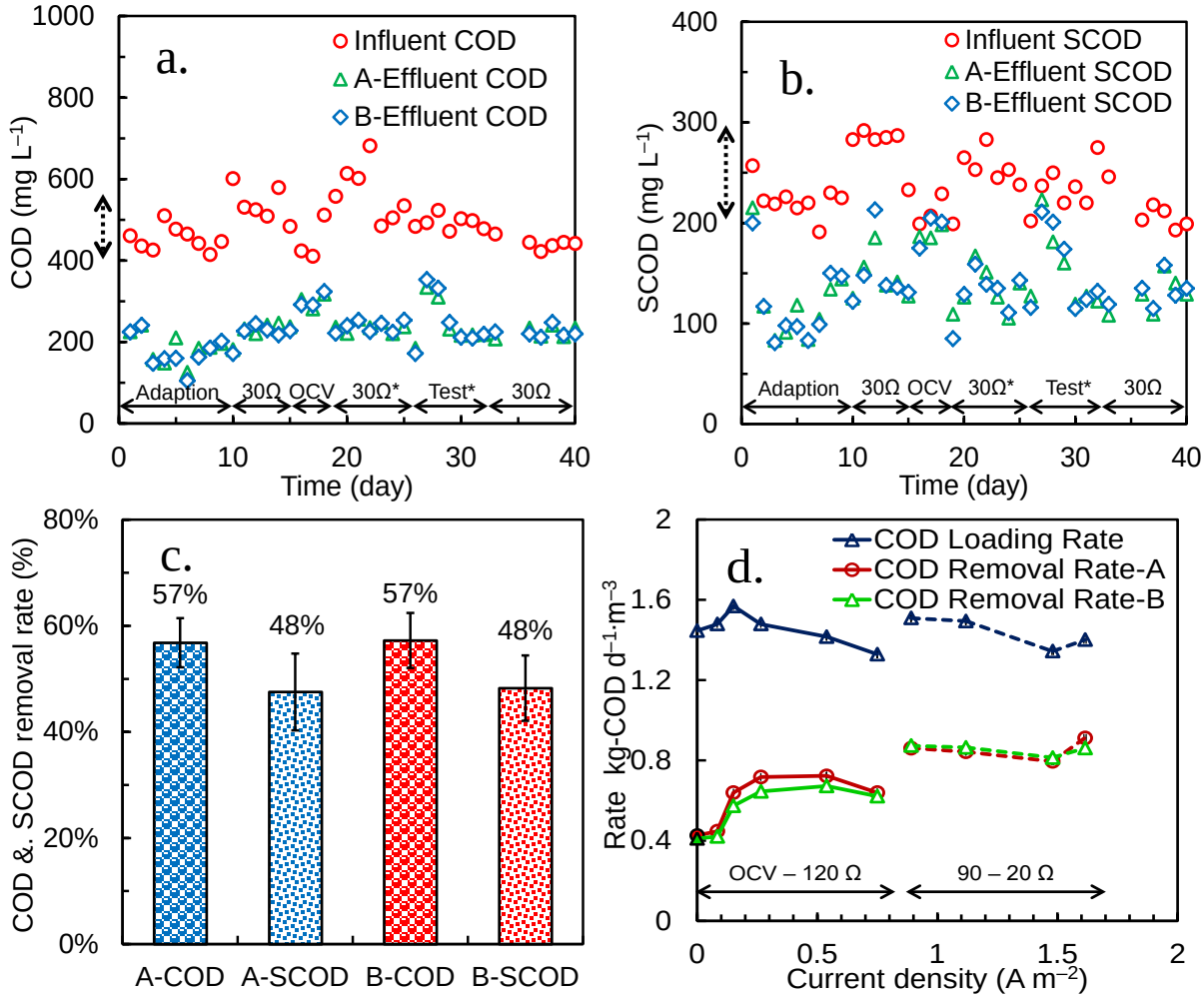

Figure 38. (a) Influent and effluent total COD and (b) SCOD for MFCs operated under continuous flow conditions using raw wastewater. Arrows above the x axis indicate data taken under different conditions: during reactor acclimation; operation at a fixed resistance (30 Ω); during polarization tests (Test*); or under open circuit conditions (OCV). (c) Average removals (error bars ± SD) of the two sides (A or B) in terms of COD or sCOD. (d) COD removal rate and current density measured with under OCV (no current) conditions, or with larger (OCV; 2000, 1000, 500, 200 and 120 Ω) or smaller (90, 60, 30, or 20 Ω) resistances. Two different wastewater samples were used, as shown by the solid or dashed lines.

4.6.3. Test with a Larger, multiple-module MFC (5.7 L)

COD removal. The MFC reactor shown in Figure 5 was tested in this section. During startup (Phase 2), total COD removal with parallel flow operation was 45 ± 4%, with 33 ± 3% SCOD removal (Figure 39) [36]. In the first series of tests following startup (Phase 3), with the flow still parallel through the modules, but the direction of the flow alternated daily (A-P), COD removals were 52 ± 5% for total COD and 46 ± 5% for SCOD. When the flow was switched to an alternating direction with a serial flow path (A-S), there was no significant change in total COD or SCOD removal ($p>0.05$, Student's t-test), with 52 ± 6% COD and 40 ± 9% SCOD removals. As the wastewater was treated at the same rate (i.e. the flow into four modules in parallel operation was the same as the total flow applied to the entry module for serial flow), this showed that there was

no impact in these tests on the percent of COD removal by parallel or serial flow operation, when the flow was alternately switched between exit and entrance points.

The flow was then fixed to always enter the same module. In these fixed direction tests, with parallel flow through the modules (F-P), the percent of COD removal was slightly higher (57 ± 15%), with a similar SCOD removal (43 ± 21%) compared to the previous tests. During the final series of tests using a fixed flow direction, with serial flow through all four anode modules (F-S), COD removal was only slightly reduced to 51 ± 15%, with a lower SCOD removal of 35 ± 10%.

These results for the different operational test conditions showed that there was no significant difference in total COD removal for the different flow directions or serial or parallel flow directions ($p>0.05$, Student's t-test). For SCOD, the only significant difference among these operational conditions was for the case of parallel and alternating flow conditions (A-P), compared to serial and fixed (F-S) operational conditions ($p=0.0024$). However, the lack of changes for all other comparisons on COD or SCOD suggested that this difference may have been due more to changes in wastewater characteristics than operational conditions. The wastewater COD concentrations were not significantly different for the two tests with alternating flow (A-P and A-S), but the influent CODs in the last series of tests with fixed flow (F-P and F-S) were significantly different from the first series of tests and from each other. For example, for the COD of Phase 3 was 480 ± 70 mg/L but the averaged COD of Phase 6 was only 240 ± 80 mg/L (Table 2). These results show that although the COD concentrations changed, the percentage removals of MFC reactor were relatively constant for all four operational modes.

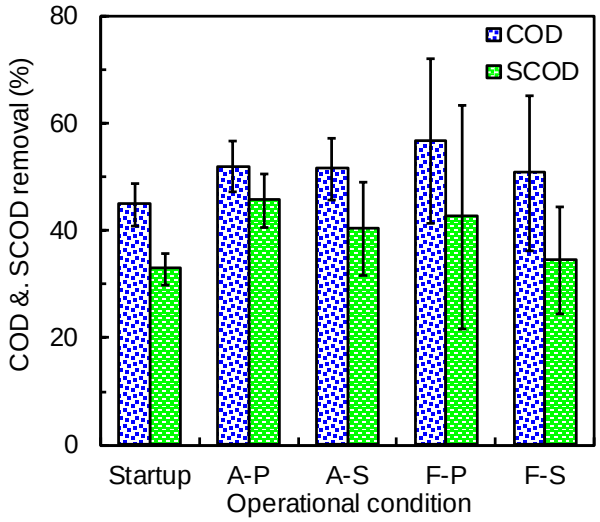

Figure 39. The COD and SCOD removal with different flow mode. (In-COD/SCOD: the influent COD/SCOD; Eff-COD/SCOD: the effluent COD/SCOD. Start: startup period; S-P: flow direction switch parallel flow mode; S-S: flow direction switch serial flow mode, N-P: parallel flow mode with fixed flow direction, N-S: serial flow mode with fixed flow direction).

Alternating flow, parallel direction (A-P), Phase 3. While COD removals were not appreciably affected by reactor operational mode, power production was substantially influenced by reactor operational conditions and wastewater strength. The impact of the operational mode was observed by obtaining polarization data following acclimation of the reactor to the different set conditions. Following the startup period, the MFC was operated in parallel flow mode with an alternating flow direction (A-P, Phase 3, Table 1) every 2 days. For these tests and all subsequent

tests, the MFCs were operated at fixed external resistance of 20 Ω for maximum power output, which was the resistance that produced the maximum power density in the fed-batch polarization tests following Phase 2. At the end of Phase 3 (A-P), anodes 2 and 3 with two cathodes produced an average power density of 236 ± 11 mW/m^2, while anodes 1 and 4 (single cathode) produced 255 ± 14 mW/m^2. Based on volumetric power, the anode modules connected to two cathodes (anode 2 and 3) produced 6.2 ± 0.2 W/m^3, which was 1.9 times that produced by the anodes connected to a single cathode (3.3 ± 0.2 W/m^3, anodes 1 and 4). In this period, the total volumetric power density for whole reactor in fed-batch tests was 4.8 W/m^3 (Figure 40) [36], which was very similar to that obtained during the startup period. The average volumetric power density under continuous flow was 4.2 ± 0.5 W/m^3.

Alternating flow, serial direction (A-S), Phase 4. The MFC flow direction was next changed to serial flow mode. The power densities following serial flow operation in Phase 4 were only slightly lower than those obtained in parallel flow operation (Phase 3), suggesting comparable overall performance under parallel or serial flow with alternating flow direction. The average power densities for the anodes with two cathodes were 216 ± 22 mW/m^2, compared to 235 ± 50 mW/m^2 for anodes with single cathodes. On a volumetric power basis, anodes 2 and 3 produced 5.7 ± 0.5 W/m^3, compared to 3.1 ± 0.7 W/m^3 for anodes 1 and 4, with an overall fed-batch volumetric power density of 4.2 W/m^3 (Figure 40). Under continuous flow conditions, the average volumetric power density was 3.9 ± 0.5 W/m^3. The key reason for the slightly lower power densities in Phase 4, compared to Phase 3, was likely reduced performance of the cathodes over time, and not serial versus parallel flow direction. The COD concentration was not thought to be a factor as the influent CODs during these tests were not significantly different for the two operational periods (Table 2).

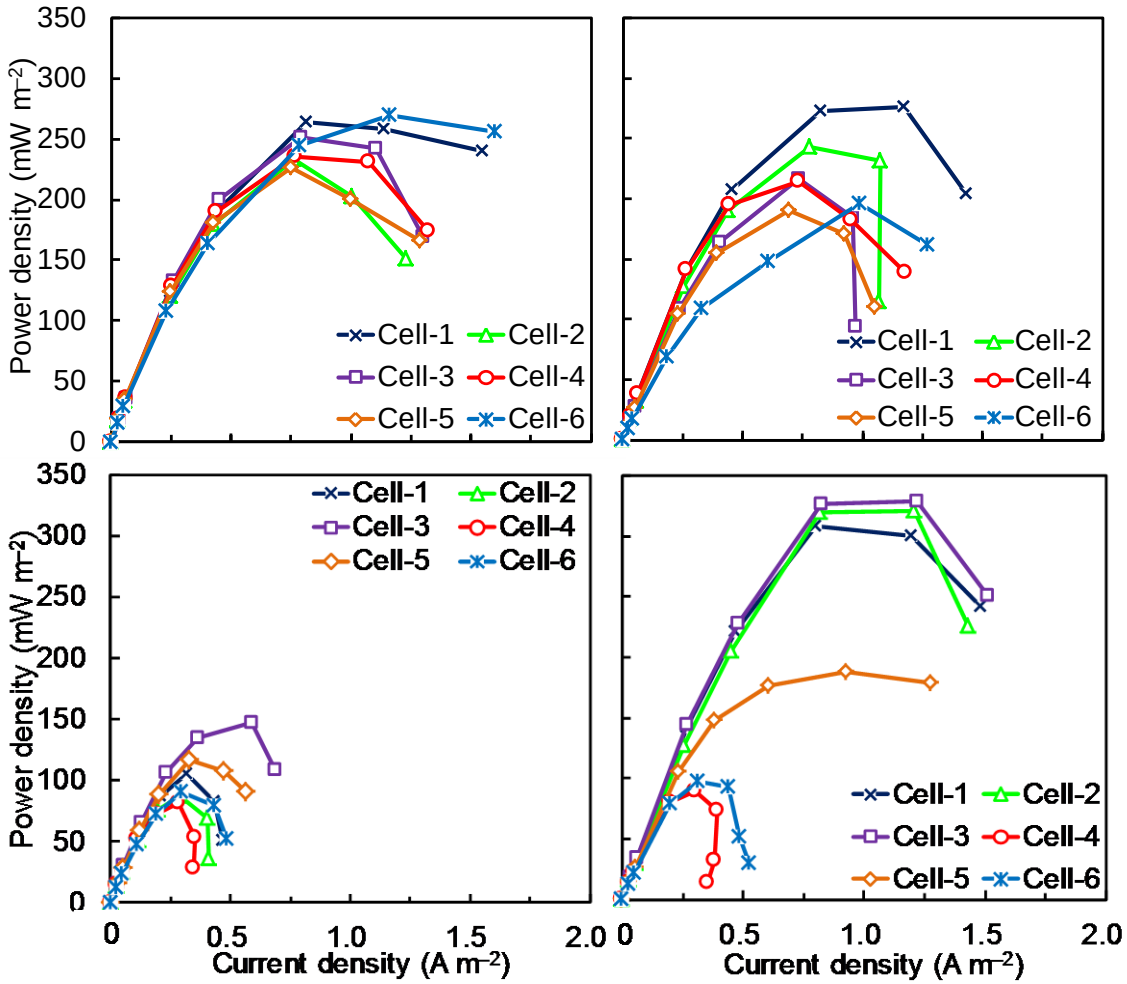

Figure 40. Power density curves for the power generation of multi-module MFC following operation under various continuous flow modes: (a) alternating direction, parallel flow, A-P, Phase 3; (b) alternating direction, serial flow, A-S, Phase 4; (c) fixed direction, parallel flow, F-P, Phase 5b; (d) fixed direction, serial flow, F-S, Phase 6 (All tests under fed-batch conditions).

Fixed flow, parallel direction (F-P), Phase 5. The reactor was next operated in a fixed, parallel flow direction. The performance of the reactor in this operational mode was divided into two periods due to a significant decrease in average COD concentration from 550 ± 100 mg/L (Phase 5a) to 350 ± 95 mg/L (Phase 5b), with an average of 430 ± 140 mg/L over the complete Phase 5 compared to 540 ± 85 mg/L in the previous tests (Table 2). From Phase 5a, the power output gradually declined, with an overall average power density under continuous flow for this period of only 1.1 ± 0.6 W/m^3. Possible reasons for this lower power density compared to previous tests include: cathode degradation; a lower influent COD which would reduce power production; or the operational flow direction (fixed versus alternating flow). Of these, cathode degradation was suspected to be the main reason for the decline in power, as the COD concentration was similar Phase 5a compared to the previous days of operation. Therefore, new cathodes were installed for data collected in Phase 5b. However, after cathode replacement the COD concentrations in the wastewater sharply decreased, as did the power production, making it difficult to separate the impact of these different factors on reactor performance (data not shown).

To try to account for the impact of the change in COD, polarization tests were conducted following Phase 5b using a wastewater sample with a COD above 400 mg/L, which was thought to be sufficiently high to avoid differences in power generation due to low COD concentration of the wastewater. In these fed-batch polarization tests, the overall volumetric power density was only 2.0 W/m^3. The anodes combined with two cathodes generated an average power density of 105 ± 25 mW/m^2 (2.8 ± 0.2 W/m^3), while the anodes connected to only one cathode produced 97 ± 10 mW/m^2 (1.3 ± 0.1 W/m^3) (Figure 40) [36]. Therefore, the use of a higher COD concentration could not immediately restore performance to its previous normal level (4.8 W/m^3 in A-P; 4.2 W/m^3 in A-S). The poorer performance could have been due to fixed flow operation compared to that under alternating flow conditions, or a combination of the fixed flow direction and parallel flow operation. In Phase 5b, the low strength influent wastewater was distributed to four parallel anode modules. Therefore, all the modules were acclimated with low COD. The sustained operation of the reactor under low COD conditions has impaired the performance of the anodes in these short-term tests with the higher COD concentration wastewater.

Fixed flow, serial direction (F-S), Phase 6. For the final period of operation (Phase 6), the MFC was operated with a fixed flow direction, but with flow through the modules in series. The average influent COD concentration during this period was only 240 ± 80 mg/L, which was likely the reason for the low overall power output under continuous flow conditions of 0.45 ± 0.10 W/m^3 (Figure 40) [36]. Polarization tests following this F-S mode operation were conducted using wastewater that had a COD above 400 mg/L, in order to better compare reactor performance to previous tests. With this higher COD concentration, the power output in continuous flow mode (20 Ω) reached 3.3 ± 0.4 W/m^3, which was close to maximum power densities obtained in previous tests in Phases 3 (4.2 ± 0.5 W/m^3) and 4 (3.9 ± 0.5 W/m^3). This confirmed that the low power density during the F-S operational period was primarily due to the low COD concentration.

In Phase 6, the influent COD concentration was very low, and only slightly higher than the ~150-200 mg/L previously shown to greatly reduce current generation with a filtered domestic wastewater fed single anode reactor in batch mode tests [46], and ~250 mg/L that reduced current production and increase internal resistance by a brush anodes multi-electrode MFCs [47]. The upstream modules were acclimated to fresh influent wastewater with a higher COD, but the downstream anodes were exposed to much lower CODs. As a result of these different conditions, the first two anode modules 1 and 2 produced power densities comparable to that obtained in Phase 2–4. However, the two downstream anode modules 3 and 4 had much lower maximum power densities in Phase 6. This degradation of downstream anode performance was also observed under continuous flow conditions.

Overall assessment of operational conditions on power generation. Power generation by MFCs has usually been considered to be limited by the cathode, based on tests using high concentrations of acetate, industrial wastewaters or domestic wastewater [48, 49]. However, the results obtained in this study demonstrate that the anode can be the main factor in MFC performance at low COD concentrations. When the anodes were connected to two cathodes, and the COD concentration of the wastewater entering the MFCs was relatively high (~500 mg/L), power production was higher (6.0 ± 0.5 W/m^3 for anode 2, and 5.8 ± 0.5 W/m^3 for anode 3) than power densities obtained with anodes connected to single cathodes (3.6 ± 0.2 W/m^3 for anode 1 and 3.2 ± 0.5 W/m^3 for anode 4). These results are consistent with previous findings that increasing the cathode area per volume of reactor can increase power per area of anode and volumetric power density [21, 34, 48, 50, 51]. However, when the influent COD concentrations became much lower, as they did in the later fixed flow tests (average influent CODs of 350 and 240 mg/L), anodes with

two cathodes did not consistently produce more power than anodes connected to a single cathode. This signaled a shift from cathode-limited performance to anode-limited performance. To avoid anode-limited performance, and to maintain higher power densities, the MFC should be operated with higher influent and effluent CODs so that the electrode is not operated for extended periods with wastewater at a low COD. Water quality needed for discharge in terms of a much lower COD can be obtained using a secondary process, such as an anaerobic fluidized bed membrane bioreactor, as previously demonstrated [42].

Low COD concentrations in MFCs did not impact the percentage of COD removed in the reactor, but they did affect reactor stability and performance in terms of power production. The percentage of COD removed was relatively unaffected by the different operational conditions (serial or parallel, alternating or fixed flow) with no clear pattern associated with these conditions. With alternating flow, either in serial or parallel flow conditions, power production was very stable with the high influent COD concentrations, suggesting little difference due to serial or parallel flow conditions. The impact of fixed flow operation compared to alternating flow, however, was inconclusive due to the low COD concentrations in the fixed flow tests. Initial tests with fixed flow at high COD concentrations showed a decrease in performance even with high COD, due to deterioration of cathode performance. However, a change in the COD from high to low concentrations did not permit direct comparisons of alternating and fixed flow conditions based only on power. Electrochemical tests using EIS showed an increase in internal resistance during operation in fixed flow conditions with serial flow, but CV results showed the opposite trend. Continued operation of the MFC under low COD concentrations therefore precluded determination of the impact of the operational condition on performance.

For the practical operation of pilot multi-module MFC stack, parallel flow with alternating flow direction may be the best choice to avoid the lower power output in some unit resulted from the imbalance regional COD distribution between modules. Matching with one anode array with an additional cathode layer will also be useful for improving anode performance and increasing overall power generation. The outer anode banks (first and last) could likely be constrained to always having a single cathode, but as additional anode banks are added, for example having 100 anode arrays as opposed to 4 here, the impact of these outer anode arrays on overall power production would be relatively limited.

4.6.4. Black Water Test using MFCs

Current generation under different external resistances. After operation for 15 days without reactor and electrode cleaning (Figure 41) [52], both MFCs (SMFC-U and SMFC-D) produced similar current (SMFC-U: 2.4 ± 0.2 mA; SMFC-D: 2.1 ± 0.1 mA) with Rext= 50 Ω until day 7. After switching the external resistance to 5 Ω, the current increased to 7.6 mA for SMFC-U and 6.8 mA for SMFC-D then decreased to 5.0 mA (SMFC-U) and 4.9 mA (SMFC-D) over the next 14 days of operation. The two MFCs were then switched back to the lower resistance. Lower current generation was observed for both MFCs after switching back to Rext= 50 Ω, suggesting fouling of the cathode. Energy production (kWh/m3) was similar using the different external resistances, with 0.04 ± 0.01 kWh/m3 produced until day 8, and 0.03 kWh/m3 produced between day 22 and 27.

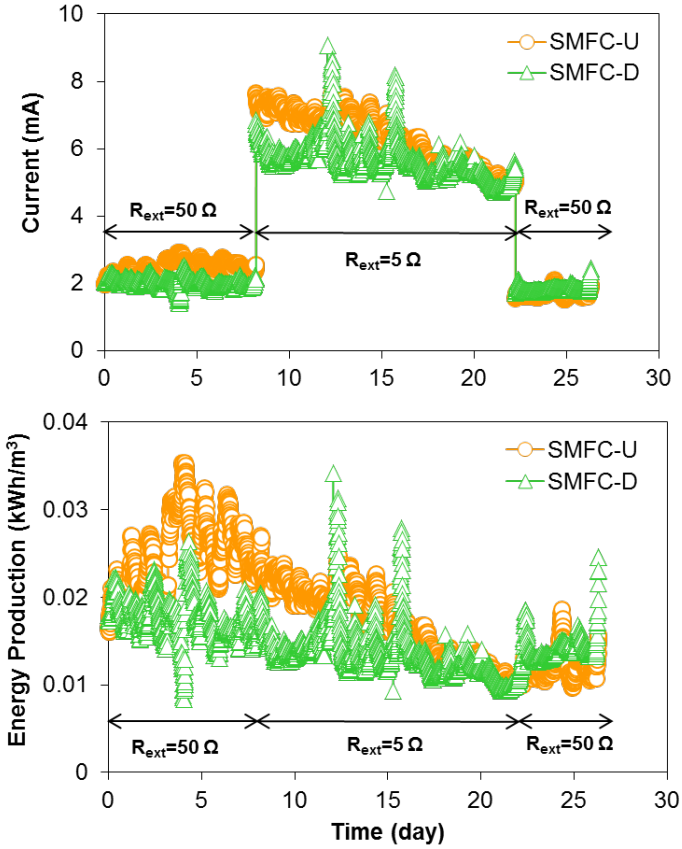

Figure 41. Current (mA) and energy production (kWh/m^3) of swine wastewater-fed MFCs (SMFCs) under different external resistances during 27 days operation.

COD removal under different external resistances. Effluent COD of the SMFC-D was 6020 ± 150 mg/L (19 ± 6 % overall removal) at R_{ext} = 50 Ω, with a significantly lower effluent COD ($p<0.05$, Student *t*-test) was at R_{ext} = 5 Ω (576 ± 170 mg/L, 22 ± 6% removal). This result indicated that a lower external resistance could significantly impact COD removal of the MFCs. A higher COD removal of the SMFCs at R_{ext} = 5 Ω also improved the CE, with 17 ± 7 % for the SMFC-U reactor and 23 ± 7 % for SMFC-D reactor (Figure 42) [52].

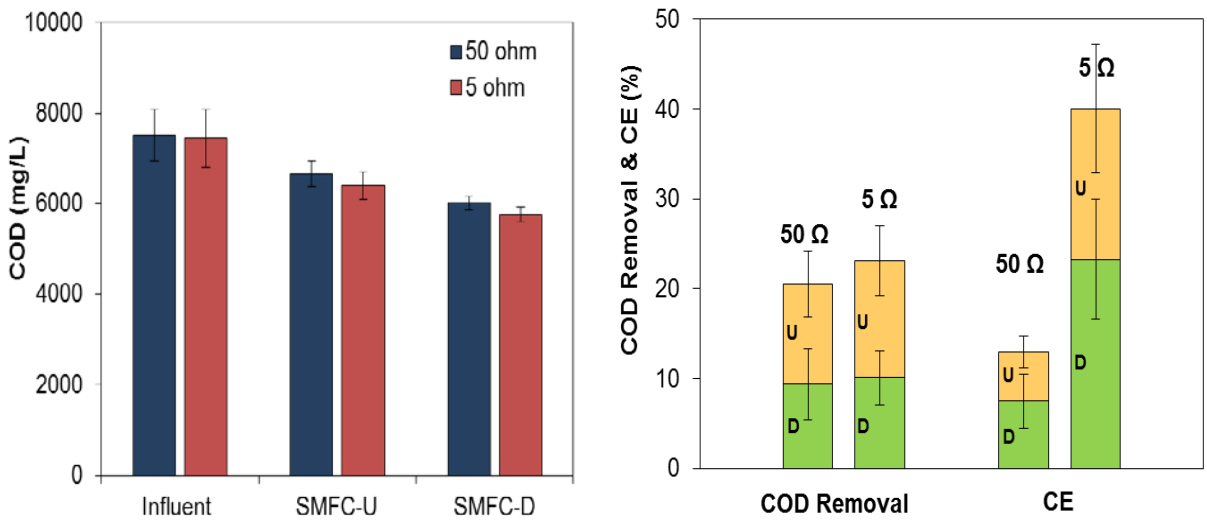

Figure 42. Influent and effluent COD (left side), COD removal and Coulombic efficiencies (right side) of swine wastewater-fed MFCs (SMFCs) under different external resistances (U: upstream; D: downstream).

COD removal rates. Assuming a first-order reaction with respect to COD removal by reaction time, COD removal rate for the black wastewater treatment using MFC was quite low (0.3–0.4 d^{-1}) compared with the removal rate constant obtained for gray wastewater treatment (4.0 d^{-1}). It was therefore concluded that for MFC operation, combining black and gray water will provide better MFC performance on the basis of overall COD removal rate and short HRTs for wastewater treatment The highly concentrated black water might would likely result in higher maintenance demands due to the high solids concentration and the high wastewater COD, with only a small percentage of the COD be converted to electrical current under these conditions.

4.7. Engineering and Economic Analysis (Task 7)

The original scope of Task 7 included engineering design and economic analysis of the MFC. The scope was expanded to include a life cycle assessment (LCA) which was conducted in collaboration with SERDP project ER-2239. Section 4.7.1 presents results of the engineering design specifically focused on a pilot-scale system that can be demonstrated under ESTCP. Section 4.7.2 presents the LCA approach for MFC systems at different FOB scales (company, battalion, brigade, and division) as well as comparisons to conventional systems. A complete report on the LCA will be included in the final report for ER-2239.

4.7.1. Engineering Design of a Pilot-Scale MFC

Objectives. The main objective of this task was to develop an engineering design for a pilot-scale MFC that can be demonstrated under ESTCP. Additional objectives included evaluation of capital and operating cost drivers for the process. Finally, comparison of the MFC process to conventional wastewater treatment processes using the LCA methodology was an objective.

To achieve these objectives, the following subtasks were conducted and are described in the following sections:

- Develop the design concept for the MFC.

- Develop a design basis for the MFC concept.
- Prepare engineering drawings and specifications suitable for pilot-scale system fabrication by a design-build contractor.
- Identify cost drivers for the MFC.
- Compare conventional and MFC wastewater treatment platforms for different scale FOBs using LCA methodology.

Engineering design concept. The conceptual design for the pilot-scale MFC was based on modular reactor concepts described in Sections 3 and 6 and is illustrated in Figure 43. This conceptual design has several attributes that are intended to promote efficient COD removal, power recovery, operational flexibility, and ease of operations and maintenance. Specific mechanical attributes include:

- Plug flow to take advantage of first-order kinetics and minimize required hydraulic residence time.
- Baffled flow path to promote plug flow and minimize short circuiting.
- Modular construction to promote scalability.
- Brush anodes that are easily and cost-effectively mass produced.
- Air cathode design that facilitate free air convection and diffusion in the spacer.
- Closely spaced and removable cathode and anode modules to maximize cathode area per unit volume and simultaneously facilitate maintenance and management of accumulated solids.

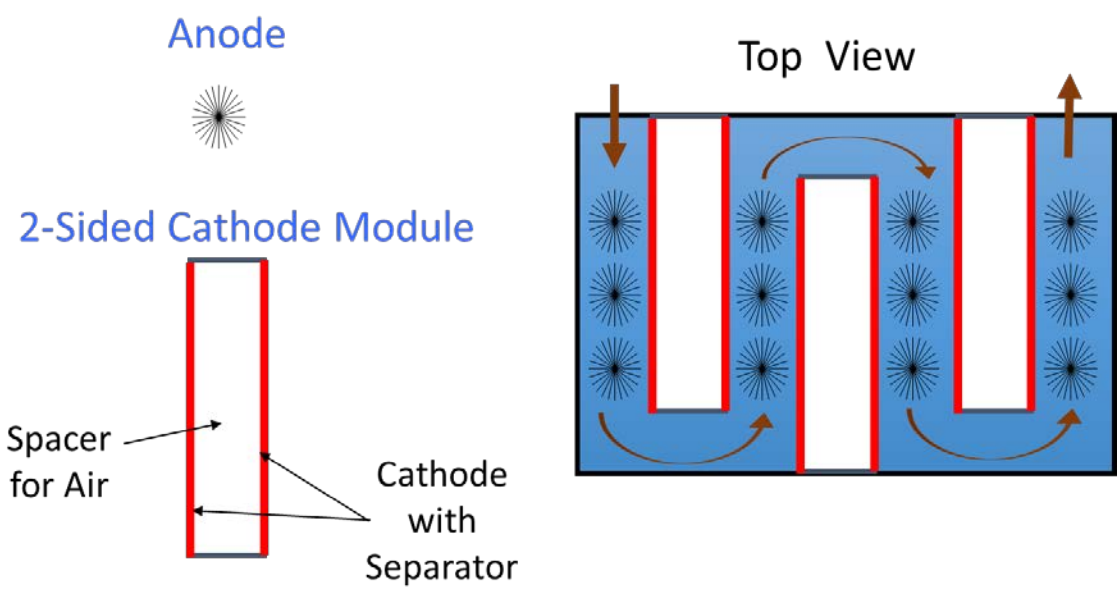

Figure 43. Conceptual design of the pilot-scale MFC. The number of anodes and cathode modules are for concept illustration only and do not reflect the actual pilot-scale MFC design.

The MFC is capable of reducing COD to about 100 to 200 mg/L while producing power as described previously. Therefore, the MFC is not considered to be a standalone wastewater treatment process and requires downstream polishing. In addition, upstream processes are required to prevent large solids and grit from entering the MFC. An overall process flow diagram (PFD) is

shown in Figure 44. This PFD illustrates one of several possible treatment trains for wastewater treatment and reuse. In this example, wastewater is pumped through a screen to remove solids larger 6.4 mm (0.25 in). Variations in screened wastewater composition and shock loads are attenuated in an equalization tank with a hydraulic residence time of about 4 to 8 hours. The screened and equalized wastewater then flows to the MFC where COD is partially reduced and power is generated. The effluent is then treated using a granular activated carbon biofilter (GAC-BF). This system (Figure 45), developed by Construction Engineering Research Laboratory (CERL) at the US Army Engineer Research and Development Center (ERDC). The GAC-BF process removes addition COD and employs intermittent operation, whereby water is passed through the GAC media in an up-flow manner for about 6 h, followed by a 6-h bio-regeneration phase in which the filter is drained. The adsorption capacity of the media is recovered during the bio-regeneration phase as microbes consume the adsorbed organic contaminants in the presence of oxygen that flows into the filter bed during liquid draining. This approach promotes aerobic treatment of residual COD along with removal of suspended solids without the high energy requirements of conventional aeration. Thus, it is a good complementary technology to be used in conjunction with MFC where the MFC potentially generates enough power to operate the GAC-BAF. Other technologies such as the anaerobic fluidized membrane biofilm reactor (AFMBR) can also be considered. Downstream of the GAC-BF process additional filtration (e.g., multimedia or ultrafiltration) can be conducted as well as disinfection. The treated water will contain nutrients such as ammonia and phosphorus, and can be used for a variety of purposes including dust suppression, irrigation and fertilization, vehicle washing, etc. Additional unit processes for nutrient removal could optionally be added if warranted.

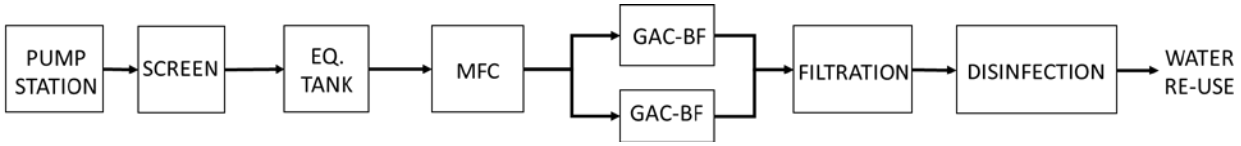

Figure 44. Process flow diagram concept of a process train for wastewater treatment and reuse based on the MFC. Eq. tank: equalization tank. GAC-BF: granular activated carbon biological filtration.

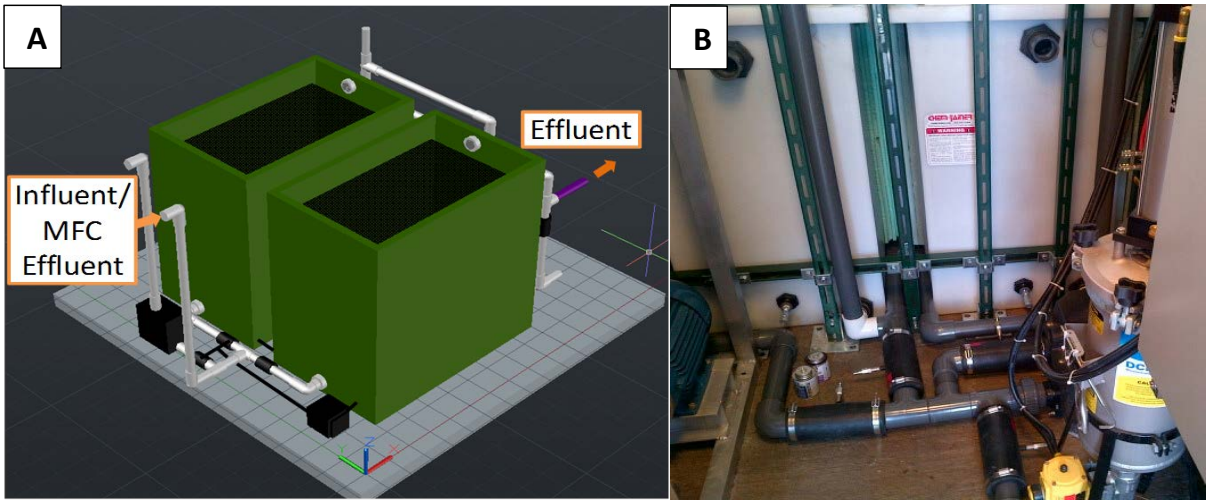

Figure 45. GAC-BAF system developed by ERDC-CERL that can be used to polish MFC effluent. A) isometric design illustrating two GAC vessels. B) pilot-scale system.

Engineering design basis. The design basis was developed for a system capable of treating domestic wastewater. Development of the design basis involved evaluation of expected wastewater composition and flow rates; anticipated treatment requirements including applicable regulations; reaction rates and removal efficiencies; electrical power production and associated voltage and currents; and production rates of residuals (e.g., sludge).

Anticipated wastewater flow rates and composition. Anticipated wastewater flow rates for a variety of FOB scales has previously been estimated [53]. These estimates were used to specify the wastewater flow design basis and results are summarized in Table 3.

Table 3. Wastewater flow rates for different scale FOBs.

FOB	Number of personnel		Flow rate (gal/day)		
	Typical [53]	Assumed Basis	Gray Water	Black Water	Total*
Company	70 to 250	150	4,463	788	5,250
Battalion	300 to 1,000	600	17,850	3,150	21,000
Brigade	2,000 to 5,000	6,000	178,500	31,500	210,000
Division	10,000 to 20,000	20,000	595,000	105,000	700,000

*Assumes 15% of combined wastewater is black water and average wastewater production rate is 35 gal/person/day [53].

Development of estimates for wastewater composition is challenging and varies widely. Anticipated wastewater composition with respect to COD, BOD_5, and TSS was evaluated using a variety of data sources. These sources included engineering handbooks, USEPA publications,

journal articles, theses, and engineering reports. The results are summarized in Table 4 and design basis is presented in Table 5. This basis was used for scale-up and the economic evaluations. In comparison, wastewater composition for Ft. Riley in Kansas are presented in Figure 46. The wastewater composition at Ft. Riley is more dilute than the wastewater composition presented in Table 5. The MFC design presented in this report will be demonstrated under ESTCP at an installation in the US. Therefore, the Ft. Riley wastewater composition with a BOD_5 of 320 mg/L and a calculated COD of 640 mg/L (i.e., twice the BOD_5) was used as the design basis.

Table 4. Gray water and black water composition documented in a selection of the literature.

Wastewater type	Source	COD (mg/L)	BOD_5 (mg/L)	TSS (mg/L)
Black water	European vacuum toilets [54]	9,500 to 19,000	NA	NA
Black water	Nature park toilets [55]	1,675.9±709.1* to 2,718.8±1,009.3	1,108.6±581.1 to 1,480.2±604.4	721.5±158.5 to 1,676.7±682.3
Black water	Vacuum toilets [56]	9,966±8,920 to 38,835±20,347	NA	NA
Black water	Vacuum toilets [57]	7,700 to 9,800	NA	NA
Black water	Vacuum toilets [58]	8,700±3,980	NA	NA
Black water	Naval shipboard [59]	NA	780 to 1,700	2,100 to 3,500
Black water	U.S. Septage [60]	1,500 to 703,000 (average 31,900)	440 to 78,600 (average 6,480)	310 to 93,378 (average 12,862)
Black water	Lodging house [61]	1,218	406	560
Black water	Housing area [62]	806 to 3,138	410 to 1,400**	920 to 4,320**
Black water	Cruise ship [63]	NA	1,950	1,510
Gray water	Lodging house [61]	245	90	48
Gray water	Bath and shower [61]	100 to 200	50 to 100	NA
Gray water	Hand basin [61]	263	109	NA
Gray water	Shower [61]	109	59	NA
Gray water	Housing area [62]	495 to 682	350 to 500***	570 to 700**
Gray water	Cruise ship [63]	NA	153 to 270	85 to 170
Combined black and gray water	Naval shipboard [59]	NA	530 to 1,300	700 to 2,400
Combined black and gray water	Untreated domestic strong wastewater [64]	1000	400	350

*± Reported standard deviation.

**Total solids

***BOD_7

Table 5. Wastewater composition basis.

Wastewater type	COD (mg/L)	BOD_5* (mg/L)	TSS (mg/L)
Gray water	285	142.5	215
Black water	8,350	4,175	4,600
Combined wastewater**	1,500	750	875

*Assumed to be half the COD.

**Assumes 15% of combined wastewater is black water.[53]

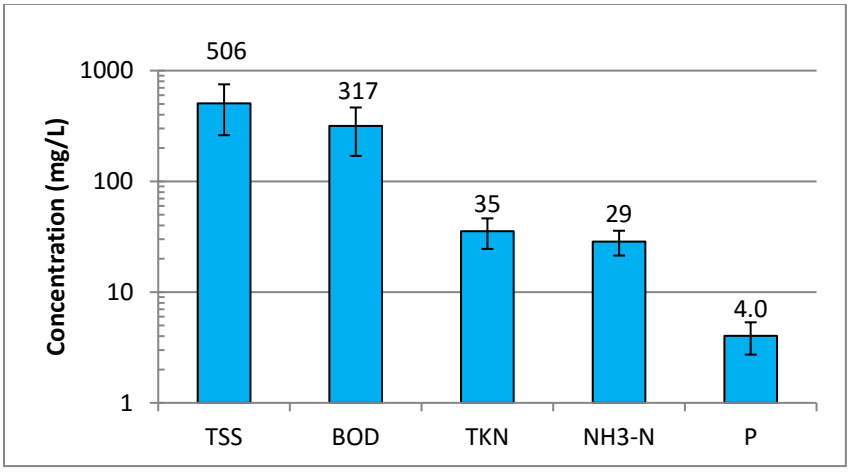

Figure 46. Ft. Riley Camp Funston wastewater composition for data reported from June 1, 2012 through May 31, 2013.

Treatment requirements. Treatment requirements depend on ultimate end use and disposition. Treated water that is discharged to surface water will need to meet requirements of the USEPA National Discharge Pollution Elimination System. These requirements are based on statutory regulations and characteristics of the receiving water body. Certain receiving waters will require more stringent treatment requirements. This is especially the case with respect to nutrients. In general, the minimum treatment requirements (USEPA Secondary Standards) for BOD_5 and TSS are 30 mg/L each (monthly averages). Treated water that is being considered for either indirect or direct potable reuse will likely have more stringent treatment requirements. For example, Virginia requires COD to be less than 10 mg/L and California requires TOC to be less than 3 mg/L. Additional treatment requirements also apply. Non-potable reuse applications have varying treatment requirements if they are established at all. Reuse of treated wastewater for irrigation and fertilization would typically not require treatment for nitrogen and phosphorus nutrients. Additional information on water reuse has been compiled in the USEPA Guidelines for Water Reuse.[65]

The focus of this research has been on organics removal. Therefore, the design basis includes treatment requirement of 30 mg/L BOD_5 or 60 mg/L COD (assuming COD in the effluent equals twice the BOD_5). Additional treatment requirements included in the design basis are 30 mg/L TSS

and 100 cfu/100 mL for fecal coliforms. These treatment requirements are suitable for restricted reuse.

Estimation of design parameters from laboratory experiments. Laboratory data from this research were reviewed to establish the design basis for COD removal in the MFC. Specifically, the kinetics of COD removal and the relationship to treatment effectiveness and power generation were considered. COD removal rates were characterized for wastewater under 100 Ω in fed-batch mode (Figure 47). COD removal followed apparent first-order kinetics, with a removal rate constant of 0.047 hr^{-1}. Overall COD removal during a fed batch cycle was 82%. Further evaluation of COD removal was conducted using acetate and wastewater.

Two sets of preliminary experiments were conducted with acetate. The first set involved acetate and varied the MFC size (2 cm and 4 cm). The model was calibrated to the 4-cm MFC and used to predict the performance of the 2-cm MFC. In general, the prediction improved with decreasing resistance (i.e., increasing current). The model under-predicted the first-order rate constant for open-cell voltage (OCV – infinite resistance), 1000 Ω, and 100 Ω conditions by 43%, 24%, and 3%. A second set of experiments was conducted with acetate and wastewater to evaluate the relationship between resistance and COD removal. The rate constant increased with decreasing resistance as expected when using acetate. Additionally, the coulombic efficiency decreased significantly as the resistance increased. To explain these results we developed two hypotheses. First, we hypothesized that wastewater fermentation to acetate was rate limiting. Second, we hypothesized that oxygen diffusion through the cathode (and potentially presence of other electron acceptors), led to competition for COD. This competition was relatively greater when MFC resistance was high. Initial calculations indicate that COD removal facilitated by oxygen diffusion through the cathode was significant: recalculation of coulombic efficiency after accounting for aerobic biodegradation resulted in an increase from about 40% to about 80%.

Comparative experiments were then conducted with acetate and wastewater to understand the relationship between current and COD removal. The results of these experiments (Figure 47) demonstrated first-order decline of COD concentration.[46] The current was initially stable with both acetate and wastewater but then suddenly decreased. The rapid decrease in current was associated with a COD concentration of about 100 to 200 mg/L and is consistent with results for a larger scale MFC presented in Figure 11. Figure 48 illustrates that, regardless of cell resistance, current density in the smaller scale MFC was high and stable at COD concentrations greater than ~100 mg/L for both acetate and wastewater. The reason for the rapid decrease in current appears to be associated with a balance between COD removal by exoelectrogenic and aerobic bacterial processes. Current density is high when COD concentrations are high and COD removal is dominated by exoelectrogenic bacterial activity. Under these conditions, oxygen is consumed in the cathode and oxygen diffusion into the MFC is relatively reduced compared to the same period of time under open-circuit conditions. Current density is low when COD concentrations are low (< ~100 mg/L) and therefore COD removal becomes dominated by oxygen diffusion through the cathode and aerobic bacterial activity in the MFC. The lower COD removal rates at COD concentrations < ~100mg/L support the need for a downstream polishing process.

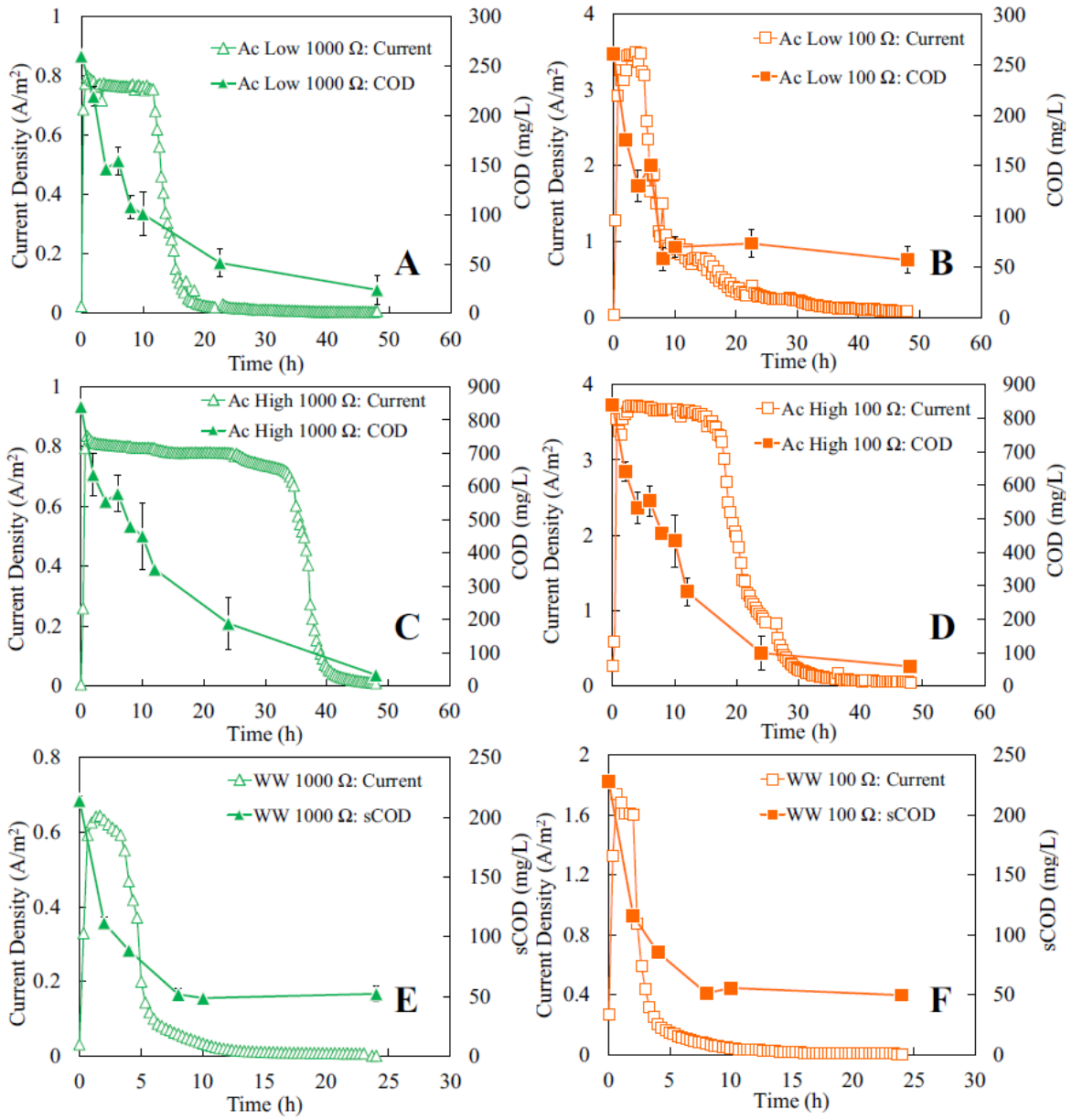

Figure 47. Trends of COD concentration and current density for acetate (A-D) and wastewater (E-F) at high (A,C,E), and low (B,D,F) cell resistance.[46]

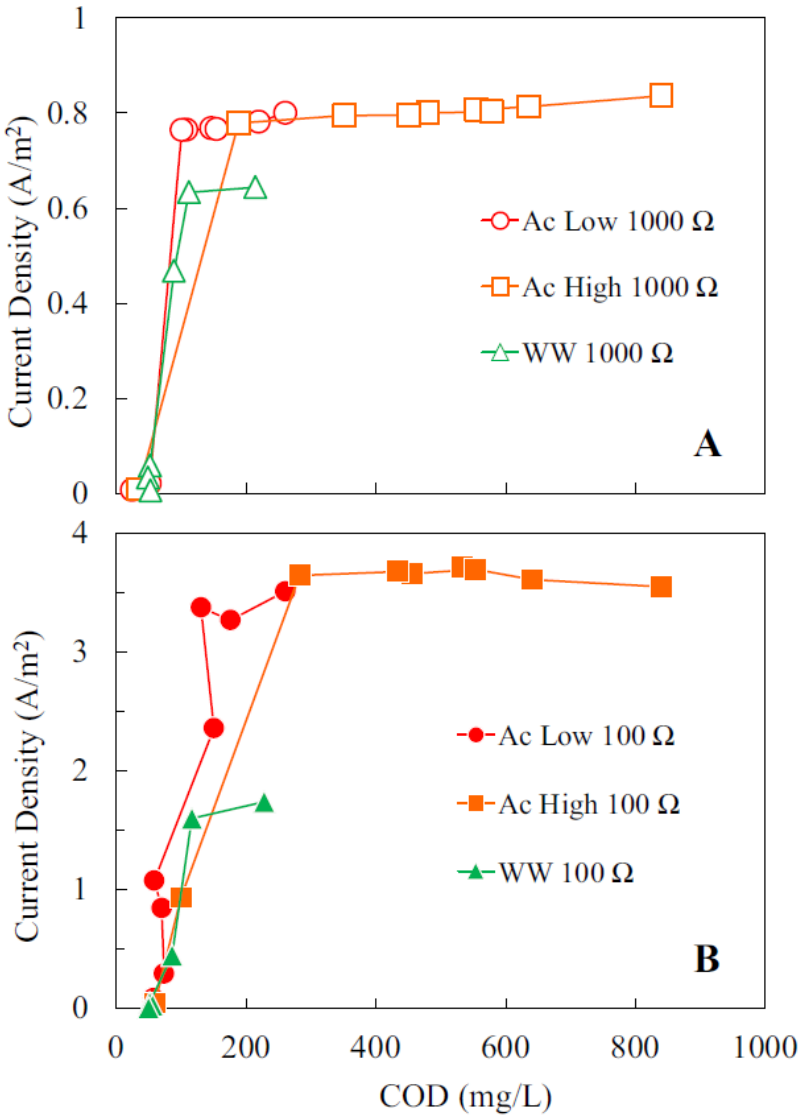

Figure 48. Current density relationship to COD concentration at high (A) and low (B) cell resistance.[46]

The COD removal process with raw domestic wastewater (without filtration) was more complex than that observed using filtered domestic wastewater (only sCOD) (Figure 49). COD removal with the raw wastewater appeared to have two different stages: one with high current production from 0 to 4 h, followed by one with little current production from 4 to 24 h. COD removal fit a first-order reaction for each stage but with much different rates. The rate constants of the first stage were 0.23 ± 0.03 h^{-1} for sCOD and 0.21 ± 0.01 h^{-1} for tCOD, and these were much higher than those of the second stage with little current production (0.04 ± 0.01 h^{-1} for sCOD and 0.06 ± 0.01 h^{-1} for tCOD) (Figure 49). These two different rates were probably due to the different characteristics of the readily- and slowly-degradable COD. The CE of raw wastewater was 21% (100 Ω), which was essentially the same as that with filtered wastewater (22%) under the same operation conditions. The peak current density of 1.7 A/m^2 was sustained for 4 h, followed by a rapid decreased in current density when the tCOD was below ~200 mg/L, and the sCOD was below

~100 mg/L (Figure 49). The final CODs after 24 h were 53 ± 6 mg/L (sCOD) and 72 ± 2 mg/L (tCOD) based on four parallel MFC reactors.

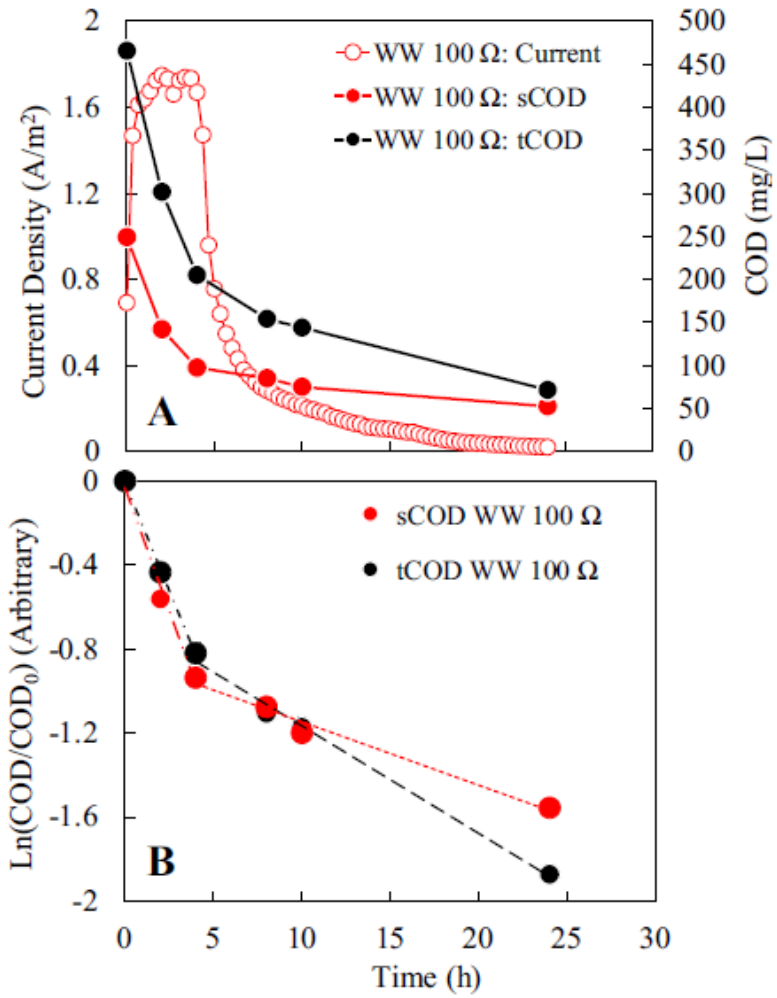

Figure 49. (A) Current density, soluble (sCOD) and total COD (tCOD) changes with time in the MFCs fed with raw domestic wastewater; (B) first-order model fits for the two phases.

The biphasic COD removal pattern and the rapid decline in current density (Figure 49) was also used to determine how the two stage MFC/GAC-BAF should be operated. If power generation and COD removal by the MFC is the goal, then the MFC is best suited for reducing total COD and soluble COD to ~200 mg/L and ~100 mg/L, respectively. The GAC-BAF would then be used to reduce the remaining COD to effluent requirements. Alternatively, the MFC could be used alone to reduce COD to the treatment goal (60 mg/L). This approach is not considered the most efficient use of the MFC considering that COD reduction in the second phase (after ~ 4h in Figure 49) is associated with low current density and thus low potential for power generation. Therefore, the treatment goal for the MFC was selected to be 150 mg/L total COD with the intention of the using the GAC-BF to reduce the remaining COD to the overall treatment goal of 60 mg/L.

Continuous flow tests demonstrated a clear relationship between COD removal efficiency and HRT (Figures 35 and 36). A comparison of these experimental results to modeled COD removal based on a first-order model with plug flow and no dispersion was made (Figure 50). The data do not fit to the model as expected because first-order kinetics were previously shown to be biphasic. On the other hand, model runs with overall first-order rate constant between 0.12 and 0.20 h^{-1} bracket the data which is consistent with the previously determined rate constant of 0.21 ± 0.01 h^{-1} for tCOD (Figure 49). The 0.20 h^{-1} first-order rate constant model result is similar to results at an HRT of 2 hours whereas the 0.012 h^{-1} first-order rate constant model result is similar to results at an HRT of 10 hours. This is expected – at lower HRTs the COD removal is low and the COD in the MFC is greater than 200 mg/L leading to higher rate constants driven by exoelectrogenic COD removal. At higher HRTs the COD removal is high and the COD in the MFC is less than 200 mg/L and COD removal is driven more by aerobic processes via oxygen mass transfer across the cathode. A first-order rate constant of 0.16 h^{-1} (4 d^{-1}) was used for the design basis.

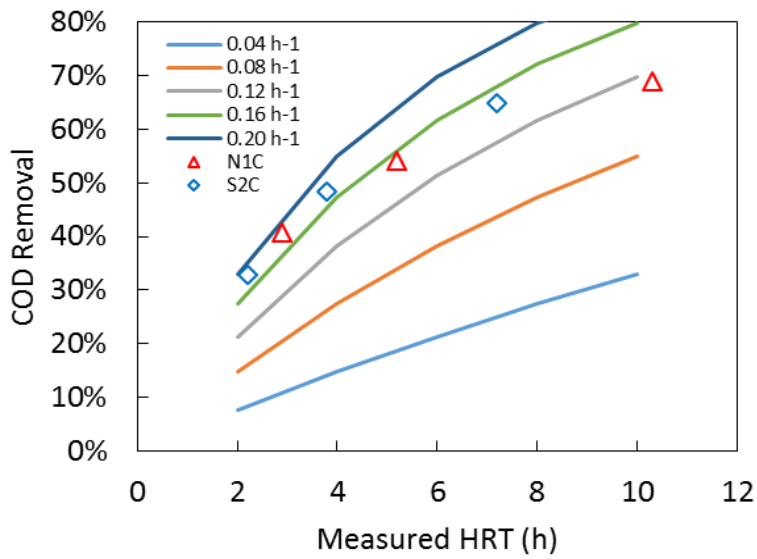

Figure 50. Comparison of COD removal in continuous-flow MFCs to theoretical COD removals based on first-order kinetics. Solids lines: model. Symbols: data based on measured HRTs taken from Figure 36.

Process Engineering Calculations. Engineering calculations were conducted to finalize the design basis and estimate reactor size and performance. These calculations are included in Appendix A and results are summarized in Table 6.

Table 6. MFC design basis summary

Parameter	Units	Value	Notes
BOD_5 influent	mg/L	320	Historical data from Ft. Riley
COD influent	mg/L	640	Assumed to be twice BOD_5
COD effluent	mg/L	150	No power generated at lower COD. Further treatment needed using a downstream polishing process.
COD removal	%	77	Calculated
First-order rate constant for COD	day^{-1}	4	Based on laboratory experiments
Hydraulic residence time	day	8.7	Calculated assuming first-order kinetics, plug flow, and no dispersion
Flow rate	gal/min	0.5	Assumed
Required reactor water volume	L	989	Calculated
Organic loading rate	$kg\ m^{-3}\ h^{-1}$	0.07	Calculated based on reactor liquid volume
Maximum water depth and cathode height	ft	2	Water depth is limited by the ability of the cathode material to sustain water pressure.
Cathode specific area	cm^2/mL	0.57	Laboratory MFC design
Total cathode area	m^2	56	Calculated
Cathode module width	ft	3.5	Assumed
Cathode module depth	in	1	Estimated including spacer for passive air flow
Number of cathodes	-	88	Calculated
Number of cathodes per module	-	2	Basis for 2-sided cathode module with air spacer
Number of cathode modules	-	44	Calculated
Anode specific projected area	cm^2/mL	0.19	Laboratory MFC design
Total projected anode area	m^2	19	Calculated
Anode diameter	in	1	Based on laboratory MFC experiments
Anode length	ft	1.83	Based on maximum liquid depth
Number of anodes	-	1323	Calculated
Number of anode modules	-	45	Number of cathode module plus 1
Number of anodes per anode module	-	29	Calculated
Reactor length	ft	8.1	Includes space occupied by cathode modules
Reactor width	ft	3.8	Includes space for flow around cathodes which also serve as baffles
Reactor height	ft	3.0	Includes freeboard above water
Overall coulombic efficiency	%	1.7 to 30%	Range of values measured in laboratory
Total current	A	11 to 190	Calculated
Areal current density	A/m^2	0.11 to 1.9	Calculated. Laboratory experiments demonstrated 0.04 A/m^2.
Voltage	V	0.2	Assumed
Total power	W	2.1 to 37	Calculated
Areal power density	mW/m^2	73 to 1300	Calculated. Laboratory experiments demonstrated 240 mW/m^2.
Energy generated per unit volume water treated	kWh/m^3	0.019 to 0.33	Calculated
Energy generated per unit COD destroyed	kJ/g	0.14 to 2.4	Calculated

Power harvesting. The overall electrical scope of this task can be broken down into two challenges: (1) how to harvest the energy produced by the microbial fuel cell reactor with systems currently in the market, and (2) how to convert the given voltage potential into a more usable voltage potential.

Energy harvesting from fuel cells, typically the hydrogen fuel cell (HFC), has been around since the 1800's. Fuel cells provide DC electricity by means of a constant chemical reaction which normally requires a constant source of fuel. In the case of HFCs, the fuel sources are hydrogen and oxygen. Maintaining a constant flow of these fuels will provide a constant chemical reaction which will in turn provide a constant flow of electricity, usually at voltages ranging between 0.5 VDC and 0.8 VDC for HFCs.[66] Typically, fuel cells are stacked in series and/or parallel combinations, increasing the voltage and/or current produced, and connected to a battery charge controller. From the batteries, the electricity may flow directly to a load or be converted into a different form (AC/DC), as determined by the load requirements.

However, when MFCs are stacked in a similar fashion to traditional fuel cells, a phenomenon known as voltage reversal occurs, resulting in a low or nearly 0 VDC stack potential.[67] Voltage reversal occurs due to a lack of chemical reaction at any given cell, causing each cell to turn into an electrolytic cell. These electrolytic cells become parasitic, drawing current from the series/parallel connected cells, forcing chemical reactions which drain current from the system instead of generating electricity.

To mitigate the voltage reversal problem, each MFC needs to be electrically isolated from the next cell. A circuit we previously proposed[67] – the capacitor-based system – proved to be an effective, yet inefficient, method to accomplish this isolation. The approach is a two-step process: (1) Charge four capacitors by using a relay to connect each capacitor to each MFC in parallel, (2) after the capacitors have become adequately charged, switch the relay contacts, thereby disconnecting the capacitors from the MFCs and connecting the capacitors in a series connected loop to discharge to a load. During each cycle, while one set of four capacitors is charging, a separate set of four capacitors will be discharging (see Figure 51). Unfortunately, the microcontroller and control relays necessary to control the process require significant power, greatly reducing the efficiency of the circuit.

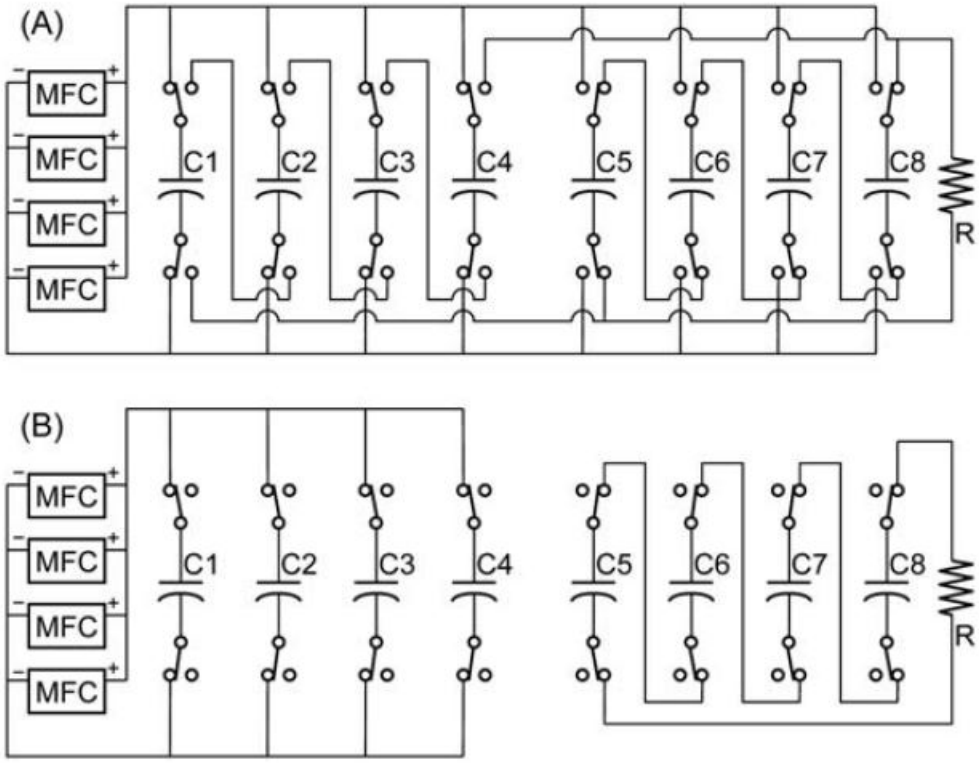

Figure 51: Energy harvesting from arrays of MFCs at boosted voltages without voltage reversal: (A) whole electric circuit diagram, (B) simplified diagram without unnecessary lines which are used in the alternating charging and discharging time period. While 4 MFCs and 8 capacitors are shown in this figure, various numbers of MFCs and capacitors can be used. (C: capacitor; R: external resistance; +: MFC cathode; –: MFC anode).[67]

Different energy harvesting circuits have been previously summarized.[68] The techniques are organized into three categories: (1) capacitor-based systems, (2) charge pump-based systems, and (3) boost converter-based systems. These are summarized in Figure 52 and Table 7.

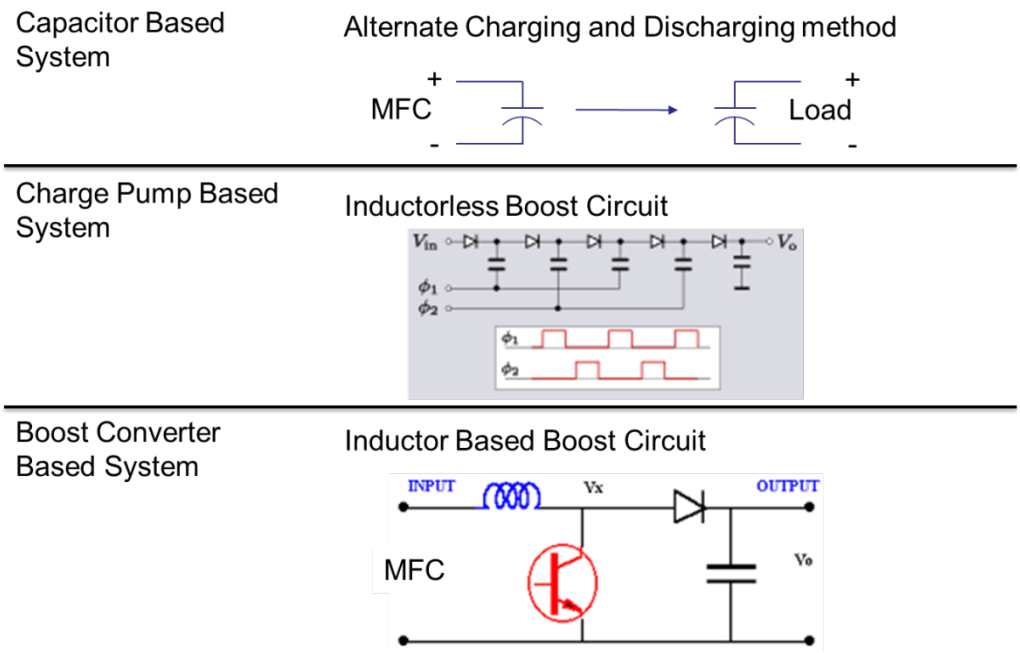

Figure 52. Power harvesting systems.

Table 7. Voltage boosting options for MFCs

Attribute	**Voltage Boost Option**		
	Capacitor Based System	**Charge Pump Based System**	**Boost Converter**
Main Charging Component	Capacitor	Capacitor, diodes	Inductor, Capacitors
Disadvantages	External Power needed control circuit needed switching circuit needed	Low efficiency due to high number of components. Requires a control circuit Long Startup Time (~2+ hrs)	Requires a control circuit
Advantages	Series of capacitors Switching Design Complete Source-Load Isolation	Passive switching Integrated circuit	Relatively small amount of components Integrated Circuit Form of Isolation
Efficiency	~70%	~80%	~90%

Capacitor-based systems require a control circuit to charge and discharge capacitors accounting for the control circuit's energy consumption reduces the system's efficiency to 74%. In theory, replacing the switching relays with semiconductor-based switching could increase the system efficiency dramatically; however, the complexity of the control circuit would also increase.

Charge pumps have low operating voltages, but can also have long startup times, depending on the current output of the MFC. Startup of an MFC to be 22 hours before reaching an output

voltage of 3.3VDC.[68] This “pre-charge” time can be a detrimental to critical applications when a quick startup is required.

Boost converters typically have efficiencies of 90% or greater, but are designed to operate at 1VDC and higher. Using boost converters at such low voltages would require a voltage input to kick start the circuitry as well as external power to run the control circuit, lowering the overall efficiency of energy harvesting.

Finding a converter designed for low voltage application is crucial for MFC energy harvesting. TXL Group (El Paso, Texas) specializes in thermoelectric generation. They design and produce a readily available inventory of boost convertors that operate at low voltage and power ranges. Their ultra-low voltage bootstrap converter (product number W0422-1, see attached data sheet in Appendix B) operates at 0.1VDC to 0.6VDC and can boost the voltage to 10VDC.

Based on the relatively high efficiencies of boost converters and the availability of commercially available off the shelf low voltage devices, boost converters were selected for the MFC design. The system will use boost converters designed for thermoelectric generation to isolate the MFCs from each other and boost each cell’s potential to a usable voltage. The system design will be broken into two boosting stages. The first stage will use TXL’s ultra-low voltage bootstrap converter to step up the voltage from 0.2VDC – 0.3VDC to 10VDC. The second stage will take the first stage output and step it up to a 24VDC (Figure 53). If desired, an inverter can be used to further boost and transform 24 VDC to 120 VAC. The overall efficiency for the boost converter system is reasonable (Table 8).

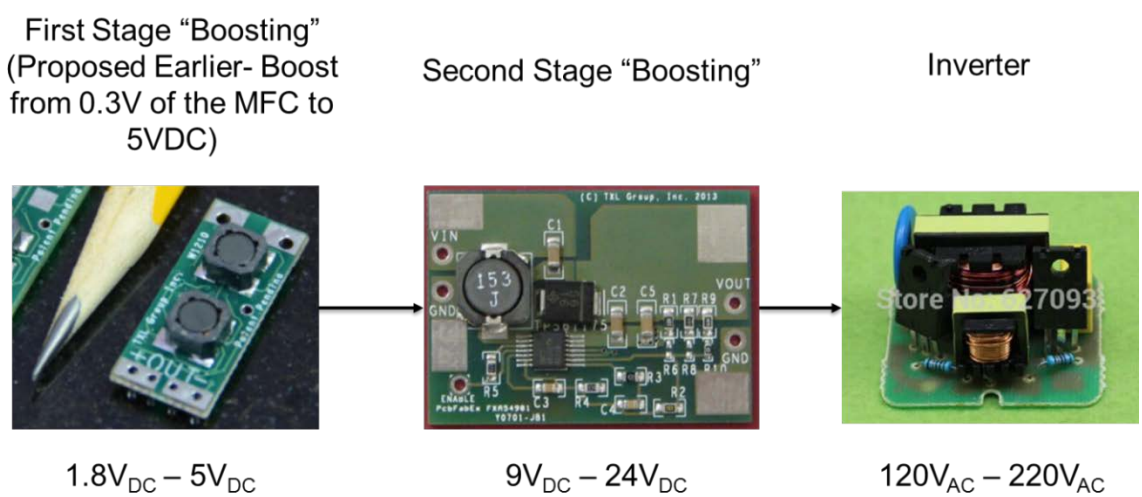

Figure 53. Two-stage voltage boost converter system with optional third-stage inverter.

Table 8. Estimated boost converter efficiencies

Device	Voltage	Efficiency	Overall Efficiency
MFC	≤ 0.7 VDC	-	-
1st Stage Boost Converter	1.8 – 5.0 VDC	70 – 90%	70 – 90%
2nd Stage Boost Converter	9 – 24 VDC	90 – 95%	63 – 86%
DC-AC Inverter	120 VAC	85 – 90%	54 – 77%

Because of the low voltages generated with MFCs, it is important to ensure that excessive voltage loss does not occur in system wiring and electrical connections. The power loss was estimated for each cathode module at the range of estimated coulombic efficiencies (1.7 to 30%). Table 9 illustrates the power loss is substantial (100%) at the higher efficiency but acceptable (6%) at the higher efficiency. There are several aspects of this design that contribute to loss of power, but the main culprit is the ohmic loss of the transmission system. Ohmic loss is power (in the form of heat) that is lost in the transmission system. The more resistance there is between the MFC and the boosters, the more power is lost. A 16 gauge wire has a DC resistance of 5.25 ohms/1000 ft while 14 gauge wire has a DC resistance of 3.26 ohms/1000 ft. The 14 gauge wire size was used in the design. Use of a larger diameter (i.e., smaller gauge) wire would be necessary to offset the loss at the higher coulombic efficiency. Transition resistance also contributes to the total resistance in this transmission system. This resistance occurs when the surface area of the contact point of one conductor does not match the surface area of the contact point of the second conductor. The best method to get around transition resistance is to minimize the number of transitions and/or maximize their surface area contact (usually through soldering/brazing or welding). Our power loss calculations do not take into account these transition resistances.

Table 9. Power loss calculation for current transmission

Parameter	MFC Designs		Units
MFC Efficiency	1.7	30	%
Power per MFC anode module (P_{MFC})	47	830	mW
Maximum current per anode module (I_{MFC})	0.24	4.16	A
Wire Resistance (#14 AWG)	3.26	3.26	Ω/1000FT
Distance Between MFC & Control Panel	15	15	Ft
Resistance of 1 Wire (Ω_W)	0.049	0.049	Ω
Power Loss across Wire (P_{1W})	2.8	846	mW
Power @ Booster (P_{IN}) (P_{MFC}-P_W)	44.183	0.000	mW
% Power Loss	6%	100.0%	%

Engineering design drawings and specifications.

Mechanical engineering design. The main components of the microbial fuel cell are reactor tank, the cathode modules, and the anode modules. The general approach to mechanical design was to have a modular system that is easily maintainable with removable anode and cathode modules. The design builds upon the concept presented above in Figure 43. Figure 54 is a plan view of the reactor tank showing the 45 anode modules and 44 cathode modules along with tank inlet and outlet valving that will be discussed later. The serpentine flow is shown whereby the wastewater flows past the anodes in each anode module and around each cathode module.

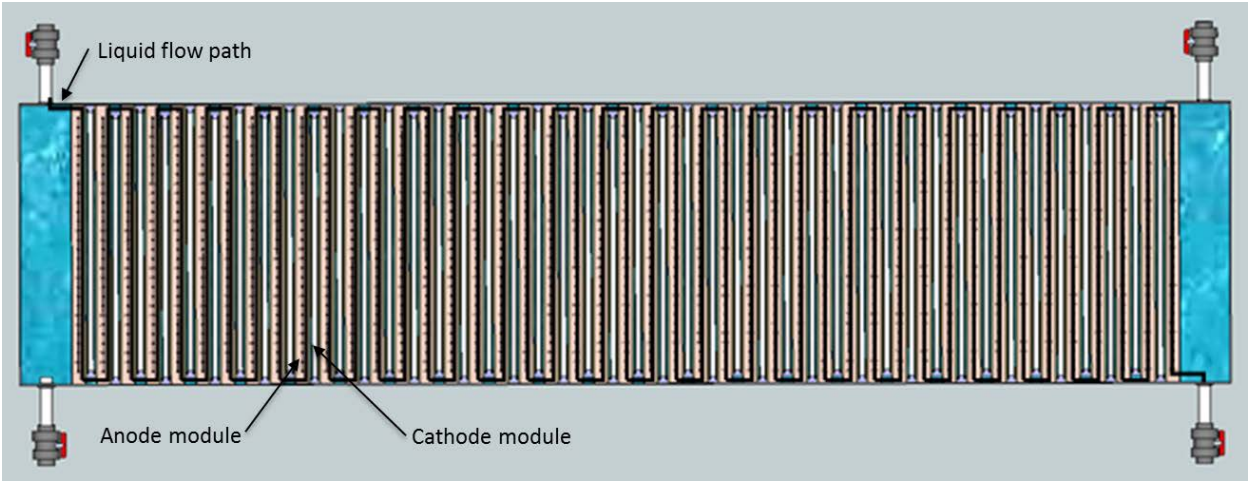

Figure 54: Reactor plan view showing serpentine flow through the anodes in the 45 anode modules and around the 44 cathode modules.

Figure 55 shows several reactor details reactor attributes including:

- Removable anode and cathode modules supported by epoxy-coated angle iron brackets that are welded to the epoxy-coated tank walls. A tank cut-away illustrating the angle iron brackets and their function is shown in Figure 56.
- The tank width is four inches greater than the cathode module width. Cathode modules are four inches that can be placed in the tank either next to the tank wall or offset from the tank wall thus allowing the modules to act as baffles and promote serpentine flow.
- Quick disconnect cabling to the anode and cathode modules to facilitate easy removal and replacement during maintenance.

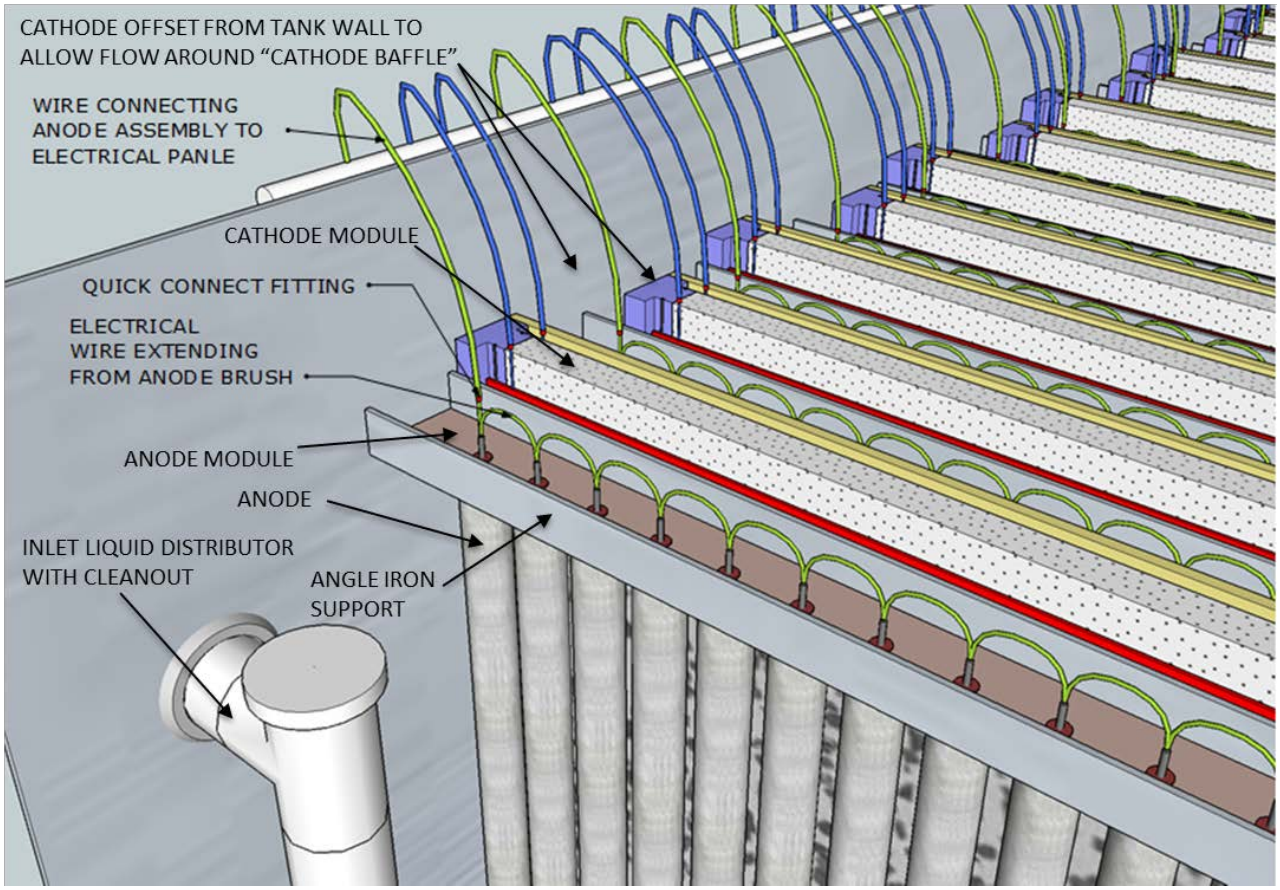

Figure 55. Reactor detail showing individual anode and cathode modules.

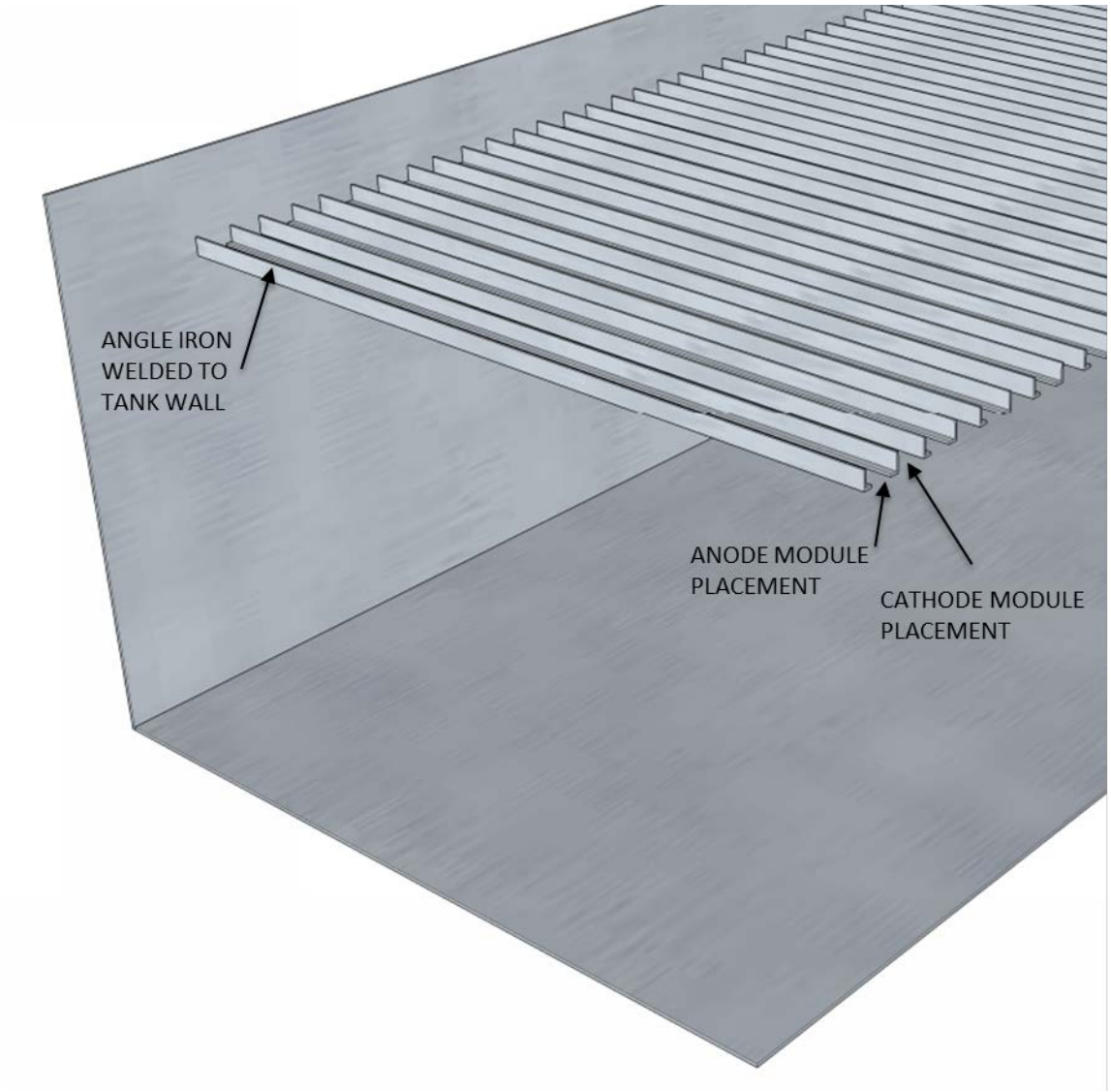

Figure 56. Tank cutaway showing angle iron brackets used to support both anode and cathode modules.

Figure 57 shows a section view of the reactor. In addition to the previously mentioned attributes, a box channel is shown at the bottom. The anodes are secured into the anode module by this epoxy-coated metal box channel at the bottom and by a flat plate at the top (see Figure 55). The box channel ensures the anodes are separated from the cathode and also provide a means for periodically air scouring the anodes. Compressed air (or nitrogen) can be directed to the box channels which then exits via evenly-spaced holes in the channel. The gas then flows upwards past the anodes and disengages loose biomass or particulates by souring. Figure 58 further illustrates this concept.

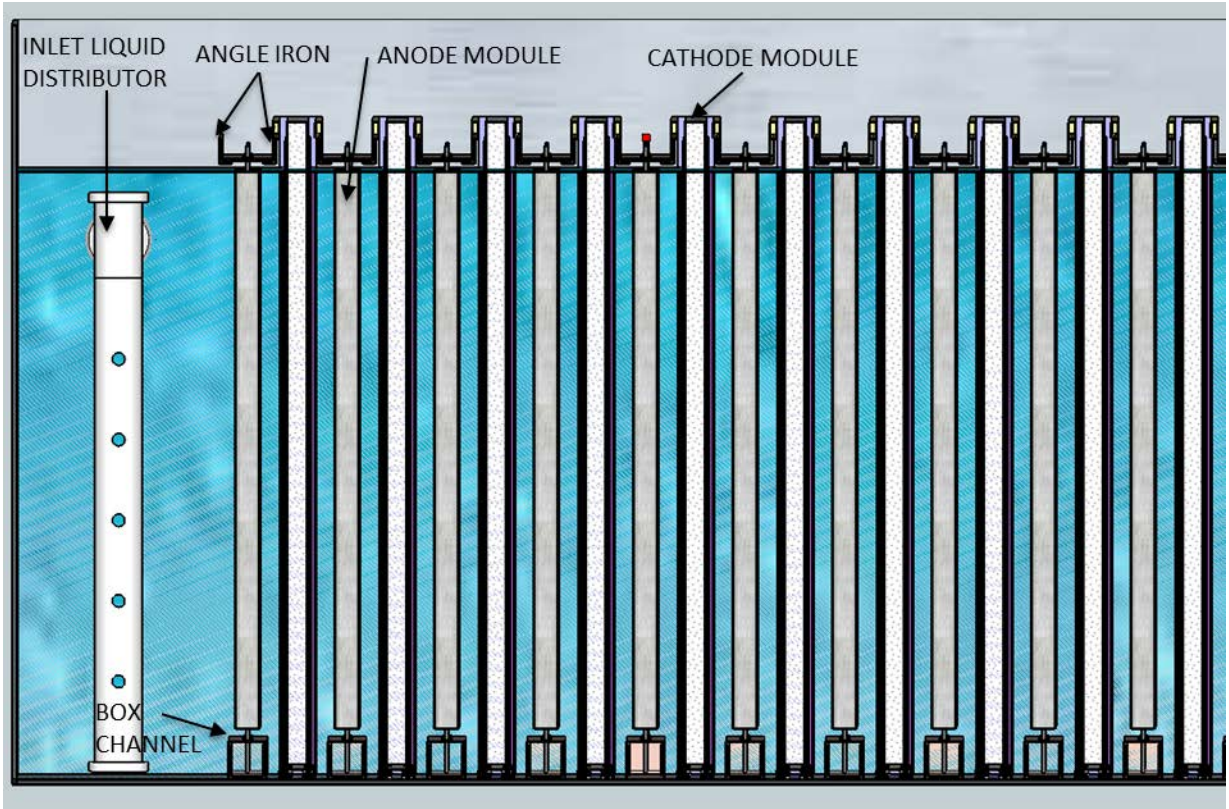

Figure 57. Section view of the reactor showing liquid distributor piping, anode and cathode modules, angle iron supports, and rectangular box channel supports.

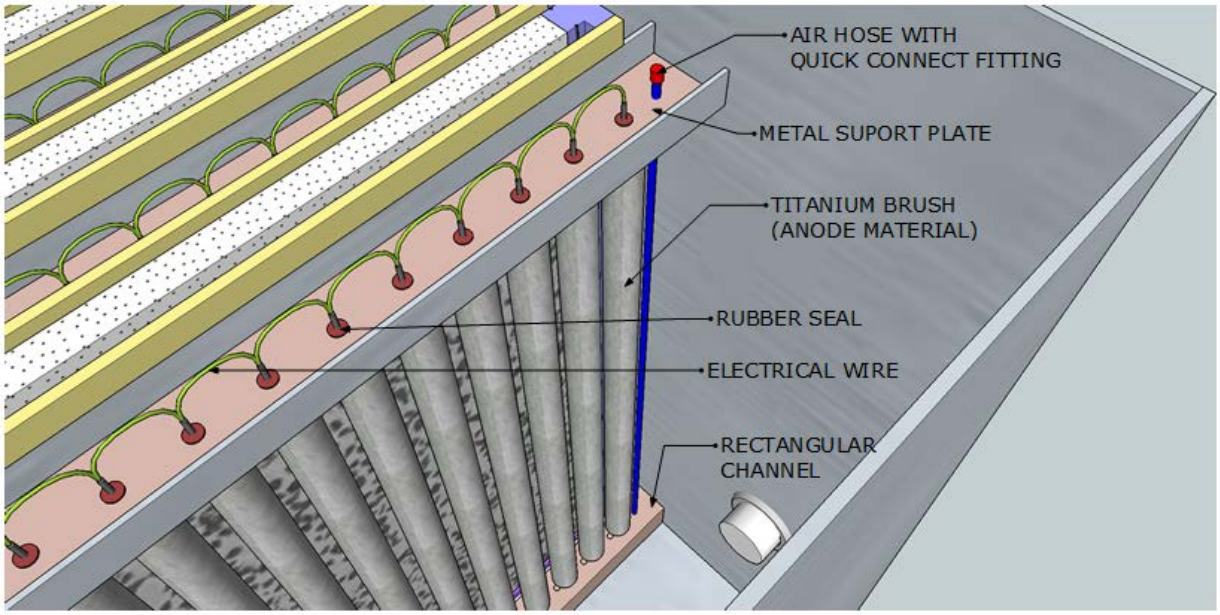

Figure 58. Anode module and air scour system. Note holes in rectangular channel adjacent to anodes.

Each cathode module (Figures 59 and 60) consists of a multicomponent plastic frame, a spacer for passive air flow, two cathode sheets with current collector bars (shown in red in Figure 59) to which wiring is connected, and two separators. The spacer is comprised of commercially available welded and perforated plastic tubes that provide structural support for the cathode and high porosity for air transport (Figure 61). Assembly of the cathode module generally follows the sequence illustrated in Figure 62. Details on the reactor tank and associated piping and valving are show in Figure 63. Additional design drawings, calculations, and a bill of materials are included in Appendix A.

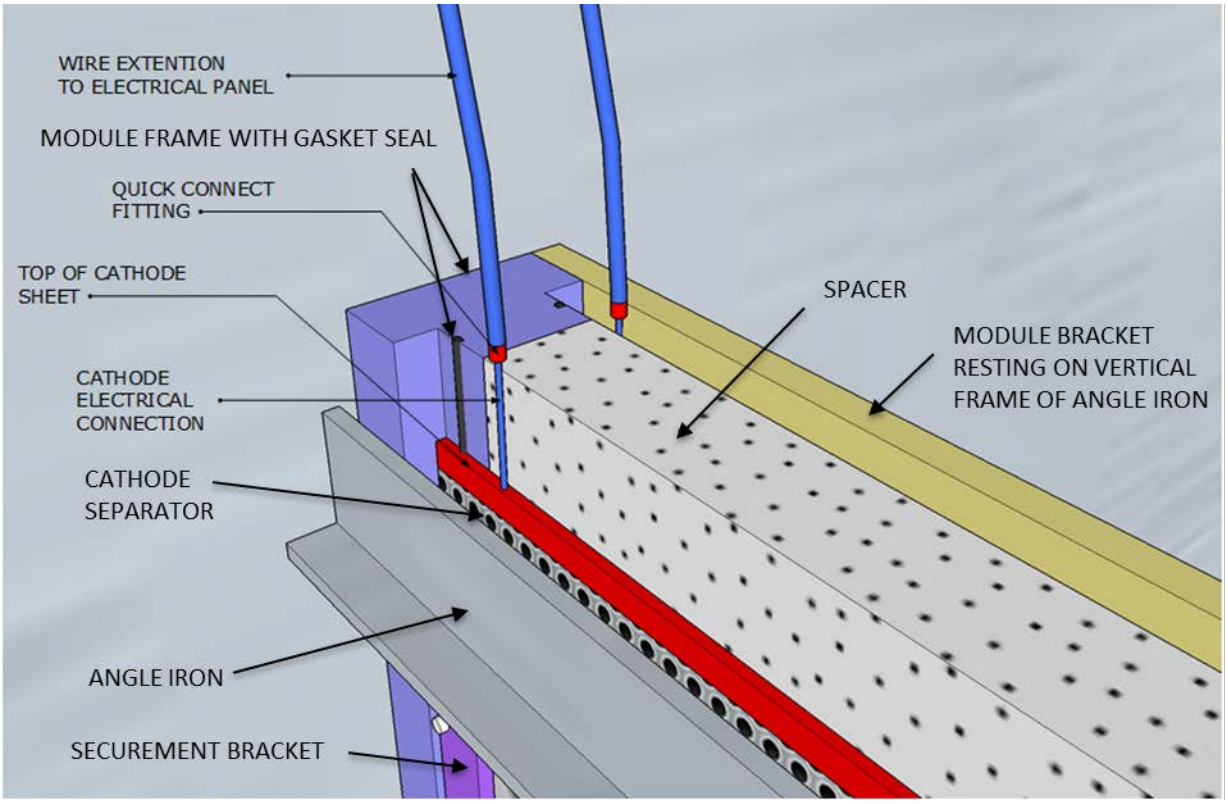

Figure 59. Cathode module details (yellow module bracket on left removed for clarity).

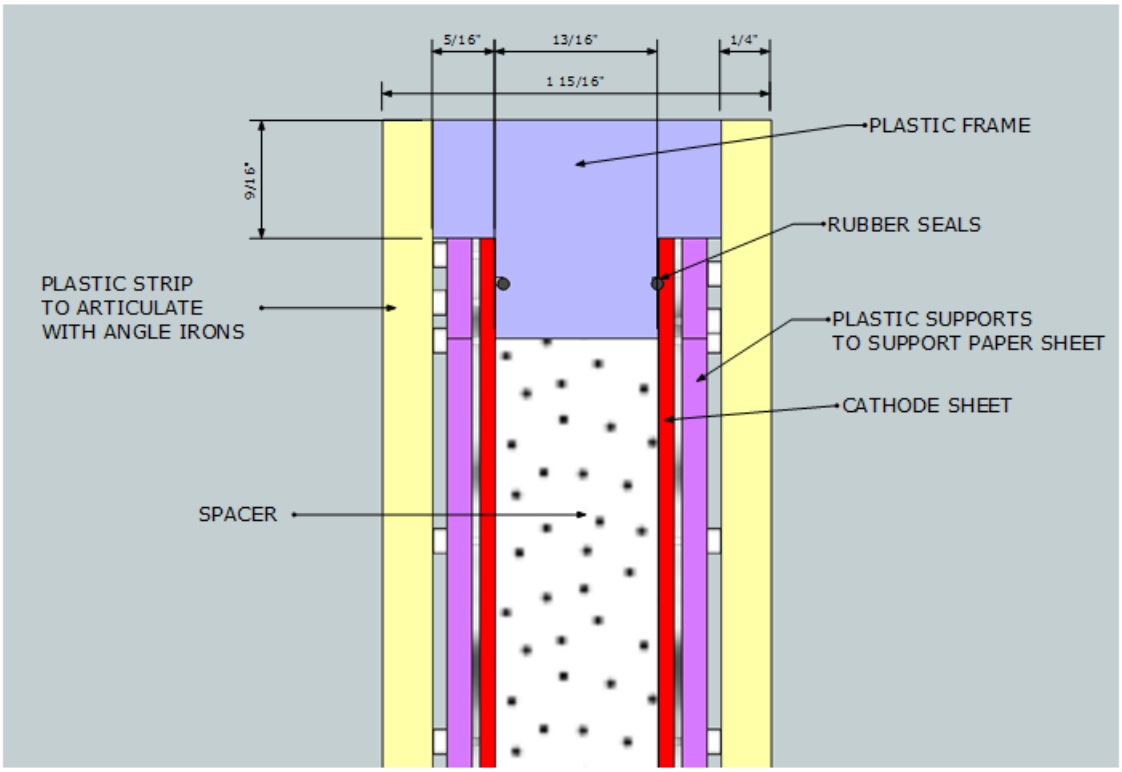

Figure 60. Cathode assembly plan view

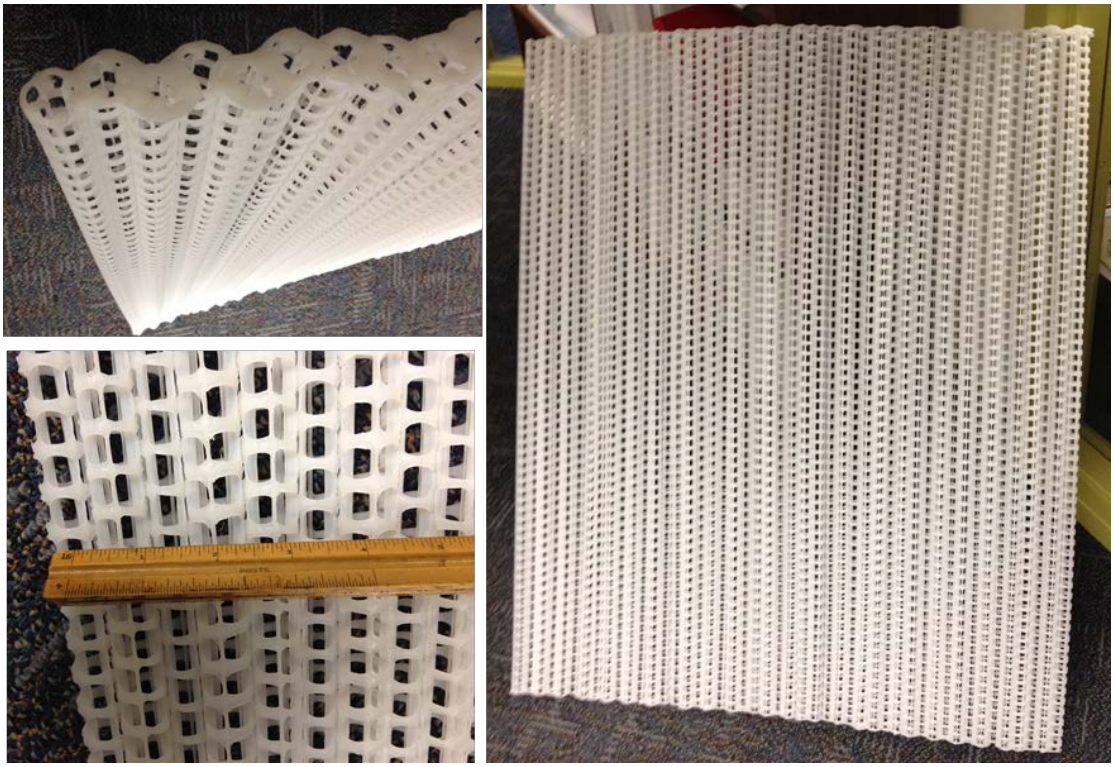

Figure 61. Spacer photographs.

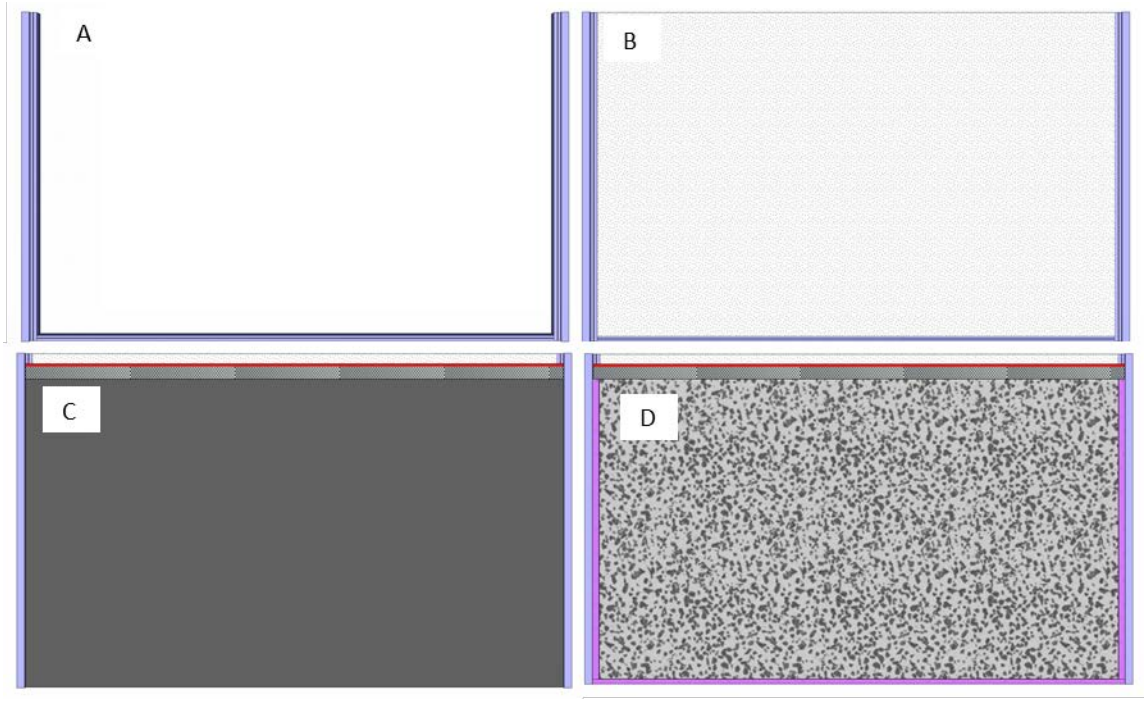

Figure 62. Cathode module assembly. A) Plastic module frame with rubber seal on sides and bottom. B) Spacer inserted into frame. C) Cathodes with current collector rod (top in red) mounted on both sides of spacer. D) Separators laid on top of cathode sheets and held in place with securement brackets that are bolted to the plastic module frame.

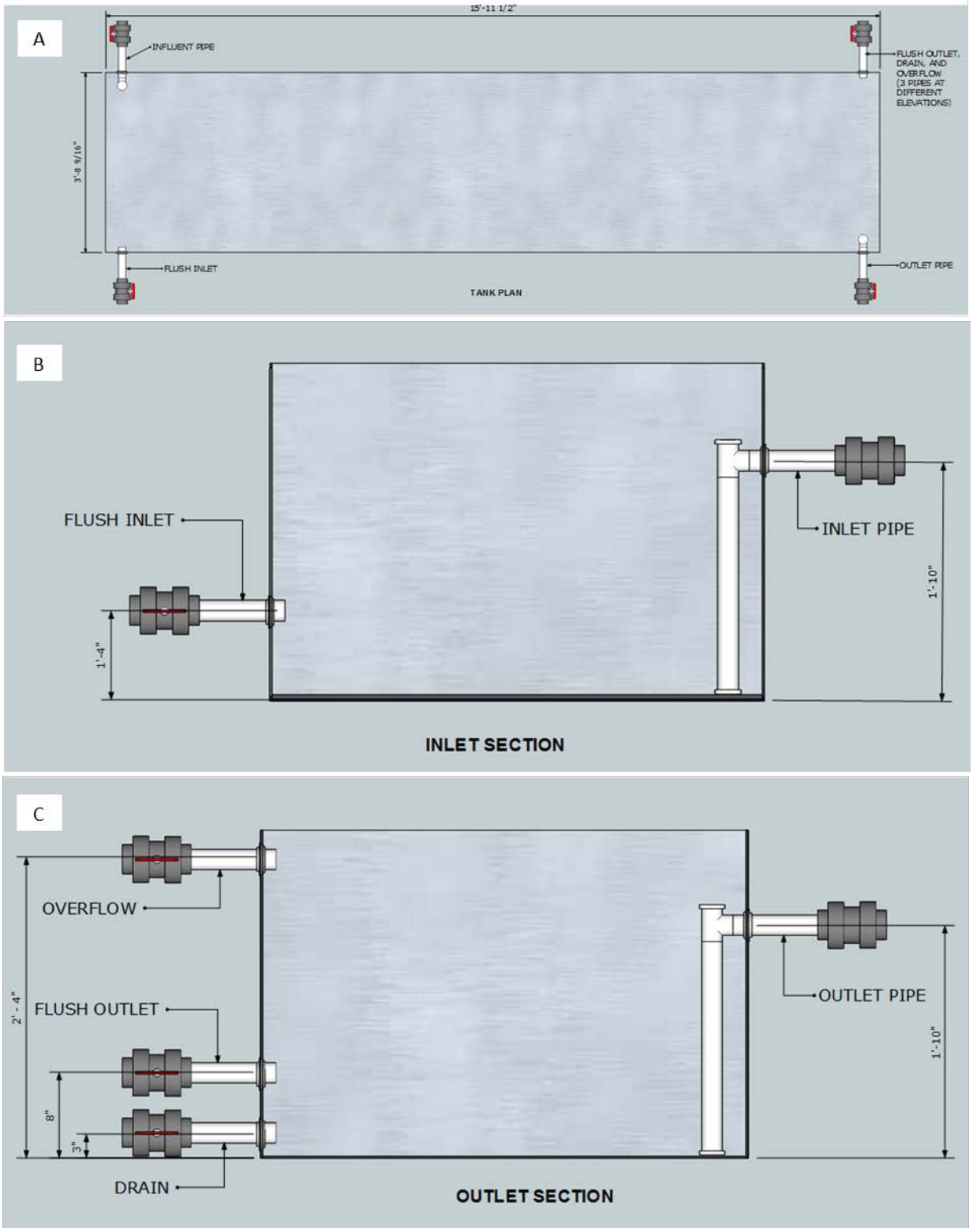

Figure 63. Reactor tank dimensional drawings showing plan view (a), inlet section (b), and outlet section (c).

Electrical engineering design. Each MFC anode-cathode module pair will be wired to one first stage booster, therefore the first stage boost will consist of 44 first stage boosters. The output of all 44 first stage boosters will be connected to super capacitor to serve as an interim energy storage (see Figure 64). The booster system will be enclosed in a NEMA 4X enclosure located outside within 10 feet of the MFC reactor. Within the NEMA 4X enclosure, there will be a human-machine interface/programmable logic controller (HMI/PLC) unit which will act as the control system. An office trailer will be furnished and installed with the power distribution detailed on drawings E-1 and E-2 (Appendix B).

Such critical loads include process feed pump, air compressors, 1.5 kVA universal power supply (UPS), the operator workstation and the data acquisition system. Between the MFC reactor and local control panel, there will be a junction box for ease of access to the wiring. Since the anodes and cathode assemblies will be exposed to raw sewage, there will be some maintenance (cleaning of probes and/or cathodes) will be required, thus cathode and anode modules will need to be disassembled periodically. The junction box will be installed on the side of the MFC reactor to minimize wire length (and ohmic losses) and provide easy operator access.

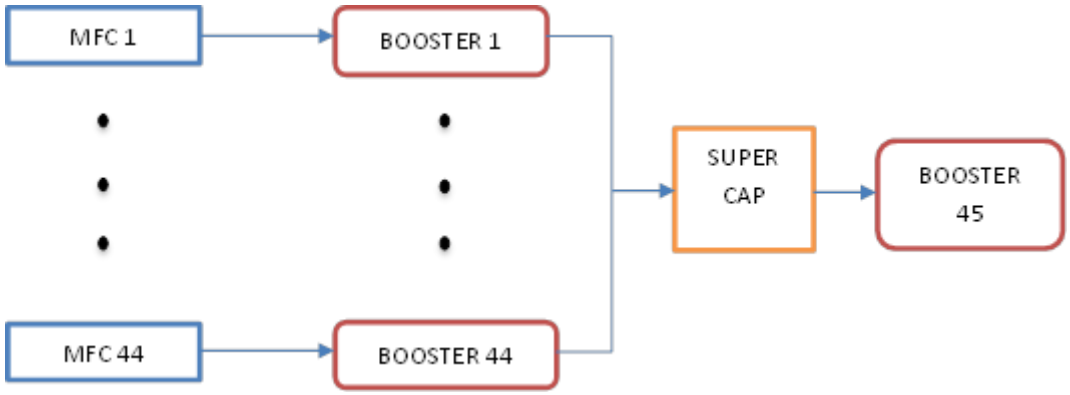

Figure 64. System for harvesting energy from the MFC anode/cathode modules.

Instrumentation engineering design. Figure 65 is a process and instrumentation diagram (P&ID) for the MFC system and Figure 66 is a control architecture drawing. The purpose of the P&ID is to provide a diagram of the physical process, show the instruments with associated loop numbers, and show how the information flows around the system. The reactor is shown near the center of the image with the cathode / anode array contained and all inputs and outputs connected. The destination / source of all signals is represented at the top of the drawing. The purpose of the Control Architecture Drawing is to provide a conceptual visualization of how the components of the system are connected on the network. The boundaries of the physical locations are shown in dashed lines.

The following parameters will be monitored:

- Influent wastewater flowrate into the bioreactor
- Temperature of wastewater in the bioreactor
- Fluid level in the bioreactor
- Voltage and current from each anode/cathode module pair
- Current and voltage output from the stage 2 boost converters, which represents the final power output of the bioreactor

A Keithley 2750 digital multimeter will be used as the data acquisition tool and will be connected to the operator workstation for data storage and analysis. The 2750 is designed to sense low voltages; leads from the fuel cells are connected directly to expansion cards which plug in to the back of the 2750. Three 7708 multiplexer module expansion cards will be used to bring the total available channels to 120. For current measurement, a shunt with known resistance will be installed in the anode lead and the voltage drop across it measured. The current channels will be programmed in the Keithley to divide the measured voltage by the known resistance to calculate current.

KickStart control software from Keithley will be installed on the Operator Workstation to view, process, and export the recorded data. The software can be configured to record data at specified intervals to collect "snapshots" of the process over time. It can also be automated to export data to the hard drive of the operator workstation at specified times.

The Vision 1040 PLC/HMI with I/O expansion card V200-18-E3XB from Unitronics will collect the influent wastewater flowrate, temperature, and liquid level data from the process sensors and output them to the Keithley 2750. The main purpose of the PLC is to communicate with the influent pump VFD over ethernet: sending start/stop and speed commands and receiving fault, running, and speed feedback commands. A low flow alarm will be configured in the PLC to shut down the pump should the flowrate remain below a configurable set point for a configurable time.

The Vision HMI graphics will display the influent flowrate, temperature of the wastewater, and reactor liquid level, and will have an alarm screen where the low flow alarm will be configured and acknowledged.

Additional details including a bill of materials and instrument cut sheets are provided in Appendix C.

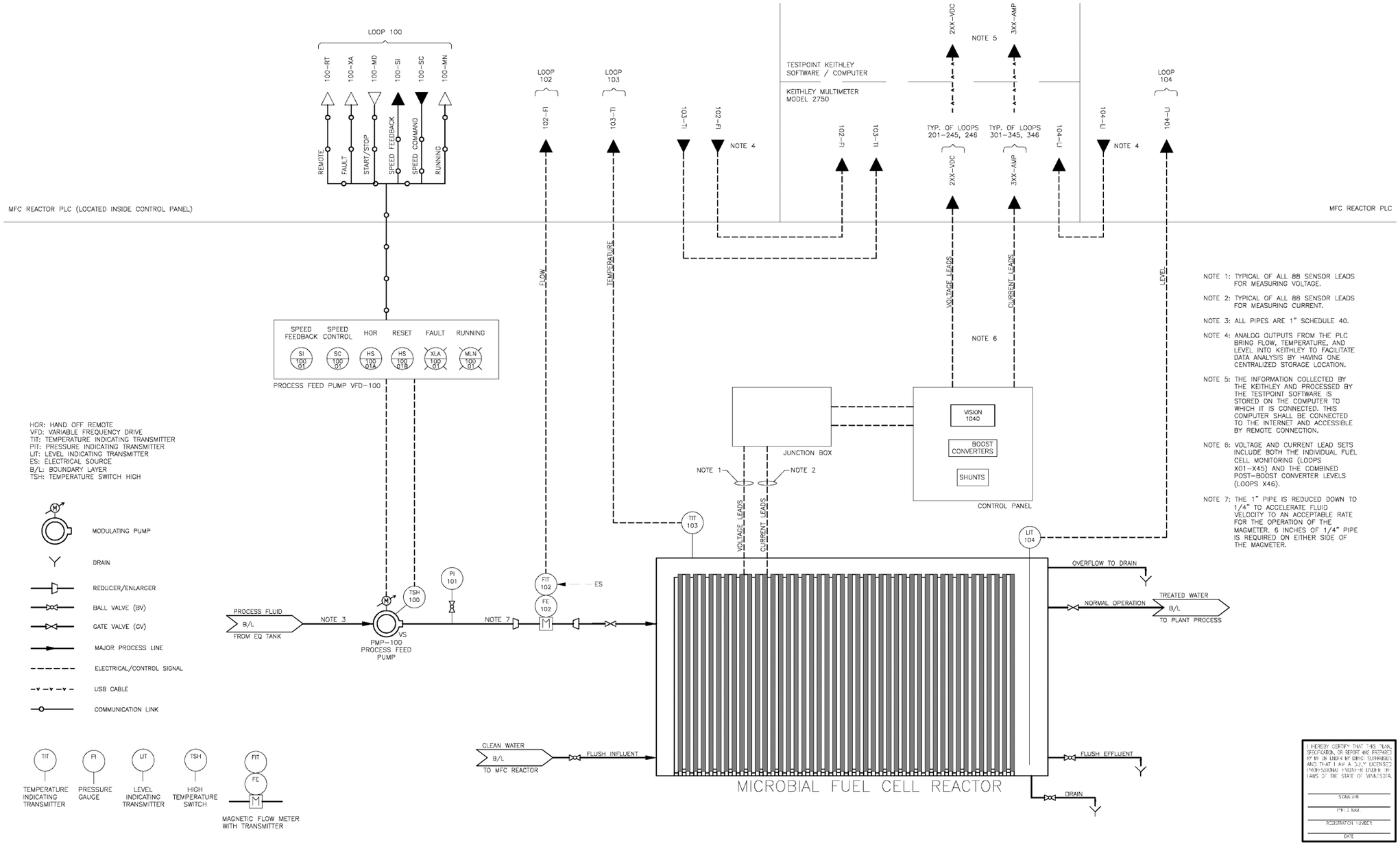

Figure 65. Process and instrumentation diagram for the MFC system.

BILL OF MATERIALS:

DATA ACQUISITION:
KEITHLEY 2750 DIGITAL MULTIMETER
3 7708 MULTIPLEXER MODULE EXPANSION CARDS
USB–GPIB INTERFACE ADAPTER MODEL KUSB–488B

DESKTOP COMPUTER:
REUSE AN EXISTING CDM SMITH MACHINE

PLC/HMI:
VISION V1040–T20B
I/O EXPANSION CARD: V200–18–E3XB

MAGNETIC FLOWMETER:
SIEMENS SITRANS F M MAG 1100 SENSOR
SIEMENS SITRANS F M MAG 5000 TRANSMITTER

TEMPERATURE INDICATING TRANSMITTER:
MORE INDUSTRIES TDY

LEVEL INDICATING TRANSMITTER:
SIEMENS LC300 CAPACITANCE LEVEL PROBE 3/4"

UPS:
APC BACK–UPS PRO 865 WATTS / 1500 VA

INTERNET MODEM:
VERIZON WIRELESS PANTECH 4G LTE USB MODEM AIRCARD UML295 4G

PRESSURE GAUGE:
ASHCROFT TYPE 1279 DURAGAUGE

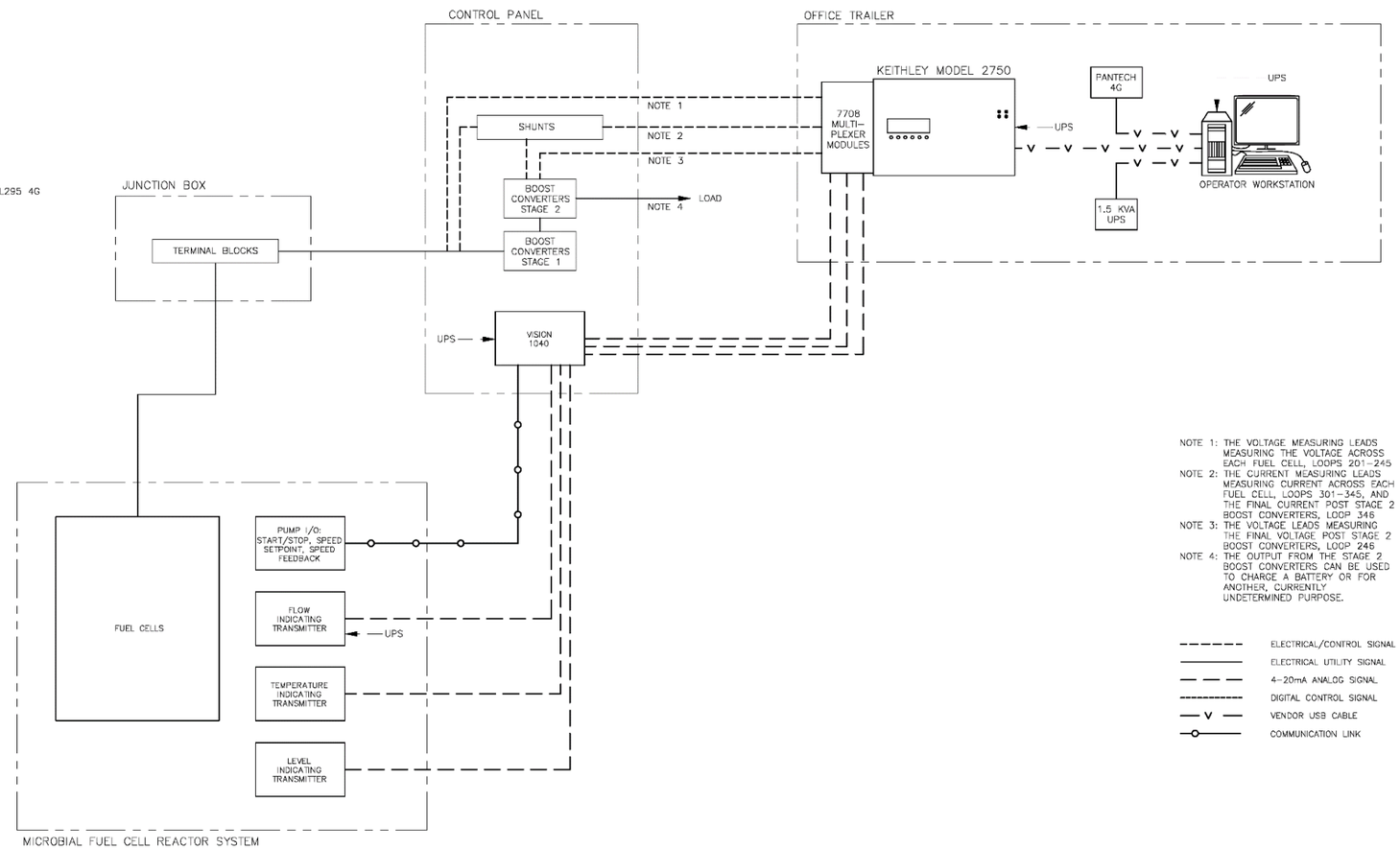

NOTE 1: THE VOLTAGE MEASURING LEADS MEASURING THE VOLTAGE ACROSS EACH FUEL CELL, LOOPS 201–245

NOTE 2: THE CURRENT MEASURING LEADS MEASURING CURRENT ACROSS EACH FUEL CELL, LOOPS 301–345, AND THE FINAL CURRENT POST STAGE 2 BOOST CONVERTERS, LOOP 346

NOTE 3: THE VOLTAGE LEADS MEASURING THE FINAL VOLTAGE POST STAGE 2 BOOST CONVERTERS, LOOP 246

NOTE 4: THE OUTPUT FROM THE STAGE 2 BOOST CONVERTERS CAN BE USED TO CHARGE A BATTERY OR FOR ANOTHER, CURRENTLY UNDETERMINED PURPOSE.

ELECTRICAL/CONTROL SIGNAL
ELECTRICAL UTILITY SIGNAL
4–20mA ANALOG SIGNAL
DIGITAL CONTROL SIGNAL
VENDOR USB CABLE
COMMUNICATION LINK

I HEREBY CERTIFY THAT THIS PLAN, SPECIFICATION, OR REPORT WAS PREPARED BY ME OR UNDER MY DIRECT SUPERVISION AND THAT I AM A DULY LICENSED PROFESSIONAL ENGINEER UNDER THE LAWS OF THE STATE OF MINNESOTA.

SIGNATURE

PRINTED NAME

REGISTRATION NUMBER

DATE

Figure 66. Process and instrumentation diagram for the MFC system.

Economic evaluation. Cost drivers for the process include those associated with capital equipment, operations and maintenance (O&M)), and downstream processing to meet discharge requirements. Capital equipment costs are difficult to estimate at this stage but the primary cost drivers are discussed below. O&M include labor, chemicals, power, and residuals management.

Cathode materials and fabrication. The cathode materials and associated fabrication costs are likely to be the greatest component of the capital cost until the day when they can be mass produced in quantity. Currently, no full-scale manufacturing process is available for manufacturing the cathodes. However, various such processes are being evaluated separately as part of ESTCP Project ER-201635: Hybrid Microbial Fuel Cell-Biofiltration System for Energy-Neutral Wastewater Treatment. In addition to the cathode material itself, several other components of the cathode module are required (e.g., spacer, separator, frame) and these need to be assembled. These other components are not necessarily expensive, but manufacturing can be expensive until molds have been made and the cathode modules are fabricated in bulk.

Anode materials and fabrication. The anodes are much simpler than the cathodes and essentially require carbon fiber and titanium wire. Standard brush manufacturing equipment is used to make the anodes.

Tankage, piping, and appurtenances. Tankage, piping, and appurtenances such as valves and fittings are standard materials and are not expected to be costly. Use of inexpensive epoxy coating technology on carbon steel avoids the use of more expensive materials such as stainless steel. As the technology matures fiberglass reinforced plastic (FRP) tanks can be design and manufactured at lower cost yet and also with lower weight.

Electrical, instrumentation, and controls

Electrical system for power recovery use inexpensive voltage booster devices that are commercially available. Instrumentation and controls are used to monitor voltage and current. Relatively expensive instrumentation is required to accurately monitor the lower voltages that are generated by MFCs. Additionally, wiring and associated electrical fittings need to be designed to minimize ohmic losses. These designs require use of larger wire diameters which add to the cost.

Labor. Labor is initially anticipated to be greater for any innovative systems because certified wastewater treatment plant operators are not familiar with the technology. However, as the technology becomes standard then the labor costs are anticipated to be similar to those for traditional processes. In the mean-time certain aspects are unknown such as the frequency of anode/cathode cleaning and maintenance. These activities will affect labor effort and cost.

Chemicals. Chemical use is anticipated to be a minor component. Acids may be required to regenerate the cathodes but the amount and cost of acid is expected to be small. Waste disposal will also be a cost but the volume is again expected to be small.

Power. One major advantage of the MFC is the power is generated rather than consumed. Thus electrical power is not an O&M cost.

Residuals management. Residuals include waste sludge that must be removed from the MFC and disposed. The characteristics (e.g., concentration, settleability) of this sludge are unknown. But standard technologies (coagulation, flocculation, settling, dewatering, drying) are available for use. The solids would then need to be landfilled or land applied in accordance with applicable regulations. Depending on the quality of the biosolids the residual disposal may be a cost or a revenue.

Additional capital and O&M costs will be associated with downstream treatment. A variety approaches are and ideally the process would be one that can cost-effectively meet treatment

objectives and operate on the power generated by the MFC. Options include the granular activated carbon biofilter (GAC-BF) and the anaerobic fluidized membrane biofilm reactor (AFMBR).[42]

4.7.2. Life Cycle Assessment

Life cycle assessments (LCAs) are conducted to quantify the environmental impacts over the useful life of different products, services and activities. In the case of this research, performing a LCA on these innovative technologies and comparing them to the status quo provides insight into whether or not replacing an existing technology with a new technology actually has a benefit with regard to the environment, on a life cycle basis. In this comparative LCA, each of the different life cycle categories are broken out into five distinct groups including, chemical use, capital goods, energy use, sludge disposal, and transportation. Additionally, four scales of typical FOBs were assessed, which included appropriate treatment technologies. The four scales ranging from smallest to largest included, company, battalion, brigade and division. By breaking out the LCA into categories and by size, the environmental differences of the innovative approaches to wastewater treatment at FOBs can be seen in direct comparison to what's currently being used. The results of the LCA, when coupled with financial and social impacts provides a tiered approach to decision making. The LCA introduced herein couples SERDP projects ER-2216 led by PSU and ER-2239 led by Arizona State University. As such the LCA is not complete; complete results will be reported in the SERDP report for ER-2239.

The basis of flow for each scale was developed using the information from SERDP Sustainable Forward Operating Bases,[53] where ranges of typical military group quantities are provided. The averages of these ranges were assumed for Company and Battalion size bases and the higher of the provided range of values is assumed for Brigade and Division groups, in order to be conservative. The same report also presents that 35 gal/day/person is an acceptable estimation of per capita wastewater production at military bases. Furthermore, it is assumed that an average of 15 percent of all wastewater could be classified as blackwater (BW) while rest would be gray water (GW).[53] These flows were applied to nominally sized Company, Battalion, Brigade, and Division nominally having 150, 600, 6000, and 20000 soldiers, respectively.

Typical wastewater compositions for BW and GW were obtained from various technical literature that related to similar scenarios as our chosen configurations. Using these values, average influent concentrations are calculated for chemical oxygen demand (COD), biochemical oxygen demand (BOD) and total suspended solids (TSS). In order to simplify the mass balance calculations, it was assumed that influent BOD_5 concentration is equal to half of the assumed influent COD value. The wastewater composition used in the basis of design for the treatment alternatives is summarized in Table 10.

Table 10. Assumed wastewater composition used for the LCA

Parameter	Blackwater	Graywater	Combined Wastewater
COD (mg/L)	8350	285	1500
TSS (mg/L)	4600	215	875

Once the scales of treatment and wastewater composition were established, it was important to identify primary treatment scenarios to be further developed. The scenarios were developed and revised over several iterations as part of finalizing the project objectives. The scenarios selected for evaluation are summarized as follows. For each of the four FOB scales, three scenarios were

evaluated corresponding to: conventional treatment, MFC with electricity production, and microbial electrolysis cell (MEC) with H_2O_2 production. For each of these scenarios, an additional evaluation was included to account for water re-use options, for a total of six alternative design scenarios as tabulated in Table 11.

Table 11. Scenarios evaluated in the LCA

Scenario	Process	Water Reuse
1	Conventional	No
2	MFC with electricity generation	No
3	MEC with H_2O_2 production	No
4	Conventional	Yes
5	MFC with electricity generation	Yes
6	MEC with H_2O_2 production	Yes

The methodology follows four stages of an LCA as defined in ISO 14040 standards: (1) definition of goals and scope; (2) life cycle inventory (LCI) analysis using various databases available in SimaPro 7.3.3, a LCA software which serves as the tool to collect and analyze the relative sustainability of a product or process; (3) life cycle impact assessment (LCIA) using ReCiPe v1.08 method using a hierarchist model typically applied to scientific LCAs; and (4) interpretation of results. The life cycle inventory (LCI), which is the raw data that will be entered into the LCA software, and LCIA were completed in SimaPro 7.3.3 using Ecoinvent 2.0 database, a vast compilation of pre-established life cycle inventory data for complete processes or materials and average world datasets when available. Average world datasets are used when location specific information is not available in the Ecoinvent 2.0 database.

The goal of this work is to compare the environmental impacts of the three main wastewater treatment processes at a FOB located 10-250 km from the source of potable drinking water. The functional unit, which is the definition of what is being studied and all subsequent LCI data is relative to this unit, chosen is one cubic meter of effluent wastewater produced during the two years the FOB is operational, which is the maximum operational time frame specified by the U.S. Army. The time frame encompasses wastewater treatment process construction and FOB operation and neglects decommissioning and warfare losses (excluding casualties). The system boundary (Figure 67) is a cradle-to-grave analysis of capital and supplies distribution to the FOB through treatment for a distribution center through wastewater treatment. The impacts from final disposal of the wastewater treatment plant at the FOB is not included in the scope of this research, however, the impact from disposal of sludge produced during the useful life of the FOB is assessed. The upstream processes include the distribution of capital, supplies and water to the FOB, water consumption, and wastewater treatment processes. Background processes include the materials, energy, transport and waste from capital goods manufacturing (including truck, water tank, and chemicals manufacturing) and transportation to and from the FOB.

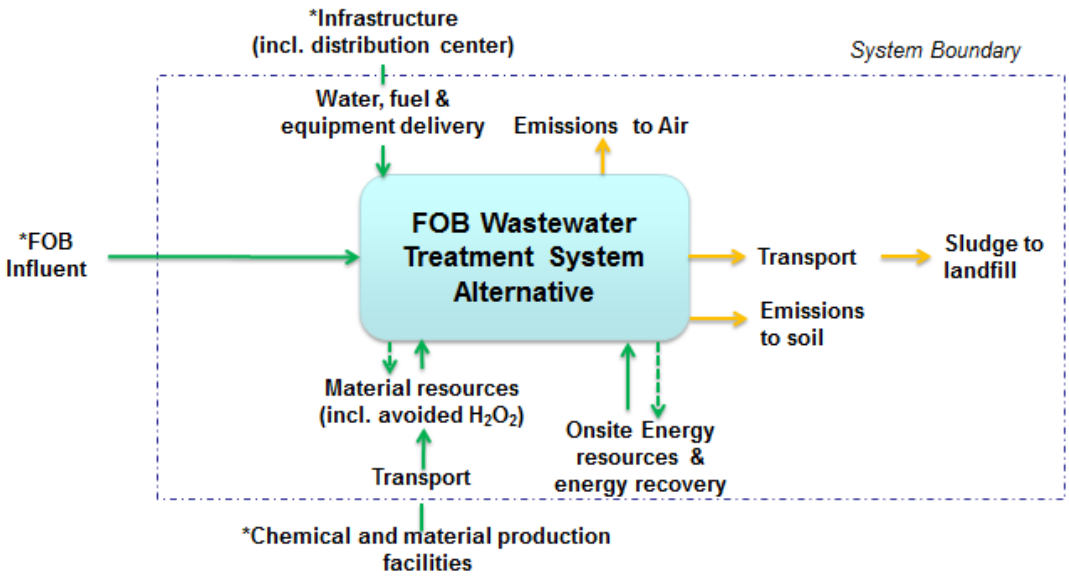

Figure 67. System boundary for the LCA.

The LCA includes an assessment of the environmental impacts of the six scenarios discussed above in SimaPro 7.3.3 using ReCiPe v1.08. We will show the results for the midpoint categories. Midpoint category values are determined by applying scientifically established characterization factors to relevant materials and processes from life cycle assessment to equate all materials and processes against a common reference substance. For example, all materials and processes included in the global warming potential midpoint category are expressed in terms of kg CO_2 equivalents. To equate methane as CO_2 equivalents, the scientific community has determined that methane is 25 times more potent a greenhouse gas than CO_2; thus the global warming potential characterization factor for methane is 24. For this analysis, we have chosen six midpoint categories to represent human health and environmental impacts: climate change, ozone depletion, human toxicity, particulate matter formation, climate change to ecosystems, terrestrial ecotoxicity, freshwater ecotoxicity, and fossil depletion.

In addition to the environmental impacts, we are estimating the impact on soldier causalities based on the number of truck trips required to supply the FOB. We will determine casualty factors based on data obtained from both wars in Iraq and Afghanistan during the year 2007.[69] We will create casualty factors for both water and fuel resupply convoys. We will allocate the total number of casualties in the reference year to the movement of a commodity using the following percentages: 50% for fuel and 20% for drinking water. To estimate the total number of casualties for fuel resupply, the total number of gallons transported by a Theater will be divided by the average capacity of a 16 Supply Truck Convoy. The same methodology will be employed for calculating the total number of casualties for water resupply convoys in the reference year, but also assuming that 80% of the treated water is available for reuse in the reuse scenarios. The total number of casualties by convoy type, using the percentages referenced above, will then divided by the total number of convoys in 2007 to determine the casualty factor for water and fuel resupply convoys respectively.[69] The number of convoys for both water and fuel resupply over the entire two year operating period will be multiplied by the average casualty factor calculated from each war to obtain the total number of casualties over the useful life of the FOB.

5. Conclusions and Implications for Future Research/Implementation

These results clearly showed that it was necessary to keep the anode brushes fully covering the cathode, and that brush mass (total amount of carbon fiber in the brush) was less important that full cathode coverage. Thus, brushes should be placed to fully cover the cathode in order to obtain the maximum performance of the reactors. Brush diameter was a more complex issue as small brushes (<1 cm diameter) that fully covered the cathode projected area worked better than larger brushes when acetate was used at high concentrations, in a well buffered system. However, when these were used with wastewater, performance was erratic. Therefore, we concluded that the optimum cathode sizes are the larger brushes that have diameters of 2-2.5 cm. These brushes will therefore be used in all future tests with the wastewater.

All tests with PVA separators were completed in fed-batch tests with acetate or wastewater. The PVA can be used as a separator in MFCs with comparable results to wipe separators in both AC and Pt cathode MFCs. In a low conductivity solution, where solution resistance is a main component of total resistance, addition of a PVA separator had no effect on power densities. In higher conductivity solutions, where solution resistance is a smaller part of total resistance, the impact of PVA on power production became larger with solution conductivity. A spray-on separator can be used in place of a cast separator to achieve similar power densities and CEs, but with increased cycle times. We concluded the performance with PVA separators was about the same as the cloth separators, but the cloth performance was more stable over time and therefore that cloth separators should be used.

Of the different spacers examined, the wire spacers produced the best performance as they minimized blockage of the cathode surface and allowed good air flow to the cathode, resulting in a reactor design that produced the highest power densities obtained to date in larger reactors using domestic wastewater. This new design provides an easy method to construct and install electrodes, and at the same time it produced relatively high power densities with domestic wastewater. It was concluded that wire spacers provided the best operation relative to COD removal and current densities.

Cathode performance is important for good power generation. Of the different cathode materials and preparation methods, the best results were obtained by blending 10% CB into AC, resulting in improved performance with the maximum power densities increased by 16% in the first week, and by 29% after 3.5 months, compared to MFCs with plain AC. MFCs with Fe-modified and heat-treated AC produced maximum power densities that were approximately 35% higher than plain AC. During long-term operation, all AC-based cathodes had significantly improved power densities compared with Pt cathodes. The PVDF binder with activated carbon using a phase inversion process provided an excellent best cathode binder as it is inexpensive, and easy to apply by immersion in water. Cathode fouling is a challenge, and to explore possible reasons for fouling we examined the impact of high concentration of humic acids on cathodes. Substantial adsorption of humic acids reduced power, but only by $\leq$14%. This suggests that there are other more critical reasons for a reduction in power over long periods of time, such as microbially produced biopolymers or precipitated salts.

COD was effectively removed using modular MFCs containing arrays of brush anodes and dual cathodes modules. Experiments conducted with domestic wastewater, similar gray water at an FOB, and diluted swine wastewater to simulate black water, indicated that treating combined gray and black water will be more efficient than individual treatment, as black water COD was difficult to treat. Combining the two wastewaters produces a COD suitable for effective treatment.

For MFC operation, careful consideration will need to be given in the future to whether they are operated to maximize power or to produce high current densities. Increasing current density, by using reduced electrical loads (lower external resistors), will increase the rate of COD removal and thus could lead to shorter HRTs. However, higher current densities will lower the voltage, reducing recoverable power. The tradeoffs in HRT and COD removal rate with power production should be further examined in future pilot scale tests. Thus the MFC may be operated under energy-positive, energy-neutral, or energy-negative conditions depending on the overall objectives for wastewater treatment.

The startup time for a larger, pilot scale reactor is anticipated to be on the order of 2-6 weeks. In the laboratory, small reactors (0.1 L size) required startup times of ~2-4 weeks. Larger reactors (2-6 L) required slightly longer times, of ~4 weeks. We estimate that a field reactor, if fed with effluent from smaller reactors and wastewater, could start within this time frame. However, as such a large scale reactor has never been started up in the field, this remains a research question.

Long-term reliability is difficult to assess based on the short-term experiments conducted in this study. Planned ESTCP demonstration work will address this data gap.

Implications for future research

The results of this work produced design parameters that enabled the development of a prototype design with specifications for anode area, cathode area, catalysts, HRTs, electrical resistance specifications for the load, spacer requirements, and overall MFC architecture. The next step in the development of MFCs for FOBs is construction and testing of this reactor under the ESTCP program, as this would allow performance of a larger MFC to be examined at a DOD site. ESTCP project Number ER-201635, Hybrid Microbial Fuel Cell-Biofiltration System for Energy-Neutral Wastewater Treatment, is currently underway which will fulfill this next step. The objectives of this ESTCP project are to:

- Integrate the MFC and BF technologies in an operator friendly configuration.
- Demonstrate the production of high-quality re-usable water that meets U.S. Environmental Protection Agency (USEPA) Guidelines for Water Reuse.
- Demonstrate a reduction in energy consumption relative to conventional aerobic wastewater treatment technology.
- Demonstrate a reduction in residuals (sludge) compared to aerobic bioreactors.
- Compare the cost and performance of the MFC-BF system to conventional treatment systems used for water reuse such as ultrafiltration/reverse osmosis.
- Generate life cycle cost data to confirm a payback period of less than 10 years.

These objectives will address specific questions regarding: 1) the energy footprint of the overall process considering that downstream polishing is required to reduce the MFC effluent COD to less than 100-200 mg/L; and 2) relative benefits of the MFC-BF system compared to conventional treatment processes. The demonstration will involve final design, manufacture and testing of a pilot-scale MFC-BF system capable of treating about 2 L/min (0.5 gpm). Several scale-up parameters should be monitored that will facilitate FOB implementation. These include:

- BOD and COD removal
- Organic loading rate
- Hydraulic residence time
- Solids production
- Power consumption or generation
- Voltage and current

- Cathode cleaning frequency and requirements
- Other maintenance requirements

6. Literature Cited

1. Logan, B.E. and J.M. Regan, *Microbial fuel cells—challenges and applications.* Environmental Science & Technology, 2006. **40**(17): p. 5172-5180.
2. Liu, H., R. Ramnarayanan, and B.E. Logan, *Production of electricity during wastewater treatment using a single chamber microbial fuel cell.* Environmental Science & Technology, 2004. **38**(7): p. 2281-2285.
3. Logan, B.E., *Extracting hydrogen and electricity from renewable resources.* Environmental Science & Technology, 2004. **38**(9): p. 160A-167A.
4. Logan, B.E., et al., *Microbial fuel cells: methodology and technology.* Environmental Science & Technology, 2006. **40**(17): p. 5181-5192.
5. Cheng, S., H. Liu, and B.E. Logan, *Power densities using different cathode catalysts (Pt and CoTMPP) and polymer binders (Nafion and PTFE) in single chamber microbial fuel cells.* Environmental Science & Technology, 2006. **40**: p. 364-369.
6. Zhao, F., et al., *Application of pyrolysed iron (II) phthalocyanine and CoTMPP based oxygen reduction catalysts as cathode materials in microbial fuel cells.* Electrochemistry Communications, 2005. **7**: p. 1405-1410.
7. Logan, B.E., *Materials for BES*, in *Bioelectrochemical systems: from extracellular electron transfer to biotechnological applications*, K. Rabaey, et al., Editors. 2010, IWA Publishing: London. p. 184-204.
8. Logan, B.E., *Microbial fuel cells*. 2008, Hoboken, NJ: John Wiley & Sons, Inc. 300.
9. Logan, B.E., et al., *Graphite fiber brush anodes for increased power production in air-cathode microbial fuel cells.* Environmental Science & Technology, 2007. **41**(9): p. 3341-3346.
10. Xie, X., et al., *Three-dimensional carbon nanotube−textile anode for high-performance microbial fuel cells.* Nano Letters, 2010. **11**(1): p. 291-296.
11. Saito, T., et al., *Effect of nitrogen addition on the performance of microbial fuel cell anodes.* Bioresource Technology, 2011. **102**(1): p. 395-398.
12. Zhu, N., et al., *Improved performance of membrane free single-chamber air-cathode microbial fuel cells with nitric acid and ethylenediamine surface modified activated carbon fiber felt anodes.* Bioresource Technology, 2011. **102**(1): p. 422-426.
13. Fan, Y., et al., *Nanoparticle decorated anodes for enhanced current generation in microbial electrochemical cells.* Biosensors and Bioelectronics, 2011. **26**(5): p. 1908-1912.
14. Selembo, P.A., M.D. Merrill, and B.E. Logan, *The use of stainless steel and nickel alloys as low-cost cathodes in microbial electrolysis cells.* Journal of Power Sources, 2009. **190**(2): p. 271-278.
15. Zhang, Y., M.D. Merrill, and B.E. Logan, *The use and optimization of stainless steel mesh cathodes in microbial electrolysis cells* International Journal of Hydrogen Energy, 2010. **35**(21): p. 12020-12028.
16. Zhang, F., et al., *Microbial fuel cells cathodes constructed from stainless steel mesh that use poly(dimethylsiloxane) diffusion layers.* Environmental Science & Technology, 2010. **44**(4): p. 1490-1495.
17. Rozendal, R.A., H.V.V. Hamelers, and C.J.N. Buisman, *Effects of membrane cation transport on pH and microbial fuel cell performance.* Environmental Science & Technology, 2006. **40**(17): p. 5206-5211.
18. Rozendal, R.A., et al., *Effect of the type of ion exchange membrane on performance, ion*

transport, and pH in biocatalyzed electrolysis of wastewater. Water Science and Technology, 2008. **57**(11): p. 1757-1762.
19. Kim, J.R., et al., *Power generation using different cation, anion and ultrafiltration membranes in microbial fuel cells.* Environmental Science & Technology, 2007. **41**(3): p. 1004-1009.
20. Zhang, X., et al., *Separator characteristics for increasing performance of microbial fuel cells.* Environmental Science & Technology, 2009. **43**(21): p. 8456-8461.
21. Zhang, X., et al., *Scalable air cathode microbial fuel cells using glass fiber separators, plastic mesh supporters, and graphite fiber brush anodes.* Bioresource Technology, 2011. **102**(1): p. 372-375.
22. Watson, V.J., et al., *Polymer coatings as separator layers for microbial fuel cell cathodes.* Journal of Power Sources, 2011. **196**(6): p. 3009-3014.
23. Fan, Y., H. Hu, and H. Liu, *Enhanced coulombic efficiency and power density of air-cathode microbial fuel cells with an improved cell configuration.* Journal of Power Sources, 2007. **171**(2): p. 348-354.
24. Shizas, I. and D.M. Bagley, *Experimental determination of energy content of unknown organics in municipal wastewater streams.* Journal of Energy Engineering, 2004. **130**(2): p. 45-53.
25. Heidrich, E.S., T.P. Curtis, and J. Dolfing, *Determination of the internal chemical energy of wastewater.* Environmental Science & Technology, 2011. **45**(2): p. 827–832.
26. Ahn, Y. and B.E. Logan, *Domestic wastewater treatment using microbial fuel cells and electrical energy production.* Bioresource Technology, 2009. **101**(2): p. 469-475.
27. Hays, S., *Performance of membrane electrode assembly microbial fuel cells using activated carbon cathodes with various diffusion layers*, in *Department of Civil & Environmental Engineering*. 2011, Penn State University: University Park.
28. Cusick, R.D., et al., *Performance of a pilot-scale continuous flow microbial electrolysis cell fed winery wastewater.* Applied Microbiology and Biotechnology, 2011. **89**(6): p. 2053–2063.
29. Liu, H., S. Cheng, and B.E. Logan, *Production of electricity from acetate or butyrate in a single chamber microbial fuel cell.* Environmental Science & Technology, 2005. **39**(2): p. 658-662.
30. Pant, D., et al., *A review of the substrates used in microbial fuel cells (MFCs) for sustainable energy production.* Bioresource Technology, 2009. **101**(6): p. 1533–1543.
31. Lanas, V. and B.E. Logan, *Evaluation of multi-brush anode systems in microbial fuel cells.* Bioresource technology, 2013. **148**: p. 379-385.
32. Lanas, V., Y. Ahn, and B.E. Logan, *Effects of carbon brush anode size and loading on microbial fuel cell performance in batch and continuous mode.* Journal of Power Sources, 2014. **247**: p. 228-234.
33. Hoskins, D.L., et al., *Spray-on polyvinyl alcohol separators and impact on power production in air-cathode microbial fuel cells with different solution conductivities.* Bioresource technology, 2014. **172**: p. 156-161.
34. Kim, K.-Y., W. Yang, and B.E. Logan, *Impact of electrode configurations on retention time and domestic wastewater treatment efficiency using microbial fuel cells.* Water research, 2015. **80**: p. 41-46.
35. He, W., et al., *Microbial fuel cells with an integrated spacer and separate anode and cathode modules.* Environmental Science: Water Research & Technology, 2016. **2**(1): p.

186-195.
36. He, W., et al., *The effect of flow modes and electrode combinations on the performance of a multiple module microbial fuel cell installed at wastewater treatment plant.* Water Research, 2016. **105**: p. 351-360.
37. Dong, Y., et al., *A 90-liter stackable baffled microbial fuel cell for brewery wastewater treatment based on energy self-sufficient mode.* Bioresource technology, 2015. **195**: p. 66-72.
38. Yang, W., et al., *Single-step fabrication using a phase inversion method of poly (vinylidene fluoride)(PVDF) activated carbon air cathodes for microbial fuel cells.* Environmental Science & Technology Letters, 2014. **1**(10): p. 416-420.
39. Ahn, Y. and B. Logan, *Domestic wastewater treatment using multi-electrode continuous flow MFCs with a separator electrode assembly design.* Applied Microbiology and Biotechnology, 2013. **97**(1): p. 409-416.
40. Yang, W., K.-Y. Kim, and B.E. Logan, *Development of carbon free diffusion layer for activated carbon air cathode of microbial fuel cells.* Bioresource Technology, 2015. **197**: p. 318-322.
41. Wei, B., et al., *Development and evaluation of carbon and binder loading in low-cost activated carbon cathodes for air-cathode microbial fuel cells.* Rsc Adv., 2012. **2**(33): p. 12751-12758.
42. Ren, L., Y. Ahn, and B.E. Logan, *A Two-Stage Microbial Fuel Cell and Anaerobic Fluidized Bed Membrane Bioreactor (MFC-AFMBR) System for Effective Domestic Wastewater Treatment.* Environmental Science & Technology, 2014. **48**(7): p. 4199-4206.
43. Zhang, X., et al., *Enhanced activated carbon cathode performance for microbial fuel cell by blending carbon black.* Environmental science & technology, 2014. **48**(3): p. 2075-2081.
44. Zhang, X., et al., *Long-term performance of chemically and physically modified activated carbons in air cathodes of microbial fuel cells.* ChemElectroChem, 2014. **1**(11): p. 1859-1866.
45. Yang, W., V.J. Watson, and B.E. Logan, *Substantial humic acid adsorption to activated carbon air cathodes produces a small reduction in catalytic activity.* Environmental Science & Technology, 2016. **50**(16): p. 8904-8909.
46. Zhang, X., et al., *COD removal characteristics in air-cathode microbial fuel cells.* Bioresource technology, 2015. **176**: p. 23-31.
47. He, W.H., et al., *Microbial fuel cells with an integrated spacer and separate anode and cathode modules.* Environ. Sci. Water Res. Technol., 2016. **2**: p. 186-195.
48. Oh, S., B. Min, and B.E. Logan, *Cathode performance as a factor in electricity generation in microbial fuel cells.* Environmental science & technology, 2004. **38**(18): p. 4900-4904.
49. Logan, B.E., et al., *Assessment of microbial fuel cell configurations and power densities.* Environmental Science & Technology Letters, 2015. **2**(8): p. 206-214.
50. Cheng, S. and B.E. Logan, *Increasing power generation for scaling up single-chamber air cathode microbial fuel cells.* Bioresource Technology, 2011. **102**(6): p. 4468-4473.
51. Fan, Y., S.-K. Han, and H. Liu, *Improved performance of CEA microbial fuel cells with increased reactor size.* Energy & Environmental Science, 2012. **5**(8): p. 8273-8280.
52. Kim, K.-Y., et al., *Continuous treatment of high strength wastewaters using air-cathode microbial fuel cells.* Bioresource Technology, 2016. **221**: p. 96-101.
53. Barry, J.A., *Characterization of DoD Installation Wastewater Treatment.* *http://www.serdp.org/Program-Areas/Environmental-Restoration/Wastewater-and-*

Drinking-Water/Noblis-Report. 2012.
54. Wendland, C., *Anaerobic digestion of blackwater and kitchen refuse*. 2008, Technical University of Hamburg-Harburg.
55. Oarga, A., *Blackwater treatment at tourist facilities*. 2013, University of Nova Gorica Graduate School.
56. Elimitwalli, T., *Treatment of concentrated black-water and kitchen organic-wastes in accumulation systems*, in *Tenth International Water Technology Conference, IWTC10* 2006: Alexandria, Egypt.
57. de Graaff, M.S., *Resource recovery from black water*. 2010, Wageningen University.
58. Wendland, C., et al., *Anaerobic digestion of blackwater from vacuum toilets and kitchen refuse in a continuous stirred tank reactor (CSTR)* Water Science and Technology, 2007. **55**(7): p. 187-194.
59. Lerke, T., S. Riggs, and H. Castle, *Demonstration of advanced oxidation treatment of shipboard blackwater and graywater. ESTCP report WP-200802*. 2010.
60. USEPA, *Handbook. Septage treatment and disposal. EPA-625/6-84-009*. 1984.
61. Atasoy, E., et al., *Membrane bioreactor (MBR) for treatment of segregated household wastewater for reuse.* Clean, 2007. **35**(5): p. 465-472.
62. Palmquist, H. and J. Hanaeus, *Hazardous substances in separately collected grey- and black-water from ordinary Swedish households.* Science of the Total Environment, 2005. **348**: p. 151-163.
63. CDM Smith, *Cruise ship wastewater study.* 2000.
64. Tchobanoglous, G., F.L. Burton, and H.D. Stensel, *Wastewater Engineering. Treatment, Disposal, and Reuse*. Fourth ed. 2003, New York: McGraw Hill.
65. USEPA, USAID, and CDM Smith, *2012 Guidelines for Water Reuse. EPA/600/R-12/618*. 2012.
66. SEPUP. *Hydrogen and fuel cells: science behind fuel cells.* *http://sepuplhs.org/high/hydrogen/hydrogen.html*. 2015.
67. Kim, Y., et al., *Capturing power at higher voltages from arrays of microbial fuel cells without voltage reversal.* Energy & Environmental Science, 2011. **4**: p. 4662-4667.
68. Wang, H., J.D. Park, and Z.J. Ren, *Practical energy harvesting for microbial fuel cells: a review.* Environ Sci Technol, 2015. **49**(6): p. 3267-77.
69. Army Environmental Policy Institute, *Sustain the Mission Project: Casualty Factors for Fuel and Water Resupply Convoys Final Technical Report*. 2009.

Appendix A

Process-Mechanical Engineering Calculations and Details

MFC Pilot System Design

1.0 Purpose/Objective

These calculations are to support the design of a microbial fuel cell (MFC) for an ESTCP demonstration. The objective of the calculation is to determine the number of anode and cathode modules required to treat wastewater from Ft. Riley

2.0 Procedure

2.1 State assumptions and constants. These include water quality and flow assumptions, material related constants, and anode and cathode dimensions.
2.2 Sizing calculations
2.21 Calculate required liquid volume of reactor based on design COD removal.
2.22 Calculate required number of anode and cathode modules.
2.23 Calculate required tank volume based on required liquid volume and volume of electrode modules.
2.24 Calculate required tank length based on electrode module dimensions.
2.25 Calculate required tank length based required volume (water and electrodes), cathode width, and max water depth. This length must be less than or equal to length based on electrode dimensions.
2.3 Electrical calculations
2.31 State assumptions and constants. These include the Coulombic efficiency, the molecular weight of COD, and the Faraday constant.
2.32 Calculate the volumetric and areal current density.
2.32 Calculate the maximum current derived from the first module based on it's volume (used volume based on 3-D model)
2.33 Calculate the power for one anode module based on the voltage and the max current.
2.34 Caculate the total power generated in the MFC by mulitplying the power for one anode module by the total number of modules.
2.35 Calculate the power generated per gram of COD based on the total power of the MFC, the flow rate, and the change in COD through the MFC.
2.36 Calculate the power generated per volume of water treated based on the total power and the flow rate.

3.0 References/Data Sources

3.1 PSU data from SERDP project - Section 5
3.2 Ft. Riley wastewater data

4.0 Assumptions

Water Quality and Flow

$BOD := 320 \frac{mg}{L}$

Based on historical data from Ft. Riley.

$COD_{Influent} := 2 \bullet BOD = 640 \bullet \frac{mg}{L}$

Based on laboratory observations from Penn State and general understanding of relationship between BOD and COD.

$COD_{Effluent} := 150 \frac{mg}{L}$

At COD concentrations less than 150ppm, no power is generated. There will be a biologically active carbon filter downstream to remove remaining COD.

$COD_{removal} := \frac{COD_{Influent} - COD_{Effluent}}{COD_{Influent}} = 0.77$

Will be used in kinetic equation to determine required hydraulic residence time.

$Q_{water} := 0.5 \frac{gal}{min}$

Wastewater flow rate - these are arbitrary and may change based on the cost of the reactor.

Material Related Constants

$Depth_{max.water} := 2ft$

Water depth is limited by the ability of the cathode material to sustain water pressure. This may change based on cathode material.

$Specific_Area_{Cathode} := 0.57 \frac{cm^2}{mL}$

This is the cathode area required per unit volume of wastewater, based on experiments at Penn State.

$Specific_Projected_Area_{Anode} := 0.19 \frac{cm^2}{mL}$

This is the anode projected area required per unit volume of wastewater, based on experiments at Penn State.

Anode Related Material Dimensions

$Diameter_{Anode} := 1in$ This is the diameter of anodes that are available for use.

$Length_{Anode} := 1ft + 10in = 1.83 \bullet ft$ Based on the maximum water depth defined above.

$Anode_Cathode_Spacing := \frac{1}{2}in$ This is the spacing between the edge of the anode brush and the angle iron This is the minimum amount of space that is required to remove the anode module from the reactor without contacting the cathode module. Penn State research indicated 0.8mm, but they did not use the angle irons.

$Width_{anode_module} := Diameter_{Anode} + 2 \bullet Anode_Cathode_Spacing = 2 \bullet in$

Cathode Related Material Dimensions

$Width_{Frame.Components} := \frac{13}{16}in + 2 \bullet (2mm + 1mm) + 2 \bullet \frac{1}{8}in + 2 \bullet 1.7mm + 2 \bullet \frac{1}{4}in = 1.93 \bullet in$

$Width_{Cathode.module} := 1in + \frac{15}{16}in = 1.94 \bullet in$ From model

The frame width comprises the spacer width (see **Calc # XX**, 20 mm or about 13/16"), the width of two cathode (2mm each) meshes plus separators (1mm each), the width of two cathode fasteners (1/8" each), the width of two sets of fastener bolts heads (1.7mm each), and the width of 2 plastic pieces that rest on the angle irons.

5.0 Calculations

Required Reactor Volume

$k_{COD} := \frac{4}{day}$ First-order rate constant for COD removal, determined through experiments at Penn State.

$$t_{HRT} := \frac{\ln\left(\frac{1}{1 - COD_{removal}}\right)}{k_{COD}} = 8.7 \bullet hr$$

Hydralic residence time based on first order decay.

$V_{water} := Q_{water} \bullet t_{HRT} = 989 \bullet L$ Required liquid volume at each flow rate defined above.

Required Number of Cathode Assemblies

$Area_{Cathode_total} := Specific_Area_{Cathode} \bullet V_{water} = 56.35\,m^2$

Required cathode area.

$Height_{Cathode.sheet} := 2ft \quad Width_{Cathode.sheet} := 3.5ft$

$Area_{Cathode.sheet} := Height_{Cathode.sheet} \bullet Width_{Cathode.sheet} = 0.65 \bullet m^2$

$Width_{Fastener} := \frac{1}{2}in = 0.5 \bullet in$

$Area_{Fastener.1} := 2 \bullet (Width_{Fastener} \bullet Height_{Cathode.sheet}) = 0.17 \bullet ft^2$

$Area_{Fastener.2} := (Width_{Cathode.sheet} - 2 \bullet Width_{Fastener}) \bullet Width_{Fastener} = 0.14 \bullet ft^2$

$Area_{Fastener} := Area_{Fastener.1} + Area_{Fastener.2} = 0.03 \bullet m^2$

$EffectiveArea_{Cathode.sheet} := Area_{Cathode.sheet} - Area_{Fastener} = 6.69 \bullet ft^2$

$Number_{Cathodes} := round\left(\frac{Area_{Cathode_total}}{Area_{Cathode.sheet}}\right) = 87 \qquad Number_{Cathodes_per_module} := 2$

$Number_{Cathode.modules} := Round\left(\frac{Number_{Cathodes}}{Number_{Cathodes_per_module}}, 1\right) = 44$

Required Number of Anode Assemblies

$Area_{Anode_total} := Specific_Projected_Area_{Anode} \bullet V_{water} = 18.78\,m^2$

Required anode proejcted area.

$Diameter_{Anode} = 1 \bullet in$

$Area_Projected_{Anode_single} := Diameter_{Anode} \bullet Length_{Anode} = 0.01\,m^2$

$Number_{Anodes} := Round\left(\frac{Area_{Anode_total}}{Area_Projected_{Anode_single}}, 1\right) = 1323$

$Number_{Anode.modules} := Number_{Cathode.modules} + 1 = 45$

This accounts for the one extra anode module at the end of the reactor.

$Number_{Anodes_per_module} := Round\left(\frac{Number_{Anodes}}{Number_{Anode.modules}}, 1\right) = 29$

Required Tank Volume

$V_{water} = 988.56\,L$

$V_{Anode} := 0$ Anode volume is mostly water

$Width_{Spacer} := \frac{13}{16}in$ $Width_{Mesh} := 2mm$ $Width_{Separator} := 1mm$

These are the elements on the cathode assembly that are under water.

$Width_{CathodeUnderWater} := Width_{Spacer} + 2 \bullet (Width_{Mesh} + Width_{Separator}) = 1.05 \bullet in$

$V_{cathode.assembly} := 1018.49in^3 = 16.69\,L$

From 3-D model based on cathode assembly components described above. Model is more accurate because it includes frame.

$V_{cathode.assembly.check} := Area_{Cathode.sheet} \bullet Width_{CathodeUnderWater} = 17.32\,L$

$V_{nonwater} := V_{cathode.assembly} \bullet Number_{Cathode.modules} = 734.36\,L$

$V_{total} := V_{water} + V_{nonwater} = 1722.92\,L$

Required Tank Length Based on Required Number of Anodes and Cathodes

$Width_{Cathode.module} = 1.94 \bullet in$

$Length_1 := Number_{Cathode.modules} \bullet Width_{Cathode.module} = 7.1 \bullet ft$

$Width_{Anode.plate} := \frac{35}{16}in = 2.19 \bullet in$

$Length_2 := Number_{Anode.modules} \bullet Width_{Anode.plate} = 8.2 \bullet ft$

$Length_{Edge} := 8in$ Length between anode reactors at ends of tank and tank edge.

$Min_Length_{Reactor} := Length_1 + Length_2 + 2 \bullet Length_{Edge} = 5.07 \bullet m$

Required Tank Length Based on Required Volume of Water Plus Electrode Dimensions

$Length_{Spacer} := 3ft + 5in = 1.04\,m$ $\quad Length_{Frame} := 1in + \frac{1}{16}in = 0.03\,m$

$Length_{Cathode.module} := Length_{Spacer} + 2 \bullet Length_{Frame} = 3.59 \bullet ft$

$Width_{Reactor} := Length_{Cathode.module} + 2 \bullet 1in = 3.76 \bullet ft$

$$Length_{Reactor} := \frac{V_{total}}{(Depth_{max.water} \bullet Width_{Reactor})} = 8.09 \bullet ft$$

Design is OK if this length is less than or equal to the length required based soley on required number of electrodes.

Cost

$dollars := ¤$

$$Unit_Cost_{cathode} := \frac{70dollars}{(20cm \bullet 20cm)}$$

$Cost_{cathode} := Area_{Cathode_total} \bullet Unit_Cost_{cathode} = 98609 \bullet dollars$

Electrical Calculations

Assumptions - to match 3-D "model"

$Q_e := 0.5gpm$ $\quad Number_{Anodes.per.module.e} := 29$

$V_{water.e} := Q_e \bullet t_{HRT} = 989 \bullet L$ $\quad Number_{Anode.modules.e} := 45$

$$CE := \begin{pmatrix} 1.7 \\ 30 \end{pmatrix}\%$$

Coulombic efficiency based on Penn State experiments.

$$R_{COD_max} := k_{COD} \bullet COD_{Influent} = 2560 \bullet \frac{mg}{L \bullet day}$$

Maximum COD removal rate.

$FW_{COD} := 32\frac{gm}{mol}$ $\quad n := 4\frac{mol}{mol}$ $\quad F := 26.801\frac{A \bullet hr}{mol}$

Constants

$$Volumetric_Current_Density := \frac{CE \bullet R_{COD_max} \bullet F \bullet n}{FW_{COD}} = \begin{pmatrix} 6.07 \\ 107.2 \end{pmatrix}\frac{A}{m^3}$$

Specific current density

$$Areal_current_density := \frac{Volumetric_Current_Density}{Specific_Area_{Cathode}} = \begin{pmatrix} 0.11 \\ 1.88 \end{pmatrix}\frac{A}{m^2}$$

The value at the lower efficiency is slightly greater than Kyoug-Yeol's estimate of 0.04 mA/cm2

Calculate current delivered from first anode module. First calculate volume of one anode module.

$$V_{anode_module} := \frac{V_{water.e}}{Number_{Anode.modules.e}} = 21.97\,L$$

Assume module volume is equal to space taken up in model.

$$V_{anode.module.modeled} := Depth_{max.water} \bullet Width_{Anode.plate} \bullet Width_{Reactor} = 38.82\,L$$

Calculate current for one anode module

$$Current_{anode.module} := Volumetric_Current_Density \bullet V_{anode.module.modeled} = \begin{pmatrix} 0.24 \\ 4.16 \end{pmatrix} A$$

Calculate power density for one anode module

$$Voltage := 0.2V \qquad Power := Current_{anode.module} \bullet Voltage = \begin{pmatrix} 47.17 \\ 832.37 \end{pmatrix} \bullet mW$$

$$Power_Density_{volumetric} := \frac{Power}{V_{anode.module.modeled}} = \begin{pmatrix} 1.21 \\ 21.44 \end{pmatrix} \bullet \frac{W}{m^3}$$

$$Power_Density_{areal} := \frac{Power}{Area_{Cathode.sheet}} = \begin{pmatrix} 72.53 \\ 1279.94 \end{pmatrix} \bullet \frac{mW}{m^2}$$

The PSU estimate of 280 mW/m2 is in between these two values.

Calculate power for total MFC

$$Power_{MFC} := Power \bullet Number_{Anode.modules.e} = \begin{pmatrix} 2.12 \\ 37.46 \end{pmatrix} W$$

Total current

$$Current_{MFC} := \frac{Power_{MFC}}{Voltage} = \begin{pmatrix} 10.61 \\ 187.28 \end{pmatrix} A$$

Calculate energy per unit COD removed from the reactor

$$kJ := 1000J$$

$$Energy_{COD} := \frac{Power_{MFC}}{\left(COD_{Influent} - COD_{Effluent}\right) \bullet Q_e} = \begin{pmatrix} 0.14 \\ 2.42 \end{pmatrix} \bullet \frac{kJ}{gm}$$

This is low compared to Kyoung-Yeol's number of 14.7 kJ/g which is from Shizas and Bagley, 2004. See 7/2/15 email from Bruce Logan.

Now calculate the energy generated per unit volume water treated.

$$Energy_{volume} := \frac{Power_{MFC}}{Q_e} = \begin{pmatrix} 0.019 \\ 0.33 \end{pmatrix} \bullet \frac{kW \bullet hr}{m^3}$$

This is 0.02 kWh/m3 which is similar to Logan data presented in our proposal supporting information (0.0197)

Calculate organic loading rate (OLR)

$$OLR := Q_e \bullet \frac{COD_{Influent}}{V_{water.e}} = 0.07 \bullet \frac{kg}{m^3 hr}$$

Determination of Optimal Spacer Thickness

1.0 Purpose/Objective

Determine the optimal thickness of the spacer to allow passive oxygen transfer and not limit reaction rate at the cathode

2.0 Procedure

Calculate stoichiometry for oxygen consumption, rate of oxygen consumption, and rate of oxygen transfer via equimolar counter diffusion for different space thicknesses.

3.0 References/Data Sources

Logan Lab data
Fick's law
Diffusivity for oxygen in air
Faraday's law

4.0 Assumptions

Wire frame support in spacer does not hinder mass transfer
Equimolar counterdiffusion drives oxygen transfer in spacer

5.0 Calculations

Logan data for cathode performance

$$I_{cathode} := 0.04 \frac{mA}{cm^2}$$

Assumed spacer dimensions.

$$Spacer_{thickness} := (10mm \quad 20mm)$$

$$Spacer_{height} := 2ft = 0.6096\,m$$

$$Spacer_{width} := 2m$$

Calculate area for a cathode on both sides of a single spacer

$$Cathode_{area} := 2Spacer_{height} \cdot Spacer_{width} = 2.4384\,m^2$$

Calculate current for the cathodes on a single spacer

$$I := Cathode_{area} \cdot I_{cathode} = 0.9754\,A$$

Reaction of oxygen with electrons to form water at cathode

$O_2 + 2H_2O + 4e^- \text{-->} 4OH^-$

Calculate oxygen consumption rate

Faraday's law

$$F := 96485 \frac{C}{mol} = 96485 \frac{A \cdot s}{mol}$$

$$z := 4$$

$$Rate_{oxygen.consumption} := \frac{I}{F \cdot z} = 0.2184 \cdot \frac{mol}{day}$$

Ideal gas law standard volume

$$V := 22.4 \frac{L}{mol}$$

$$Flow_{oxygen.consumption} := Rate_{oxygen.consumption} \cdot V = 4.8911 \cdot \frac{L}{day}$$

$$Flow_{air} := \frac{Flow_{oxygen.consumption}}{0.21} = 23.291 \cdot \frac{L}{day}$$

$$Spacer_{volume} := Spacer_{height} \cdot Spacer_{width} \cdot Spacer_{thickness} = (12.192 \quad 24.384)\ L$$

Calculate average residence time for air in spacer

$$t_{air} := \frac{Spacer_{volume}}{Flow_{air}} = (0.5235 \quad 1.0469) \cdot day$$

Fick's Law for equimolar counterdiffusion

Diffusivity of oxygen (A) in nitrogen (B) (from Perry)

$$D_{AB} := 0.181 \frac{cm^2}{s}$$

Ideal gas constant

$$R := 0.082 \frac{L}{mol} \frac{atm}{K}$$

Partial pressures (p) of oxygen at top (1) and bottom (2) of spacer. Assume the following:

$$p_{A1} := 0.21atm$$

Calculate pA2 as different fractions of pA1. This represents having the range of 10% t0 90% oxygen depletion at the bottom of the spacer.

$$p_{A2} := \begin{pmatrix} 0.1p_{A1} \\ 0.3p_{A1} \\ 0.5p_{A1} \\ 0.7p_{A1} \\ 0.9p_{A1} \end{pmatrix} = \begin{pmatrix} 0.021 \\ 0.063 \\ 0.105 \\ 0.147 \\ 0.189 \end{pmatrix} \cdot atm$$

$$z_1 := 0m$$

$$z_2 := Spacer_{height} = 0.6096\ m$$

$$T := 298K$$

Calculate flux J_A for oxygen from bottom to top of spacer for different pA2

$$J_A := D_{AB} \cdot \frac{(p_{A1} - p_{A2})}{R \cdot T \cdot (z_2 - z_1)} = \begin{pmatrix} 19.8417 \\ 15.4324 \\ 11.0232 \\ 6.6139 \\ 2.2046 \end{pmatrix} \cdot \frac{mol}{m^2 day}$$

$$Area_{flux} := Spacer_{thickness} \cdot Spacer_{width} = (0.02 \quad 0.04)\, m^2$$

Calculate diffusive oxygen flow for different pA2 (rows) and different spacer thickness (columns)

$$Rate_{oxygen.diffusion} := J_A \cdot Area_{flux} = \begin{pmatrix} 0.3968 & 0.7937 \\ 0.3086 & 0.6173 \\ 0.2205 & 0.4409 \\ 0.1323 & 0.2646 \\ 0.0441 & 0.0882 \end{pmatrix} \cdot \frac{mol}{day}$$

$$Flow_{oxygen.diffusion} := Rate_{oxygen.diffusion} \cdot V = \begin{pmatrix} 8.8891 & 17.7782 \\ 6.9137 & 13.8275 \\ 4.9384 & 9.8768 \\ 2.963 & 5.9261 \\ 0.9877 & 1.9754 \end{pmatrix} \cdot \frac{L}{day}$$

Compare flow via oxygen diffusion to flow via oxygen consumption

$$Excess_{oxygen} := \frac{Flow_{oxygen.diffusion}}{Flow_{oxygen.consumption}} = \begin{array}{c} \text{Spacer thickness} \\ \begin{array}{cc} \text{10 mm} & \text{20 mm} \end{array} \\ \begin{pmatrix} 181.7398 & 363.4797 \\ 141.3532 & 282.7064 \\ 100.9666 & 201.9332 \\ 60.5799 & 121.1599 \\ 20.1933 & 40.3866 \end{pmatrix} \end{array} \cdot \% \quad \begin{array}{c} \text{pA2/pA1} \\ 10\% \\ 30\% \\ 50\% \\ 70\% \\ 90\% \end{array}$$

Graphical relationship of excess oxygen to oxygen concentration at bottom of spacer. Top curve is for a 20-mm spacer and bottom curve is for a 10-mm spacer.

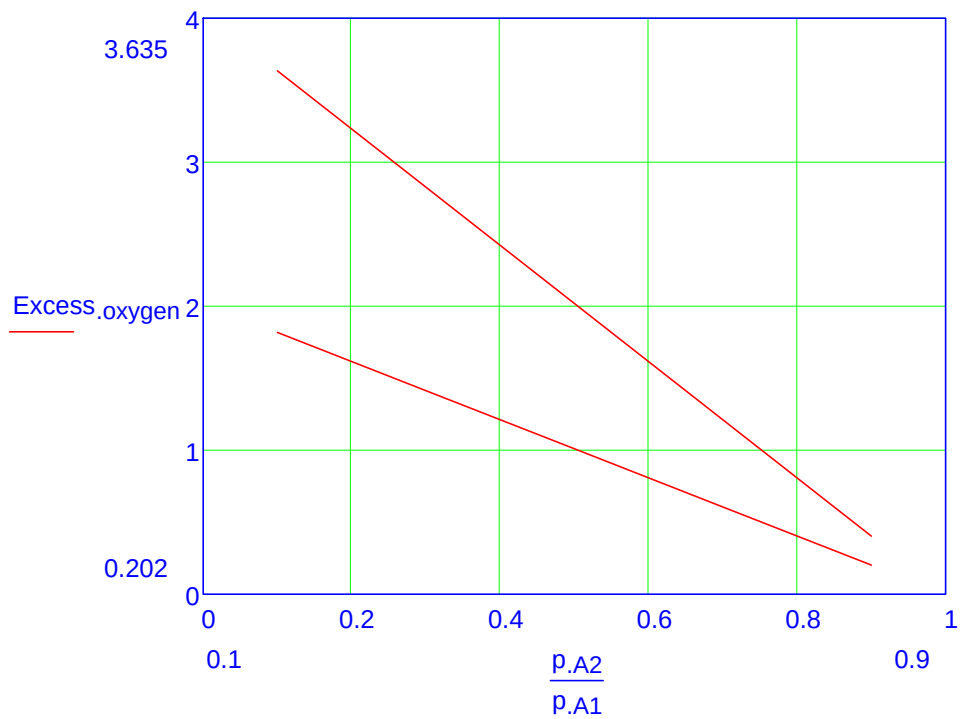

6.0 Conclusions/Results

A 20-mm spacer is recommended to minimize oxygen limitations at the bottom of the spacer

CDM Smith	**Job #**	**Calc By:** J. Goldman
Client: SERDP	**Checked By:** Chris Stillwell	**Date:** 11/2/15
Project: MFC Design	**Date:** 11/5/15	**Calc.No.**
Detail: Water Distribution Manifold Design	**Reviewed By:**	**Revision #** 1
	Date:	**Date:**

1.0 PURPOSE/ OBJECTIVE

1.1 Determine the number of distribution holes and the hole diameter required to distribute flow equally through the holes.

2.0 PROCEDURE / APPROACH

2.1 Define assumptions

2.11 Total flow is equal fo 0.5 gpm (1.114×10^{-3} ft3/s)

2.12 Diffuser pipe ID is 1.5 in (0.125 ft)

2.13 K (flow coefficient) at the first port is 0.675

2.14 Energy at the end of the pipe

$$E_{end} := \frac{V^2}{2g} + \left(\frac{v_{orafice}}{K^2}\right)\frac{1}{2g}$$

2.14a Velocity head is equal to 0 at the end of the pipe.

2.14b Assume equal flow through all orafices. Start with orafice diameter of 0.5 in.

2.15 Constants: g = 32.2 ft/s2, γ = 62.4 lb/ft3, ν = 1.47×10^{-5} ft2/s, Ks (PVC roughness) = 9.84×10^{-6} ft

2.2 Define equations

Velocity in pipe before hole n $\quad V_{n-1} := \frac{Q_{n-1}}{A_{diffuser}}$

Flow coefficient at hole n $\quad K_n := 0.675\sqrt{\frac{1 - V_{n-1}^2}{2g \cdot E_n}}$

Flow through hole n $\quad q_n := K_n \cdot a_n \cdot \sqrt{2g \cdot E_n}$

Change in pipe velocity after hole n $\quad \Delta V_n := \frac{q_n}{\pi \frac{D^2}{4}}$

Reynold's number at hole n $\quad Re_n := V_n \cdot \frac{D}{\upsilon}$

Friction factor at hole n $\quad f_n := \frac{0.25}{\left(\log\left(\frac{k_s}{3.7 \cdot D} + \frac{5.74}{Re^{0.9}}\right)\right)^2}$

Head loss at hole n $\quad h_n := f_n \cdot \left(\frac{L}{D}\right)\left(\frac{V_n^2}{2g}\right)$

Total head in pipe after hole n $\quad E_{n+1} := E_n + h_{fn}$

2.3 Set up spreadsheet to solve these equations in order, starting at the terminal end of the distribution pipe.

2.4 Sum total discharge from all the holes (sum of qn for each hole) and define as a percentage of total flow in pipe. (E35

2.5 Calculate percent difference in flow between first and last hole. (E37)

2.6 Iterate on number of holes and hole diameter to achieve maximum percent flow discharge and minimum percent difference between first and last hole.

3.0 DATA & REFERENCES

See also references on calcs attached

3.1 Roberson, J. A., Cassidy, J. J., & Chaudhry, M. H. (1998). *Hydraulic engineering*. New York: Wiley.

4.0 ASSUMPTIONS/ LIMITATIONS

4.1 Total flow is equal fo 0.5 gpm (1.114×10^{-3} ft3/s)

4.2 Diffuser pipe ID is 1.5 in (0.125 ft)

4.3 K (flow coefficient) at the first port is 0.675

4.4 Total length of distribution pipe is 1.75 ft (from 3-D model)

4.5 Constants: g = 32.2 ft/s2, γ = 62.4 lb/ft3, ν = 1.47×10^{-5} ft2/s, Ks (PVC roughness) = 9.84×10^{-6} ft

5.0 CALCULATIONS

Total Q	ft3/s	1.114E-03	L (spacing)	ft	0.317
Diffuser Pipe ID	ft	0.125	L (distribution pipe)	ft	1.375
a, diffuser pipe	ft2	0.0123	# holes	#	5.0
V, diffuser pipe	ft/s	0.0908	Kend		0.675
Port D	ft	0.0417	Eend	ft	0.0009
Port a	ft2	0.0014	Required Head		
V.oriface	ft/s	0.1634			
g	ft/s2	32.2			
γ	lb/ft3	62.4			
ν	ft2/s	1.47E-05			
Ks	ft	9.84E-06			

Water Flow →→→

Port	Vn-1	Kn	qn	ΔVn	Vn	Re.n	fn	hfn	En+1
	ft/s	--	f3/s	ft/s	ft/s	--	--	ft	ft
1	0.000	0.675	2.23E-04	0.01816	0.018155	154	0.170562698	2.21157E-06	0.000912
2	0.018	0.673	2.22E-04	0.01813	0.036282	309	0.11395558	5.9009E-06	0.000918
3	0.036	0.667	2.21E-04	0.01803	0.054314	462	0.093093897	1.08031E-05	0.000929
4	0.054	0.658	2.19E-04	0.01789	0.072199	614	0.081643987	1.67413E-05	0.000946
5	0.072	0.645	2.17E-04	0.01770	0.089897	764	0.07420812	2.35909E-05	0.000969
Tot			1.103E-03						0.005

% Discharge	99
% Diff in q between first and last port	-2.59

6.0 CONCLUSIONS/ RESULTS

6.1 Percent discharge through the distribution holes is maximized at 99% of the total flow.

6.2 Percent difference in flow between the first and last holes is equal to 2.59%

6.3 The hole diameter is 0.5 in, and there are 5 holes in the pipe. They are spaced 0.32 ft apart.

CDM Smith	**Job #**	**Calc By:** J. Goldman
Client: SERDP	**Checked By:** P. Evans	**Date:** 11/2/15
Project: MFC Design	**Date:**	**Calc.No.**
Detail: Air Distribution Manifold Design	**Reviewed By:**	**Revision #** 1
	Date:	**Date:**

1.0 PURPOSE/ OBJECTIVE

1.1 Determine the number of distribution holes and the hole diameter required to distribute air flow equally through the holes.

2.0 PROCEDURE / APPROACH

2.1 Define assumptions

2.11 Relationship between flow and pressure is defined by standard air compressor curve (shown in References tab)

2.12 Diffuser pipe ID is 1.25 in (0.104 ft)

2.13 K (flow coefficient) at the first port is 0.675

2.14 Energy at the end of the pipe

$$E_{end} := \frac{V^2}{2g} + \left(\frac{v_{orafice}}{K^2}\right)\frac{1}{2g}$$

2.14a Velocity head is equal to 0 at the end of the pipe.

2.14b Assume equal flow through all orafices. Start with orafice diameter of 0.5 in.

2.15 Constants: g = 32.2 ft/s2,, Ks (PVC roughness) = 9.84 x 10^{-6} ft

γ = .2902 lb/ft3, ν = 1.52 x 10^{-4} ft2/s (See References tab)

2.2 Define equations

Velocity in pipe before hole n $V_{n-1} := \frac{Q_{n-1}}{A_{diffuser}}$

Flow coefficient at hole n $K_n := 0.675\sqrt{\frac{1 - V_{n-1}^2}{2g \cdot E_n}}$

Flow through hole n $q_n := K_n \cdot a_n \cdot \sqrt{2g \cdot E_n}$

Change in pipe velocity after hole n $\Delta V_n := \frac{q_n}{\pi \frac{D^2}{4}}$

Reynold's number at hole n $Re_n := V_n \cdot \frac{D}{\upsilon}$

Friction factor at hole n $f_n := \frac{0.25}{\left(\log\left(\frac{k_s}{3.7 \cdot D} + \frac{5.74}{Re^{0.9}}\right)\right)^2}$

Head loss at hole n $h_n := f_n \cdot \left(\frac{L}{D}\right)\left(\frac{V_n^2}{2g}\right)$

Total head in pipe after hole n $E_{n+1} := E_n + h_{fn}$

2.3 Set up spreadsheet to solve these equations in order, starting at the terminal end of the distribution pipe.

2.4 Sum total discharge from all the holes (sum of qn for each hole) and define as a percentage of total flow in pipe. (E35)

2.5 Calculate percent difference in flow between first and last hole. (E37)

2.6 Iterate on air pressure, number of holes, and hole diameter to achieve maximum percent flow discharge and minimum percent difference between first and last hole.

3.0 DATA & REFERENCES

See also references on calcs attached

3.1 Roberson, J. A., Cassidy, J. J., & Chaudhry, M. H. (1998). *Hydraulic engineering*. New York: Wiley.

4.0 ASSUMPTIONS/ LIMITATIONS

4.1 Relationship between flow and pressure is defined by standard air compressor curve (shown in References tab)

4.2 Diffuser pipe ID is 1.25 in (0.104 ft)

4.3 K (flow coefficient) at the first port is 0.675

4.4 Total length of distribution pipe is 44.12 ft (from 3-D model)

4.5 Constants: g = 32.2 ft/s2,, Ks (PVC roughness) = 9.84 x 10^{-6} ft

γ = .2902 lb/ft3, ν = 1.52 x 10^{-4} ft2/s (See References tab)

5.0 CALCULATIONS

Air Pressure	psi	30		L (spacing)	ft	0.126
Total Q	ft3/s	0.055333333		L (distribution pipe)	ft	3.682
Diffuser Pipe ID	ft	0.104166667		# holes	#	25.0
a, diffuser pipe	ft2	0.0109		Kend		0.675
V, diffuser pipe	ft/s	5.0995		Eend	ft	1.4368
Port D	ft	0.0208				
Port a	ft2	0.0003				
V.oriface	ft/s	6.4929				
Temperature	F	60				
g	ft/s2	32.2				
γ	lb/ft3	0.2372				
ν	ft2/s	1.52E-04				
Ks	ft	9.84E-06				

Air Flow →→→

Port	Vn-1	Kn	qn	ΔVn	Vn	Re.n	fn	hfn	En+1
	ft/s	--	f3/s	ft/s	ft/s	--	--	ft	ft
1	0.000	0.675	2.21E-03	0.20398	0.203981	140	0.182052102	0.000142765	1.436907
2	0.204	0.675	2.21E-03	0.20395	0.407926	280	0.120129	0.000376754	1.437283
3	0.408	0.674	2.21E-03	0.20383	0.611760	419	0.097550727	0.000688081	1.437972
4	0.612	0.674	2.21E-03	0.20365	0.815414	559	0.085192037	0.001067584	1.439039
5	0.815	0.673	2.21E-03	0.20341	1.018822	698	0.077162799	0.001509565	1.440549
6	1.019	0.671	2.20E-03	0.20310	1.221926	837	0.07142309	0.002009904	1.442559
7	1.222	0.670	2.20E-03	0.20274	1.424668	976	0.067061646	0.002565363	1.445124
8	1.425	0.668	2.20E-03	0.20233	1.626999	1115	0.063604007	0.003173261	1.448297
9	1.627	0.665	2.19E-03	0.20187	1.828869	1253	0.060776233	0.0038313	1.452129
10	1.829	0.663	2.18E-03	0.20137	2.030237	1391	0.058407873	0.004537451	1.456666
11	2.030	0.660	2.18E-03	0.20083	2.231063	1529	0.056386668	0.005289896	1.461956
12	2.231	0.657	2.17E-03	0.20025	2.431311	1666	0.054635316	0.006086976	1.468043
13	2.431	0.654	2.17E-03	0.19964	2.630951	1803	0.053098627	0.006927166	1.474970
14	2.631	0.650	2.16E-03	0.19900	2.829953	1939	0.051736018	0.007809053	1.482779
15	2.830	0.646	2.15E-03	0.19834	3.028294	2075	0.050516888	0.008731317	1.491510
16	3.028	0.642	2.14E-03	0.19766	3.225955	2211	0.049417669	0.009692724	1.501203
17	3.226	0.638	2.14E-03	0.19696	3.422918	2346	0.048419878	0.010692118	1.511895
18	3.423	0.633	2.13E-03	0.19625	3.619172	2480	0.047508783	0.011728412	1.523624
19	3.619	0.628	2.12E-03	0.19553	3.814705	2614	0.04667248	0.012800585	1.536424
20	3.815	0.623	2.11E-03	0.19481	4.009514	2748	0.045901228	0.013907683	1.550332
21	4.010	0.618	2.11E-03	0.19408	4.203596	2881	0.045186967	0.015048809	1.565381
22	4.204	0.613	2.10E-03	0.19336	4.396953	3013	0.044522964	0.016223131	1.581604
23	4.397	0.608	2.09E-03	0.19264	4.589590	3145	0.043903539	0.017429872	1.599034
24	4.590	0.602	2.08E-03	0.19192	4.781514	3277	0.043323867	0.018668315	1.617702
25	4.782	0.596	2.07E-03	0.19122	4.972739	3408	0.042779814	0.019937801	1.637640
Tot			5.396E-02						10.079
% Discharge			98						
% Diff in q between first and last port			-6.67						

6.0 CONCLUSIONS/ RESULTS

6.1 Percent discharge through the distribution holes is maximized at 98% of the total flow.

6.2 Percent difference in flow between the first and last holes is equal to -6.67%

6.3 The hole diameter is 0.25 in, and there are 25 holes in the pipe. They are spaced 0.126 ft apart.

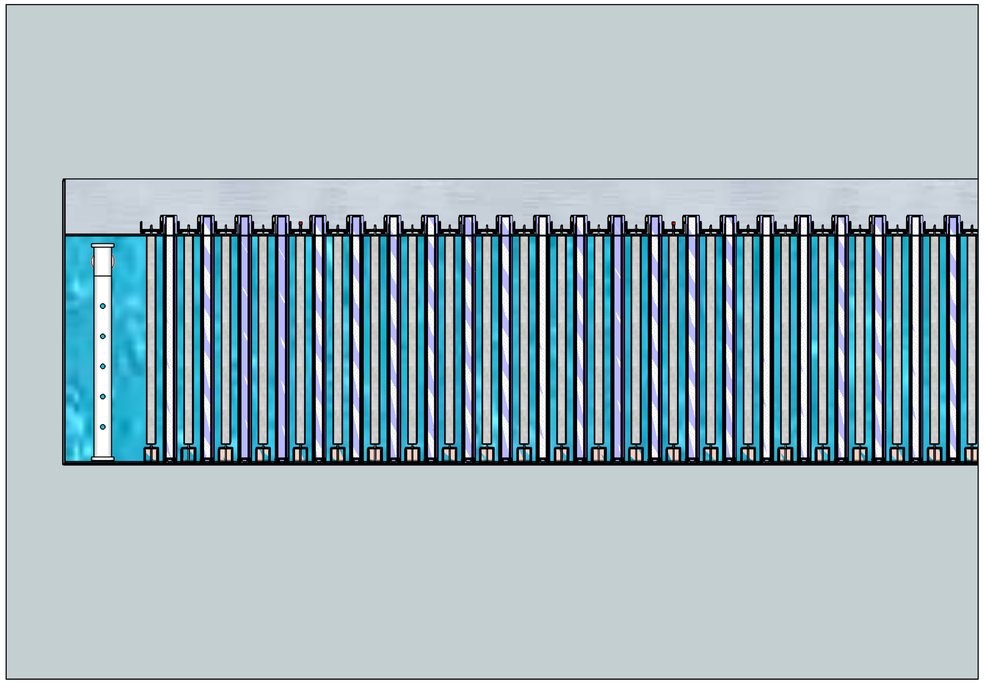

A 1 SECTION
Scale: 3/4" : 1'

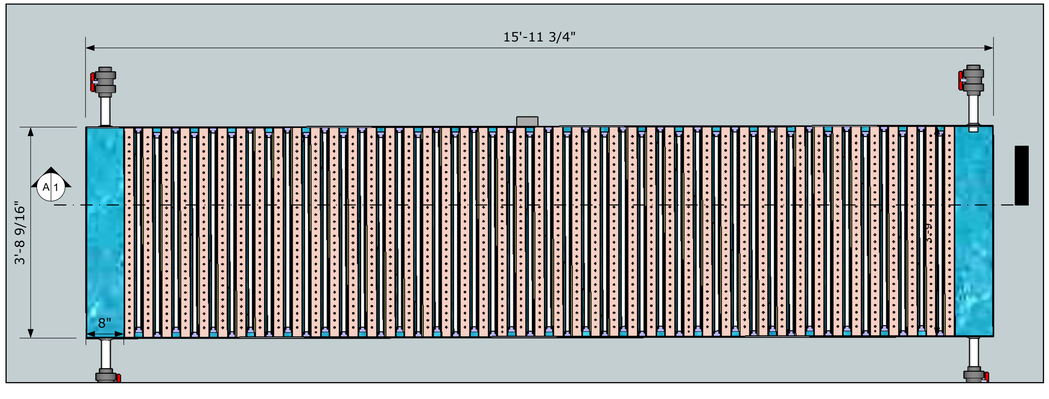

PLAN
Scale: 3/4" : 1'

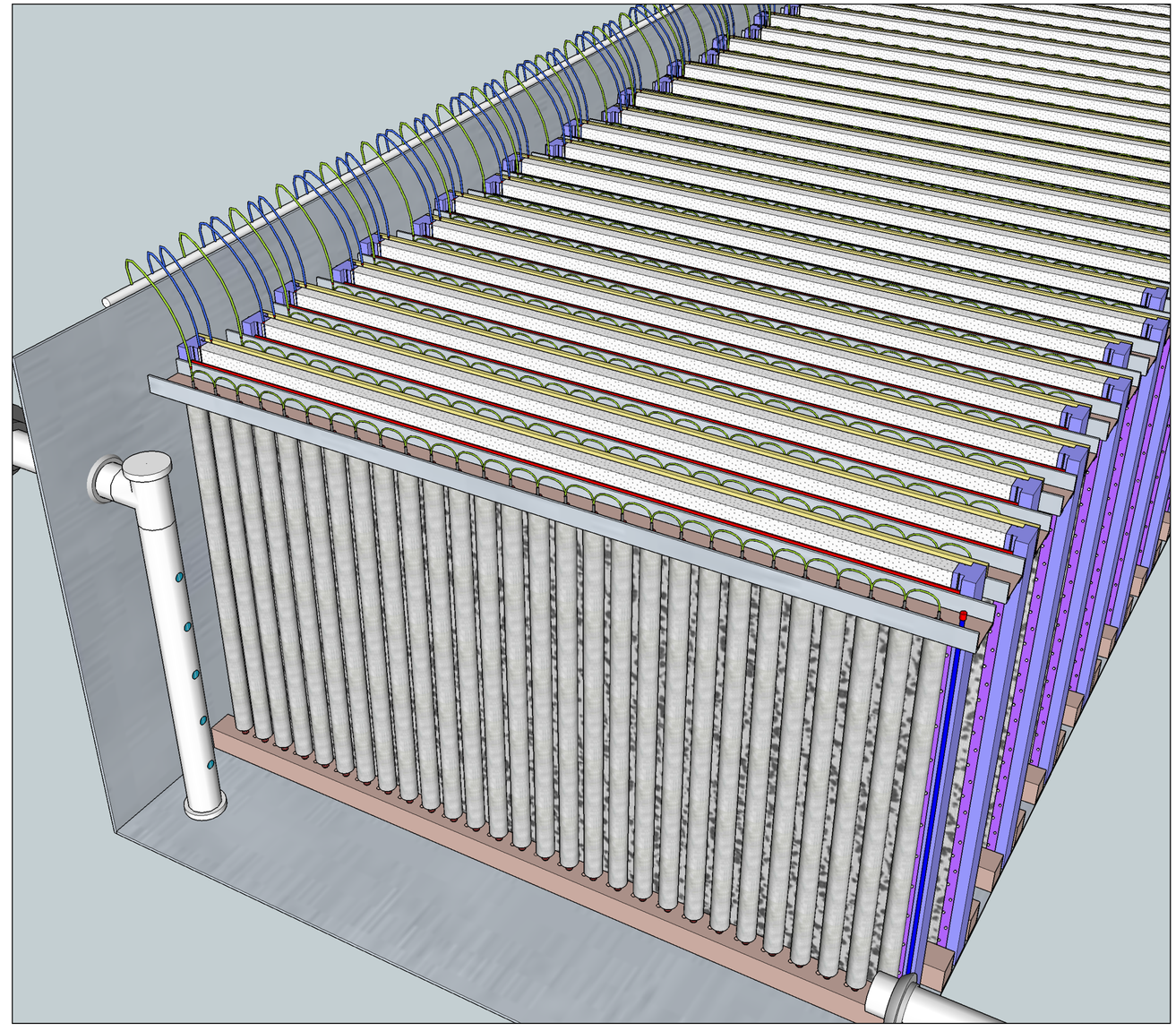

PERSPECTIVE
NTS

REV. NO.	DATE	DRWN	CHKD	REMARKS
XXX	XXX	XXX	XXX	XXX
XXX	XXX	XXX	XXX	XXX
XXX	XXX	XXX	XXX	XXX
XXX	XXX	XXX	XXX	XXX
XXX	XXX	XXX	XXX	XXX

0 1
IF THIS BAR DOES NOT MEASURE 1" THEN DRAWING IS NOT TO SCALE

DESIGNED BY: Pat Evans
DRAWN BY: Josh Goldman
SHEET CHK'D BY: XXXXX
CROSS CHK'D BY: XXXXX
APPROVED BY: XXXXX
DATE: 4/13/2015

CDM Smith
555 17th Street, Suite 1100
Denver, CO 80202
Tel: (303) 383-2300

ESTCP
MICROBIAL FUEL CELL

REACTOR

PROJECT NO. 83278-95598
FILE NAME: Fuel Cell Sheets
SHEET NO.
1

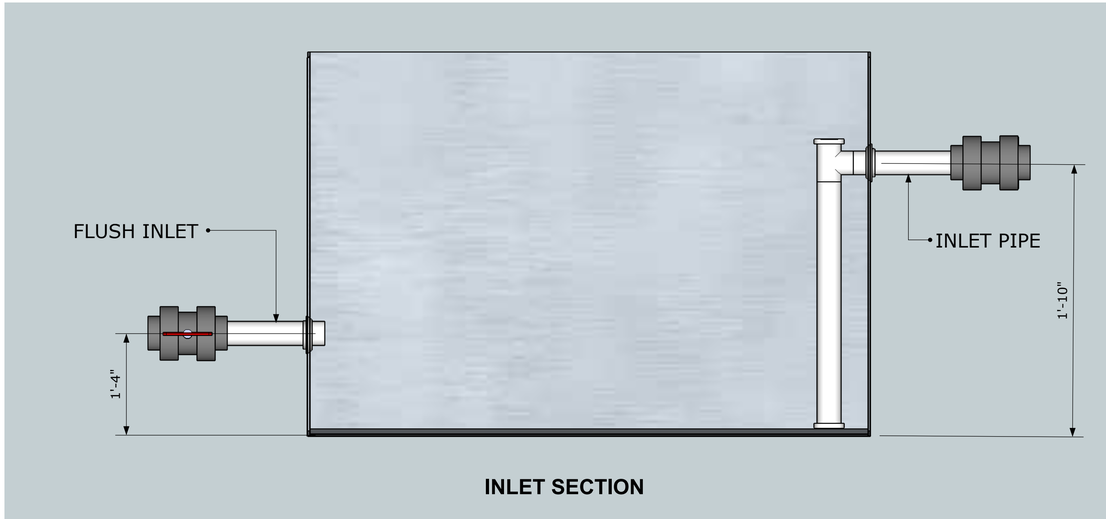

INLET SECTION

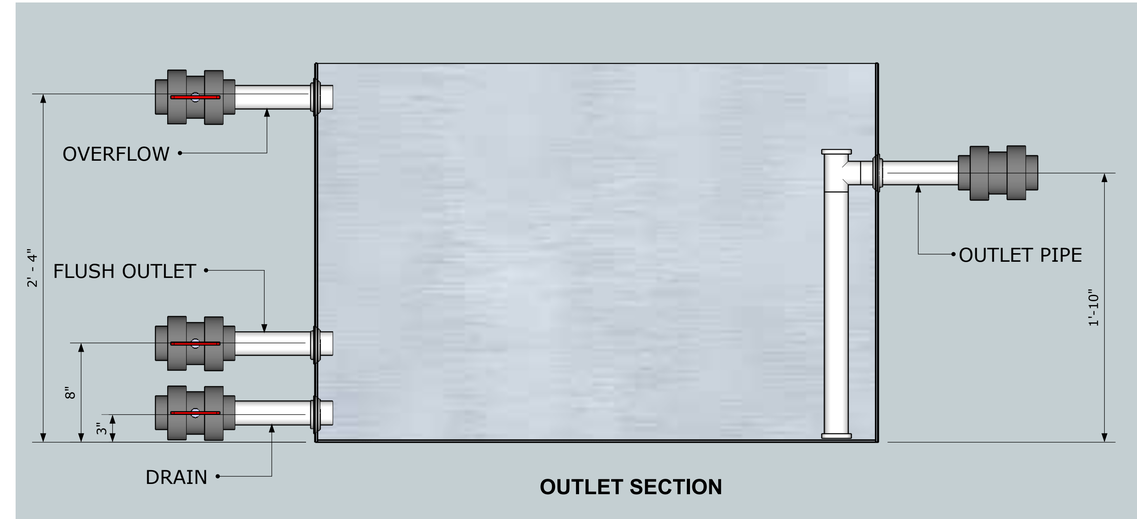

OUTLET SECTION

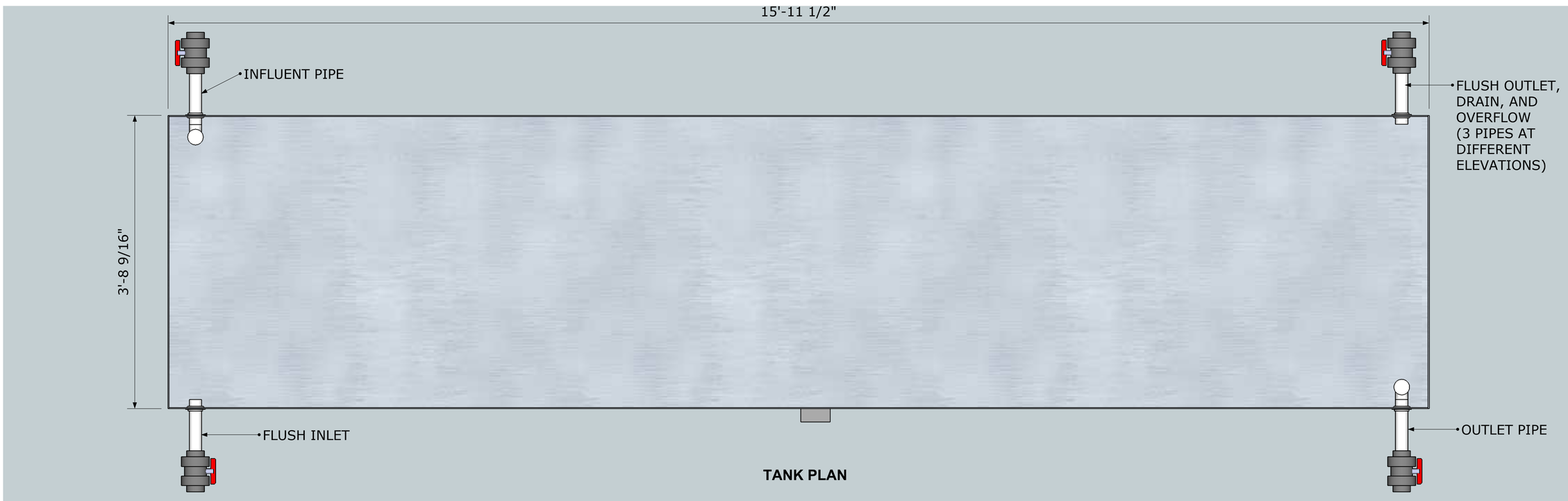

TANK PLAN

REV. NO.	DATE	DRWN	CHKD	REMARKS
XXX	XXX	XXX	XXX	XXX
XXX	XXX	XXX	XXX	XXX
XXX	XXX	XXX	XXX	XXX
XXX	XXX	XXX	XXX	XXX
XXX	XXX	XXX	XXX	XXX

0 1

IF THIS BAR DOES NOT MEASURE 1" THEN DRAWING IS NOT TO SCALE

DESIGNED BY: Pat Evans
DRAWN BY: Josh Goldman
SHEET CHK'D BY: XXXXX
CROSS CHK'D BY: XXXXX
APPROVED BY: XXXXX
DATE: 4/13/2015

CDM Smith
555 17th Street, Suite 1100
Denver, CO 80202
Tel: (303) 383-2300

ESTCP

MICROBIAL FUEL CELL

TANK

PROJECT NO. 83278-95598
FILE NAME: Fuel Cell Sheets
SHEET NO.
2

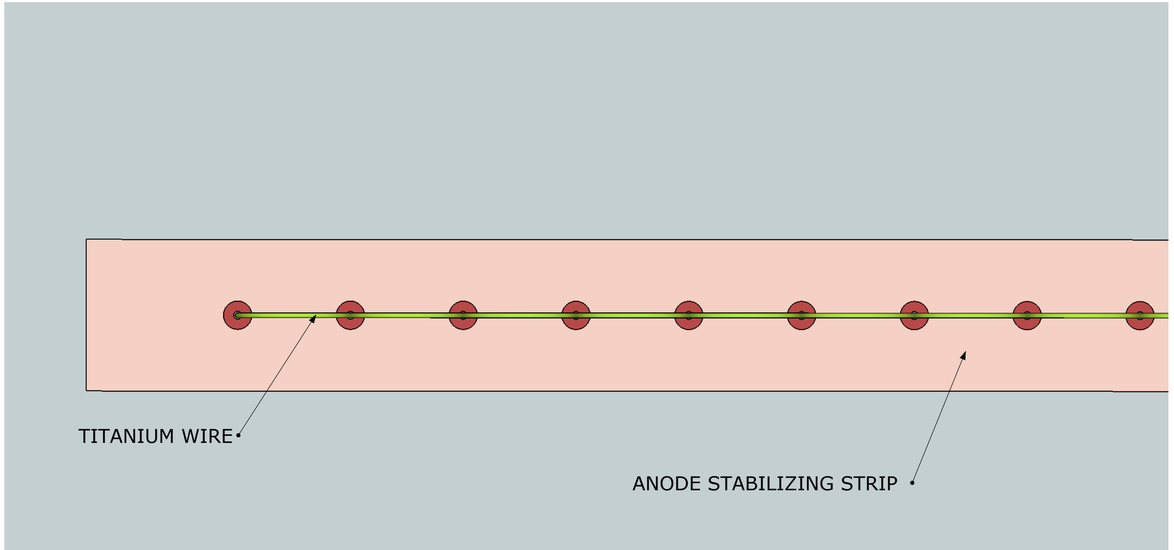

A 1 ANNODE ASSEMBLY PLAN
Scale: 2.5" : 1"

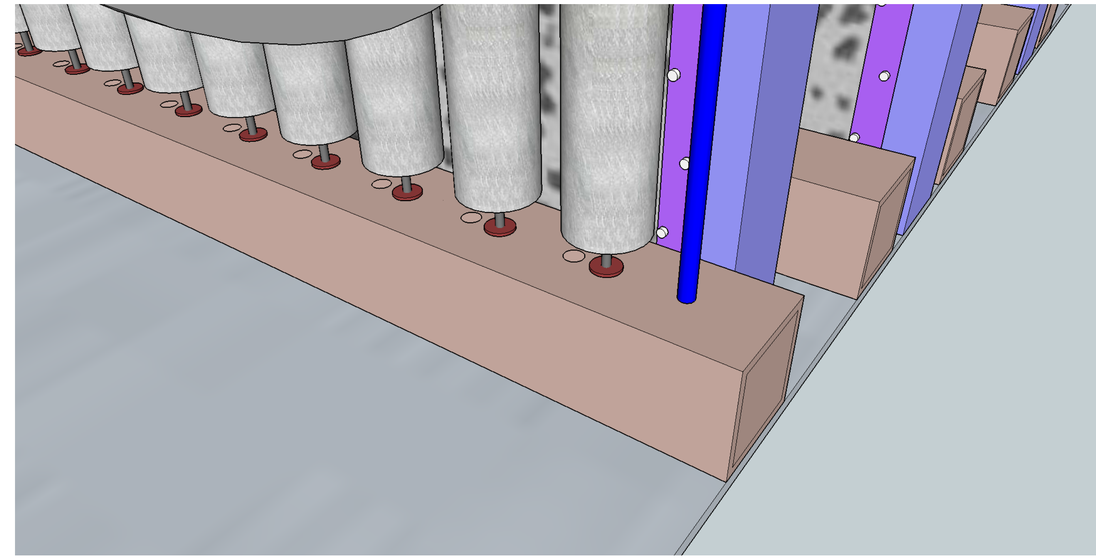

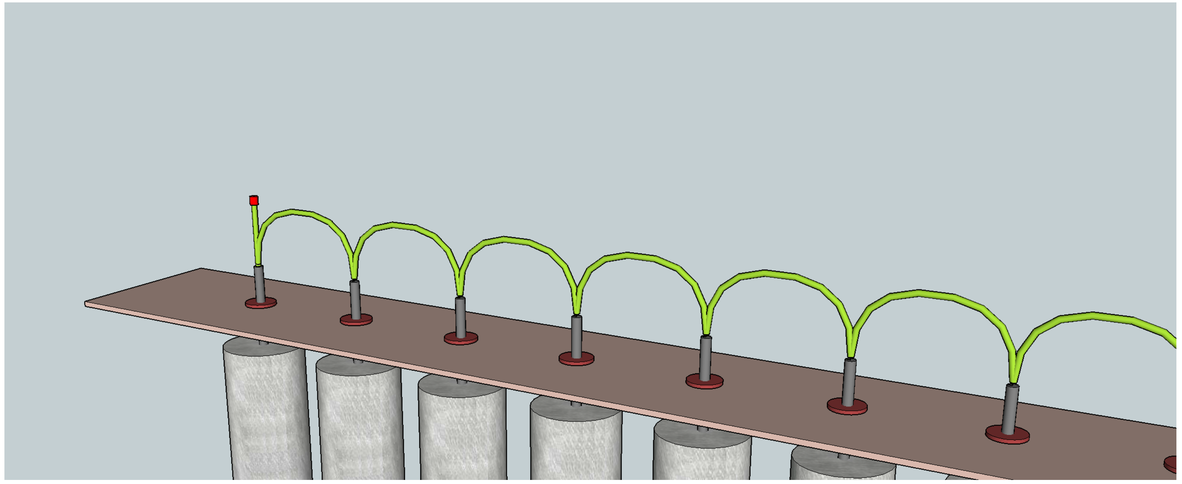

ANNODE PERSPECTIVE
NTS

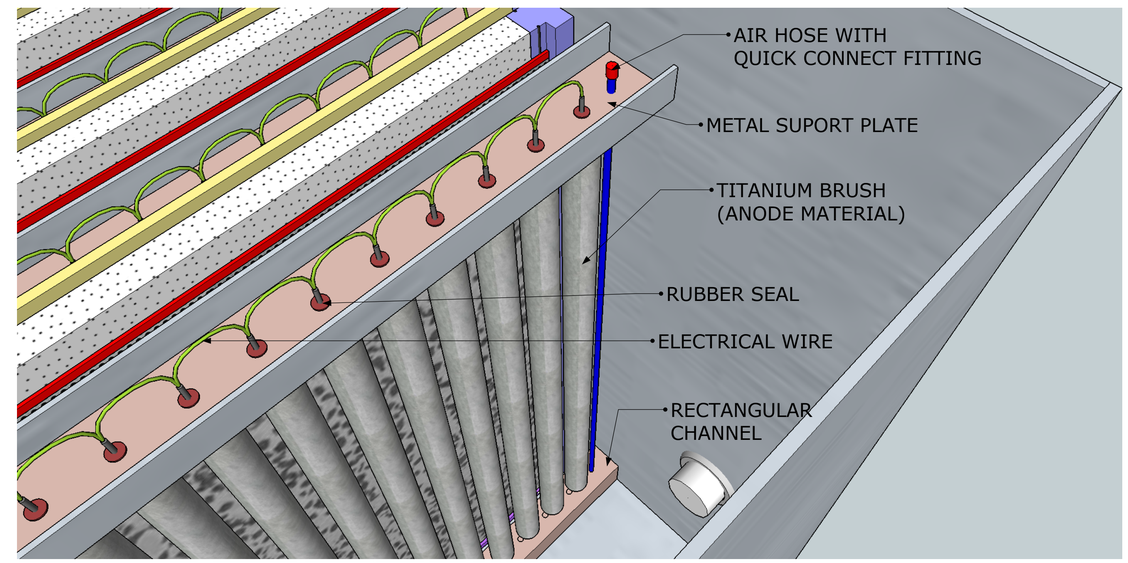

REV. NO.	DATE	DRWN	CHKD	REMARKS
XXX	XXX	XXX	XXX	XXX
XXX	XXX	XXX	XXX	XXX
XXX	XXX	XXX	XXX	XXX
XXX	XXX	XXX	XXX	XXX
XXX	XXX	XXX	XXX	XXX

0 1
IF THIS BAR DOES NOT MEASURE 1" THEN DRAWING IS NOT TO SCALE

DESIGNED BY: Pat Evans
DRAWN BY: Josh Goldman
SHEET CHK'D BY: XXXXX
CROSS CHK'D BY: XXXXX
APPROVED BY: XXXXX
DATE: 4/13/2015

CDM Smith
555 17th Street, Suite 1100
Denver, CO 80202
Tel: (303) 383-2300

ESTCP
MICROBIAL FUEL CELL

ANODE

PROJECT NO. 83278-95598
FILE NAME: Fuel Cell Sheets
SHEET NO.
3

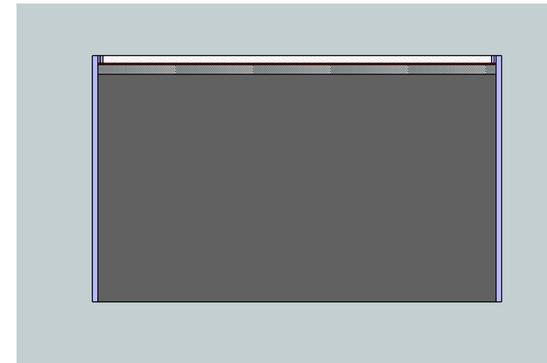

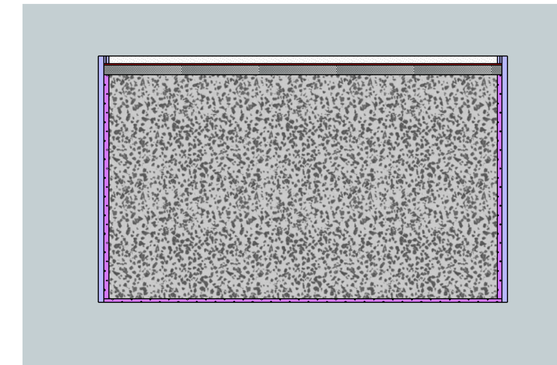

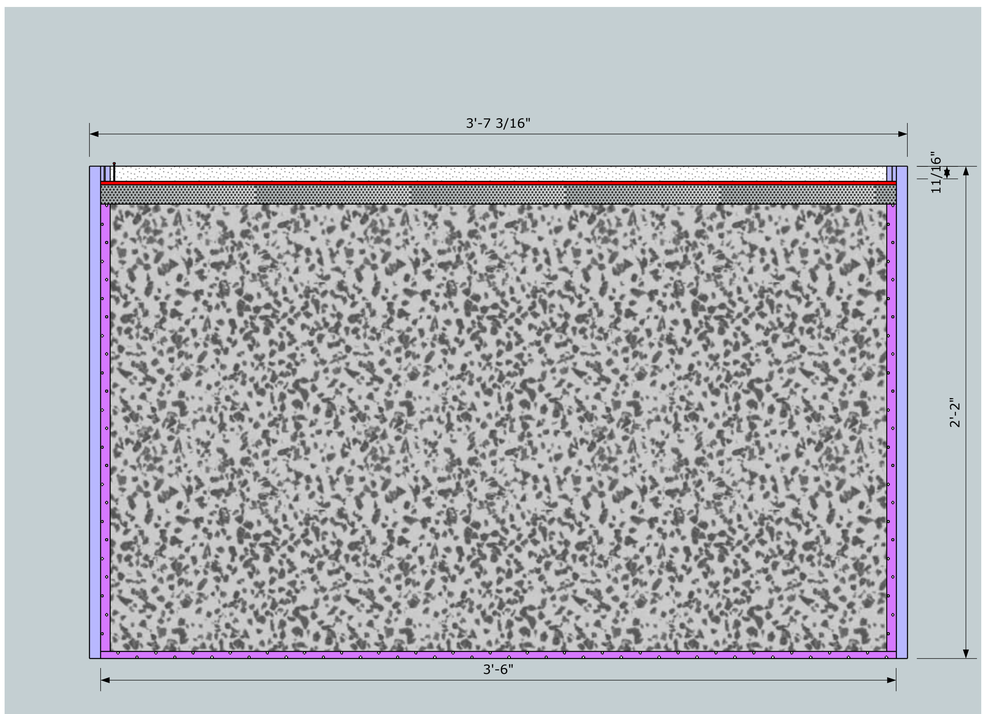

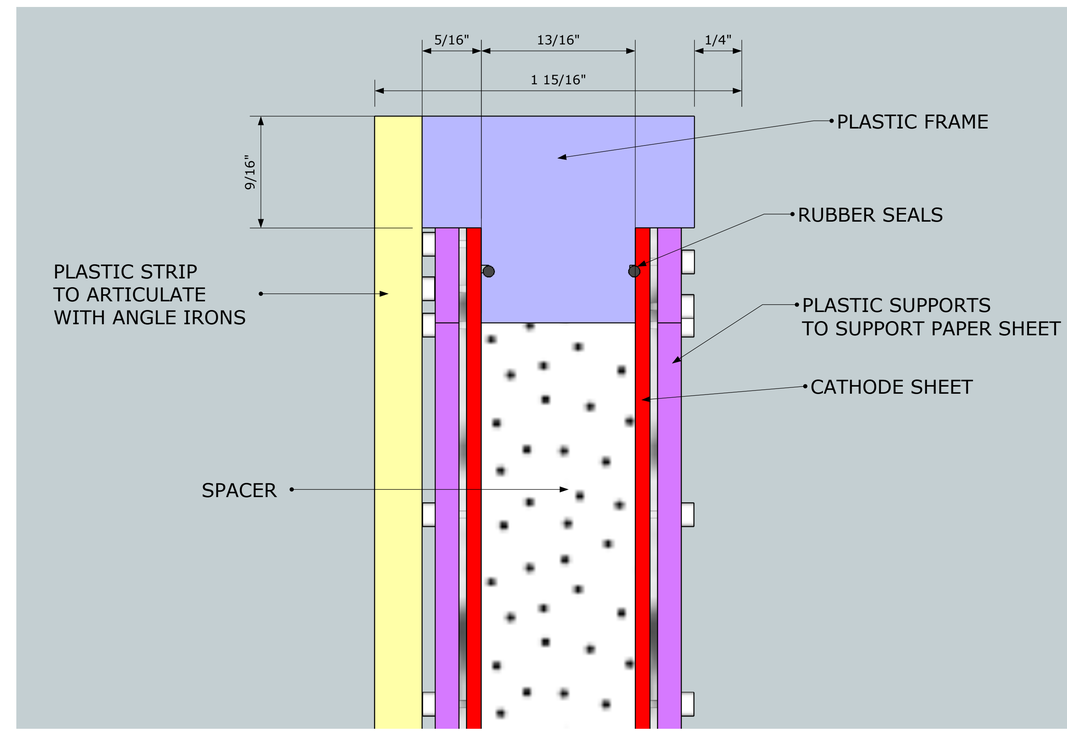

REV. NO.	DATE	DRWN	CHKD	REMARKS
XXX	XXX	XXX	XXX	XXX
XXX	XXX	XXX	XXX	XXX
XXX	XXX	XXX	XXX	XXX
XXX	XXX	XXX	XXX	XXX
XXX	XXX	XXX	XXX	XXX

0 1

IF THIS BAR DOES NOT MEASURE 1" THEN DRAWING IS NOT TO SCALE

DESIGNED BY: Pat Evans
DRAWN BY: Josh Goldman
SHEET CHK'D BY: XXXXX
CROSS CHK'D BY: XXXXX
APPROVED BY: XXXXX
DATE: 4/13/2015

CDM Smith
555 17th Street, Suite 1100
Denver, CO 80202
Tel: (303) 383-2300

ESTCP

MICROBIAL FUEL CELL

CATHODE

PROJECT NO. 83278-95598
FILE NAME: Fuel Cell Sheets
SHEET NO.
4

	MFC Bioreactor Design												
	Bioreactor Mechanical Parts List												
	General Information							**Notes**					
	Cathode Modules	44						Cathode modules are two-faced frames constructed of milled PVC stock; the frames hold carbon-coated stainless steel mesh on each face; the stainless steel mesh is covered with a textile separator. The mesh and textile are attached to the cathode frame using strips of PVC bar stock secured by multiple small bolts. A circular core-stock gasket is set between the perimeter of the mesh/textile layer and the frame to prevent water leakage	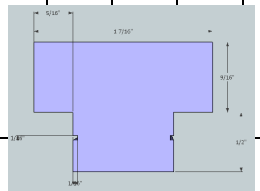				
	Anode Modules	45						An anode module consists of 29 anodes (which resemble test tube cleaning brushes) aligned in a row, suspended vertically. The individual anodes are secured to a top plate, and wired in a daisy chain above the top plate. The bottom tips of the 29 anodes are secured in a plastic strip to ensure that the anodes remain aligned vertically. This bottom plastic strip is also perforated with holes through which air or nitrogen can be introduced to remove settled solids and clear solids that may have deposited on the anodes					
	Anodes per Module	29											
Part #	**Part**	**L/Diameter**	**Width**	**Height**	**Description**	**Quantity**	**Unit**	**Notes**					
Bioreactor Tank and Piping Connections													
T-1	Carbon Steel Tank 3/16" Wall Thickness	16' 8 1/8"	3' 8 9/16"	2' 6"	A-36 Carbon Steel with white blast, one coat primer and two coats chemical resistant epoxy paint	1	tank	If cost effective, other materials besides carbon steel are acceptable; design criteria are for a chemically resistant, non-conductive shell					
T-2	Angle Brackets for supporting cathode and anode modules	3' 8 3/16"	1/2"	1"	A-36 Carbon Steel, welded to tank wall; with white blast, one coat primer and two coats chemical resistant epoxy paint	90	pieces	Angle "iron" lengths span from side to side of reactor to support the anode and cathode modules. The 29 anode modules are secured to a polycarbonate plate that sits on the horizontal legs of adjacent angle pieces. The cathode modules drop in between adjacent vertical legs of the angle pieces					
T-3	Weld on Fittings for Tank	1-in ID female pipe thread			McMaster Carr 1145K47 316 stainless steel or equal	6	pieces	Threaded, weld-on fittings to which to attach the 1-in diameter threaded pipe; hole size to be drilled in tank is larger					
P-1	Straight Pipe to distributor pipe	1-in diameter		7 3/4"	PVC Sch 80	6	pieces						
P-2	Tee	1-in diameter			PVC Sch 80	1	piece						
P-3	Perforated Distributor Pipe	1-in diameter		1'6"	PVC Sch 80 with 1/8-in diam holes 2 inches on-center vertically	1	piece	Stock PVC pipe with 1/8-in diameter holes 2-in on-center drilled in shop					
P-4	Pipe Cap at bottom of distributor pipe and other locations	1-in diameter			PVC Sch 80	4	pieces						
P-5	Ball Valves	1-in diameter			PVC; McMaster Carr 4876K13 or equal	6	pieces						
Cathode Modules													
C-1	Cathode Frame (Vertical members - 2 per module)			2'2"	1-in square PVC square stock. McMaster Carr 8740K16 or equal	88	pieces	Mill adjacent corners of PVC square stock to create rabbet on each corner. Rabbet cut serves as inset for mesh and textile layers. Also create 1/8-in diameter, half-circle groove along rabbeted edge for gasket placement					
C-2	Cathode Frame (Horizontal members - 1 per module)	3'5"	13/16"	3/8"	1-in square PVC square stock. McMaster Carr 8740K16 or equal	44	pieces	Mill adjacent corners of PVC square stock to create rabbet on each corner. Rabbet cut serves as inset for mesh and textile layers. Also create 1/8-in diameter, half-circle groove along rabbeted edge for gasket placement					
C-3	Cathode Gasket (Vertical)	1/8-in diameter		2'2"	O-ring, circular cross section cord stock; silicone; 1/8-in round; McMaster Carr 96505K23	approx 400	linear feet						
C-4	Cathode Fastener (Vertical)	2' 2"	1/8"	1/2"	PVC strip stock; McMaster Carr 8740K11	176	pieces	Consider ripping from 1-in wide stock if 1/2 width is not available					
C-5	Cathode Fastener (Horizontal)	3'6"	1/8"	1/2"	PVC strip stock; McMaster Carr 8740K11	88	pieces						

C-6	Cathode Fastener Bolts	1/8"		1/2"	Stainless steel threaded tapered -head with philips or star head	7920	pieces	Consider nylon bolts as alternative if stripping is a concern					
C-7	Cathode Support for Angle Bracket	3'7 3/16"	1/8"	1"	PVC strip stock; McMaster Carr 8740K11	88	pieces						
C-8	Separator Cloth	2'	3'6"	0.3 mm thick	Textile separator cloth; 46% cellulose/54% polyester; 0.3 mm thick. Amplitude Prozorb by Contec Inc or equal	88	sheets	These are what we might call "lab towels." May require contacting manufacturer to obtain larger sizes than commonly sold.					
C-9	Cathode (top inch is uncoated)	3'6"	2'1"	estm 1/16" thick	Stainless steel mesh with "carbon" coating; custom fabrication	88	sheets	Specialty item supplied by other					
C-10	Cathode Bus	Approx 3' 4 "	approx 1/2"	Approx 1/16" thick	Electrically conductive material suitable for soldering or welding to stainless steel mesh and corrosion resistant	88	pieces	Solder or MIG weld to stainless steel mesh					
C-11	Cathode Spacer	3'5"	2'2"	approx 11/16" thick	Raschig Kompakt polyethylene, custom plates	44	sheets	Custom fabrication by Raschig. Contact is Chris Harden, Raschig USA Corp 540-862-8426; charden@raschig-usa.com					
Anode Modules													
A-1	Anode Bottom Channel	3' 8 3/16"	1"	1"	Chemical resistant PVC square tube; McMaster Carr 85095K74 or equal	45	pieces	Anode channel secures anode tips and is also perforated; perforations must be drilled. Perforations are for periodic injection of pressurized air or nitrogen for cleaning purposes. Walls are 0.12" with 28 1/4-inch diameter circular holes on top. Each anode channel to be fitted with compressed air fitting and about 2 feet of flexible, nylon compressed air hose.					
A-2	Anode Brushes with Titanium Wire	1'10"		approx 1-in diameter	Custom fabrication	1305	pieces	Specialty item supplied by other					
A-3	Rubber Discs to Hold Anode Brushes to Plate (1/8" cutouts)	3/8" diameter			Flexible PVC snap-in grommets; McMaster Carr 63595K31	2610	pieces	Size may change slightly to fit anode shaft diameter					
A-4	Anode Top Plate	3' 8 3/16"	2"	3/8"	Polycarbonate rectangular bar, McMaster Carr 1749K339	45	pieces	Polycarbonate stock drilled in shop to secure 29 anode modules per 45 top plates; hole diameter to be determined, but approximately 1/4-inch		3/8-in thick			
Compressed Air Piping to Anode Bottom Channel													
CA-1	Air Piping (Hose)	3/8-in inside diameter			Retractable "yellow" nylon hose; McMaster Carr 9150K39 as an example	approx 150	linear feet	Air tubing sizes may be adjusted to fit reactor dimensions					
CA-2	Air Piping (quick disconnect fittings)	3/8-in diameter				5	pairs	Quick disconnects for connection to 2-gallon compressor (compressor by others)					
CA-3	Compressed air fittings	3/8-in diameter				45	pieces	1 connected to each anode bottom channel					

Overview

The pupose of this project is to construct a pilot scale bioreactor under development as a microbial fuel cell. The bioreactor treats domestic wastewater with high BOD content and is able to generate small amounts of electrical current. It is envisioned that the pilot scale reactor will be tested at a military facility and may, in the future, be a model for use in military field applications.

CDM Smith is seeking the services of a specialty fabricator to construct the bioreactor in consultation with our engineers and scientists.

The system consists of a bioreactor tank, appurtanances, and fittings; 44 cathode modules; 45 anode assemblies; and electrical wiring/meters/devices.

While many details are provided in the attached drawings, figures, parts lists, part descriptions, CDM Smith welcomes alternative concepts that meet the intent and design criteria of this design

System Description

The bioreactor is sized to treat a wastewater flow rate of 0.5 gpm and has a hydraulic retention time of about 8 hours. The reactor is configured for a serpentine flow through numerous rectangular plate-type modules. These plates are "cathode modules" and resemble double-sided window screens. In between adacent cathode modules are rows of anodes, which resemble bottle brushes. Above the operating liquid level of the tank, the anode assemblies and cathode modules are electrically wired to measure electrical output.

Because of the goal to generate electrical current and because the process will be anaerobic, certain materials of construction are prescribed, such as PVC, stainless steel, and other non-corrosive materials. Plastics are use for other significant features, such as the top plates that suspend the anodes and the frames for the cathode modules.

Bioreactor

The bioreactor is a simple box, but must retain its basic shape when filled with water. We believe that 3/16-in thick steel will provide sufficient strength.

The bioreactor will be moved, so lifting eyes at the 4 corners and base pieces suitable to allow a forklift to lift the reactor are to be added per the fabricators design. The bioreactor is not intended to be moved when full of water.

The reactor is designed as a rectangular tank, with the general flow path down the long axis of the reactor, currently about 16 feet in length. Inlet, outlet, overflow, and drain ports are at the front and end of the reactor.

A signficant feature of the reactor is the system for holding the anode assemblies and cathode modules. Multiple rows of "angle iron" run the width of the reactor. When seen from the side, the angle pieces will appear as an "L" the adjacent angle as a reverse "L", then an "L", then a reverse "L", and so on. Adjacent lengths of angle pieces hold the top plate of the anode assemblies on the horizontal leg. The cathode modules have horizontal strips on each side, at the top. These strips are intended to rest atop adjacent vertical legs of the angle pieces, such that the cathode modules are set in (and removable) as one might set a slice of bread in a toaster. Because the bioreactor is fairly precisely designed, tolerances for the angle pieces and other features is 1/32 of an inch.

One option under consideration is to mount the angle pieces to a separate top frame that would be about 4 inches in height and match the roughly 3 ft, 9-in wide, 16-ft, 8-in long reactor plan. The main reactor tank and the top frame could be bolted together by fabricating a roughly 2-inch wide flange on each.

Anode Assemblies and suggested assembly steps

Each anode assembly holds 29 anodes vertically, suspended from a polycarbonate (plexliglass or lucite) top plate. The anodes will be produced by others and shipped to the fabricator. To keep the lower tips of the anodes from moving, the tips will be set into a "bottom channel" that will rest in the bottomn of the reactor. The current design calls for square PVC tube as the bottom channel.

The top plate is to be drilled by the fabricator to the diameter of the anode shaft, about 1/4-inch. Rubber, flexible PVC, or similar grommets are to be placed to secure the anode shaft.

The bottom channel serves a second purpose. It is designed to also be a source of compressed air (less than 50 psi) to provide a purge flow of air or nitrogen that will clean solids that may collect on the anodes. Fabricator is to drill holes in the bottom channel to provide the purge air flow. Fabricator is also to attach compressed air fittings and flexible air tubing to the bottom channel. The bottom channel will need to be sealed with end plates to provide an eclosed chamber. CDM Smith envisions PVC plate plate glued to the end of the PVC square tube, but fabricator may elect to use a different method.

The anode assembly is to be removable as an entire assembly (all 29 anodes, top plate and bottom channel together). As such, it will need to have a fair amount of rigidity. Fabricator may elect to affix additional vertical members to hold togther the top plate and bottom channel.

The air or nitrogen supply for purging will be periodic, not continuous, so CDM Smith envisions quick disconnects at the top of the anode plate, such that the air supply can be disconnected when not in use.

Cathode modules and suggested assembly steps

Each of the 44 cathode modules resembles a double-pane glass window, except that the panes of glass are stainless steel mesh coated with an electrically conductive "carbon" coating. The window frame is to be built of PVC shapes, milled and assembled (welded or glued using PVC glue) to provide a rigid frame. In the "air space" between the two sheets of stainless steel screen there will be a flexible plastic layer (spacer) measuring the size of the open pane. This spacer will be about 20 mm thick. A celluose/polyester (cloth) layer will cover the carbon-coated stainless steel mesh. This cloth layer is intended to be removable.

The carbon-coated stainless steel screens will be supplied by others.

The plastic spacers will be supplied by others.

The cathode module assembly method is suggested below, but fabricator is welcome to consider other methods. Note that there will be 44 two-faced modules, so a custom jig is recommended.

1 Procure and mill the square PVC stock to produce a rabbet on adjacent edges. The two vertical members and the bottom horizontal member shall be similarly milled and are also to include a half-circle groove into which a solicone gasket will be placed. The frame may be glued or welded together. Fabricator is welcome to use other mortise/tenon or similar jointing methods at the corners to better secure the frame.

2 Procure and cut to size the cathode mounting strip from PVC stock.

3 Secure the mounting strip to the U-shaped frame by welding or gluing

4 Procure and, if necessary, cut to width, the PVC mounting strip. There will be mounting strips to match the U-shaped frame (two vertical and one horizontal).

5 Set the mounting strip inside the U-shaped frame. Drill into both to match the mounting holes. Using a drill tap, tap the holes to match the stainless steel bolt thread size.

6 Place the silicone gasket material in the half circle groove.

7 Precut 88 stainless steel mesh pieces to fit the inset frame created by the rabbeted edge. Do not cut them too small or you are doomed!

8 Precut 88 cloth layers to this same size.

9 Set one layer of the stainless steel mesh, carbon-layer facing "out" (with respect to the "air space" of the frame). Ensure the mesh fits exactly within the frame. Note that there will be an upper, exposed edge of the stainless steel

10 Place the cloth layer on top of the mesh layer.

11 Secure double layer using the PVC strip and multiple stainless steel bolts. Set your DC-drill on low torque to prevent stripping the threads.

12 Flip the module over.

13 Repeat the process of drilling and tapping the mounting strip and frame

14 Set the plastic spacer sheet against the inside of the first sheet of stainless steel mesh.

15 Set the gasket on this face

16 Set the stainless steel mesh layer.

17 Set the cloth layer

18 Set the PVC mounting strips and secure with stainless steel bolts. Yes, there are a lot of these little bolts.

19 Repeat to produce 44 cathode modules

Appendix B

Electrical Design Details

NOTES:

1. EACH INDIVIDUAL ANODE/CATHODE PAIR WILL BE CONNECTED TO ONE BOOST CONVERTER (1ST STAGE).
2. BUNDLED WIRING FROM MICROBIAL FUEL CELL TO JUNCTION BOX.
3. BOOSTERS 1 – 44 OUTPUTS SHALL BE PARALLELED AND FEED BOOSTER 45 VIA A SUPER CAPACITOR.
4. CONNECTION POINT FOR THE KEITHLEY DIGITAL MULTIMETER WILL BE AT TERMINAL BLOCK, TO MEASURE VOLTAGE AND CURRENT.
5. PROVIDE NUMBER OF RECEPTACLES AS REQUIRED.
6. CAPACITOR RATINGS ARE 90 MILLIFARAD AT 12 VOLTS. SUPER CAPACITOR SHALL BE SOLDERED IN PARALLEL TO THE INPUT OF BOOSTER 45.

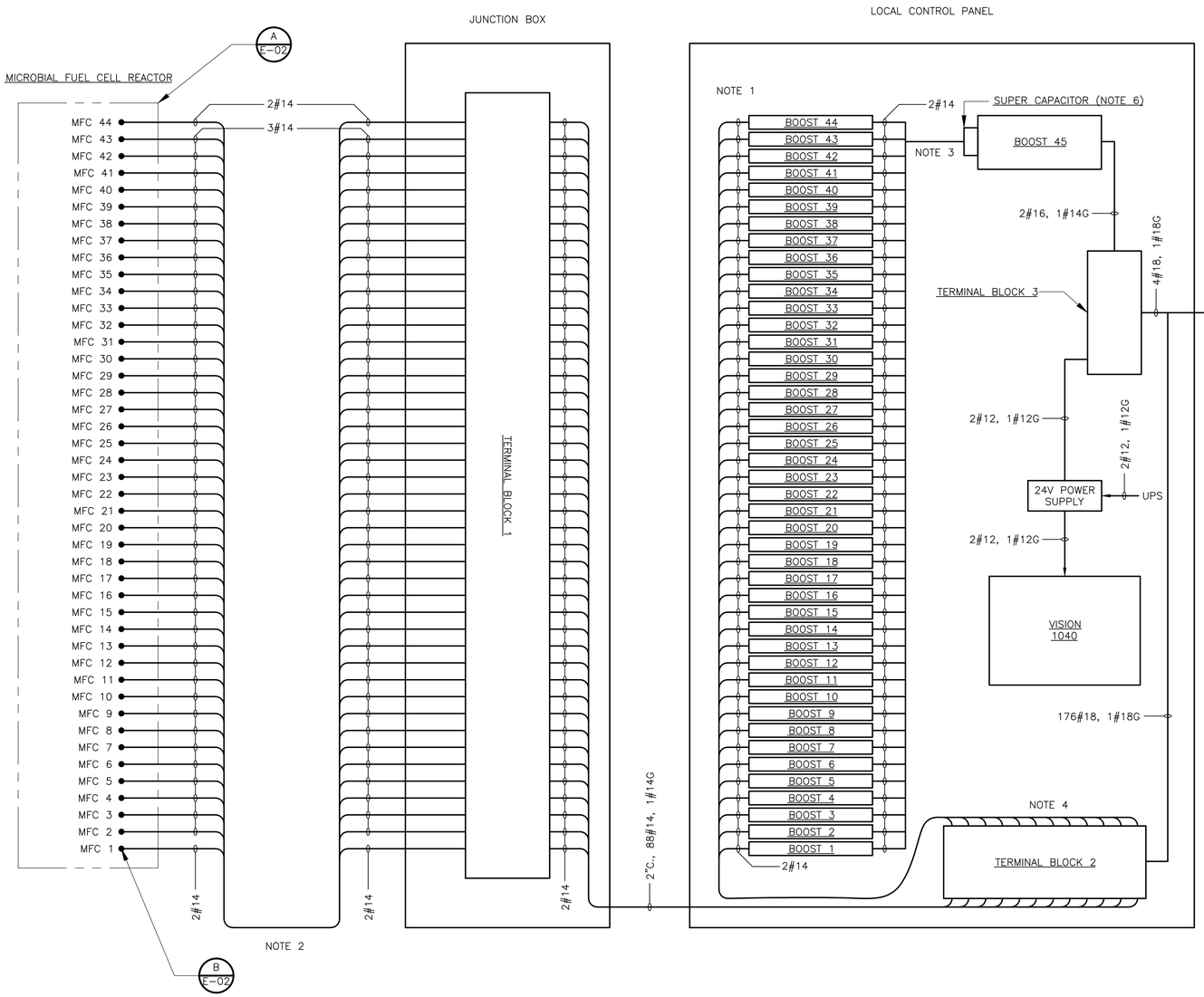

MICROBIAL FUEL CELL

WIRING DIAGRAM

N.T.S.

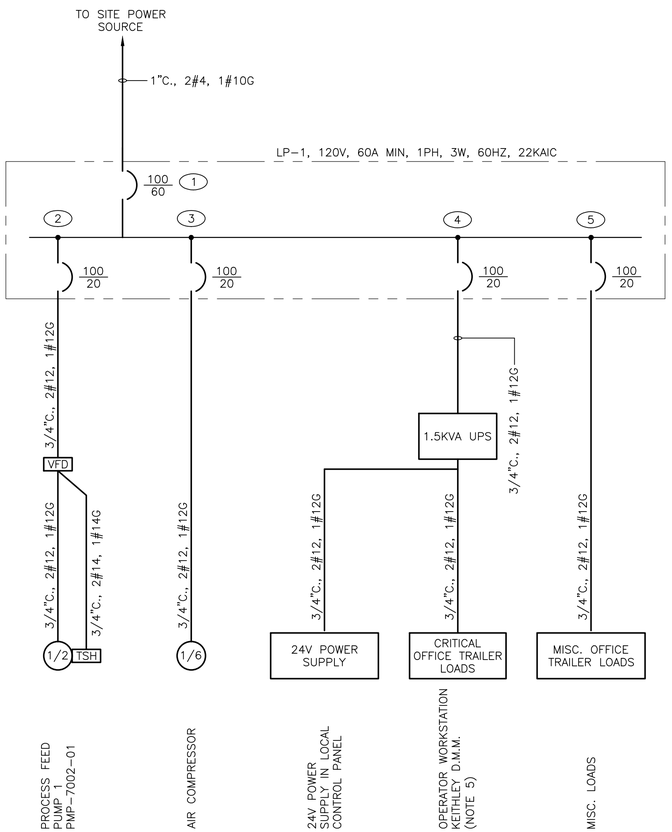

SITE

ONE-LINE DIAGRAM

N.T.S.

I HEREBY CERTIFY THAT THIS PLAN, SPECIFICATION, OR REPORT WAS PREPARED BY ME OR UNDER MY DIRECT SUPERVISION AND THAT I AM A DULY LICENSED PROFESSIONAL ENGINEER UNDER THE LAWS OF THE STATE OF MINNESOTA.

SIGNATURE

TYPED NAME

REGISTRATION NUMBER

DATE

REV. NO.	DATE	DRWN	CHKD	REMARKS

DESIGNED BY: O. DEL OLMO
DRAWN BY: O. DEL OLMO
SHEET CHK'D BY: T. MOHAMMAD
CROSS CHK'D BY: P. EVANS
APPROVED BY:
DATE: JUNE 2015

CDM Smith
75 State Street, Suite 701
Boston, MA 02109
Tel: (617) 452-6000

PENN STATE UNIVERSITY

MICROBIAL FUEL CELL DESIGN

ELECTRICAL
ONE - LINE DIAGRAM

PROJECT NO. 83278-95598
FILE NAME: E-01

SHEET NO.

E-01

PRELIMINARY DESIGN SUBMITTAL - NOT FOR CONSTRUCTION

© 2015 CDM SMITH ALL RIGHTS RESERVED.
REUSE OF DOCUMENTS: THESE DOCUMENTS AND DESIGNS PROVIDED BY PROFESSIONAL SERVICE, INCORPORATED HEREIN, ARE THE PROPERTY OF CDM SMITH AND ARE NOT TO BE USED, IN WHOLE OR PART, FOR ANY OTHER PROJECT WITHOUT THE WRITTEN AUTHORIZATION OF CDM SMITH.

© 2015 CDM SMITH ALL RIGHTS RESERVED.
REUSE OF DOCUMENTS: THESE DOCUMENTS AND DESIGNS PROVIDED BY PROFESSIONAL SERVICE, INCORPORATED HEREIN, ARE THE PROPERTY OF CDM SMITH AND ARE NOT TO BE USED, IN WHOLE OR PART, FOR ANY OTHER PROJECT WITHOUT THE WRITTEN AUTHORIZATION OF CDM SMITH.

NOTES:

1. NICKEL PLATED TITANIUM ROD ENDS.
2. CATHODE EDGE IS TO BE SOLDERED ONTO 39.37" × $\frac{1}{16}$" × $\frac{1}{4}$" NICKEL PLATED STAINLESS STEEL ROD.
3. 16 AWG WIRE TO BE SOLDERED ONTO THE NICKEL PLATED ROD, THE SIDE CLOSES TO THE NEMA 4X JUNCTION BOX
4. CORROSION COATING IS TO BE APPLIED TO ALL SOLDERED JUNCTIONS.
5. ONE MICROBIAL FUEL CELL WILL BE DETERMINED AS ONE ANODE ASSEMBLY PAIRED WITH THE NEAREST CATHODE.

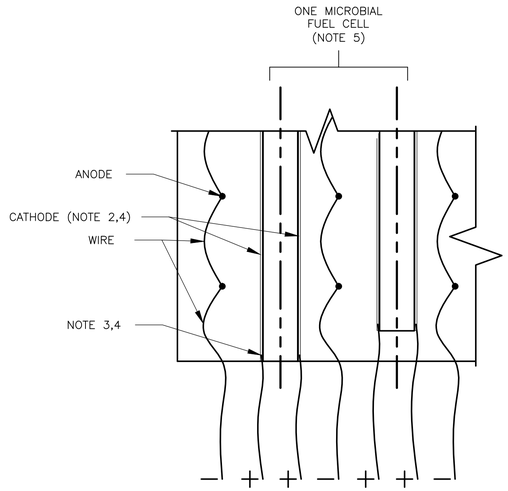

MICROBIAL FUEL CELL
DETAIL A / E−01
N.T.S

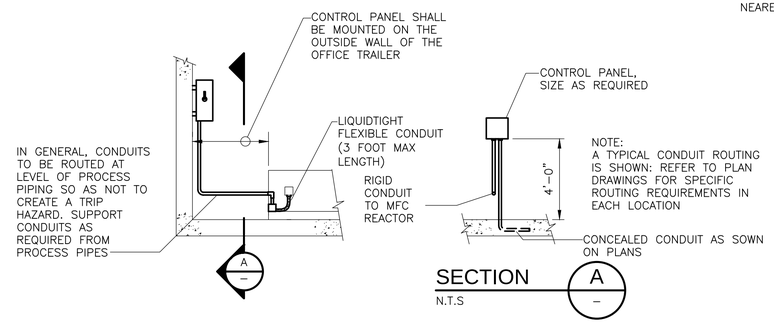

SECTION A / –
N.T.S

WALL MOUNTED CONTROL STATION
DETAIL D / –
N.T.S

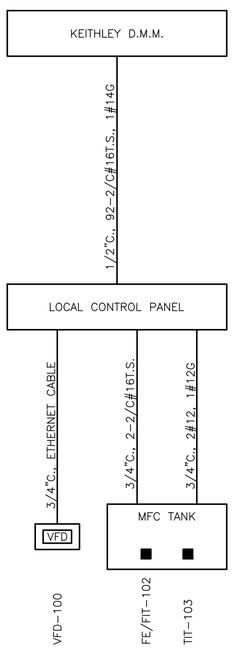

MICROBIAL FUEL CELL RISER DIAGRAM
RISER DIAGRAM
N.T.S.

BILL OF MATERIALS:

1. 16 AWG WIRE, XHHW – RED
2. 16 AWG WIRE, XHHW – BLACK
3. 18 AWG WIRE, THHW – RED
4. 18 AWG WIRE, THHW – WHITE
5. 12 AWG WIRE, XHHW – RED
6. 12 AWG WIRE, XHHW – GREEN
7. 2 CONDUCTOR 14 AWG TWISTED SHIELDED WIRE
8. CAT 6 CABLE
9. NEMA 4X JUNCTION BOX
10. DIN RAIL
11. QUICK CONNECTS TERMINAL BLOCK
12. TERMINAL BLOCK LABELS
13. STANDARD TERMINAL BLOCK – GROUND
14. STANDARD TERMINAL BLOCK – GREY
15. BOOST CONVERTER (.2V TO 10V) – W0422–1 (44 PCS)
16. BOOST CONVERTER (10V TO 24Vout)– Y0701 (1 PCS)
17. DIN RAIL HOUSINGS FOR PCBS
18. NEMA 4X NON–METALLIC PANEL
19. ALUMINUM BACK PLATE
20. 2" LIQUID TIGHT CONDUIT
21. 2" LIQUID TIGHT FITTINGS
22. CORROSION RESISTANT COATING (ZRC 221)
23. 3" FLEXIBLE METAL CONDUIT
24. 3" FLEXIBLE METAL CONDUIT FITTINGS
25. 3/4" RIGID METAL CONDUIT
26. 3/4" RIGID METAL CONDUIT FITTINGS

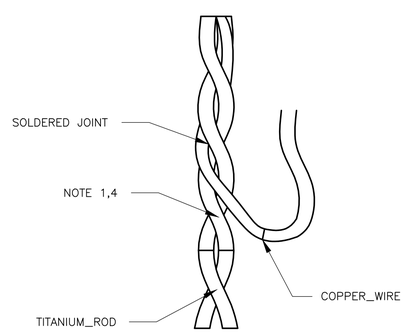

CATHODE–WIRE CONNECTION
DETAIL B / E−01
N.T.S

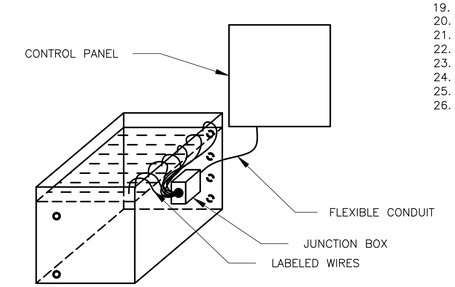

SYSTEM OVERVIEW
DETAIL C / –
N.T.S

I HEREBY CERTIFY THAT THIS PLAN, SPECIFICATION, OR REPORT WAS PREPARED BY ME OR UNDER MY DIRECT SUPERVISION AND THAT I AM A DULY LICENSED PROFESSIONAL ENGINEER UNDER THE LAWS OF THE STATE OF MINNESOTA.

SIGNATURE
TYPED NAME
REGISTRATION NUMBER
DATE

REV. NO.	DATE	DRWN	CHKD	REMARKS

DESIGNED BY: O. DEL OLMO
DRAWN BY: O. DEL OLMO
SHEET CHK'D BY: T. MOHAMMAD
CROSS CHK'D BY: P. EVANS
APPROVED BY:
DATE: JUNE 2015

CDM Smith
75 State Street, Suite 701
Boston, MA 02109
Tel: (617) 452-6000

PENN STATE UNIVERSITY

MICROBIAL FUEL CELL DESIGN

ELECTRICAL
RISER DIAGRAM & STANDARD DETAILS

PROJECT NO. 83278–95598
FILE NAME: E00
SHEET NO.
E-02

PRELIMINARY DESIGN SUBMITTAL - NOT FOR CONSTRUCTION

BILL OF MATERIALS:

Item	Description	Manufacturer	Part Number	Qty	Unit Measure	Notes
1	16 AWG WIRE, XHHW - RED	-	-	2	spools	approximate
2	16 AWG WIRE, XHHW - BLACK	-	-	2	spools	approximate
3	18 AWG WIRE, THHW - RED	-	-	1	spools	approximate
4	18 AWG WIRE, THHW - WHITE	-	-	1	spools	approximate
5	12 AWG WIRE, XHHW	-	-	1	spool	approximate
6	12 AWG WIRE, XHHW - GREEN	-	-	50	ft	approximate
7	2 CONDUCTOR 14 AWG TWISTED SHIELDED WIRE	-	-	50	ft	approximate
8	CAT 6 CABLE	-	-	25	ft	approximate
9	NEMA 4X JUNCTION BOX	Hoffman	-	1	each	
10	DIN RAIL	-	-	as needed		
11	QUICK CONNECTS TERMINAL BLOCK	-	-	as needed	267 (approx)	
12	TERMINAL BLOCK LABELS	-	-	as needed	267 (approx)	
13	STANDARD TERMINAL BLOCK - GROUND	-	-	as needed		
14	STANDARD TERMINAL BLOCK - GREY	-	-	as needed		
15	BOOST CONVERTER (.2V TO 10V)	TXL Group	W0422-1	44	each	
16	BOOST CONVERTER (10V TO 24Vout)	TXL Group	Y0701	1	each	
17	DIN RAIL HOUSINGS FOR PCBS	-	-	45	each	
18	NEMA 4X NON-METALLIC PANEL	Hoffman	-	1	each	
19	ALUMINUM BACK PLATE	Hoffman	-	1	each	
20	2" LIQUID TIGHT CONDUIT	-	-	as needed		
21	2" LIQUID TIGHT FITTINGS	-	-	as needed		
22	CORROSION RESISTANT COATING (ZRC 221)	ZRC	ZRC 221	as needed		or equivalent
23	3" FLEXIBLE METAL CONDUIT	-	-	as needed		
24	3" FLEXIBLE METAL CONDUIT FITTINGS	-	-	as needed		
25	3/4" RIGID METAL CONDUIT	-	-	as needed		
26	3/4" RIGID METAL CONDUIT FITTINGS	-	-	as needed		
27	90 MILLIFARAD SUPER CAPACITOR, 12V	-	-	1	each	

The following discussion details the necessary preparation work required to make solid electrical connections to the anode assembly in order to mitigate transition resistance between the anode assemblies and the homeruns to the boost converters. As part of anode preparation, the ends of each titanium current collector should be nickel plated to facilitate the soldering junction between the copper wire and the titanium rod (it should be noted that alternatives to nickel plating do exist for this specific application, i.e., SBond 220). Each anode module contains 29 titanium rods, which will be daisy-chained together using a copper cable. Cutting a piece of black wire, stripping both ends and wrapping each end to two adjacent rods (see Detail B on Drawing E-02). If the titanium rods are nickel plated, using standard rosin-less solder and a hot soldering iron can solder the wrapped copper wire to the titanium rod. If the titanium rods were not nickel plated, use the recommended "SBond 220" and hot soldering iron to solder the copper wire to the titanium rod. It is crucial not to overheat the copper wire, as it may damage the wire's insulation which is crucial to protect the copper strands from corrosion. Inspection for fractures of each solder joint will be required after installing each anode assembly to the MFC reactor. (NOTE: corrosion coating will need to be applied after all the system has been commissioned and each solder joint has been cleaned with rubbing alcohol and ready for long-term operation.)

The following preparation work is needed to make solid electrical connections to the cathode modules to mitigate transition resistance between the cathode assemblies to the homeruns back to the boost converters. The top edge of the cathode stainless steel mesh current collector (the "exposed" edge, see mechanical details) should be nickel plated as well as welded to a 1/4-in x 1/16-in stainless steel bar (it should be noted that alternatives to nickel plating do exists for this specific application, i.e., Silvaloy 505). Each cathode module will have two SS mesh and two SS rods and the installation of the SS rods to the SS mesh should be done prior to the full assembly of the cathode assembly. The SS rod will be lined up to the "exposed" edge of the SS mesh, as detailed by the mechanical plans (see Figure 60). If the SS mesh and rods were nickel plated, using standard rosin-less solder and a blow torch can be used to bond the two metals together. If no nickel plating was done, use the recommended "Silvaloy 505" & recommend flux with a blow torch to bond the two metals together. Be sure to use plenty of flux to ensure proper bonding and wicking has been achieved between the mesh and rod. Inspection for fractures of each SS mesh and rod bond will be required after installing each cathode assembly to the MFC reactor. (NOTE: corrosion coating can be applied after both metals have cooled down to a safe handling temperature and have been thoroughly cleaned with rubbing alcohol.)

The following discussion is provided to help understand the system topology and wiring scheme. Drawing E-01 shows the high level wiring of the MFC system. Included on Drawing E-01 is the electrical connection required to have the electrical infrastructure to power the trailer office. Drawing E-02 contains a riser diagram detailing the instrumentation connections required by process control.

After completing all the sub-assemblies, the full system can be built. Each anode assembly and cathode assembly will be paired and counted as one cell (See attached Detail A on Drawing E-02). Each paired cell will be wired to a quick connect terminal block found inside the NEMA 4X

junction box. From the junction box, the paired cells will be wired to a second terminal block located inside the local control panel via a liquid tight conduit fastened to the junction box and connects the local control panel. This terminal block will be the junction point where the supervisory control and data acquisition (SCADA, Keithley Model 2750) system will tap each MFC connected to each boost converter, measuring each low voltage and current from each MFC. A shunt resistor will need to be provided to help measure current of each MFC. The shunt resistor will be installed between terminal block 2 and each boost converter. The Keithley will also tap each output of the first stage converters to measure each boost converter's current output.

A super capacitor will be used to connect all 44 low voltage boost converters as an interim storage device provided by TXL Group Inc. The super capacitor (see Figure 65) will feed its stored energy to a second stage boost converter (TXL Group Inc.'s product number Y0701) to step the voltage to the desired voltage level of 24VDC. One boost converter will be used, therefore all the low voltage boost converters' outputs will be parallel connected to the super capacitor. There will be two channels from the Keithley measuring device used to measure the total voltage and total current feeding the second stage converter. A second pair of channels and connections will be made at the output of the second stage converter to measure both voltage and current. The final piece to the system is connecting a 24VDC load to the output of the final stage boost converter.

ULTRA-LOW VOLTAGE BOOTSTRAP CONVERTER

DATASHEET W0422-1,2

INTRODUCTION

The W0422 line of bootstrap converters are self-oscillating DC/DC converters that convert DC power at very low voltages into power at higher, more usable voltages. These converters are specifically designed for thermoelectric generation, where temperature gradients that are harvested for power may be only a few degrees, causing generated voltages that are too low for direct use.

THERMOELECTRIC GENERATION

Thermoelectric (TE) phenomena arise from the intercoupled electrical and thermal currents in a material. A thermoelectric generator is constructed by connecting multiple n-type and p-type thermoelements in electrical series with all elements in thermal parallel between a heat source and a heat sink. A scaffolding is often used on the top and the bottom of a device to lend mechanical support to the thermoelements. Figure 1 depicts a commercially available device with the top scaffolding removed.

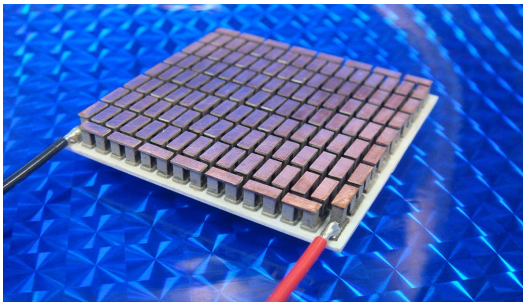

Figure 1 – A 254 Element TE Module
(model TXL-127-03L)

Any thermoelectric device can be used for either generation or for heat pumping. In a heat pumping application, the TE device is often referred to as a Peltier module or cell. When an electrical current is applied, heat is moved from one side to the other side of the device. The W0422 bootstrap converters can work with TE devices that have been designed for either generation or heat pumping.

TE-GENERATED VOLTAGE

The open circuit voltage that is generated from a temperature differential across a thermoelectric module is a function of the temperature gradient, ΔT, the number of series connected elements, j, and a material constant called the Seebeck coefficient, S. If it is assumed that the n-type and p-type thermoelements have the same magnitude of thermoelectric properties, then the open circuit voltage may be written as

$$V_{OC} = j \times S \times \Delta T \qquad (1)$$

The ΔT in eq. (1) will always be less than the difference between heat source and heat sink temperatures due to thermal resistances between source/sink and the actual thermoelements. These “parasitic” thermal resistances should be minimized to the greatest extent possible.

OBTAINING MAXIMUM POWER

Every generator has an internal electrical impedance, often referred to as the source resistance, R_S. When a thermoelectric module is used for generation, this source resistance is primarily due to the electrical resistance of the individual thermoelectric elements. If we assume that there is a constant resistance, $R_{element}$, for both n-type and p-type thermoelements, then for a generator having a total of j elements, the source resistance is

$$R_s = j \times R_{element} \qquad (2)$$

The source resistance serves to reduce the power that can be delivered to an electrical load. A well-known result from electric circuit theory is that the maximum power that can be delivered by a source to an electrical load is obtained when the load impedance is designed to be the same as the source impedance. This is called impedance matching. The W0422 line of bootstrap generators are designed for operation over the range of $R_S = 1\Omega$ to $R_S = 10\Omega$ with an optimal efficiency for $R_S = 3\Omega$.

UNIPOLAR AND BIPOLAR CONVERSION

The W0422-1 is a unipolar DC/DC converter that steps up an input voltage of fixed polarity. The W0422-2 is a bipolar DC/DC converter that can accept voltages of either polarity. Both converters measure 0.45 inches by 1.05 inches (11 mm X 26.7 mm).

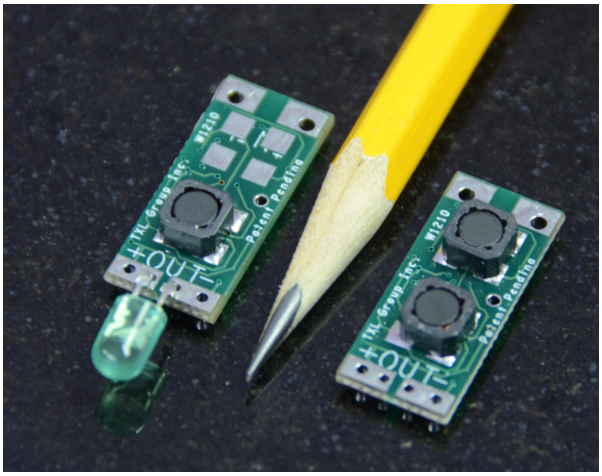

Figure 2 – On left, W04022-1 with optional LED Load;
On right, W04022-2

The amount of output power that can be obtained from any

thermoelectric device depends upon the open circuit voltage V_{oc}, the internal resistance of the module, R_S, and the nature of the load. In most applications for harvesting energy from environmental heat, fluctuations in ΔT may cause intermittent charging, so it is desirable to intermittently charge an electrochemical cell (the load) which then furnishes power as needed for sensing or wireless transmission duties. Figure 3 depicts the power delivered by the W0422 converter to a 3 volt Lithium-Ion rechargeable cell as a function of the open circuit (unloaded) voltage, V_{OC}. The curves in Figure 3 correspond to three cases of TE cell internal resistance. The actual performance that is obtained will depend upon the particular internal resistance, R_S, of the chosen thermoelectric module.

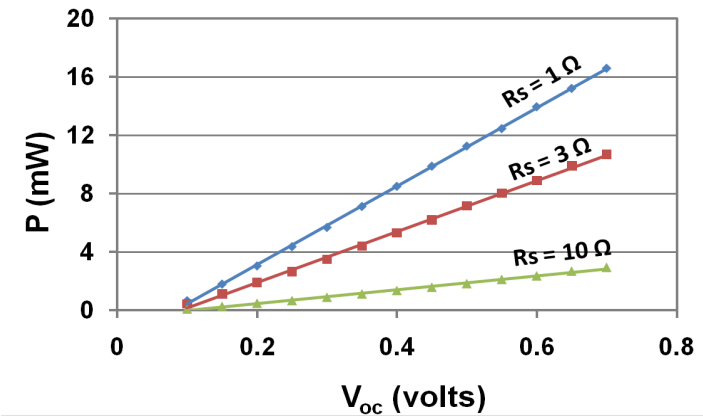

Figure 3 – Output Power vs V_{OC} When Charging a 3V Cell

Figure 4 depicts the input voltage to the W0422-1 module as a function of V_{OC}, when charging a 3 volt cell. The output current delivered to the cell (load) is calculated by dividing the output power by 3. The input current to the W0422-1 is obtained by taking the difference between V_{OC} and V_{in} and dividing by R_S. The input power to the W0422-1 is the product of input current and input voltage.

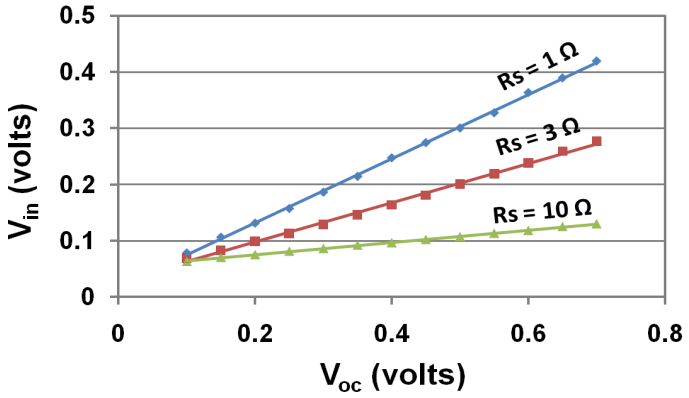

Figure 4 – Input Voltage vs V_{OC} When Charging a 3V Cell

A DESIGN EXAMPLE

Eq. (1) and Figures 3 and 4 may be used to estimate power and charge current for a given thermoelectric module and a given ΔT. Consider the TXL Group model TXL-127-03L, 254 element module depicted in Figure 1 with R_S = 6 Ω. The elements are made of n-type and p-type bismuth telluride alloys with an approximate Seebeck coefficient of S = 180 μV/C. For ΔT = 6°C, by equation (1), the open circuit voltage is V_{OC} = 274 mV. From Figures 3 and 4, the output power and input voltage (corresponding to V_{OC}=0.274 V and interpolating for R_S =6 Ω) are determined to be, respectively, 2 mW and 100 mV. The charging current delivered to the Li-Ion cell is 2mW/3V = 666 μA. The input power is the product of input current and V_{in}, so

$$P_{input} = \frac{0.274 - 0.100}{6} \times 0.100 = 2.9\,mW \qquad (3)$$

and the electronic conversion efficiency may be calculated as:

$$\eta = \frac{P_{out}}{P_{input}} = \frac{2\ mW}{2.9\ mW} = 69\% \qquad (4)$$

RESTRICTIONS ON THE LOAD

Other rechargeable cells can be used with this circuit, including series connected NiCad cells with nominal battery voltage of up to six volts. Or, instead of an electrochemical cell, a high capacitance, low leakage, "super cap" can serve as the load[1]. ***The W0422 bootstrap converter yields an unregulated output, so care should be taken not to overcharge a cell or to exceed a capacitor voltage rating.***

USING THE ENABLE PIN

For applications in which the W0422-1 or W0422-2 converters will be interfaced to a microcontroller, an enable port is provided that can be used to hold the microcontroller in a reset mode until the power supply has stabilized to a sufficiently high value. In Figure 2, this is seen as the port that is between the words "Patent" and "Pending". When the output voltage is under 1.1 volts, the resistance between the enable pin and the minus side of V_{out}^- is less than 2 kΩ. When the output voltage is greater than 1.4 volts, the resistance between the enable pin and V_{out}^- is greater than 1 MΩ. In a microcontroller application, the W0422 furnishes power at V_{out}. An active low reset line of the microcontroller can be tied to the enable port and use a 10 kΩ pull-up from reset to V_{out}^+. So, when the microcontroller has an applied voltage of under 1.1 volts, it is held in a reset condition by the enable line. When the W0422 output voltage goes above about 1.2 volts, the reset line goes high and the microcontroller is enabled.

ABOUT TXL

TXL Group, Inc. is an El Paso, Texas company developing industrial Waste Heat Harvest® solutions[2]. Part of this effort entails developing electronic devices for efficient energy power conversion from the low voltages typical of thermoelectric generation devices. This has led the Company to investigate a range of solutions for scalable thermoelectric power generation. TXL offers a range of thermoelectric devices and electronic conversion solutions from microwatts and up. Since thermoelectric generation solutions are scalable, the potential is huge. It's an endless harvest!

1 A series resistance of >100 Ω should be used with a super cap.
2 *Waste Heat Harvest*® is a U.S. Registered Trademark of TXL Group, Inc.

PROGRAMMABLE BOOST CONVERTER

DATASHEET Y0701

INTRODUCTION

The Y0701 programmable boost converter is a self-oscillating DC/DC converter that can be hardware programmed to convert an input voltage as low as 2.8 volts into a selectable, regulated DC output voltage. On-board resistors are provided to allow jumper selectable voltages of +9, +12, +14 or +24 volts. By adding a single 0805 style resistor, an arbitrary output voltage of between 6 to 36 volts may be selected. These converters are specifically designed for use with thermoelectric generators, where thermoelectrically generated voltages may be either variable or too low for direct use.

THERMOELECTRIC GENERATION

Thermoelectric (TE) phenomena arise from the intercoupled electrical and thermal currents in a material. A thermoelectric generator is constructed by connecting multiple n-type and p-type thermoelements in electrical series with all elements in thermal parallel between a heat source and a heat sink. A white alumina scaffold is often used on the top and the bottom of a device to lend mechanical support to the thermoelements.

Any thermoelectric device can be used for either generation or for heat pumping. In a heat pumping application, the TE device is often referred to as a Peltier module or cell. When an electrical current is applied, heat is moved from one side to the other side of the device. The Y0701 Programmable Boost Converter can work with TE devices that have been designed for either generation or heat pumping.

TE-GENERATED VOLTAGE

The open circuit voltage that is generated from a temperature differential across a thermoelectric module is a function of the temperature gradient, ΔT, the number of series connected elements, j, and a material constant called the Seebeck coefficient, S. If it is assumed that the n-type and p-type thermoelements have the same magnitude of thermoelectric properties, then the open circuit voltage may be written as

$$V_{OC} = j \times S \times \Delta T \quad (1)$$

The ΔT in eq. (1) will always be less than the difference between heat source and heat sink temperatures due to thermal resistances between source/sink and the actual thermoelements. These "parasitic" thermal resistances should be minimized to the greatest extent possible.

OBTAINING MAXIMUM POWER

Every generator has an internal electrical impedance, often referred to as the source resistance, R_S. When a thermoelectric module is used for generation, this source resistance is primarily due to the electrical resistance of the individual thermoelectric elements. Assuming a constant resistance, $R_{element}$, for both n-type and p-type thermoelements, then for a generator having a total of j elements, the source resistance is

$$R_s = j \times R_{element} \quad (2)$$

The source resistance serves to reduce the power that can be delivered to an electrical load.

THEORY OF OPERATION

The Y0701 is a unipolar DC/DC up-converter that takes a DC voltage and converts it to a higher, preselected, regulated voltage. The approach is based upon a pulse width modulation (PWM) control scheme whereby input power is stored within a magnetic field in an inductor and then released into an output capacitor to supply load current and maintain a selected output voltage.

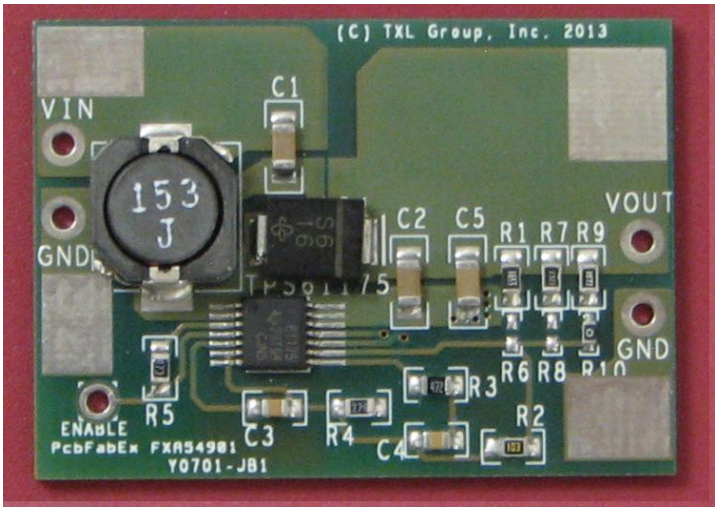

Figure 1 – The Y0701 Programmable Boost Converter

Figure 1 depicts the Y0701. There are five external connections. The input voltage is applied at the nodes labeled VIN and GND. The nodes labeled VOUT and GND are the output. Pads above and below these four nodes allow easy clip lead and solder attachment. The GND nodes for the input and output are electrically connected. In a correct application, VIN and VOUT will have a positive polarity with respect to ground. The node labeled ENABLE in the lower left represents a means to turn on and off the converter. This has an internal pull-up. When the enable input is pulled to ground, the device is disabled and no power will be supplied at VOUT.

PROGRAMMING THE OUTPUT VOLTAGE

The Y0701 has a preprogrammed jumper selectable output voltage. By placing 0 Ω, size 0604 shorting resistors in positions R6, R8 and/or R10, it is possible to program an output voltage of +24, +14, +12 or +9 VDC. Equivalently, R6, R8 and R10 may be shorted with a wire or solder blob to select the output voltage. All units are shipped from the factory with R6 and R8 open and R10 shorted to provide a default voltage of +24V. Table 1 lists the different setpoint voltages that can be obtained by opening (o) or shorting (s).

R6	R8	R10	Vout
O	O	S	+ 24 V (default)
O	S	O	+ 29.7 V
O	S	S	+ 14 V
S	O	O	+ 21.5 V
S	O	S	+ 12 V
S	S	O	+ 13.1V
S	S	S	+ 9 V

Table 1 – Jumper Configurations to Select Vout

DO NOT OPERATE WITH ALL OPEN! It is possible to program other output voltages over the range of +6 to +36 volts by keeping R6 and R8 open, R10 short, and changing the value of R9 according to the equation

$$R9 = 10{,}000\left(\frac{Vout}{1.229} - 1\right) \qquad (3)$$

So, for example, to select an output of +36 V, use the default configuration with R9 changed to a value of 283 kΩ.

ELECTRICAL SPECIFICATIONS

VIN: +2.8 VDC to +18 VDC
VOUT: + 6 VDC to +36 VDC
PMAX: 8 Watts

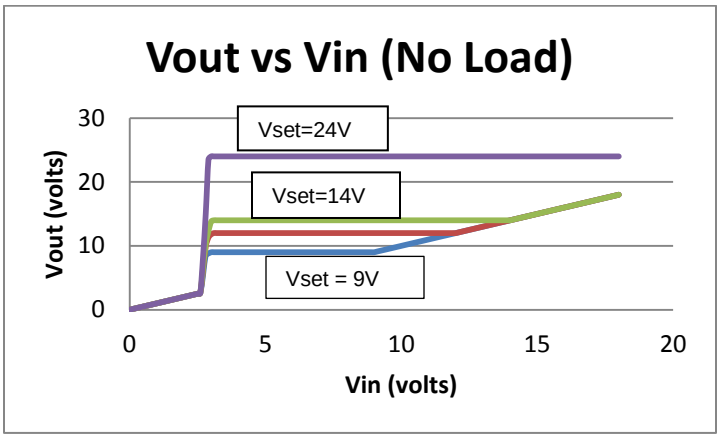

Figure 2 – Vout vs Vin Under No-Load Conditions

It is important to note that the Y0701 converter module can only step up a voltage. When the input voltage exceeds the setpoint voltage, then the output voltage will exceed the setpoint voltage and will track the input voltage. This is seen in Figure 2.

CONVERSION EFFICIENCY AND RIPPLE

Conversion efficiency is highly dependent upon source impedance, input voltage, output voltage and the power drawn by the load. The maximum power at all programmed voltages is 8 watts, corresponding to 333 mA at 24 volts, 667 mA at 12 volts, etc. For light loading of under 4 watts, the efficiency will typically exceed 90%.

Conversion efficiency and output regulation, particularly at relatively heavy loads, are dependent upon the source resistance and the load characteristics. In particular, for heavy loads, a ripple voltage may be observed at the output. This can be reduced by adding output capacitance in parallel with the load.

TYPICAL APPLICATIONS

When the input power is thermoelectrically generated, the voltage will vary with the temperature gradient. In these cases, if the desired voltage is higher than the thermoelectrically generated voltage, the Y0701 converter can serve to deliver power at a known regulated voltage. This is well suited for rechargeable battery applications either with or without a dropping resistor. The enable pin on the Y0701 may be a useful feature for controlling power to the load.

The starting point for any design is to determine if the input can source enough power to boost and furnish to the load. From circuit theory, the maximum power that can be drawn from a source is obtained when the load impedance matches the source impedance. So, for example, if the open circuit (no load) voltage from a thermoelectric module is + 4 volts and that module has an input resistance of 1 Ω, the maximum power that can be delivered by that source occurs for a load of 1 Ω, in which case the load would have 2 volts and the power delivered to that load would be 4 watts. So the maximum power that can be delivered by the source in this example is 4 watts, irrespective of the output voltage setpoint. Of course, the power delivered to a load at any given voltage setpoint will be somewhat less than the maximum possible input power due to efficiency losses.

Each application will present its own challenges and should be tested for extreme cases of anticipated input voltage and loading. In particular, the input voltage must be clamped to a not-to-exceed voltage of +18 V.

ABOUT TXL

TXL Group, Inc. is an El Paso, Texas company developing industrial Waste Heat Harvest® solutions[1]. In many applications, thermoelectric generation alone does not directly provide the desired voltage level. As such, high efficiency conversion is an important part of any design as an arbitrary X% improvement in conversion efficiency has the same overall impact on systems efficiency as an X% improvement in thermoelectric generation. This has led TXL Group to investigate a range of solutions for scalable thermoelectric power generation from microwatts and up.

1 *Waste Heat Harvest®* is a U.S. Registered Trademark of TXL Group, Inc.

Appendix C

Instrumentation Design Details

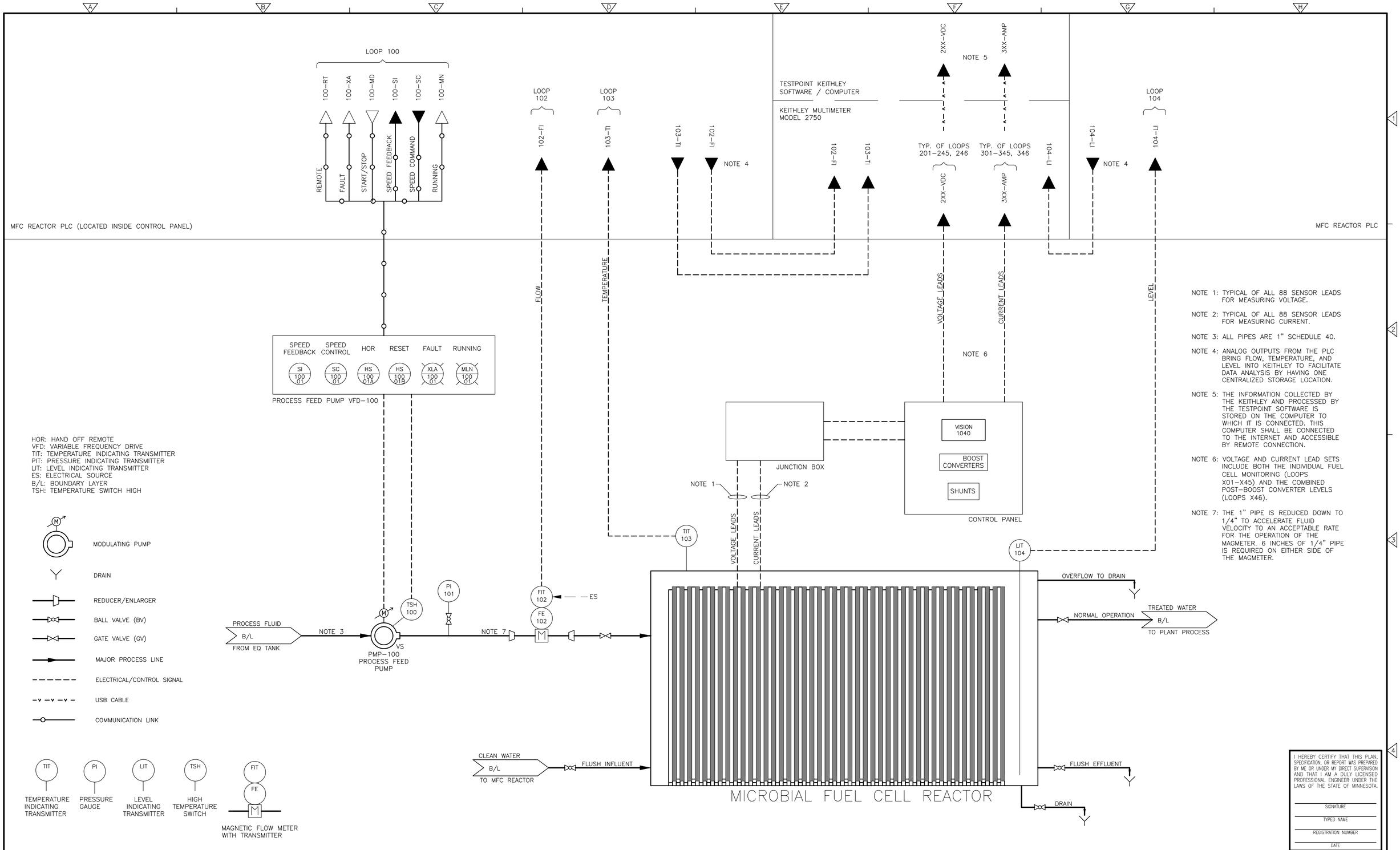

NOTE 1: TYPICAL OF ALL 88 SENSOR LEADS FOR MEASURING VOLTAGE.

NOTE 2: TYPICAL OF ALL 88 SENSOR LEADS FOR MEASURING CURRENT.

NOTE 3: ALL PIPES ARE 1" SCHEDULE 40.

NOTE 4: ANALOG OUTPUTS FROM THE PLC BRING FLOW, TEMPERATURE, AND LEVEL INTO KEITHLEY TO FACILITATE DATA ANALYSIS BY HAVING ONE CENTRALIZED STORAGE LOCATION.

NOTE 5: THE INFORMATION COLLECTED BY THE KEITHLEY AND PROCESSED BY THE TESTPOINT SOFTWARE IS STORED ON THE COMPUTER TO WHICH IT IS CONNECTED. THIS COMPUTER SHALL BE CONNECTED TO THE INTERNET AND ACCESSIBLE BY REMOTE CONNECTION.

NOTE 6: VOLTAGE AND CURRENT LEAD SETS INCLUDE BOTH THE INDIVIDUAL FUEL CELL MONITORING (LOOPS X01-X45) AND THE COMBINED POST-BOOST CONVERTER LEVELS (LOOPS X46).

NOTE 7: THE 1" PIPE IS REDUCED DOWN TO 1/4" TO ACCELERATE FLUID VELOCITY TO AN ACCEPTABLE RATE FOR THE OPERATION OF THE MAGMETER. 6 INCHES OF 1/4" PIPE IS REQUIRED ON EITHER SIDE OF THE MAGMETER.

I HEREBY CERTIFY THAT THIS PLAN, SPECIFICATION, OR REPORT WAS PREPARED BY ME OR UNDER MY DIRECT SUPERVISION AND THAT I AM A DULY LICENSED PROFESSIONAL ENGINEER UNDER THE LAWS OF THE STATE OF MINNESOTA.

SIGNATURE

TYPED NAME

REGISTRATION NUMBER

DATE

REV. NO.	DATE	DRWN	CHKD	REMARKS

DESIGNED BY: M. DELISO
DRAWN BY: M. DELISO
SHEET CHK'D BY: E. SILVERMAN
CROSS CHK'D BY: M. TAHA
APPROVED BY:
DATE: JUNE 2015

CDM Smith
75 State Street, Suite 701
Boston, MA 02109
Tel: (617) 452-6000

PENN STATE UNIVERSITY

MICROBIAL FUEL CELL DESIGN

PENN STATE / CDM SMITH COLLABORATION
MICROBIAL FUEL CELL PILOT UNIT
PROCESS AND INSTRUMENTATION DIAGRAM

PROJECT NO. 83278-95598
FILE NAME: 1001PIDI.DWG
SHEET NO.
I-1

PRELIMINARY DESIGN SUBMITTAL - NOT FOR CONSTRUCTION

xREFs: [CDMS_2234] Images: []
Last saved by: DELISOMA Time: 10/16/2015 10:35:32 AM
pw:\\bdcpwpp1.PW_AM1\83278\95598\03 Reports and Studies\15 MFC Design\Instrumentation\001PIDI.dwg
© 2015 CDM SMITH ALL RIGHTS RESERVED.
REUSE OF DOCUMENTS: THESE DOCUMENTS AND DESIGNS PROVIDED BY PROFESSIONAL SERVICE, INCORPORATED HEREIN, ARE THE PROPERTY OF CDM SMITH AND ARE NOT TO BE USED, IN WHOLE OR PART, FOR ANY OTHER PROJECT WITHOUT THE WRITTEN AUTHORIZATION OF CDM SMITH.

BILL OF MATERIALS:

DATA ACQUISITION:
- KEITHLEY 2750 DIGITAL MULTIMETER
- 3 7708 MULTIPLEXER MODULE EXPANSION CARDS
- USB-GPIB INTERFACE ADAPTER MODEL KUSB-488B

DESKTOP COMPUTER:
- REUSE AN EXISTING CDM SMITH MACHINE

PLC/HMI:
- VISION V1040-T20B
- I/O EXPANSION CARD: V200-18-E3XB

MAGNETIC FLOWMETER:
- SIEMENS SITRANS F M MAG 1100 SENSOR
- SIEMENS SITRANS F M MAG 5000 TRANSMITTER

TEMPERATURE INDICATING TRANSMITTER:
- MORE INDUSTRIES TDY

LEVEL INDICATING TRANSMITTER:
- SIEMENS LC300 CAPACITANCE LEVEL PROBE 3/4"

UPS:
- APC BACK-UPS PRO 865 WATTS / 1500 VA

INTERNET MODEM:
- VERIZON WIRELESS PANTECH 4G LTE USB MODEM AIRCARD UML295 4G

PRESSURE GAUGE:
- ASHCROFT TYPE 1279 DURAGAUGE

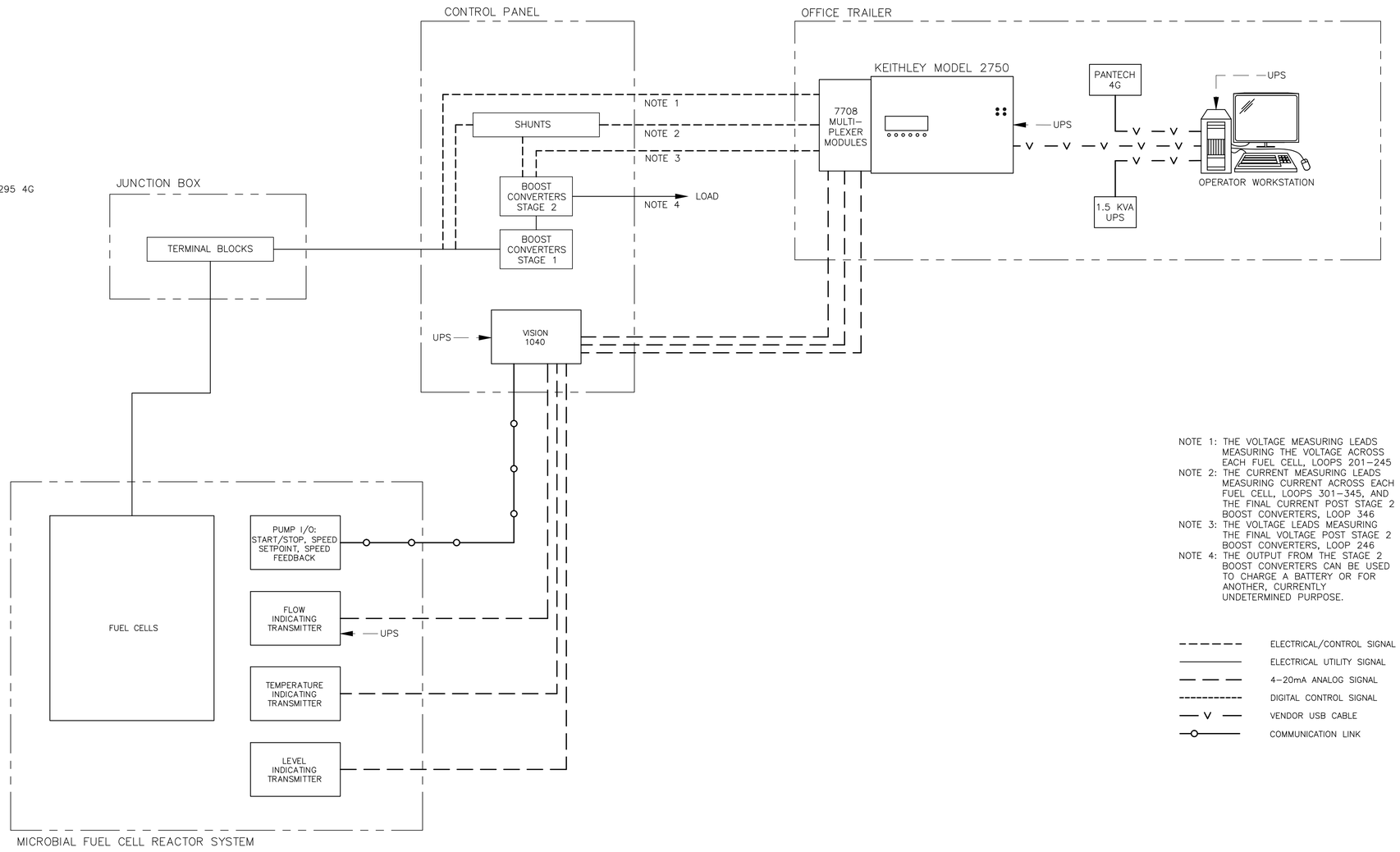

NOTE 1: THE VOLTAGE MEASURING LEADS MEASURING THE VOLTAGE ACROSS EACH FUEL CELL, LOOPS 201-245

NOTE 2: THE CURRENT MEASURING LEADS MEASURING CURRENT ACROSS EACH FUEL CELL, LOOPS 301-345, AND THE FINAL CURRENT POST STAGE 2 BOOST CONVERTERS, LOOP 346

NOTE 3: THE VOLTAGE LEADS MEASURING THE FINAL VOLTAGE POST STAGE 2 BOOST CONVERTERS, LOOP 246

NOTE 4: THE OUTPUT FROM THE STAGE 2 BOOST CONVERTERS CAN BE USED TO CHARGE A BATTERY OR FOR ANOTHER, CURRENTLY UNDETERMINED PURPOSE.

- ELECTRICAL/CONTROL SIGNAL
- ELECTRICAL UTILITY SIGNAL
- 4-20mA ANALOG SIGNAL
- DIGITAL CONTROL SIGNAL
- VENDOR USB CABLE
- COMMUNICATION LINK

I HEREBY CERTIFY THAT THIS PLAN, SPECIFICATION, OR REPORT WAS PREPARED BY ME OR UNDER MY DIRECT SUPERVISION AND THAT I AM A DULY LICENSED PROFESSIONAL ENGINEER UNDER THE LAWS OF THE STATE OF MINNESOTA.

SIGNATURE

TYPED NAME

REGISTRATION NUMBER

DATE

REV. NO.	DATE	DRWN	CHKD	REMARKS

DESIGNED BY: M. DELISO
DRAWN BY: M. DELISO
SHEET CHK'D BY: E. SILVERMAN
CROSS CHK'D BY: M. TAHA
APPROVED BY:
DATE: JUNE 2015

CDM Smith
75 State Street, Suite 701
Boston, MA 02109
Tel: (617) 452-6000

PENN STATE UNIVERSITY

MICROBIAL FUEL CELL DESIGN

PENN STATE / CDM SMITH COLLABORATION
MICROBIAL FUEL CELL PILOT UNIT
CONTROL ARCHITECTURE DRAWING

PROJECT NO. 83278-95598
FILE NAME: I001GDSA.DWG
SHEET NO.
I-1

PRELIMINARY DESIGN SUBMITTAL - NOT FOR CONSTRUCTION

XREFs: [CDMS_2234] Images: []
Last saved by: DELISOMA Time: 10/16/2015 10:14:55 AM
pw:\\bdcpwapp1:PW_XM1\83278\95598\03 Reports and Studies\15 MFC Design\Instrumentation\I001GDSA.dwg
©2015 CDM SMITH ALL RIGHTS RESERVED.
REUSE OF DOCUMENTS: THESE DOCUMENTS AND DESIGNS PROVIDED BY PROFESSIONAL SERVICE, INCORPORATED HEREIN, ARE THE PROPERTY OF CDM SMITH AND ARE NOT TO BE USED, IN WHOLE OR PART, FOR ANY OTHER PROJECT WITHOUT THE WRITTEN AUTHORIZATION OF CDM SMITH.

Item	description	price / unit ($)	quantity	total price	URL
Keithley 2750	multimeter	2460	1	2460	http://www.keithley.com/products/data/datalogger/?mn=2750
Keithley 7708 Multiplexer module	input card	951	3	2853	http://www.keithley.com/products/switch/rfmicrowave/?mn=7708
USB-GPIB Interface Adapter	cable adapter	539	1	539	http://www.keithley.com/products/accessories/ieee/usb/?mn=KUSB-488B
Vision V1040 -T20B	PLC/HMI	1240	1	1240	http://www.unitronics.com/plc-hmi/plc-vision-enhanced/v1040-
V200-18-E3XB	Snap-in I/O	349	1	349	http://www.unitronics.com/docs/technical-library/v200-18-e3xb.pdf?sfvrsn=0
Siemens Sitrans F M Mag 5000 transmitter	flowmeter transmitter	1	1	3400	http://w3.siemens.com/mcms/sensor-systems/en/process-instrumentation/flow-measurement/electromagnetic/pulsed-dc-meters/transmitters/Pages/sitrans-f-m-mag-5000.aspx
Siemens Sitrans F M Mag 1100 sensor	flowmeter sensor				http://w3.siemens.com/mcms/sensor-systems/en/process-instrumentation/flow-measurement/electromagnetic/pulsed-dc-meters/sensors/pages/sitrans-f-m-mag-1100.aspx
Siemens LC300 Capacitance Level Probe	level probe	1338	1	1338	http://w3.siemens.com/mcms/sensor-systems/en/process-instrumentation/level-measurement-with-level-measuring-instruments/continuous/capacitance/pages/sitrans-lc300.aspx
CDM machine	computer	15	1	15	($15 for shipping)
APC Back-UPS Pro, 865 Watts /1500 VA, Input 120V /Output 120V, Interface Port USB	UPS	200	1	200	http://www.apc.com/products/resource/include/techspec_index.cfm?base_sku=BX1500G&total_watts=200
More Industries TDY	temperature sensor / transmitter	1000	1	1000	http://www.miinet.com/Portals/0/DataSheets/TDY_Datasheet_Moore_Industries.pdf
Verizon Wireless Pantech 4G LTE USB Modem Aircard UML295 4G (w/out contract)	cell modem	169	1	169	http://www.amazon.com/Verizon-Wireless-Pantech-Aircard-Contract/dp/B00GOAAIMU
Verizon Internet Prepaid Jetback Plan 3GB / month	cell plan	60 / mo			
Ashcroft Type 1279 Duragause	pressure guage	100	1	100	http://www.ashcroft.com/products/pressure_gauges/process_gauges/1279-duragauge.cfm
			total price	**13663**	

ASHCROFT®
Trust the shield.™

Type 1279 Duragauge® Pressure Gauge Available With *PLUS!™* Performance Option

- ***Solid front case design, field convertible to hermetically sealed or liquid filled style***
- ***Pressure ranges from vacuum — 30,000 psi***
- ***Select from various socket and Bourdon tube materials***
- ***Micrometer adjustable pointer***
- ***400 Series stainless steel movement wears better for longer life***
- ***Teflon-coated pinion for longer life***
- ***Patented Duratube™ with as-welded tube construction controls stresses for longer life***
- ***PLUS!™ Performance Option:***
  - ***Liquid-filled performance in a dry gauge***
  - ***Fights vibration and pulsations without liquid-filled headaches***
  - ***Order as option XLL***

The Ashcroft® Duragauge® pressure gauge is the finest production gauge on the market for industrial use where precise indications are required. The product line offers a wide variety of case styles, Bourdon tubes and pressure ranges to meet your application needs.

With the component combinations available in the Duragauge gauge line, over ten million variations are possible to serve the needs of all types of industries, including process, power, nuclear, aerospace and cryogenics.

TEMPERATURE LIMITS

	Ambient	Process	Storage
Dry	–20/200°F[1] (–29/93°C)	–20/250°F[1] (–29/121°C)	–40/250°F (–40/121°C)
LF (glycerin)	20/150°F (7/66°C)	20/150°F (7/93°C)	0/150°F (–18/66°C)
(silicone)	–40/150°F (–40/66°C)	–40/200°F (–40/93°C)	–40/150°F (–40/66°C)
(halocarbon)	–40/150°F (–40/66°C)	–40/200°F (–40/93°C)	–40/150°F (–40/66°C)

Note: Other than discoloration of the dial and hardening of the gasketing that may occur as ambient or process temperatures exceeds 150°F, non-liquid-filled gauges with standard glass windows, can withstand continuous operating temperatures up to 250°F (121°C). Liquid-filled gauges can withstand 200°F (93°C) but glycerin fill and acrylic window will tend to yellow. Accuracy at temperatures above or below the reference ambient temperature of 68°F (20°C) will be affected by approximately .4% per 25°F. Gauges with welded joints will withstand 750°F (450°F (232°C) with silver brazed joints) for short times without rupture, although other parts of the gauge will be destroyed and calibration will be lost. For continuous use and for process or ambient temperatures above 250°F (121°C), a diaphragm seal or capillary or siphon is recommended.

(1) Available for temperatures below –20°F, see Product Information page ASH/PI-21B for details.

PRODUCT SPECIFICATIONS

Model Number:	1279
Accuracy:	½% full scale (Grade 2A, ASME B40.100)
Ranges:	Vac., compound to 30,000 psi
Dial Size:	4½″ diameter
Case Material:	Black phenolic, solid front
Weather Protection:	Dry Case: IP54 Liquid filled or hermetically sealed case: IP 66
Ring:	Threaded reinforced black polypropylene
Window:	Glass
Dial:	Aluminum, white background, black figures and intervals
Pointer:	Micrometer adjustable
Movement:	Rotary, 400 SS, Teflon® coated pinion gear and segment
Bourdon Tube and Socket:	C510 Phos. bronze/brass (A)[1] 316L SS/steel (R)[2] 316L SS/316L SS (S)[2] K Monel/ Monel (P)[2]
Conn. Size:	¼″, ½″ NPT
Conn. Location:	Lower or back

OPTIONAL FEATURES

Fill:	L-Glycerin-Standard XGV-Silicone-Optional XGX-Halocarbon-Optional
***PLUS!™* Performance:**	XLL
Hermetically Sealed, IP65:	H
Flush Mounting Ring:	X56
Receiver Gauge:	XPR
Shatter Proof Glass Window:	XSG
Acrylic Window:	XPD
Red Set Hand:	XSH
Maximum Pointer:	XEP

[1] Joints silver brazed
[2] Joints welded

STANDARD RANGE TABLE*

Pressure – psi		
Range	**Figure interval**	**Minor Graduation**
0/15	1	0.1
0/30	5	0.2
0/60	5	0.5
0/100	10	1
0/160	20	2
0/200	20	2
0/300	50	2
0/400	50	5
0/600	50	5
0/800	100	10
0/1000	100	10
0/1500	200	20
0/2000	200	20
0/3000	500	20
0/5000	500	50
0/6000	500	50
0/10,000	1000	100
0/20,000	2000	200
0/30,000	5000	200

* Full standard and metric equivalent range table available on our web site.

All specifications are subject to change without notice.
All sales subject to standard terms and conditions.
© Ashcroft Inc. 2014 Rev. 5/15

Ashcroft Inc., 250 East Main Street, Stratford, CT 06614 USA
Tel: 203-378-8281 • Fax: 203-385-0408
email: info@ashcroft.com • www.ashcroft.com

Type 1279 Duragauge® Pressure Gauge Available With *PLUS!*™ Performance Option

Compound				
Range	Figure Interval		Minor Grads	
	in Hg	psi	in Hg	psi
30˝ Hg/15 psi	5	3	0.5	0.2
30˝ Hg/30 psi	10	5	1	0.5
30˝ Hg/60 psi	10	10	1	1
30˝ Hg/100 psi	10	10	2	1
30˝ Hg/150 psi	10	20	5	2
30˝ Hg/200 psi	30	20	5	2
30˝ Hg/300 psi	30	50	5	2

Vacuum		
Range	Figure Interval	Minor Grads
30/0 in. Hg 34/0 ft H_2O	5 in 5 ft	0.2 in 0.5 ft

TYPE 1278M SERIES FLUSH MOUNTING RING

Used to flush mount gauge case Type 1279(*)S. Standard finish is black; optional polished stainless steel finish is available.

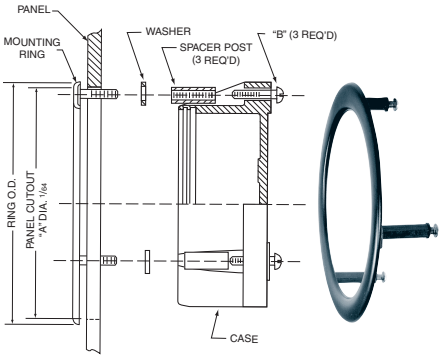

GAUGE SIZE	RING O.D.	"A" DIA.	"B" Size of 3 Screws	"C" Size of Washers
4½	6.000 (152)	5⅝ (148)	#10-24 x 1⅝	7/16 x 17/64 x ⅝

Dimensions

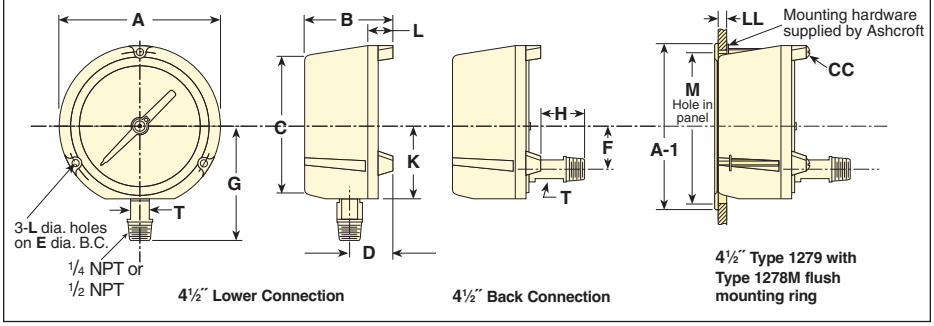

Dial Size Inches	A	B	C	D	E	F	G	H	K	L	T	V	Weight (lbs)
4½	5.81 (147.6)	3.36 (85.3)	5.07 (128.7)	1.06 (40.6)	5.375 (137)	1.62 (41.2)	4.08 (103.7)	.73 (18.4)	2.62 (66.6)	.22 (5.5)	.62 (15.7)	2.625 (67)	2.5 (Dry) 3.5 (L.F.)

Order Coding Example

45	1279	S	S	04	L	XEPNH	100	#

SIZE	TYPE	SYSTEM (TUBE & SOCKET)	CASE DESIGN SOLID FRONT	PROCESS CONNECTION SIZE	CONNECTION LOCATION	OPTIONS (X VARIATIONS)[1]	RANGE	ENGINEERING UNITS[1]
(45) 4½	**1279**	**(A)** Bronze tube, Brass socket[1] **(P)** K-Monel 500 tube, Monel 400 socket[2] **(R)** 316L st st tube, steel socket **(S)** 316L[2] [1] Max pressure 1000psi [2] Max pressure 30,000psi	**(S)** Dry(IP54) **(SH)** Dry, Hermetically Sealed, Field Fillable (IP65) **(SL)** Liquid filled (glycerin standard) (IP65)	**(02)** 1⁄4 NPT male[1] **(04)** 1⁄2 NPT male[1] **(09)** 9/16-18 UNF-2B Aminco (standard for high pressure >20,000psi) [1] Max pressure 20,000psi	**(B)** Back **(D)** Side (3:00) **(E)** Side (9:00) **(L)** Lower **(T)** Top (12:00)	**(GV)** Silicone case fill **(GX)** Halocarbon case fill **(NH)** St. St. Wired Tag **(TS)** Throttle screw[2] **(6B)** Oxygen service **(PD)** Acrylic window[2] **(SG)** Safety glass **(EP)** Maximum pointer, adjustable **(SH)** Red set hand, stationary **(LL)** ***PLUS!*** Performance **(56)** Flush mounting ring **(C4)** Individual calibration chart [1] Others on request [2] Standard with hermetically sealed or liquid filled gauge	See website for most common ranges offered	**(#)** PSI **(BR))** Bar **(KG)** Kilograms/CM2 **(KP)** Kilopascal **(IMV)** Inches of Mercury Vacuum [1] See website for more units of measure

All specifications are subject to change without notice.
All sales subject to standard terms and conditions.
© Ashcroft Inc. 2014 Rev.5/15

Ashcroft Inc., 250 East Main Street, Stratford, CT 06614 USA
Tel: 203-378-8281 • Fax: 203-385-0408
email: info@ashcroft.com • www.ashcroft.com

Technical Data

1.888.KEITHLEY (U.S. only)

www.keithley.com

KEITHLEY

A GREATER MEASURE OF CONFIDENCE

Integra Series Multimeter/Switch Systems

Introduction

The Integra Series of 6½-digit Multimeter/Switch systems blends Keithley's high performance DMM technology, switching expertise, and data acquisition knowledge into compact, affordable, easy-to-use packages. This technical data booklet provides a comprehensive overview of the systems and includes detailed specifications.

There are three Integra systems: the Model 2700, 2701, and 2750. Each consists of a mainframe and a growing line of plug-in switch/control modules. The Model 2700 and 2701 each include two slots for the plug-in modules; the Model 2750 has five slots. Each slot can support a series of multiplexer, matrix, or control modules, and all the modules in a system operate simultaneously. Input modules can be mixed or matched to provide a broad range of measurement, acquisition, and control capabilities.

While the core functionality and programming of all Integra Series systems are identical, each mainframe has unique capabilities. For example, the Model 2701 is the only system to provide a 10/100BaseTX Ethernet interface, and the Model 2750 provides extended low ohms measurement capability.

Setting up an Integra system is simple and straightforward. When a plug-in module is inserted into a slot, it is ready to be used immediately. Settings can be configured from the front panel of the system or via the computer controller (over GPIB, RS-232, or Ethernet). Also, each channel can be configured independently.

If you have any questions after reviewing this information, please contact your local Keithley representative or call one of our Application Engineers at 1-800-552-1115 (U.S. only). Check Keithley's website, www.keithley.com, for the names and numbers of our representatives around the world.

Figure 1. Typical Integra Series System Diagram

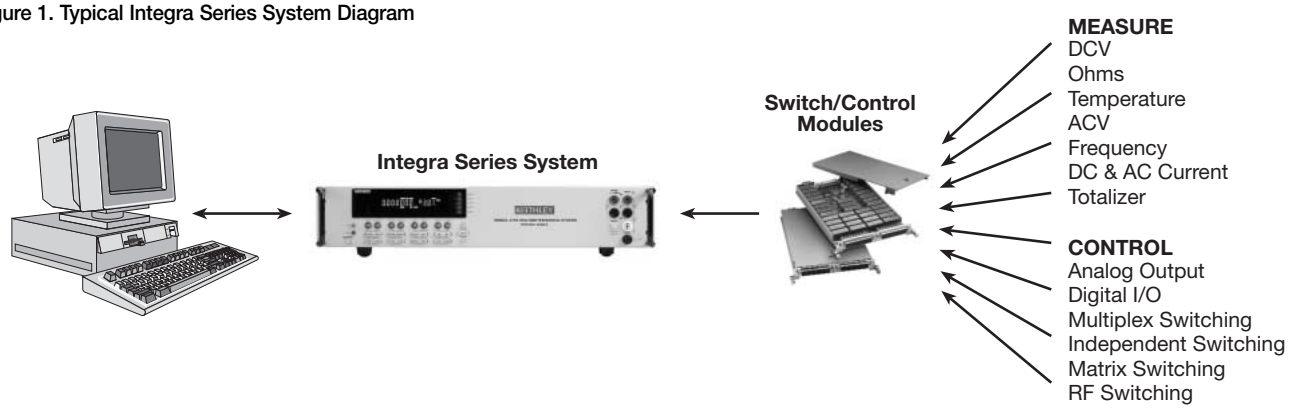

Quick Comparison of Integra Systems

	Communication Bus	No. of Slots	Max. No. of Channels or Crosspoints	Battery-Backed Memory Buffer	Maximum Measurement Speed (readings/second on one channel)	Maximum Scanning Rate (channels/second)	Other
Model 2701	Ethernet, RS-232	2	80 channels or 96 crosspoints	450,000 readings	3500	500	Hardwired Ethernet interface good to 100m from computer or network hub. Wireless Ethernet good for miles.
Model 2700	GPIB, RS-232	2	80 channels or 96 crosspoints	55,000 readings	2000	180	
Model 2750	GPIB, RS-232	5	200 channels or 240 crosspoints	110,000 readings	2500	230	Low ohms capabilities, 1μΩ sensitivity

Integra Series Multimeter/Switch Systems

Table of Contents

Overview 4
- Front and Rear Panel Views of Model 2700 5
- Front and Rear Panel Views of Model 2701 6
- Front and Rear Panel Views of Model 2750 4

Measurement Ranges 7
Switch/Control Module Capabilities 7
- Module Capabilities Overview 7
- Module Selector Guide 8
- Connector Guide for Keithley Integra Series Modules 8

Channel Configuration Capabilities 9
Scanning Capabilities 9
Choice of Communication Interfaces 10
Triggering and I/O Capabilities 11
- Trigger Sources 11
- Alarm Limits 12
- Digital Outputs 12
- Electrical Capabilities 12

On-board Data Storage 12
Saving/Recalling a Setup 13
Power Failure Recovery 13
Channel Monitor 13
Measurement Performance 13
Filtering 14
NPLC 14
Line Cycle Synchronization 14
Autozero 14
Low Ohms Measurement 14
Offset Compensation 15
Voltage Limit/Dry Circuit Ohms (DRYCKT) 15
Temperature Measurements 15
Calibration 16
Software 17
Integra Series Specifications 19
Switch/Control Module Specifications
- 7700 20-Channel Differential Multiplexer w/Automatic CJC 24
- 7701 32-Channel Differential Multiplexer 25
- 7702 40-Channel Differential Multiplexer 26
- 7703 32-Channel High Speed Differential Multiplexer 27
- 7705 40-Channel Control Module 28
- 7706 All-in-One I/O Module 29
- 7707 Multiplexer-Digital I/O Module 30
- 7708 40-Channel Differential Multiplexer Module 31
- 7709 6×8 Matrix Module 32
- 7710 20-Channel Solid State/Long Life Differential Multiplexer w/CJC 33
- 7711 2GHz 50Ω RF Module 34
- 7712 3.5GHz 50Ω RF Module 35

System Configuration Examples 36

Integra Series Multimeter/Switch Systems

Model 2700

Use mX+b or % scaling to convert sensor/transducer outputs directly into engineering units.

Measure the ratio or average of two input channels.

View a channel of interest without interrupting a scan by using the Channel Monitor feature.

Built-in linearization for thermocouples, RTDs, and thermistors.

Front panel input jacks simplify manual probing, troubleshooting, and calibration. Built-in signal conditioning with 1000V isolation simplifies system configuration and ensures good measurements.

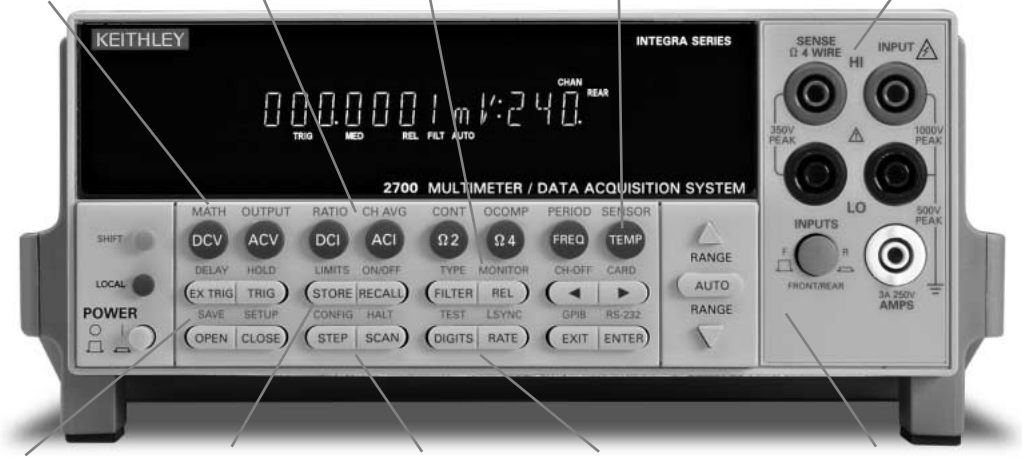

Initialize the system with one of four fully programmable set-up conditions. System configuration is stored in non-volatile memory.

Non-volatile memory allows time-stamped storage of 55k readings.

Manually step through channels or scan automatically. Configure each channel independently.

Set the number of digits to be displayed as well as the reading rate.

Familiar DMM-like front panel scheme makes it easier to use on bench or rack. Select or change functions with the simple push of a button.

Built-in digital I/O lines provide for control, external triggering, and HI/LO alarm/limit outputs.

Trigger Link enables tightly synchronized triggering with other instruments in large ATE systems

GPIB and RS-232 interfaces are standard.

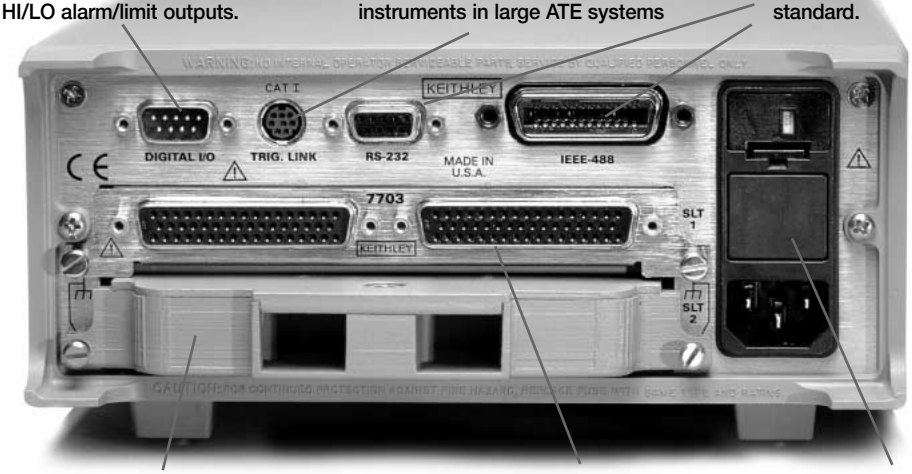

A variety of measurement and control modules let you mix, match, and change input signals or control lines any time you like. Install up to two modules at a time to create up to an 80-channel "mini-ATE" system.

Rugged 50-pin D-sub connectors ensure dependability and quick setup/teardown in production test racks.

Built-in noise rejection circuitry ensures stable, predictable measurements.

1.888.KEITHLEY (U.S. only)

www.keithley.com

KEITHLEY

A GREATER MEASURE OF CONFIDENCE

Integra Series Multimeter/Switch Systems

Model 2701

If there's a power failure, valuable data is protected with the battery-backed non-volatile memory and scans can automatically be resumed right where they stopped when power returns.

Open lead detection protects against false readings due to lead disconnections.

Front panel input jacks simplify manual probing, troubleshooting, and calibration. Includes 1000V protection in case of accidental overload.

Built-in signal conditioning and statistical analysis is configurable per channel for maximum flexibility.

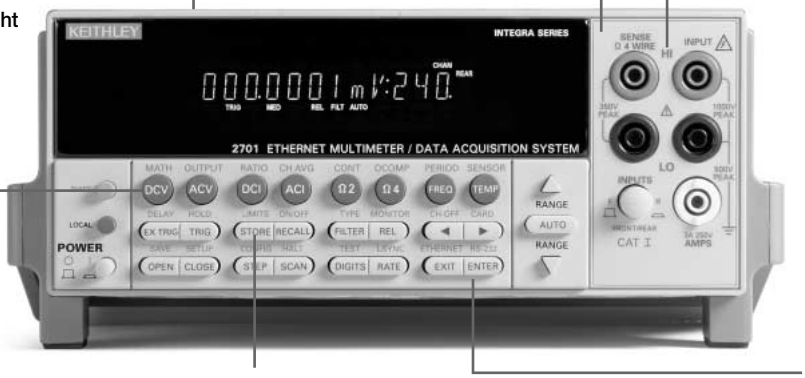

Large memory buffer (450,000 readings) for storing data without tying up the network.

Its familiar DMM-like front panel scheme makes the Model 2701 easy to use on the bench or in the rack. Select or change functions with the press of a button.

Fast and convenient 10/100BaseTX Ethernet with TCP/IP protocol.

Immediate alarm notification independent of the PC provided by built-in open-collector digital I/O lines for control, external triggering, and HI/LO alarm/limit outputs.

A variety of measurement and control modules makes it simple to mix, match, and change input signals or control lines as needed. Get up to 80 differential channels and up to 500 channels per second scanning rate.

Built-in relay cycle counters on each module for ease of maintenance.

Integra Series Multimeter/Switch Systems

Model 2750

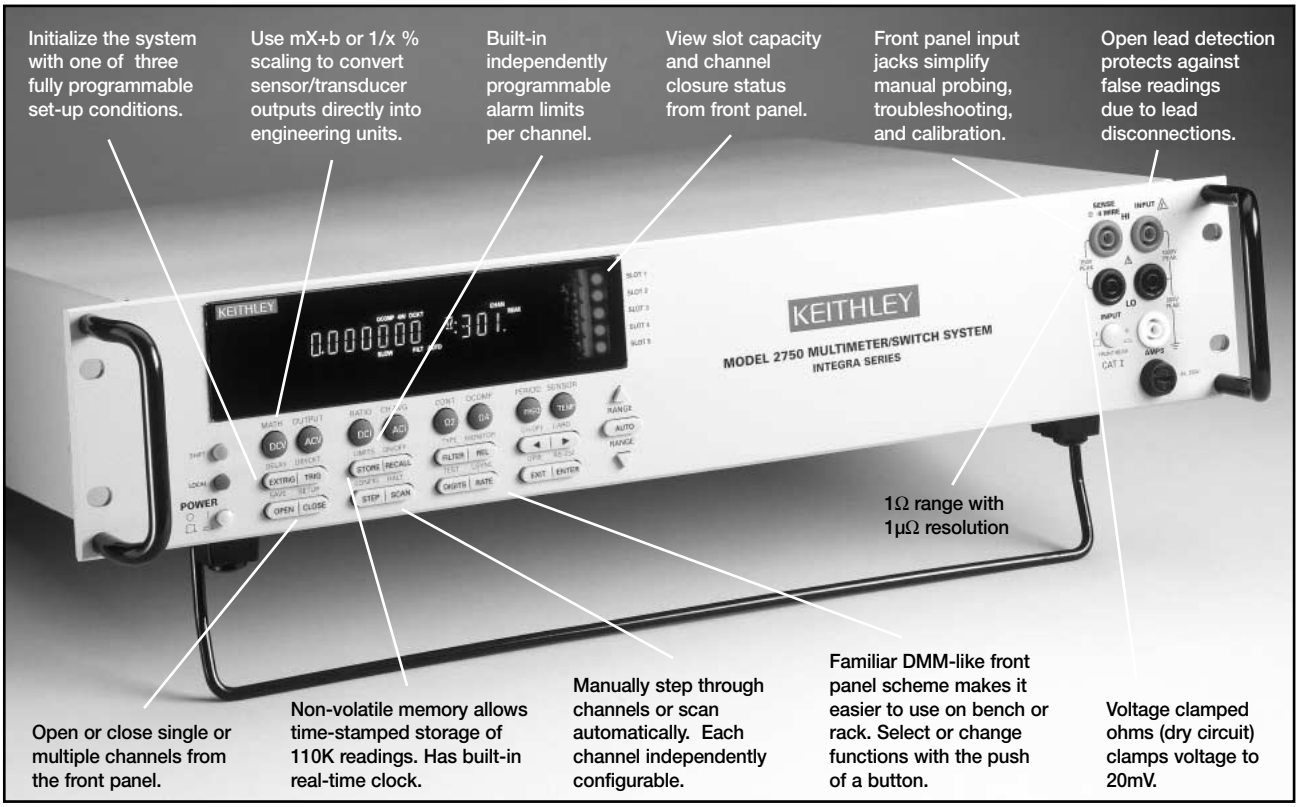

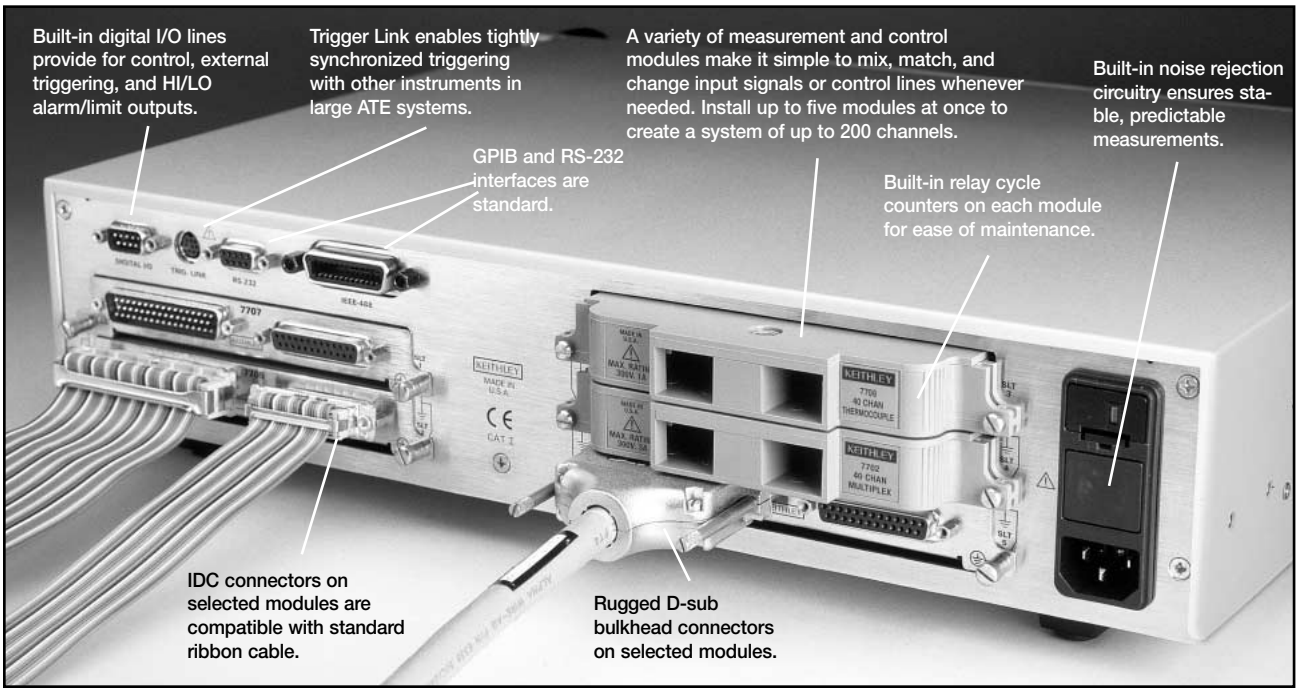

1.888.KEITHLEY (U.S. only)

www.keithley.com

KEITHLEY

A GREATER MEASURE OF CONFIDENCE

Measurement Ranges for the Integra Series Systems

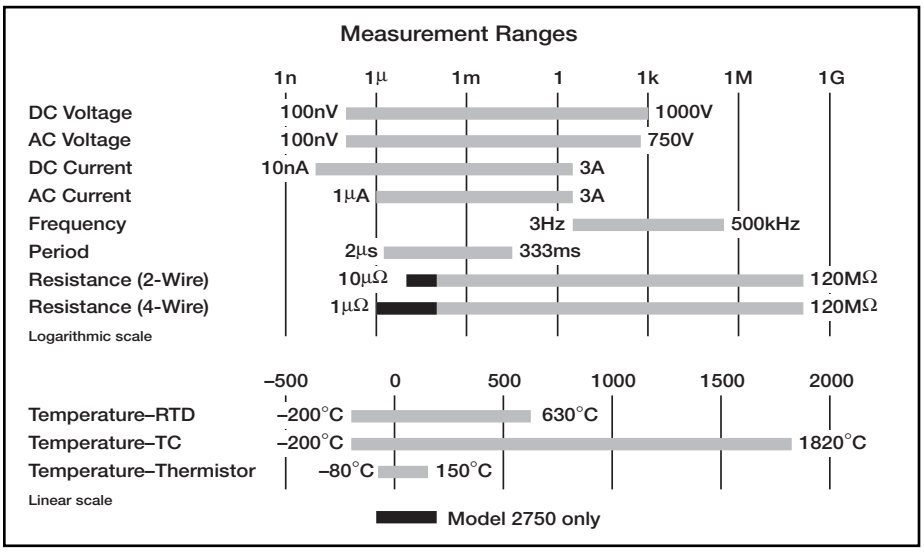

Figure 2. Measurement Ranges

Switch/Control Module Capabilities

The flexibility to mix and match switch/control modules in a single mainframe simplifies configuring Integra Series-based systems for a wide range of applications. Each module offers a different combination of capabilities, such as number of channels, speed, etc. Before selecting a module, it is critical to analyze the needs of the application carefully and consider future requirements for expansion.

Module Capabilities Overview

	7700	7701	7702	7703	7705	7706	7707	7708	7709	7710	7711	7712
DC Volts	✓	✓	✓	✓		✓	✓	✓	✓	✓		
DC Current	✓		✓									
Temperature												
T/C w/Automatic CJC	✓					✓		✓		✓		
T/C w/External CJC	✓	✓	✓	✓		✓	✓	✓	✓	✓		
RTD	✓	✓	✓	✓		✓	✓	✓	✓	✓		
Thermistor	✓	✓	✓	✓		✓	✓	✓	✓	✓		
Resistance (2- or 4-wire)	✓	✓	✓	✓		✓	✓	✓	✓	✓		
Continuity	✓	✓	✓	✓		✓	✓	✓	✓	✓		
AC Volts	✓	✓	✓	✓		✓	✓	✓	✓	✓		
AC Current	✓		✓									
Frequency	✓	✓	✓	✓		✓	✓	✓	✓	✓		
Event Counter/Totalizer						✓						
Signal Routing/Control	✓	✓	✓	✓	✓	✓	✓	✓	✓	✓	✓	✓
Digital Input							✓					
Digital Output						✓	✓					
Analog Output						✓						
RF Performance											✓	✓

Integra Series Multimeter/Switch Systems

Module Selector Guide

This selector guide may prove helpful in identifying the best module for a specific application. Install up to five modules at a time in the Model 2750 mainframe or two modules in the Model 2700 or 2701 mainframe.

Module	# Analog Inputs	Configuration		Type of Connector	Max. Voltage	Max. Switched Current	Bandwidth	Contact Life	Switch Speed	Other
7700	20	Multiplexer w/CJC	1×20 or two 1×10	Screw terminals	300 V	1	50 MHz	10^8	3 ms	Maximum power = 125VA. 2 current measure channels.
7701	32	Multiplexer	1×32 or two 1×16	D-sub	150 V	1 A	2 MHz	10^8	3 ms	Maximum power = 125VA.
7702	40	Multiplexer	1×40 or two 1×20	Screw terminals	300 V	1 A	2 MHz	10^8	3 ms	Maximum power = 125VA. 2 current measure channels.
7703	32	Multiplexer	1×32 or two 1×16	D-sub	300 V	500 mA	2 MHz	10^8	1 ms	Reed relays.
7705	40	Independent SPST	N/A	D-sub	300 V	2A	10 MHz	10^8	3 ms	Maximum power = 125VA.
7706	20	Multiplexer w/CJC	1×20 or two 1×10	Screw terminals	300 V	1 A	2 MHz	10^8	3 ms	2 analog outputs. 16 digital outputs. Maximum power = 125VA.
7707	10	Multiplexer/ Digital I/O	1×10 or two 1×5	D-sub	300 V	1 A	2 MHz	10^8	3 ms	32 digital I/O. Maximum power = 125VA.
7708	40	Multiplexer w/CJC	1×40 or two 1×20	Screw terminals	300 V	1 A	2 MHz	10^8	3 ms	Maximum power = 125VA.
7709	48	Matrix	6×8	D-sub	300 V	1 A	2 MHz	10^8	3 ms	Connects to internal DMM. Daisy chain multiple cards for up to a 6×40 matrix. Maximum power = 125VA.
7710	20	Multiplexer w/CJC	1×20 or two 1×10	Removable screw terminals	60 V	0.1 A	2 MHz	10^{10}	0.5 ms	Solid state relays, 60V max. 500 channels/second scan rate.
7711	8	Multiplexer	Dual 1×4	SMA	60 V	0.5 A	2 GHz	10^6	10 ms	Insertion loss <1.0dB @ 1GHz. VSWR <1.2 @ 1GHz.
7712	8	Multiplexer	Dual 1×4	SMA	42 V	0.5 A	3.5 GHz	10^6	10 ms	Insertion loss <1.1dB @ 2.4GHz.

* Can be disconnected from internal DMM for routing external signals

Connector Guide for Keithley Integra Series Modules

Module	Connector Type	Supplied Accessories	Available Accessories
7700	Oversized Screw Terminal	Strain Relief	7401 TC wire
7701	50-pin female D-sub & 25-pin female D-sub	7789 connector kit	7790 connector kit, 7705-MTC-2 & 7707-MTC-2 cables
7702	Oversized Screw Terminal	Strain Relief	—
7703	Two 50-pin female D-sub	7788 connector kit	7705-MTC-2 cable
7705	Two 50-pin female D-sub	7788 connector kit	7705-MTC-2 cable
7706	Screw Terminal	Strain Relief	7401 TC wire
7707	50-pin male D-sub & 25-pin female D-sub	7790 connector kit	7789 connector kit, 7705-MTC-2 & 7707-MTC-2 cables
7708	Oversized Screw Terminal	Strain Relief	7401 TC wire kit
7709	50-pin female D-sub & 25-pin female D-sub	7790 connector kit	7789 connector kit, 7705-MTC-2 & 7707-MTC-2 cables
7710	Quick Disconnect Screw Terminal	Strain Relief	7401 TC wire kit
7711	SMA	—	7711-BNC-SMA & 7712-SMA-N adapters, 7712-SMA-1 & S46-SMA-0.5,-1 SMA cables, 7051-2,-5,-10 BNC cables
7712	SMA	—	7712-SMA-N adapter, 7712-SMA-1 & S46-SMA-0.5,-1 SMA cables

Channel Configuration Capabilities

- ***Measurement functions:*** An Integra system can measure many different parameters: DC voltage, DC current, AC voltage, AC current, 2-wire Ω, 4-wire Ω, voltage clamped Ω (2750 only), temperature (using thermocouples, RTDs, and thermistors), frequency, period, and continuity.
- ***Math functions:*** A variety of math functions are available at the push of a button, including channel average and ratio, mX+b scaling, min, max, average and standard deviation. All are available on a per-channel basis.
- ***Measurement setup:*** Each channel can be configured independently for making measurements. Selectable channel parameters include:

- Speed
- Range
- Resolution
- Number of power line cycles (NPLC)
- Math functions
- Ratio calculation
- Individual "m" and "b" values in mX+b format
- Channel averaging
- Hi-Low limits
- Resistance measurement method (2- or 4-wire)
- Offset compensation
- CJC type
- Thermistor type
- Thermocouple type
- RTD type
- Voltage clamped ohms (Dry Circuit, 2750 only)

- ***DUT-to-modules connections:*** It is easy to connect the device under test to the switch/control modules. The 7703 and 7705 modules use dual 50-pin "D-sub" input connectors for secure, quick connections. The 7701, 7707, and 7709 modules use "D-sub" connectors that are compatible with off-the-shelf standard ribbon cable. These connectors are especially convenient for rapid system setup. When greater connection flexibility is required, the 7700, 7702, and 7708 modules provide oversize screw terminal connectors that simplify setup by eliminating the need to handle small connectors. The standard wires used are 20AWG. Model 7710 uses removable terminal blocks to provide the simplicity of screw terminal connections with the speed of mass terminated cables. The 7711 and 7712 RF modules use industry standard SMA connectors.
- ***Mainframe-to-modules connection:*** Secure screws connect the modules to the mainframe. At power-up, the mainframe detects any attached modules automatically, which minimizes set-up time. All signals are routed internally from module to mainframe.
- ***Front/rear switch:*** The front inputs are used for manual probing, troubleshooting, and calibration. A switch on the front panel makes it easy to shift between the front and rear inputs. This eases setting up the equipment and speeds verifying proper setup and connections prior to automating the measurement.

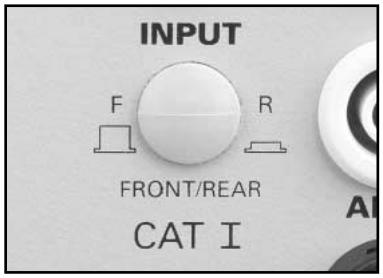

Scanning Capabilities

- ***Relay Closure Counts:*** Relay closure counts are logged every time a channel is closed. These counts are permanently written to the EEPROM on the module at a user-settable time interval (factory default of 10 minutes) or whenever the counts are queried. Valid intervals (set in integer number of minutes) are between 1 and 1440 minutes (24 hours). Relay closures are counted when a relay cycles from open to closed state.
- ***Open Sense Lead Indication.*** The system can alert the user if there is a sense lead disconnection on any channel. In this case, the front panel display will show "OVERFLOW." Therefore, the system does not need other equipment or calibration to inspect the broken connection or failed relay on the scanner card. In addition, the system will protect against erroneously passed conditions.
- ***Scan count:*** An Integra Series system can be programmed to run a given number of scans (up to 450,000) automatically and to record readings into the internal memory buffer. The instrument also allows programming the trigger source used to initiate each scan. (Refer to page 11 for more information on triggering.)

- ***Scan interval:*** The user can set the interval after which each succeeding scan will begin. Scan intervals can be set anywhere from 0 to 99 hours in increments of 1ms.
- ***Scan sequence/omitting channels:*** In addition to scanning in numerical sequence, the system can be programmed to skip any channels that are not required for a particular test. This avoids recording irrelevant data and speeds the data acquisition process. This makes scanning both faster and more flexible.
- ***Ratio (DCV only):*** The instrument can calculate and display the ratio of measurements of paired channels. Ratios can only be determined for specific channel pairs, depending upon the input module used. For example, channel pairs on the Model 7702 include Channels 1 and 21, Channels 2 and 22, etc. Hi/Lo limits are fully supported.
- ***Channel average (DCV and thermocouple only):*** The instrument can calculate and display the average of two channel measurements. As with ratio calculations, only paired channels can be averaged. Hi/Lo limits are fully supported.

Choice of Communication Interfaces

RS-232

All the Integra Series mainframes include RS-232 ports for computer control. RS-232 is a low cost point-to-point interface, allowing a computer to interface with a one mainframe per port at distances up to several hundred meters, depending on the baud rate setting. Slow baud rates can be run long distances, while the fastest baud rate settings are limited to several meters maximum distance. The Model 2700 and 2750 can receive commands and transfer data via RS-232 at various baud rates up to 19.2kBaud. The Model 2701 offers data rates up to 115.2kBaud with hardware handshaking.

GPIB

The Model 2700 and 2750 both offer a GPIB port. GPIB provides higher speed data transfers (up to 1Mbyte/sec.) than RS-232, and allows up to 32 devices to addressed from a single GPIB controller card in a host computer. The maximum cabling distance for the GPIB interface is 2 meters between each GPIB connection. Up to 20 total meters of cable may be connected to a single controller card.

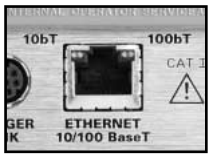

Ethernet

The Model 2701 offers a 10/100 BaseT Ethernet connection for high speed and long distance communication between a computer and a virtually infinite number of instruments. Any PC with an Ethernet port can connect to a single Model 2701 in a point-to-point configuration, to multiple 2701s through a hub, or to multiple 2701s distributed on a network. See the system configuration section on page 35 for more details on Ethernet connections.

The Model 2701 Ethernet port uses the industry-standard TCP/IP socket interface. This provides data rates up 100Mbits/sec. and allows the instrument to be located up to 100 meters from the nearest computer or network hub in hardwired systems and miles in wireless Ethernet systems. The maximum distances between a control PC and the instruments are limited only by the size of the network. The instrument also provides a built-in diagnostic web page for easy remote access to the 2701. Entering the instrument's IP address in the URL line of Microsoft® Internet Explorer® will allow communication with and control of the 2701. This Web page allows users to read and set network parameters, such as IP address, subnet mask, gateway, MAC address, and calibration dates, and to send commands to and query data from the 2701.

Triggering and I/O Capabilities

Trigger sources

Any of the following sources can be used for triggering a reading or scan sequence:

A. ***Immediate:*** An Integra Series system self-triggers automatically. This default method is the simplest way to take a measurement on a single channel.

B. An ***external trigger*** is received via the Trigger Link connector. Triggering through Trigger Link is very precise (<0.5ms trigger latency) and provides tight timing control for synchronization in larger systems. Therefore, measurements can be taken at a precise time with very little uncertainty. This capability can be valuable when optimizing coordination with other system instruments, such as the Model 2400 SourceMeter® instrument in larger rack & stack applications.

C. A ***bus trigger*** is received (GET or *TRG) on GPIB or *TRG on RS-232 and Ethernet.

D. ***Manual:*** Use of front panel TRIG key.

E. ***Analog trigger:*** A display reading on a particular channel can be programmed as an analog trigger. A scan sequence is started whenever such a reading is reached [programmed for either a greater than (>) or less than (<) condition as a trigger]. In other words, this feature can be used to initiate a scan sequence based on some external factor, such as a temperature rising above a pre-set limit. After scanning all the configured channels on the instrument, the instrument then returns to the channel that acted as the analog trigger, and checks for the reading to be in conditional limits. Depending on the limits and current reading, the instrument decides whether to start the next scan. Only the data of interest are acquired, eliminating the need to spend hours searching through reams of normal readings to find anomalous data.

F. ***Digital trigger:*** Two digital inputs (TTL-level) are standard on each mainframe—one to serve as a trigger input and one to serve as a hardware interlock. The digital trigger is logical "and"-ed with the interlock. The interlock is default true. Therefore, the digital trigger input would be recognized for triggering only when the digital trigger and the interlock are both true. Thus, the interlock provides the user with a controlling mechanism for recognizing the digital trigger if necessary (see ***Figure 3***).

Figure 3

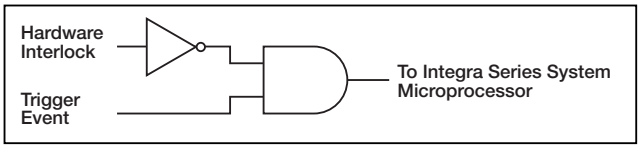

B

C

D

E

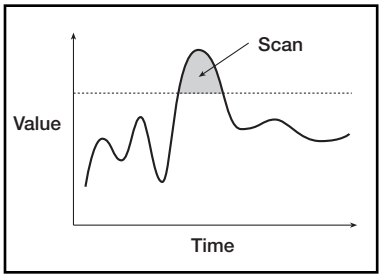

F

1.888.KEITHLEY (U.S. only)
www.keithley.com
KEITHLEY
A GREATER MEASURE OF CONFIDENCE

Alarm Limits/Digital Outputs

The digital output lines can trigger external alarms without the need for a PC connection. The instrument can be programmed to provide alarms when any pre-set limits are breached. Limits can be applied to all measurement functions except continuity, which has its own alarm beeper. The limit test is performed after "mX + b" and math operations.

Limit types: Each channel has four independently programmable limits, each of which can be assigned a value. These are:

1. Limit1 High (for example, 1% higher than the expected reading)
2. Limit1 Low (for example, 1% less than the expected reading)
3. Limit2 High (for example, 5% higher than the expected reading)
4. Limit2 Low (for example, 5% less than the expected reading)

The outputs can be positive or negative true, pulse, or fixed level. Pulse widths are programmable.

Master Limit: In addition to these limit alarms, a master limit is provided. It is logically "or"-ed with the four limits and is active every time any of the other limits are breached.

Each of the alarm limits and the master alarm is mapped to a specific output pin on the 9-pin male connector that handles the output of that alarm limit.

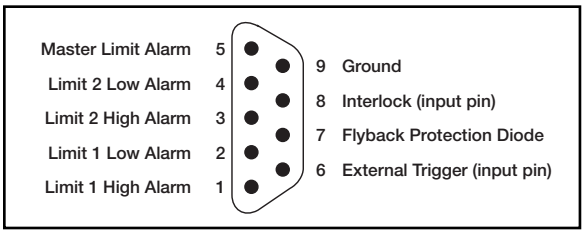

Figure 4. Structure of the 9-Pin Male Digital I/O Connector

Electrical Capabilities:

- 250mA sink (output).
- TTL level outputs (no external supply is needed).
- Open collector output up to 33V with external supply.
- Ability to trigger or start a scan by connecting to one of the digital input lines.

On-board Data Storage

Buffer: There are non-volatile "read and transmit" memory buffers (in other words, the buffer can be emptied while it is being filled) in each system. The buffer can be configured in "wrap around" mode for recording readings continuously for long periods. There is no need to stop taking data, reset the instrument, or change memory cards. The wrap around memory can be configured to issue a Service Request (SRQ) at predetermined points in the scan. An SRQ can be issued when the buffer is one-quarter full, one-half full, three-quarters full, or completely full. The instrument can be commanded to download the readings without interfering with the current acquisition; therefore, data acquisition and retrieval can occur simultaneously. When the buffer is full, the instrument returns to the beginning of the buffer and starts writing in the locations emptied by the previous download.

Timestamp: The readings in the memory can be timestamped to trace the progress of a test. The time can be configured as either:

- Real time: The actual calendar day and time.
- Relative Time: Time is relative to the first reading stored in the buffer.

1.888.KEITHLEY (U.S. only)
www.keithley.com
KEITHLEY
A GREATER MEASURE OF CONFIDENCE

Saving/Recalling a Setup

All current set-up information for individual channels and the mainframe is battery backed and the measurement data is stored in the non-volatile memory. Therefore, while the instrument is switched off, the configuration for each channel is saved in the memory, then automatically recalled when the product is switched on again. Up to five (four for Model 2700 and three for Model 2750) different sets of setups can be recorded for each channel, so it's unnecessary to set up each channel before a different test.

Power Failure Recovery

All set-up information is battery backed and data is stored in non-volatile RAM, so the system is immune to power failures and can resume scanning where it stopped once power is restored. There is no need to restart interrupted tests from the beginning. The scan resumption feature is user-selectable.

Channel Monitor

The channel monitor feature allows monitoring any specific input channel on the front panel display at any time during a scan. The system can scan across channels very rapidly, so the channel monitor offers a convenient way to view only the channel of interest without interrupting a scan.

Measurement Performance

Each Integra series system is a true 6½-digit (22-bit) instrument designed for high measurement precision. Its high precision enhances measurement repeatability and stability.

Measurement performance is a key advantage of all of Keithley's products. The Integra Series is based on a number of advanced technologies that improve its overall performance dramatically, including:

- Patented A/D converter IC circuitry design to increase the resolution, precision, and speed of measurement.
- Advanced signal conditioning hardware to filter out unwanted noise and provide necessary isolation.
- A unique "servo" front end design (***Figure 6***). While conventional DMMs typically measure and correct for the zero drift of front-end circuitry, these systems' servo front end eliminates zero drift, which also eliminates the wasted measurement time usually required to check zero, further increasing measurement speed.

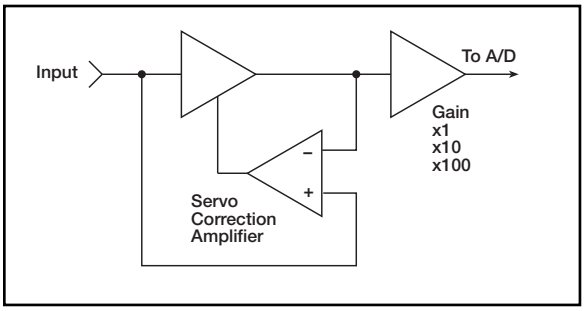

Figure 6.

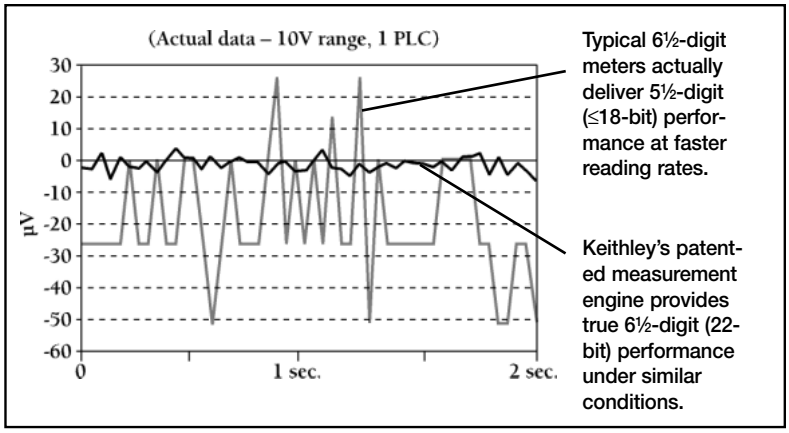

Figure 5. When the measurements matter, Keithley provides up to 10x better performance at equivalent reading rates or up to 10x faster speeds at equivalent measurement performance. Our patented A/D converter and high performance signal conditioning circuitry make this possible.

Specification Conversion Factors

Percent	PPM	Digits	Bits	dB	Portion of 10V
10%	100000	1	3.3	–20	1 V
1%	10000	2	6.6	–40	100 mV
0.1%	1000	3	10	–60	10 mV
0.01%	100	4	13.3	–80	1 mV
0.001%	10	5	16.6	–100	100 µV
0.0001%	1	6	19.9	–120	10 µV
0.00001%	0.1	7	23.3	–140	1 µV
0.000001%	0.01	8	26.6	–160	100 nV
0.0000001%	0.001	9	29.9	–180	10 nV

Integra Series Performance (6½-digit, 22-bit)

Digital Filtering

For each major measurement function, users can employ either averaging or advanced digital filtering to reduce noise and increase the effective resolution.

Averaging Filter

The averaging filter operates over a range of from two to 100 readings. All readings included in the filter range are weighted equally. A step input of any size will ramp up linearly to the final value after obtaining the number of readings specified by the user. The averaging filter may be configured as either a moving averaging or as a repeat filter. Operation over the GPIB bus is often done in "repeat" mode to ensure that all readings are fully filtered. Also, taking filtered measurements in repeat mode requires only one trigger, simplifying programming. Only the repeat filter can be used while scanning.

Advanced Filter

When a DMM is used in bench mode, it's often desirable for it to respond immediately upon connection to a test point, without the slow response associated with an averaging filter. The advanced filter addresses this need by providing a filter reset level. If the measured value deviates significantly from previous values, the filter is reset to the new value, and filtering is restarted. In this way, the user can set the filter reset level just above the maximum noise level anticipated and the multimeter will respond to new values immediately.

NPLC

Selectable power line cycle integration allows the user to specify the number of power line cycles (NPLC) over which to integrate (1, 5, 10, etc.). Use of line cycle integration provides rejection of noise from line cycle interference, the most common source of noisy readings. In general, the longer the integration time chosen, the greater the noise rejection will be. The system can also be set to less than 1 NPLC integration time, as fast as 0.002 NPLC (~33μs at 60Hz) in the Model 2701 and 0.01 NPLC (~167μs at 60Hz) in the Model 2700 and 2750 for faster data measurement (but without power line noise rejection).

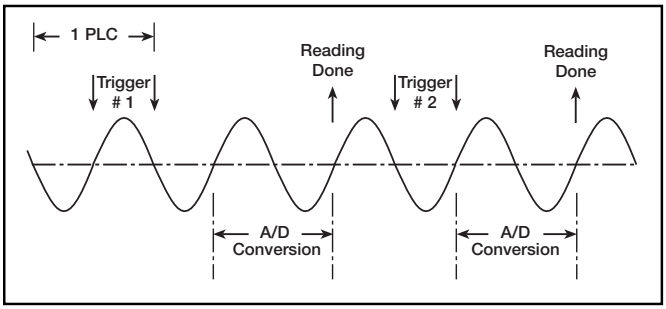

Figure 7

Line Cycle Synchronization

To attain the highest possible line cycle noise rejection, it is important to trigger the reading at the beginning of a power line cycle. The system can be set to start a measurement precisely when the power line signal crosses zero (see ***Figure 7***). This function increases the normal mode noise rejection 30dB, providing an additional ×30 reduction in noise due to line cycle interference.

Autozero

Internal autozeroing is used to maintain the best measurement performance. The advanced firmware design does the required calculation, such as CJC compensation for thermocouple measurements with the 7700, 7706, 7708, and 7710, automatically in the background. This enables the Integra system to provide faster reading rates (competitive products spend half their measurement time validating their own zero). Autozero can be disabled to increase measurement speed, but this may result in greater measurement uncertainty.

Low Ohms Measurement (Model 2750 only)

The Model 2750 can measure low ohms on all of its switch/control modules that have multiplexers or matrix configurations. The four-wire ohms measurement supports low ohms measurements down to the 1Ω range, with micro-ohm resolution. Measurements can be accommodated through ribbon cable or discrete wiring. On four-wire ohms measurements, up to five additional ohms of cable/switch card resistance can be tolerated per cable lead. This allows the use of ribbon cable without overloading the range.

1.888.KEITHLEY (U.S. only)
www.keithley.com
KEITHLEY
A GREATER MEASURE OF CONFIDENCE

Offset Compensation

For more accurate low resistance measurements, all Integra systems provide the offset compensation mode to eliminate errors from the thermoelectric EMF effects (V_{EMF}). During the measurement cycle, the built-in ohms current source is turned off, then turned on again, and the resulting EMF error is automatically subtracted. This technique is typically used when measuring values less than 100Ω using the four-wire ohms method.

Voltage Limit/Dry Circuit Ohms (Model 2750 only)

The use of dry circuit mode, when selected, limits the open-circuit voltage to 20mV. This allows resistance measurements to be made with low power. When measuring contact and connector resistances, it is important not to puncture oxides and films that may have formed. Standard resistance measurements have open-circuit voltage levels from 5.4V to 12.8V, depending on the selected range.

Dry circuit ohms can be used on the 1Ω, 10Ω, 100Ω, and 1kΩ ranges for the four-wire ohms (Ω4) function. Also, offset compensated ohms (OCOMP) can be used with dry circuit ohms to cancel the effect of thermoelectric EMFs.

Dry circuit ohms should be used for any device that could be damaged by high open-circuit voltage. If not sure, and the slightly degraded accuracy is not a consideration, it is good practice to use dry circuit ohms to measure low resistance.

The accuracy specifications for all dry circuit ohms ranges are with offset compensated ohms and line synchronization enabled.

Temperature Measurements

The Integra systems support three major types of temperature sensors with built-in signal conditioning and linearization: thermocouples, RTDs, and thermistors.

	Thermocouples	RTDs	Thermistors
Temperature Range	–200 ~ 1820°C	–200 ~ 630°C	–80 ~ 150°C
Advantage	• Self-powered • Wide temperature range	• High stability • High accuracy • No CJC required	• Interchangeability • No CJC required • High accuracy over limited temperature range
Cost	Low	High	Medium

The Integra systems provide built-in algorithms for a variety of thermocouples, RTDs, and thermistors. To begin using a sensor, simply hook it up and the system does the rest.

- Thermocouples: Type J, K, N, T, E, R, S, B
- RTDs: D100, F100, PT100, PT385, PT3916, or user type
- Thermistors: 2250Ω, 5kΩ, and 10kΩ

Cold Junction Compensation Methods

Thermocouple measurements always require that the temperature be known at the point where the thermocouple is connected to the instrument. This connection point is known as the "cold junction." The Integra systems support three different methods for including this "cold-junction" temperature in the temperature measurements.

Automatic CJC

The CJC sensors are mounted on the multiplexer module's PC board (7700, 7706, 7708, and 7710). They sense the actual temperature across the module's connector, then compensate all temperature measurements accordingly. The CJC scaling is done automatically when autozero is turned on, so the user does not have to acquire it separately. When autozero is turned off, the instrument is optimized for speed and does not refresh the CJC compensation. This allows the user to obtain faster scan rates for short periods of time while ambient temperature remains stable.

External CJC

A thermistor or RTD is attached to Channel 1 by the end user. This thermistor or RTD is then used to measure the temperature of the point(s) where the thermocouples are connected to the instrument or to copper wires leading to the instrument. The precision of the actual temperature measurement depends on the accuracy of the cold junction reading and how close the sensor is to the actual temperature of the connection.

Simulated CJC

When the "change" in temperature is of interest rather than the absolute temperature value, the user can enter a parameter as a cold junction reference point (for example, 23°C for room temperature). This parameter will be used to adjust the actual temperature measurement for each channel. This simulated temperature must be updated manually if ambient conditions change. This is also the method used when an actual ice bath is used to establish a cold junction of 0°C. The simulated parameter is then set to 0°C or 32°F.

Open Thermocouple Detect

A system can alert the user if any thermocouple becomes broken or otherwise disconnected from the input terminal blocks. When the Open T/C Detect feature is enabled, the system will perform (in the background) a two-wire resistance measurement across each thermocouple input channel. If an open connection is detected, the front panel display will show "OVERFLOW" for that channel.

Calibration

The design of the Integra Series and their calibration procedure were developed to address a variety of critical calibration issues. For example, the systems have front panel input jacks, so there's no need to disassemble the system for periodic recalibrations. There's also no need to buy, stock, and track spare "cal only" modules. The systems are connected to the calibrator through the front panel input jacks. The systems' calibration procedure covers both verification and adjustment and can be performed through either the front panel or any of the remote interfaces. The calibration interval is user-selectable.

Start-Up Software

Free built-In Web diagnostic tool (2701 only)

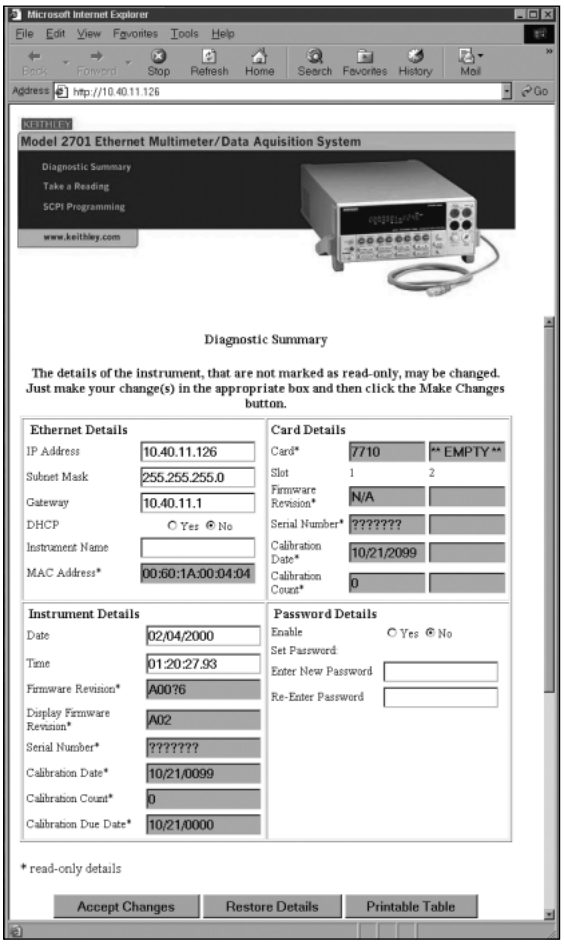

To start communicating with the Integra Series instrument, simply connect the 2701 to a PC Ethernet port using the supplied RJ-45 crossover cable, start Microsoft® Internet Explorer® version 5.0 or later, and type the instrument's IP address into the URL line. The built-in web diagnostic interface allows for easy communication and debugging, without the need to install external software. This interface makes it easy to read and set network parameters such as IP address, subnet mask, gateway, MAC address, calibration dates, and other data stored in the Integra Series instrument. It also takes readings from the instrument and allows the user to send command strings and receive data.

Free customizable start-up software

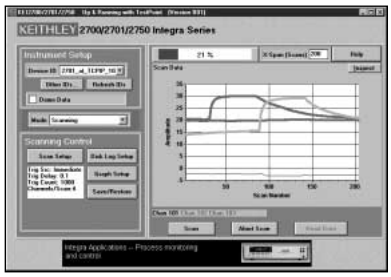

This free TestPoint runtime offers basic datalogging capabilities that can get a system "up & running" almost immediately. With just a few clicks of the mouse, this software can confirm the system's hardware, wiring, communications, and software drivers are installed and operating correctly. It can also configure instrument functions and perform simple data acquisition tasks. Data from multiple channels can be saved to disk and up to eight channels of data can be graphed automatically. If the application demands greater functionality, this runtime can be modified with the TestPoint application development package.

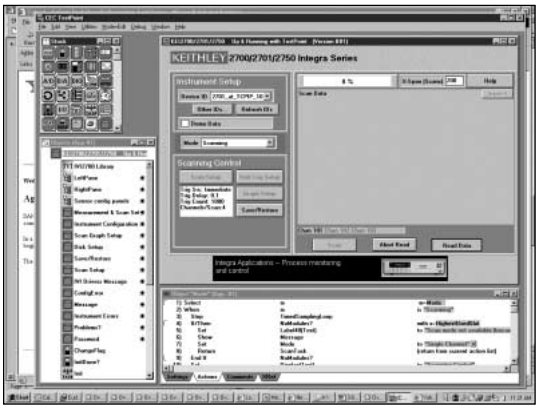

TestPoint™ Application Development Package

If Keithley's free start-up software doesn't provide a feature needed to support a specific application, the economical TestPoint application development package makes it simple to create a semi-custom solution by modifying the runtime application. By using the start-up runtime as a foundation, TestPoint offers the flexibility needed to build basic systems quickly, without in-depth programming. TestPoint uses object-oriented, drag-and-drop technology to bring both power and simplicity to data acquisition and test and measurement applications. TestWizards and pre-written application templates in a choice of graphical styles make it simple to create a complete application with a few mouse clicks. Additional objects can be modified and added to create custom enhancements.

Three optional toolkits make it easy to expand applications:

- Internet toolkit provides Web-based remote measurements and control.
- Database toolkit provides access to popular database packages like Access, SQL, Oracle, and others.
- Statistical process control (SPC) toolkit adds charts, statistics, and analysis capabilities.

Datalogging/Data Acquisition Software

ExceLINX-1A

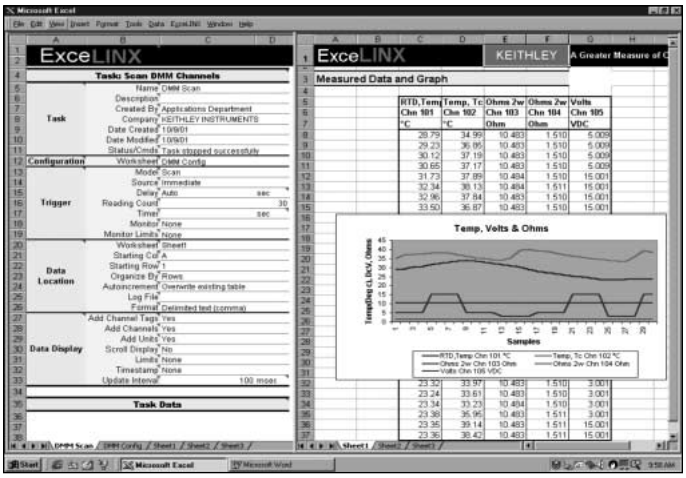

For advanced datalogging tasks, this powerful and economical add-in utility for Microsoft® Excel makes it simple to acquire data from the Integra Series instrument directly into Excel, then employ Excel's graphic, charting, and analysis capabilities to turn that data into useful information. No programming is required—a few mouse clicks are all it takes to configure channels, set parameters, configure triggers, and scan lists. ExceLINX-1A can control up to three Integra Series instruments for up to 600 channels of data acquisition. Sold separately.

Custom Application Development with VISA Based IVI Driver

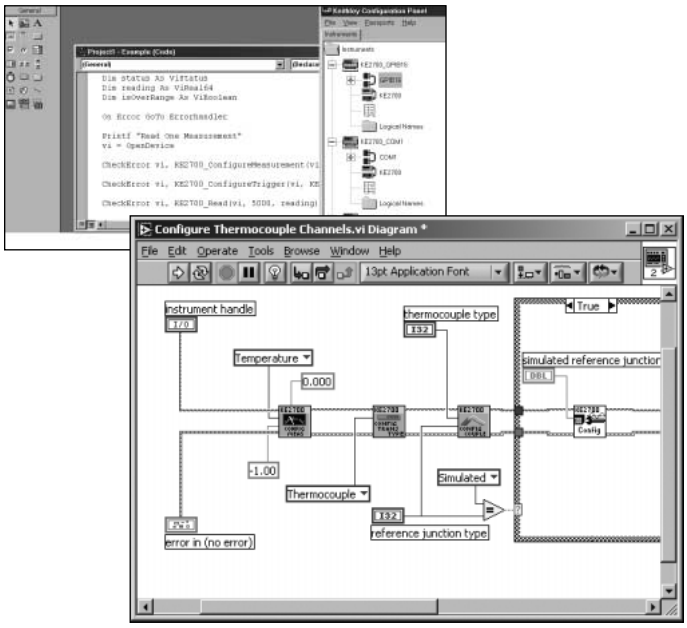

For building custom applications, programmers can take advantage of the VISA based Integra series IVI driver designed for use with software development environments like Visual Basic, Visual C/C++, LabVIEW, LabWindows/CVI, and TestPoint. The VISA (Virtual Instrument Software Architecture) layer of the driver allows the programmer to quickly reconfigure the communication bus between the PC and the instruments without changing a single line of source code. This means that changing GPIB control board vendors or switching the communication bus between GPIB, RS-232, and Ethernet requires no rework of a custom application program. The IVI (Interchangeable Virtual Instrument) layer of the driver provides a simplified command interface that is common to the entire Integra Series product family. The driver also includes a large set of examples for reference during software design.

Integra Series Multimeter/Switch Systems

Specifications are subject to change without notice.

Download the latest specs from **www.keithley.com**.

Integra Series
Mainframes

Multimeter/Switch Systems

DC CHARACTERISTICS[1]

CONDITIONS: MED (1 PLC)[2] or 10 PLC or MED (1 PLC) with Digital Filter of 10

FUNCTION	RANGE	RESOLUTION	TEST CURRENT ±5% OR BURDEN VOLTAGE	INPUT RESISTANCE OR OPEN CKT. VOLTAGE[3] 2700/2701	2750	ACCURACY: ±(ppm of reading + ppm of range) (ppm = parts per million) (e.g., 10ppm = 0.) 24 Hour[4] 23°C±1°	90 Day 23°C±5°	1 Year 23°C±5°	TEMPERATURE COEFFICIENT 0°–18°C & 28°–50°C
Voltage[11]	100.0000 mV	0.1 µV		>10 GΩ	>10 GΩ	15 + 30	25 + 35	30 + 35	(1 + 5)/°C
	1.000000 V	1.0 µV		>10 GΩ	>10 GΩ	15 + 6	25 + 7	30 + 7	(1 + 1)/°C
	10.00000 V	10 µV		>10 GΩ	>10 GΩ	10 + 4	20 + 5	30 + 5	(1 + 1)/°C
	100.0000 V	100 µV		10 MΩ ± 1%	10 MΩ ± 1%	15 + 6	35 + 9	45 + 9	(5 + 1)/°C
	1000.000 V[5]	1 mV		10 MΩ ± 1%	10 MΩ ± 1%	20 + 6	35 + 9	50 + 9	(5 + 1)/°C
Resistance[6, 8]	1.000000 Ω[24]	1 µΩ	10 mA		5.9 V	80 + 40	80 + 40	100 + 40	(8 + 1)/°C
	10.00000 Ω[24]	10 µΩ	10 mA		5.9 V	20 + 20	80 + 20	100 + 20	(8 + 1)/°C
	100.0000 Ω	100 µΩ	1 mA	6.9 V	12.2 V	20 + 20	80 + 20	100 + 20	(8 + 1)/°C
	1.000000 kΩ	1 mΩ	1 mA	6.9 V	12.2 V	20 + 6	80 + 6	100 + 6	(8 + 1)/°C
	10.00000 kΩ	10 mΩ	100 µA	6.9 V	6.8 V	20 + 6	80 + 6	100 + 6	(8 + 1)/°C
	100.0000 kΩ	100 mΩ	10 µA	12.8 V	12.8 V	20 + 6	80 + 10	100 + 10	(8 + 1)/°C
	1.000000 MΩ[23]	1.0 Ω	10 µA	12.8 V	12.8 V	20 + 6	80 + 10	100 + 10	(8 + 1)/°C
	10.00000 MΩ[7, 23]	10 Ω	0.7 µA // 10M Ω	7.0 V	7.0 V	150 + 6	200 + 10	400 + 10	(70 + 1)/°C
	100.0000 MΩ[7, 23]	100 Ω	0.7 µA // 10M Ω	7.0 V	7.0 V	800 + 30	2000 + 30	2000 + 30	(385 + 1)/°C
Dry Circuit Resistance[21, 24]	1.000000 Ω	1 µΩ	10 mA		20 mV	80 + 40	80 + 40	100 + 40	(8 + 1)/°C
	10.00000 Ω	10 µΩ	1 mA		20 mV	25 + 40	80 + 40	100 + 40	(8 + 1)/°C
	100.0000 Ω	100 µΩ	100 µA		20 mV	25 + 40	90 + 40	140 + 40	(8 + 1)/°C
	1.000000 kΩ	1 mΩ	10 µA		20 mV	25 + 90	180 + 90	400 + 90	(8 + 1)/°C
Continuity (2W)	1.000 kΩ	100 mΩ	1 mA	6.9 V	12.2 V	40 + 100	100 + 100	100 + 100	(8 + 1)/°C
Current	20.00000 mA	10 nA	< 0.2 V			60 + 30	300 + 80	500 + 80	(50 + 5)/°C
	100.0000 mA	100 nA	< 0.1 V			100 + 300	300 + 800	500 + 800	(50 + 50)/°C
	1.000000 A	1.0 µA	< 0.5 V[9]			200 + 30	500 + 80	800 + 80	(50 + 5)/°C
	3.000000 A	10 µA	< 1.5 V[9]			1000 + 15	1200 + 40	1200 + 40	(50 + 5)/°C
Channel (Ratio)[10]	Ratio Accuracy = Accuracy of selected Channel Range + Accuracy of Paired Channel Range								
Channel (Average)[10]	Average Accuracy = Accuracy of selected Channel Range + Accuracy of Paired Channel Range								

TEMPERATURE[19]

(Displayed in °C, °F, or K. Exclusive of probe errors.)

Thermocouples (Accuracy based on ITS-90.)

Type	Range	Resolution	90 Day/1 Year (23°C ± 5°C) Relative to Simulated Reference Junction	Using 77XX Module	Temperature Coefficient 0°–18°C & 28°–50°C
J	–200 to +760 °C	0.001 °C	0.2°C	1.0°C	0.03°C/°C
K	–200 to +1372°C	0.001 °C	0.2°C	1.0°C	0.03°C/°C
N	–200 to +1300°C	0.001 °C	0.2°C	1.0°C	0.03°C/°C
T	–200 to +400°C	0.001 °C	0.2°C	1.0°C	0.03°C/°C
E	–200 to +1000°C	0.001 °C	0.2°C	1.0°C	0.03°C/°C
R	0 to +1768°C	0.1 °C	0.6°C	1.8°C	0.03°C/°C
S	0 to +1768°C	0.1 °C	0.6°C	1.8°C	0.03°C/°C
B	+350 to +1820°C	0.1 °C	0.6°C	1.8°C	0.03°C/°C

4-Wire RTD:
(100Ω platinum [PT100], D100, F100, PT385, PT3916, or user type. Offset compensation On)

–200° to 630°C	0.01 °C	0.06°C		0.003°C/°C

Thermistor: (2.2kΩ, 5kΩ, and 10kΩ)[20]

–80° to 150°C	0.01 °C	0.08°C		0.002°C/°C

DC SYSTEM SPEEDS[15,18]

	2700/2750	2701
RANGE CHANGES (excludes 4WΩ)[16]:	50/s (42/s)	50/s (42/s)
FUNCTION CHANGES[16]:	50/s (42/s)	50/s (42/s)
AUTORANGE TIME[16]:	<30 ms	<30 ms
ASCII READINGS TO RS-232 (19.2k BAUD):	55/s	300/s
MAX. EXTERNAL TRIGGER RATE:	375/s	2000/s

DC MEASUREMENT SPEEDS[15]

Single Channel, 60Hz (50Hz) Operation

FUNCTION	DIGITS	READINGS/s		PLCs
DCV, DCI, Ω (<10M), Thermocouple, Thermistor	6.5[12,16]	5	(4)	10
	6.5[16]	35	(28)	1
	6.5[12,16]	45	(36)	1
	5.5[12,16]	150	(120)	0.1
	5.5[16, 17]	300	(240)	0.1
	5.5[17]	500	(400)	0.1
2701 and 2750 only	4.5[17]	2500	(2000)	0.01
2701 only	3.5	3500	(2800)	0.002
4WΩ (<10M)	6.5[16]	1.4	(1.1)	10
	6.5[16]	15	(12)	1
	5.5[17]	33	(25)	0.1
4WΩ OComp, RTD[22]	6.5[16]	0.9	(0.7)	10
	6.5[16]	8	(6.4)	1
	5.5[16, 17]	18	(14.4)	0.1
Channel (Ratio), Channel (AVG)	6.5[16]	2.5	(2)	10
	6.5[16]	15	(12)	1
	5.5[17]	25	(20)	0.1

Multiple Channels, Into Memory[18]

	Channels/s 2700	2701	2750
7710 Scanning DCV	180/s	500/s	230/s
7710 Scanning DCV with Limits or Time Stamp On	170/s	500/s	230/s
7710 Scanning DCV alternating 2WΩ	45/s	115/s	60/s

Multiple Channels, Into and Out of Memory to GPIB[16, 18] or Ethernet

	Channels/s 2700	2701	2750
7702 Scanning DCV	65/s	75/s	65/s
7700 and 7708 Scanning Temperature (T/C)	50/s	50/s	50/s
7710 Scanning DCV	145/s	440/s	210/s
7710 Scanning DCV with Limits or Time Stamp On	145/s	440/s	210/s
7710 Scanning DCV alternating 2WΩ	40/s	115/s	55/s

DC SPEED vs. NOISE REJECTION

Rate	Filter	Readings/s[12]	Digits	RMS Noise 10V Range 2700,2750	2701	NMRR	CMRR[14]
10	50	0.1 (0.08)	6.5	< 1.2 μV	< 2.5 μV	110 dB[13]	140 dB
1	Off	15 (12)	6.5	< 4 μV	< 6 μV	90 dB[13]	140 dB
0.1	Off	500 (400)	5.5	< 22 μV	< 40 μV	—	80 dB
0.01	Off	2500 (2000)	4.5	< 150 μV	< 300 μV	—	80 dB
0.002	Off	3500 (2800)	3.5	—	< 1 mV	—	60 dB

DC MEASUREMENT CHARACTERISTICS

DC VOLTS

A-D LINEARITY: 2.0 ppm of reading + 1.0 ppm of range.

INPUT IMPEDANCE:
100mV–10V Ranges: Selectable >10GΩ // with <400pF or 10MΩ ±1%.
100V, 1000V Ranges: 10MΩ ±1%.
Dry Circuit: 100kΩ ± 1% // <1μF.

EARTH ISOLATION: 500V peak, >10GΩ and <300pF any terminal to chassis.

INPUT BIAS CURRENT: <75pA at 23°C.

COMMON MODE CURRENT: <500nApp at 50Hz or 60Hz.

AUTOZERO ERROR: Add ±(2ppm of range error + 5μV) for < 10 minutes and ±1°C.

INPUT PROTECTION: 1000V, all ranges. 300V with plug in modules.

RESISTANCE

MAXIMUM 4WΩ LEAD RESISTANCE: 80% of range per lead (Dry Ckt mode). 5Ω per lead for 1Ω range; 10% of range per lead for 10Ω, 100Ω, and 1kΩ ranges; 1kΩ per lead for all other ranges.

OFFSET COMPENSATION: Selectable on 4WΩ, 1Ω, 10Ω, 100Ω, 1kΩ, and 10kΩ ranges.

CONTINUITY THRESHOLD: Adjustable 1 to 1000 Ω

INPUT PROTECTION: 1000V, all Source Inputs, 350V Sense Inputs. 300V with plug-in modules.

DC CURRENT

SHUNT RESISTORS: 100mA–3A, 0.1Ω. 20mA, 5Ω.

INPUT PROTECTION: 3A, 250V fuse.

THERMOCOUPLES

CONVERSION: ITS-90.

REFERENCE JUNCTION: Internal, External, or Simulated (Fixed).

OPEN CIRCUIT CHECK: Selectable per channel. Open >11.4kΩ ±200Ω.

DC NOTES

1. 20% overrange except on 1000V and 3A.
2. Add the following to "ppm of range" uncertainty; 100mV 15ppm; 1V and 100V 2ppm; for Model 2750 1Ω and Dry Circuit Ω 40ppm; 10→1MΩ 2ppm, for Models 2700/2701 100Ω 30ppm, 20mA and 1A 10ppm, 100mA 40ppm.
3. ±2% (measured with 10MΩ input resistance DMM, >10GΩ DMM on 10MΩ and 100MΩ ranges). For Dry Circuit Ω, ±25% with Input HI connected to Sense HI; with Sense HI disconnected add 30mV.
4. Relative to calibration accuracy.
5. For signal levels >500V, add 0.02ppm/V uncertainty for portion exceeding 500V.
6. Specifications are for 4-wire Ω, 1Ω, 10Ω, and 100Ω with offset compensation on. With 77XX plug-in modules, LSYNC on. With offset compensation on, OPEN CKT. VOLTAGE is 12.8V. For 2-wire Ω add 1.5Ω to "ppm of range" uncertainty. 1Ω range is 4-wire only.
7. Must have 10% matching of lead resistance in Input HI and LO.
8. Add the following to "ppm of reading" uncertainty when using plug in modules:

	10 kΩ	100 kΩ	1 MΩ	10 MΩ	100 MΩ
All Modules:				220 ppm	2200 ppm
7701, 7703, 7707, 7709 Modules:	10 ppm	100 ppm	1000 ppm	1%	10%
7706, 7708, 7710 Modules:	5 ppm	50 ppm	500 ppm	5000 ppm	5%
7710 Module 23°C ±5°C:	11 ppm	110 ppm	1100 ppm	1.1%	11%

9. Add 1.5V when used with plug in modules.
10. For RATIO, DCV only. For AVERAGE, DCV and Thermocouples only. Available with plug in modules only.
11. Add 6μV to "of range" uncertainty when using Models 7701, 7703, and 7707, and 3μV for Models 7706 and 7709.
12. Auto zero off.
13. For LSYNC On, line frequency ±0.1 %. For LSYNC Off, use 60dB for ≥ 1PLC.
14. For 1kΩ unbalance in LO lead. AC CMRR is 70dB.
15. Speeds are for 60Hz (50Hz) operation using factory defaults operating conditions (*RST). Autorange off, Display off, Limits off, Trigger delay = 0.
16. Speeds include measurements and binary data transfer out the GPIB or ASCII data transfer for Ethernet and RS-232 (reading element only).
17. Sample count = 1000, auto zero off (into memory buffer).
18. Auto zero off, NPLC = 0.01 (Models 2700 and 2750), NPLC = 0.002 (Model 2701).
19. Additional Uncertainty:

Type	Range	Front Terminals Sim. Ref. Junction	Plug-In Modules 7709 Sim. Ref. Junction	7701/03/07 Sim. Ref. Junction	7700/08 Using CJC	7706 Using CJC	7710 Using CJC
J	–200° to 0°C	0.1	0.1	0.3	0.8	1.6	4.5
K	–200° to 0°C	0.2	0.2	0.4	0.8	1.6	1.0
N	–200° to 0°C	0.3	0.3	0.6	0.8	1.6	2.5
T	–200° to 0°C	0.2	0.1	0.4	0.8	1.6	2.5
E	–200° to 0°C	–	0.1	0.3	0.8	1.6	2.5
R	0° to +400°C	0.4	0.6	1.2	0.5	1.0	2.2
S	0° to +400°C	0.4	0.6	1.2	0.5	1.0	2.2
B	+350° to +1100°C	0.8	0.3	1.7	0.5	1.0	2.2

Type	Range	7710 Using CJC
J	0° to +760°C	1.5
K	0° to +1372°C	–
N	0° to +1300°C	0.5
T	0° to +400°C	0.5
E	0° to +1000°C	0.5
R	+400° to +1768°C	0.9
S	+400° to +1768°C	0.9
B	+1100° to +1820°C	0.9

20. For lead resistance >0Ω, add the following uncertainty/Ω for measurement temperatures of:

		70°–100°C	100°–150°C
2.2 kΩ	(44004)	0.22°C	1.11°C
5.0 kΩ	(44007)	0.10°C	0.46°C
10 kΩ	(44006)	0.04°C	0.19°C

21. For 4-wire Ω only, offset compensation on, LSYNC on.
22. For Dry Circuit 1kΩ range, 2 readings/s max.
23. For 2750 Front Inputs, add the following to Temperature Coefficient "ppm of reading" uncertainty: 1MΩ 25ppm, 10MΩ 250ppm, 100MΩ 2500ppm. Operating environment specified for 0°C to 50°C and 50% RH at 35°C.
24. Model 2750 only.
25. Front panel resolution is limited to 0.1Ω.

AC SPECIFICATIONS[1]

Function	Range	Resolution	Calibration Cycle	Accuracy: ±(% of reading + % of range), 23°C ± 5°C				
				3 Hz–10 Hz	10 Hz–20 kHz	20 kHz–50 kHz	50 kHz–100 kHz	100 kHz–300 kHz
Voltage[2]	100.0000 mV	0.1 µV	90 Days	0.35 + 0.03	0.05 + 0.03	0.11 + 0.05	0.6 + 0.08	4.0 + 0.5
	1.000000 V	1.0 µV	(all ranges)					
	10.00000 V	10 µV	1 Year	0.35 + 0.03	0.06 + 0.03	0.12 + 0.05	0.6 + 0.08	4.0 + 0.5
	100.0000 V	100 µV	(all ranges)					
	750.000 V	1.0 µV						
			(Temp. Coeff.)/°C[3]	0.035 + .003	0.005 + .003	0.006 + .005	0.01 + .006	0.03 + .01

				3 Hz–10 Hz	10 Hz–3 kHz	3 kHz–5 kHz
Current[2]	1.000000 A	1.0 µA	90 Day/1 Year	0.30 + 0.04	0.10 + 0.04	0.14 + 0.04
	3.00000 A[14]	10 µA		0.35 + 0.06	0.16 + 0.06	0.18 + 0.06
			(Temp. Coeff.)/°C[3]	0.035 + 0.006	0.015 + 0.006	

				(3 Hz–500 kHz) (333 ms–2 µs)
Frequency[4] **and Period**	100 mV to 750 V	0.333 ppm	90 Day/1 Year	100 ppm + 0.333 ppm (SLOW, 1s gate)
		3.33 ppm		100 ppm + 3.33 ppm (MED, 100ms gate)
		33.3 ppm		100 ppm + 33.3 ppm (FAST, 10ms gate)

ADDITIONAL UNCERTAINTY ±(% OF READING)

Low Frequency Uncertainty	MED	FAST
20 Hz – 30 Hz	0.3	—
30 Hz – 50 Hz	0	—
50 Hz – 100 Hz	0	1.0
100 Hz – 200 Hz	0	0.18
200 Hz – 300 Hz	0	0.10
>300 Hz	0	0

CREST FACTOR:[5]	1–2	2–3	3–4	4–5
Additional Uncertainty:	0.05	0.15	0.30	0.40
Max. Fundamental Freq.:	50kHz	50kHz	3kHz	1kHz

Maximum Crest Factor: 5 at full-scale.

AC MEASUREMENT CHARACTERISTICS

AC VOLTS

MEASUREMENT METHOD: AC-coupled, True RMS.

INPUT IMPEDANCE: 1MΩ ±2% // by <100pF.

INPUT PROTECTION: 1000Vp or 400VDC. 300Vrms with plug in modules.

AC CURRENT

MEASUREMENT METHOD: AC-coupled, True RMS.

SHUNT RESISTANCE: 0.1Ω.

BURDEN VOLTAGE: 1A <0.5Vrms, 3A <1.5Vrms. Add 1.5Vrms when used with plug in modules.

INPUT PROTECTION: 3A, 250V fuse.

FREQUENCY AND PERIOD

MEASUREMENT METHOD: Reciprocal counting technique.

GATE TIME: SLOW 1s, MED 100ms, and FAST 10ms.

AC GENERAL

AC CMRR[6]**:** 70dB.

VOLT HERTZ PRODUCT: <= 8×10^7.

AC MEASUREMENT SPEEDS[7, 13]

Single Channel, 60Hz (50Hz) Operation

Function	Digits	Readings/s	Rate	Bandwidth
ACV, ACI	6.5	2s/Reading	SLOW	3 Hz–300 kHz
	6.5	4.8 (4)	MED	30 Hz–300 kHz
	6.5[9]	40 (32)	FAST	300 Hz–300 kHz
Frequency, Period	6.5	1 (1)	SLOW	3 Hz–300 kHz
	5.5	9 (9)	MED	30 Hz–300 kHz
	4.5	35 (35)	FAST	300 Hz–300 kHz
	4.5[10]	65 (65)	FAST	300 Hz–300 kHz

Multiple Channel

7710 SCANNING ACV[10, 11]**:** 500/s.

7710 SCANNING ACV WITH AUTO DELAY ON : 2s/reading.

AC SYSTEM SPEEDS[7, 9, 11]

	2700/2750	2701
AC System Speed:	(19.2k)	(115.2K)
Range Changes:[12]	4/s (3/s)	4/s (3/s)
Function Changes:[12]	4/s (3/s)	4/s (3/s)
Autorange Time:	< 3s	< 3s
ASCII Readings to RS-232 (19.2k baud):	50/s	300/s
Max. External Trigger Rate:	250/s	2000/s

AC NOTES

1. 20 % overrange except on 750V and 3A.
2. Specification are for SLOW mode and sine wave inputs >5% of range. SLOW and MED are multi-sample A/D conversions. FAST is DETector:BANDwidth 300 with nPLC = 1.0.
3. Applies to 0°–18°C and 28°–50°C.
4. For square wave inputs >10% of ACV range, except 100mV range. 100mV range frequency must be >10Hz if input is <20mV.
5. Applies to non-sine waves >5Hz.
6. For 1kΩ unbalance in LO lead.
7. Speeds are for 60Hz (50Hz) operation using factory defaults operating conditions (*RST). Autorange off, Display off, Limits off, Trigger delay=0..
8. For ACV inputs at frequencies of 50 or 60Hz (±10%), add the following to "% of Range" uncertainty: 100mV 0.25%, 1V 0.05%, 10V 0.13%, 100V 0.03%, 750V 0.015 (Model 2701 only)..
9. Auto Zero off.
10. Sample count = 1024.
11. DETector:BANDwidth 300 with nPLC = 0.006 (2701 only).
12. Maximum useful limit with trigger delay = 175ms.
13. Includes measurement and binary data transfer out GPIB or ASCII data transfer for Ethernet and RS-232 (Reading Element only).

GENERAL SPECIFICATIONS:

EXPANSION SLOTS: 2 (2700, 2701), 5 (2750).
POWER SUPPLY: 100V / 120V / 220V / 240V ±10%.
LINE FREQUENCY: 45Hz to 66Hz and 360Hz to 440Hz, automatically sensed at power-up.
POWER CONSUMPTION: 28VA (2700), 80VA (2701, 2750).
OPERATING ENVIRONMENT: Specified for 0°C to 50°C. Specified to 80% RH at 35°C.
STORAGE ENVIRONMENT: –40°C to 70°C.
BATTERY: Lithium battery-backed memory, 3 years @ 23°C (Models 2700, 2750) Lithium Ion battery-backed memory, 30 days of buffer storage @ 23°C and >4 hours charge time. Battery lifetime: >3 years @ 23°C, >1.5 years @ 50°C (Model 2701)
WARRANTY: 3 years excludes battery.
EMC: Conforms to European Union Directive 89/336/EEC EN61326-1.
SAFETY: Conforms to European Union Directive 73/23/EEC EN61010-1, CAT I.
VIBRATION: MIL-PRF-28800F Class 3, Random.
WARM-UP: 2 hours to rated accuracy.
DIMENSIONS:
Rack Mounting: 89mm high × 213mm wide (2700, 2701) or 485mm wide (2750) × 370mm deep (3.5 in × 8.375 in or 19 in × 14.563 in).
Bench Configuration (with handle and feet): 104mm high × 238mm wide (2700, 2701) or 485mm wide (2750) × 370mm deep (4.125 in × 9.375 in (2700, 2701) or 19 in (2750) × 14.563 in).
SHIPPING WEIGHT: 6.5kg (14 lbs.) (2700, 2701) or 13kg (28 lbs.) (2750).
DIGITAL I/O: 2 inputs, 1 for triggering and 1 for hardware interlock.
5 outputs, 4 for Reading Limits and 1 for Master Limit. Outputs are TTL compatible or can sink 250mA, diode clamped to 40V.

TRIGGERING AND MEMORY:
Window Filter Sensitivity: 0.01%, 0.1 %, 1%, 10%, or Full-scale of range (none).
Reading Hold Sensitivity: 0.01%, 0.1 %, 1%, or 10% of reading.
Trigger Delay: 0 to 99 hrs (1ms step size).
External Trigger Delay: <2ms (2700), <1ms (2701, 2750).
External Trigger Jitter: <1ms (2700), <500µs (2701), <500µs (2750).
Memory Size: 55,000 readings (2700), 450,000 readings (2701), 110,000 readings (2750).
MATH FUNCTIONS: Rel, Min/Max/Average/Std Dev/Peak-to-Peak (of stored reading), Limit Test, %, 1/x, and mX+b with user defined units displayed.
REMOTE INTERFACE:
GPIB (IEEE-488.2) (2700, 2750) and RS-232C.
Ethernet TCP/IP (10bT and 100bT) (2701)
SCPI (Standard Commands for Programmable Instruments)
LabVIEW Drivers
ACCESSORIES SUPPLIED: Model 1751 Safety Test Leads, Product Information CD-ROM. (Model 2701 only: Getting Started Foldout, 3m Ethernet crossover cable, software CD-ROM with IVI/VISA drivers for VB, VC/C++, LabVIEW, TestPoint, and LabWindows/CVI, plus free runtime start-up software.)
ACCESSORIES AVAILABLE:
4288-7Rack Mount Rear Support Kit (2750)
77XX-904A Module Manual
77XXModules
Extended Warranty
ExceLINX-1A (Excel add-in datalogger software)
TestPoint™ Software Development Package
FOR MODEL 2701:
Ethernet: RJ-45 connector, TCP/IP, 10bT and 100bTx autosensed.
IP Configuration: Static or DHCP.
Password Protection: 11 Characters.
Software: Windows 98, NT, 2000, ME, and XP compatible. Internet Explorer 5.0 or higher required. Web page server by 2701.

Integra Series
Modules

Multimeter/Switch Systems

7700 20-CHANNEL DIFFERENTIAL MULTIPLEXER W/AUTOMATIC CJC

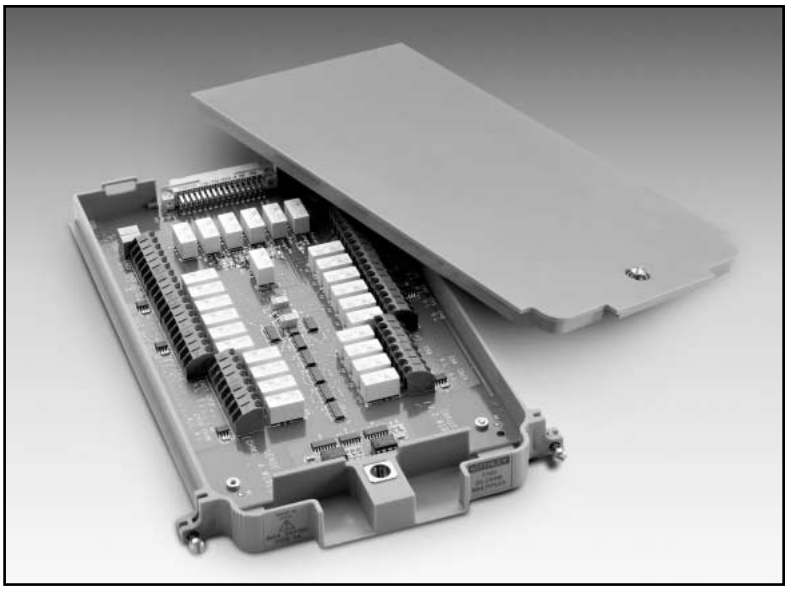

FEATURES

- 20 channels for general-purpose measurements, plus two channels to measure current.
- 2- or 4-wire measurement.
- Oversize screw terminal connection blocks are standard for easier connections.
- Automatic CJC sensors on the scanner card mean there are no other accessories are required to make thermocouple temperature measurements.
- Configurable as two independent banks of multiplexers.
- 300V, 1A capacity for voltage channels; 60W, 125VA.
- 3A capacity for current channels.
- Relay closures stored in on-board memory.

GENERAL

20 CHANNELS: 20 channels of 2-pole relay input. All channels configurable to 4-pole.

2 CHANNELS: 2 channels of current only input.

RELAY TYPE: Latching electromechanical.

ACTUATION TIME: <3ms.

FIRMWARE: Specified for Model 2700 rev. A01, 2701 rev. A01, and 2750 rev. A01 or higher.

CAPABILITIES

CHANNELS 1-20: Multiplex one of 20 2-pole or one of 10 4-pole signals into DMM.

CHANNELS 21-22: Multiplex one of 2 2-pole current signals into DMM.

INPUTS

MAXIMUM SIGNAL LEVEL:

Channels (1-20): 300V DC or 300V rms (425V peak) for AC waveforms, 1A switched, 60W, 125VA maximum.

Channels (21-22): 60V DC or 30V rms, 3A switched, 60W, 125VA maximum.

CONTACT LIFE (typ.): $>10^5$ operations at max signal level.
$>10^8$ operations cold switching.

CONTACT RESISTANCE: <1Ω at end of contact life.

CONTACT POTENTIAL: <±500nV typical per contact, 1μV max.
<±500nV typical per contact pair, 1μV max.

OFFSET CURRENT: <100pA.

CONNECTOR TYPE: Screw terminal, #20 AWG wire size.

ISOLATION BETWEEN ANY TWO TERMINALS: $>10^{10}$Ω, <100pF.

ISOLATION BETWEEN ANY TERMINAL AND EARTH: $>10^9$Ω, <200pF.

INSERTION LOSS (50Ω Source, 50Ω Load):

	w/Internal DMM	w/o Internal DMM*
<0.1 dB:	1 MHz	1 MHz
<3 dB:	2 MHz	50 MHz

CROSSTALK (50Ω Load):	w/Internal DMM	w/o Internal DMM*
10 MHz:	<–40 dB	<–40 dB
25 MHz:	**	<–25 dB

COMMON MODE VOLTAGE: 300V or 300V rms (425V peak) for AC waveforms between any terminal and chassis.

TEMPERATURE ACCURACY USING INTERNAL CJC: 1.0°C (see mainframe specification for details).

* Channels 24 and 25 are open. Refer to ROUTe:MULTiple command in 27XX User Manual.

** Not valid.

ENVIRONMENTAL:

OPERATING ENVIRONMENT: Specified for 0°C to 50°C.
Specified to 80% R.H. at 35°C.

STORAGE ENVIRONMENT: –25°C to 65°C.

WEIGHT: 0.45kg (1 lb).

ACCESSORY AVAILABLE: Model 7401 Type K Thermocouple Wire, 30.5m (100 ft).

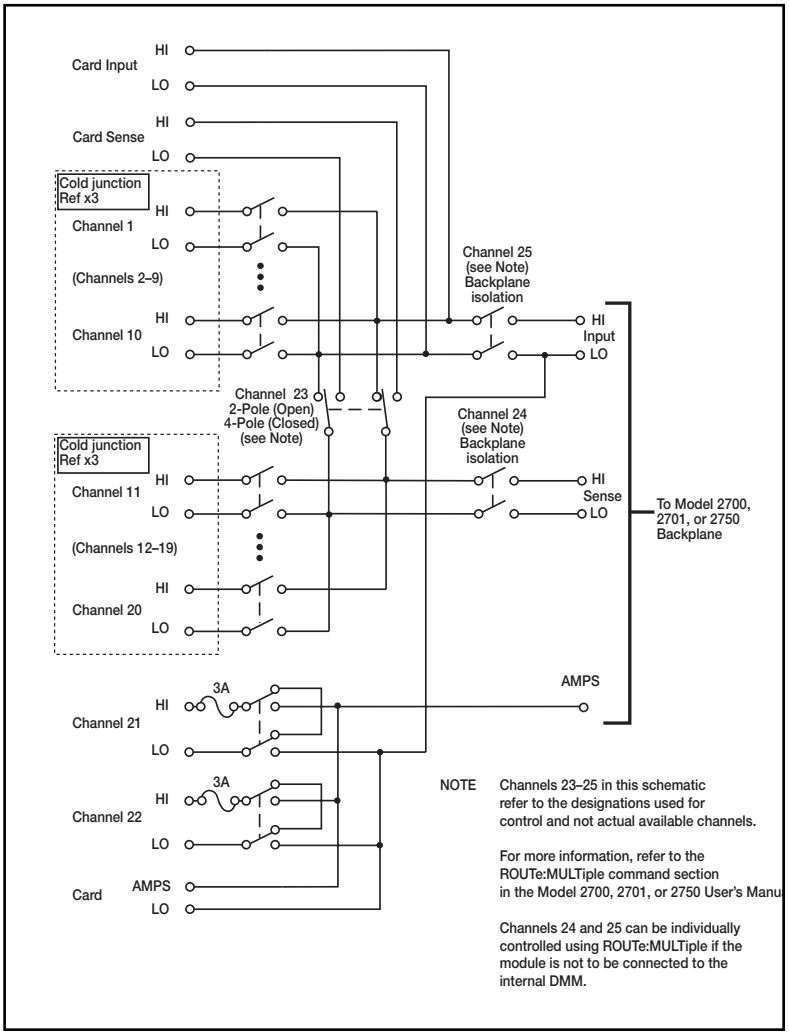

1.888.KEITHLEY (U.S. only)

www.keithley.com

KEITHLEY

A GREATER MEASURE OF CONFIDENCE

7701 LOW-VOLTAGE 32-CHANNEL DIFFERENTIAL MULTIPLEXER

FEATURES

- Configurable for 32 channels of differential measurements, with up to 16 channels of 4-pole measurements.
- Configurable for 32 channels of common-side 4-wire ohms.
- Configurable as two independent banks of multiplexers.
- Two female D-shell connectors are standard for secure hook-up and quick teardown.
- 150V, 1A capacity for voltage channels; 60W, 125VA.
- Two mating IDC connectors for ribbon cable are supplied.
- Relay closures stored in on-board memory.
- Screw terminal jumpers allow user-configurable DMM connections.

GENERAL

32 CHANNELS: 32 channels of 2-pole relay input. All channels configurable to 4-pole.

RELAY TYPE: Latching electromechanical.

ACTUATION TIME: <3ms.

FIRMWARE: Specified for Model 2700 rev. B03, Model 2701 rev. A01, and Model 2750 rev. A01 or higher.

DMM CONNECTIONS: Screw terminals provide internal DMM connections to channels 34 and 35 and connections to external wiring access.

CAPABILITIES

CHANNELS 1–32: Multiplex one of 32 2-pole or one of 16 4-pole signals into DMM. Configuration supports dual 1×16 independent multiplexers.

INPUTS

MAXIMUM SIGNAL LEVEL: Any channel to Any Channel (1–32): 150V DC or 150Vrms (212V peak) for AC waveforms, 1A switched, 60W, 125VA maximum.

SAFETY: Conforms to European Union Directive 73/23/EEC EN61010-1, CAT I.

CONTACT LIFE (typ): $>10^5$ operations at max signal level.
$>10^8$ operations cold switching.

CONTACT RESISTANCE: <1Ω any path and additional 1Ω at end of contact life.

CONTACT POTENTIAL: <6μV per contact pair.

OFFSET CURRENT: <100pA.

CONNECTOR TYPE: 50-pin female D-shell, Channels 1–24.
25-pin female D-shell, Channels 25–32.
Supplied with male IDC ribbon cable connectors.

ISOLATION BETWEEN ANY TWO TERMINALS: $>10^9$Ω, <200pF.

ISOLATION BETWEEN ANY TERMINAL AND EARTH: $>10^9$Ω, <400pF.

CROSS TALK (1MHz, 50Ω Load): <–35dB.

INSERTION LOSS (50Ω Source, 50Ω Load): <0.35dB below 1MHz.
<3dB below 2MHz.

COMMON MODE VOLTAGE: 300VDC or 300Vrms (425V peak) for AC waveforms between any terminal and chassis.

ENVIRONMENTAL:

OPERATING ENVIRONMENT: Specified for 0°C to 50°C.
Specified to 50% R.H. at 35°C.

STORAGE ENVIRONMENT: –25°C to 65°C.

WEIGHT: <0.52kg (1.16 lb).

ACCESSORIES AVAILABLE:

Model 7789	50/25 Pin Male D-Shell Solder Cup Connectors
Model 7790	50/50/25 Pin Female/Male D-Shell IDC Connectors
Model 7705-MTC-2	50 Pin Male to Female DSUB Cable, 2m (6.6 ft).
Model 7707-MTC-2	25 Pin Male to Female DSUB Cable, 2m (6.6 ft).

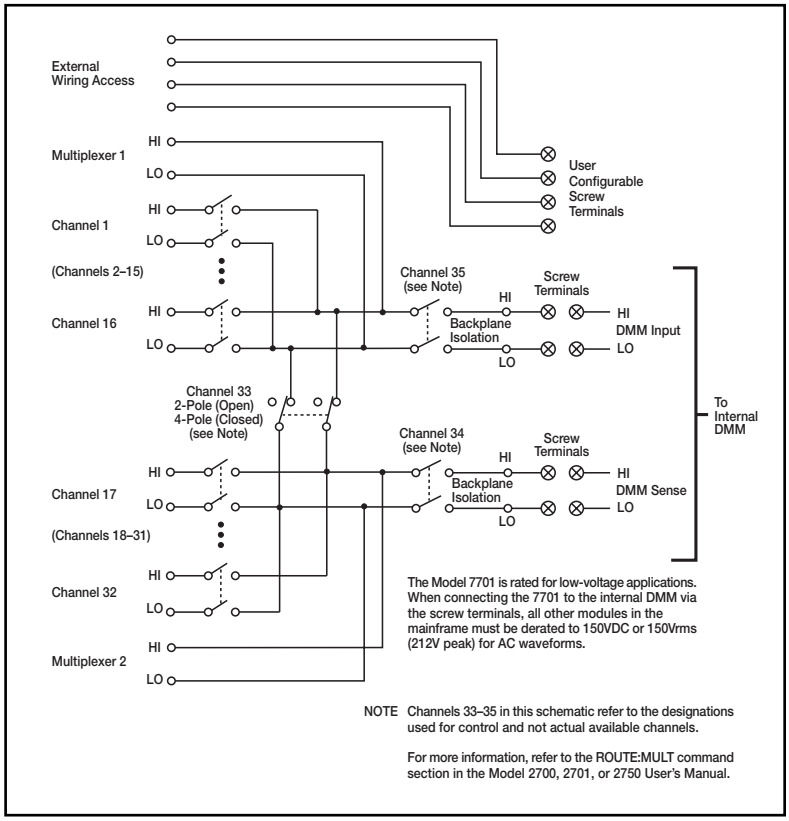

See page 43 for common-side 4-wire ohms configuration example.

Integra Series Modules

Multimeter/Switch Systems

7702 40-CHANNEL DIFFERENTIAL MULTIPLEXER

FEATURES

- There are 40 channels for general-purpose measurement, plus 2 channels to measure current.
- 2- or 4-wire measurement.
- Oversize screw terminal connection blocks are standard for easier connection.
- Configurable as two independent banks of multiplexers.
- 300V, 1A capacity for voltage channels; 60W, 125VA.
- 3A capacity for current channels.
- Relay closures stored in on-board memory.

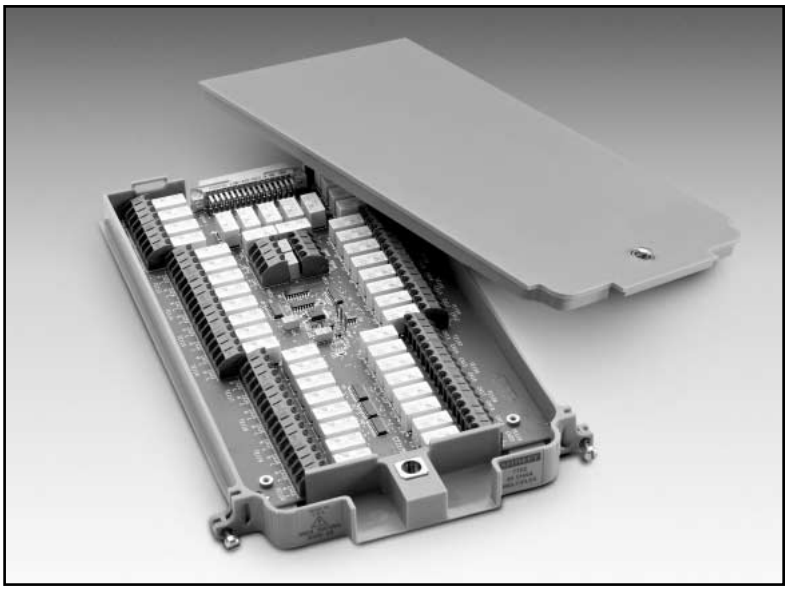

GENERAL

40 CHANNELS: 40 channels of 2-pole relay input.
All channels configurable to 4-pole.

2 CHANNELS: 2 channels of current only input.

RELAY TYPE: Latching electromechanical.

ACTUATION TIME: <3ms.

FIRMWARE: Specified for Model 2700 rev. A01, 2701 rev. A01, and 2750 rev. A01 or higher.

CAPABILITIES

CHANNELS 1-40: Multiplex one of 40 2-pole or one of 20 4-pole signals into DMM.

CHANNELS 41-42: Multiplex one of 2 2-pole current signals into DMM.

INPUTS

MAXIMUM SIGNAL LEVEL:

Channels (1-40): 300V DC or rms, 1A switched, 60W, 125VA maximum.

Channels (41-42): 60V DC or 30V rms, 3A switched, 60W, 125VA maximum.

CONTACT LIFE (typ): $>10^5$ operations at max signal level.
$>10^8$ operations cold switching.

CONTACT RESISTANCE: <1Ω at end of contact life.

CONTACT POTENTIAL: <±500nV typical per contact, 1μV max.
<±500nV typical per contact pair, 1μV max.

OFFSET CURRENT: <100pA.

CONNECTOR TYPE: Screw terminal, #20 AWG wire size.

ISOLATION BETWEEN ANY TWO TERMINALS: $>10^{10}\Omega$, <100pF.

ISOLATION BETWEEN ANY TERMINAL AND EARTH: $>10^9\Omega$, <200pF.

CROSS TALK (10MHz, 50Ω Load): <–40dB.

INSERTION LOSS (50Ω Source, 50Ω Load): <0.1dB below 1MHz.
<3dB below 2MHz.

COMMON MODE VOLTAGE: 300V between any terminal and chassis.

ENVIRONMENTAL

OPERATING ENVIRONMENT: Specified for 0°C to 50°C.
Specified to 80% R.H. at 35°C.

STORAGE ENVIRONMENT: –25°C to 65°C.

WEIGHT: 0.5kg (1.1 lb).

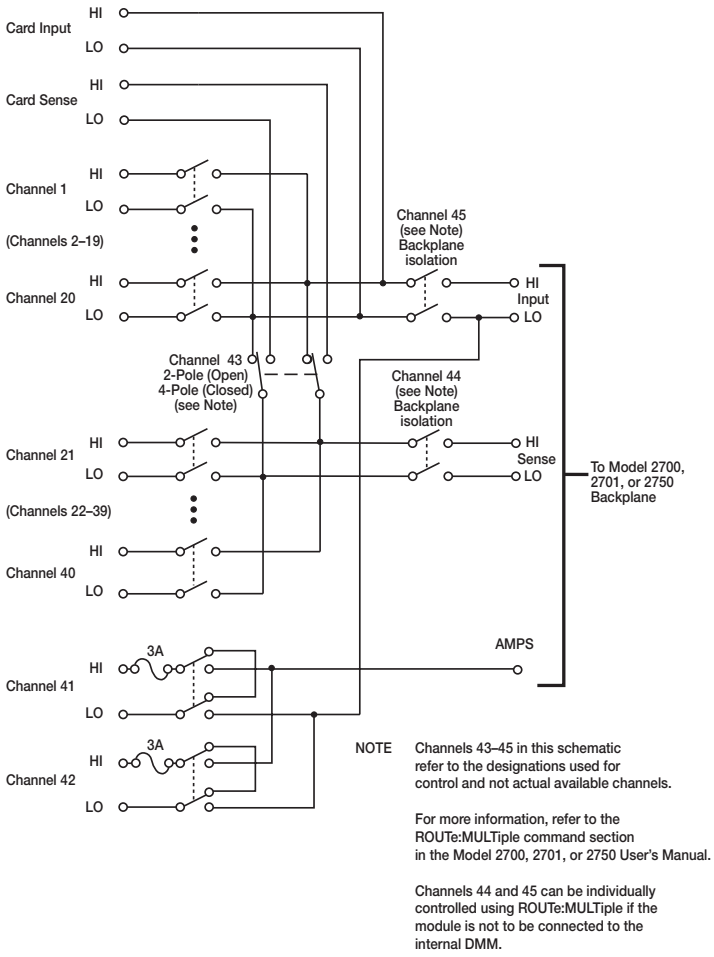

1.888.KEITHLEY (U.S. only)
www.keithley.com
KEITHLEY
A GREATER MEASURE OF CONFIDENCE

7703 32-CHANNEL HIGH SPEED DIFFERENTIAL MULTIPLEXER

FEATURES

- There are 32 channels for general purpose measurement.
- Relay actuation time of less than 1ms for high-speed scanning.
- 2 or 4 wire measurement.
- Two 50-pin female "D-sub" connectors are standard for secure hook-up and quick teardown.
- Configurable as two independent banks of multiplexers.
- Reed relay based design with 300 volt, 500mA; 10VA.
- Two mating connector with solder cup (Model 7788) are supplied.
- Relay closures stored in on-board memory.

GENERAL

32 CHANNELS: 32 channels of 2-pole relay input.
All channels configurable to 4-pole.

RELAY TYPE: Reed.

ACTUATION TIME: <1ms.

FIRMWARE: Specified for Model 2700 rev. A01, 2701 rev. A01, and 2750 rev. A01 or higher.

CAPABILITIES

CHANNELS 1-32: Multiplex one of 32 2-pole or one of 16 4-pole signals into DMM.

INPUTS

MAXIMUM SIGNAL LEVEL:

Channels (1-32): 300V DC or rms, 0.5A switched, 10W maximum.

Contact Life (typ): $>5\times10^4$ operations at max signal level.
$>10^8$ operations cold switching.

CONTACT RESISTANCE: <1Ω at end of contact life.

CONTACT POTENTIAL: <±3μV typical per contact, 6μV max.
<±3μV typical per contact pair, 6μV max.

OFFSET CURRENT: <100pA.

CONNECTOR TYPE: 50 pin D-sub×2.

RELAY DRIVE CURRENT: 20mA per channel.

ISOLATION BETWEEN ANY TWO TERMINALS: $>10^9\Omega$, <200pF.

ISOLATION BETWEEN ANY TERMINAL AND EARTH: $>10^9\Omega$, <400pF.

CROSS TALK (1 MHz, 50Ω Load): <–40dB.

INSERTION LOSS (50Ω Source, 50Ω Load): <0.35dB below 1MHz.
<3dB below 2MHz.

COMMON MODE VOLTAGE: 300V between any terminal and chassis.

ENVIRONMENTAL

OPERATING ENVIRONMENT: Specified for 0°C to 50°C.
Specified to 80% R.H. at 35°C.

STORAGE ENVIRONMENT: –25°C to 65°C.

WEIGHT: 0.8kg (1.75 lbs).

ACCESSORIES AVAILABLE:
Model 7705-MTC-2 50 Pin Male to Female DSUB Cable, 2m (6.6 ft).

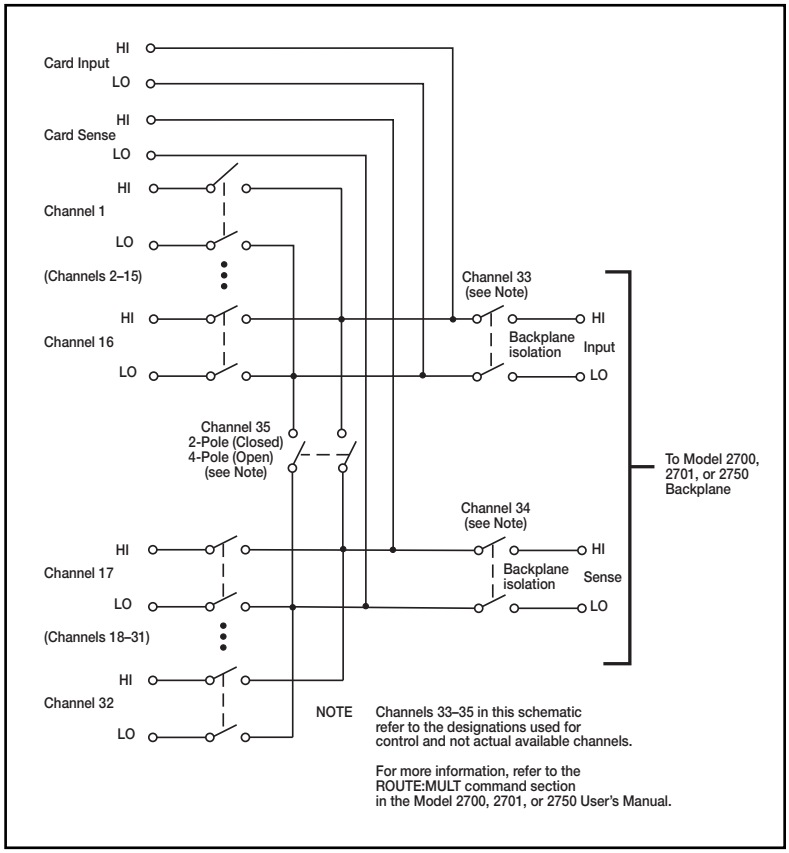

7705 40-CHANNEL CONTROL MODULE

FEATURES

- 40 channels designed for controlling power to the DUT, switching loads, controlling light indicators and relays, etc.
- Two 50-pin female "D-sub" connectors are standard for secure hook-up and quick teardown.
- 300V, 2A capacity.
- Two mating connectors with solder cup pins (Model 7788) are supplied.
- Relay closures stored in on-board memory.

GENERAL

RELAY SWITCH CONFIGURATION: 40 independent channels of 1-pole switching. Isolated from internal DMM.

CONTACT CONFIGURATION: 1 pole Form A.

RELAY TYPE: Latching electromechanical.

CONNECTOR TYPE: Two 50-pin female D-sub connectors.

FIRMWARE: Specified for Model 2700 rev. A01, 2701 rev. A01, and 2750 rev. A01 or higher.

INPUTS

MAXIMUM SIGNAL LEVEL: 300VDC or rms, 2A switched, 60W (DC, resistive), 125VA (AC, resistive).

CONTACT LIFE: **Cold Switching:** 10^8 closures.
At Maximum Signal Levels: 10^5 closures.

CHANNEL RESISTANCE (per conductor): <1Ω.

CONTACT POTENTIAL: ≤4μV per contact.

OFFSET CURRENT: <100pA.

ACTUATION TIME: 3ms.

ISOLATION: **Channel to Channel:** $>10^9\Omega$, <50pF.
Common Mode: $>10^9\Omega$, <100pF.

CROSSTALK (1MHz, 50Ω load): <–35dB.

INSERTION LOSS (50Ω source, 50Ω load): <0.3dB below 1MHz, <3dB below 10MHz.

COMMON MODE VOLTAGE: 300V between any terminal and chassis.

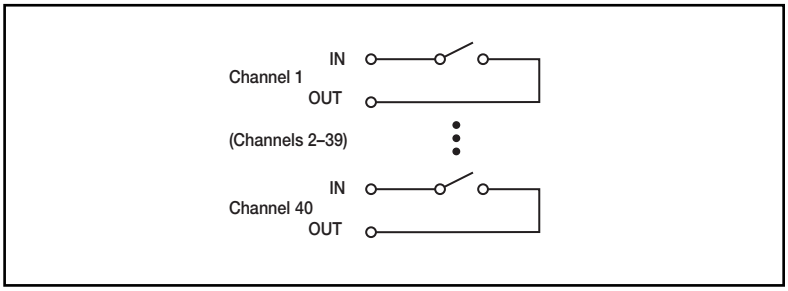

ENVIRONMENTAL

OPERATING ENVIRONMENT: Specified for 0°C to 50°C.
Specified to 80% R.H. at 35°C.

STORAGE ENVIRONMENT: –25°C to 65°C.

WEIGHT: 0.45kg (1 lb).

ACCESSORIES AVAILABLE:
Model 7705-MTC-2 50 Pin Male to Female DSUB Cable, 2m (6.6 ft).

1.888.KEITHLEY (U.S. only)
www.keithley.com
KEITHLEY
A GREATER MEASURE OF CONFIDENCE

7706 ALL-IN-ONE I/O MODULE

FEATURES

- 20 channels of analog input (w/automatic CJC) for general-purpose measurement.
- 16 channels of digital output.
- Event counter/totalizer can monitor and control system components, such as fixturing, limit switches, pass/fail indicators, external voltage sources, loads, door closures, revolutions, etc., while performing mixed signal measurement.
- 300V, 1A capacity; 60W, 125VA maximum.
- Configurable as two independent banks of multiplexers.
- Two analog outputs (±12V, 5mA).
- Relay closures stored in on-board memory.

GENERAL

20 CHANNELS: 20 channels of 2-pole relay input.
All channels configurable to 4-pole.

RELAY TYPE: Latching electromechanical.

ACTUATION TIME: <3ms.

FIRMWARE: Specified for Model 2700 rev. A02 or B01, 2701 rev. A01, and 2750 rev. A01 or higher.

CAPABILITIES

CHANNELS 1–20: Multiplex one of 20 2-pole or one of 10 4-pole signals into DMM.

Channels 21–25 are referenced to chassis ground.

CHANNELS 21–22: 16 Digital Outputs.

CHANNELS 23–24: Analog Voltage Output (2).

CHANNELS 25: Totalize Input.

INPUTS

MAXIMUM SIGNAL LEVEL (Channels 1–20): 300V DC or rms, 1A switched, 60W, 125VA maximum.

CONTACT LIFE (typ.): $>10^5$ operations at max. signal level: $>10^8$ operations cold switching.

CONTACT RESISTANCE: <1Ω at end of contact life.

CONTACT POTENTIAL: <±2μV typical per contact, 3μV max.

OFFSET CURRENT: <100pA.

CONNECTOR TYPE: Screw terminal, #20 AWG wire size.

ISOLATION BETWEEN ANY TWO TERMINALS: $>10^9$Ω, <100pF.

ISOLATION BETWEEN ANY TERMINAL AND EARTH: $> 10^9$Ω, <200pF.

CROSS TALK (10MHz, 50Ω Load): <–35dB.

INSERTION LOSS (50Ω Source, 50Ω Load): <0.1dB below 1MHz.
<3dB below 2Mhz.

COMMON MODE VOLTAGE: 300V between any terminal and chassis.

TEMPERATURE ACCURACY USING INTERNAL CJC: 1.0°C (see mainframe specification for details).

TOTALIZE INPUT

MAXIMUM COUNT: 2^{32}–1.

TOTALIZE INPUT: 100kHz (max), rising or falling edge, programmable.

SIGNAL LEVEL: 1Vp-p (min), 42Vpk (max).

THRESHOLD: 0V or TTL, jumper selectable.

DATE INPUT: TTL-Hi, TTL-Lo, or none.

COUNT RESET: manual or Read+Reset.

READ SPEED: 50/s.

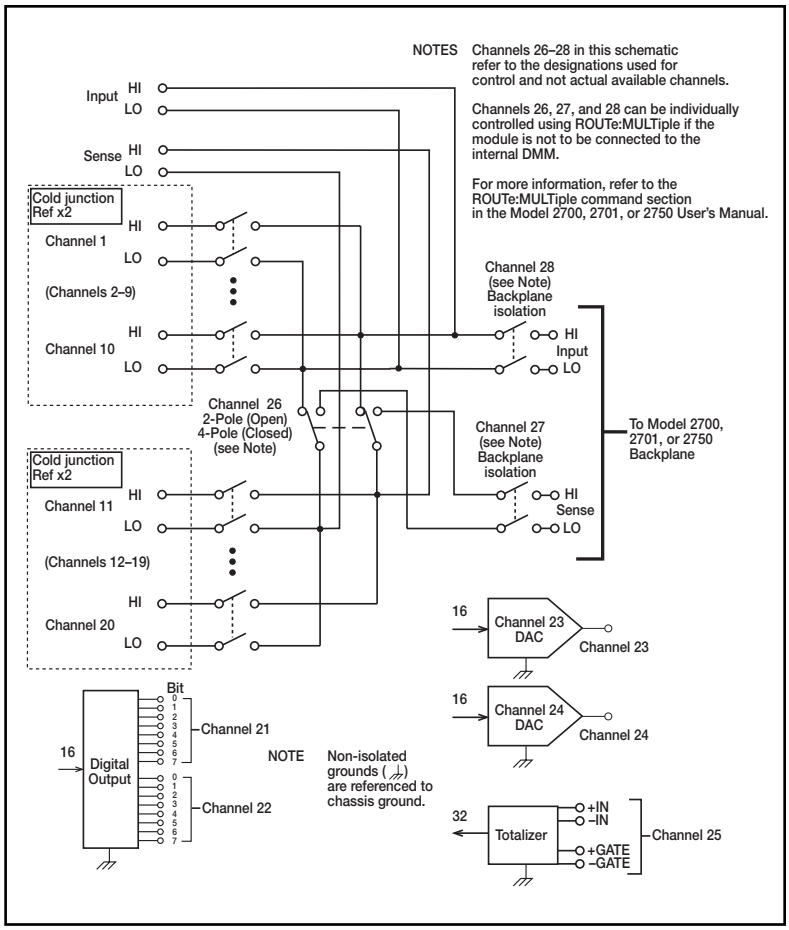

ANALOG VOLTAGE OUTPUT

DAC 1, 2: ±12V in 1mV increments, non-isolated.

RESOLUTION: 1mV.

I_{OUT}: 5mA max.

SETTLING TIME: 1ms to 0.01% of output.

ACCURACY ±(% of output + mV):
1 year ±5°C: 0.15% + 19mV;
90 day ±5°C: 0.1% + 19mV;
24 hour ±1°C: 0.04% + 19mV.

TEMPERATURE COEFFICIENT:
±(0.015% + 1mV)/°C.

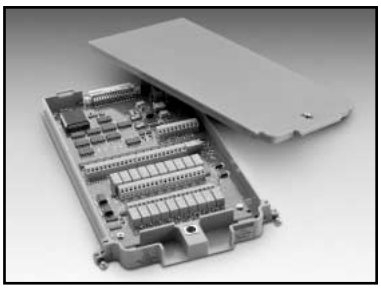

DIGITAL OUTPUT

V_{OUT}(L): <0.8V @ Iout = 400mA.

V_{OUT}(H): >2.4V @ Iout = 1mA.

V_{OUT}(H)MAX.: <42V with external open drain pull-up.

WRITE SPEED: 50/s.

ENVIRONMENTAL

OPERATING ENVIRONMENT: Specified for 0°C to 50°C.
Specified to 80% R.H. at 35°C.

STORAGE ENVIRONMENT: –25°C to 65°C.

WEIGHT: 0.5kg (1.1 lbs).

7707 MULTIPLEXER-DIGITAL I/O MODULE

GENERAL

10 CHANNELS: 10 channels of 2-pole relay input.
All channels configurable to 4-pole.

RELAY TYPE: Latching electromechanical.

ACTUATION TIME: <3ms.

FIRMWARE: Specified for Model 2700 rev. B03, 2701 rev. A01, and 2750 rev. A01 or higher.

CAPACITY: **Model 2700:** (1) 7707 and (1) 77XX, except 7706.
Model 2701: Any combination of 77XX modules.
Model 2750: (4) 7707 and (1) 77XX, except 7706. A 7706 module may be substituted for a 7707 module.

CAPABILITIES

CHANNELS 1–10: Multiplex one of 10 2-pole or one of 5 4-pole signals into DMM.

CHANNELS 11–14: 32 Digital Inputs/Outputs referenced to chassis ground.

THERMAL PROTECTION: Channels 11–14 are thermally protected to 1A.

INPUTS (CHANNELS 1–10)

MAXIMUM SIGNAL LEVEL: Any Channel to Any Channel (1–10): 300VDC or 300Vrms (425V peak) for AC waveforms, 1A switched, 60W, 125VA maximum.

SAFETY CATEGORY: Conforms to European Union Directive 73/23/EEC EN 61010-1, CAT I.

CONTACT LIFE (typ.): $>10^5$ operations at max. signal level: $>10^8$ operations cold switching.

CONTACT RESISTANCE: <1Ω any path and additional 1Ω at end of contact life.

CONTACT POTENTIAL: <6μV typical per contact pair and additional 5μV with Channels 11–14 at rate $V_{OUT}(L)$.

OFFSET CURRENT: <100pA.

CONNECTOR TYPE: 50-pin male D-shell, Channels 11–14.
25-pin female D-shell, Channels 1–10.
Supplied with female and male IDC ribbon cable connectors.

ISOLATION BETWEEN ANY TWO TERMINALS: $>10^9$Ω, <100pF with isolation channels 16 and 17 open.

ISOLATION BETWEEN ANY TERMINAL AND EARTH: $> 10^9$Ω, <200pF.

CROSS TALK (10MHz, 50Ω Load): <–35dB.

INSERTION LOSS (50Ω Source, 50Ω Load): <0.1dB below 1MHz.
<3dB below 2MHz.

COMMON MODE VOLTAGE: 300VDC or 300Vrms (425V peak) for AC waveforms between any terminal and chassis.

DIGITAL INPUT/OUTPUT (CHANNELS 11–14)

$V_{IN}(L)$: <0.8V (TTL).

$V_{IN}(H)$: >2V (TTL).

$V_{OUT}(L)$: <1.0V @ I_{OUT} = 100mA.

$V_{OUT}(H)$: >2.4V @ I_{OUT} = 1mA.

$V_{OUT}(H)$MAX.: <40V with external open drain pull-up.

READ/WRITE SPEED: 50/s.

ENVIRONMENTAL

OPERATING ENVIRONMENT: Specified for 0°C to 50°C.
Specified to 50% R.H. at 35°C.

STORAGE ENVIRONMENT: –25°C to 65°C.

WEIGHT: <0.5kg (1.1 lbs).

ACCESSORIES AVAILABLE:

Model 7790	50/50/25 Pin Female/Male D-Shell IDC Connectors
Model 7705-MTC-2	50 Pin Male to Female DSUB Cable, 2m (6.6 ft).
Model 7707-MTC-2	25 Pin Male to Female DSUB Cable, 2m (6.6 ft).

FEATURES

- 10 channels of analog input for general-purpose measurement.
- 32 channels of digital input and output (four 8-bit ports) for I/O control.
- 300V, 1A capacity; 60W, 125VA maximum (analog).
- Configurable as two independent banks of multiplexers.
- 33V, 100mA capacity (digital).
- Two mating IDC connectors supplied.
- Digital outputs are short circuit protected.
- Relay closures stored in on-board memory.

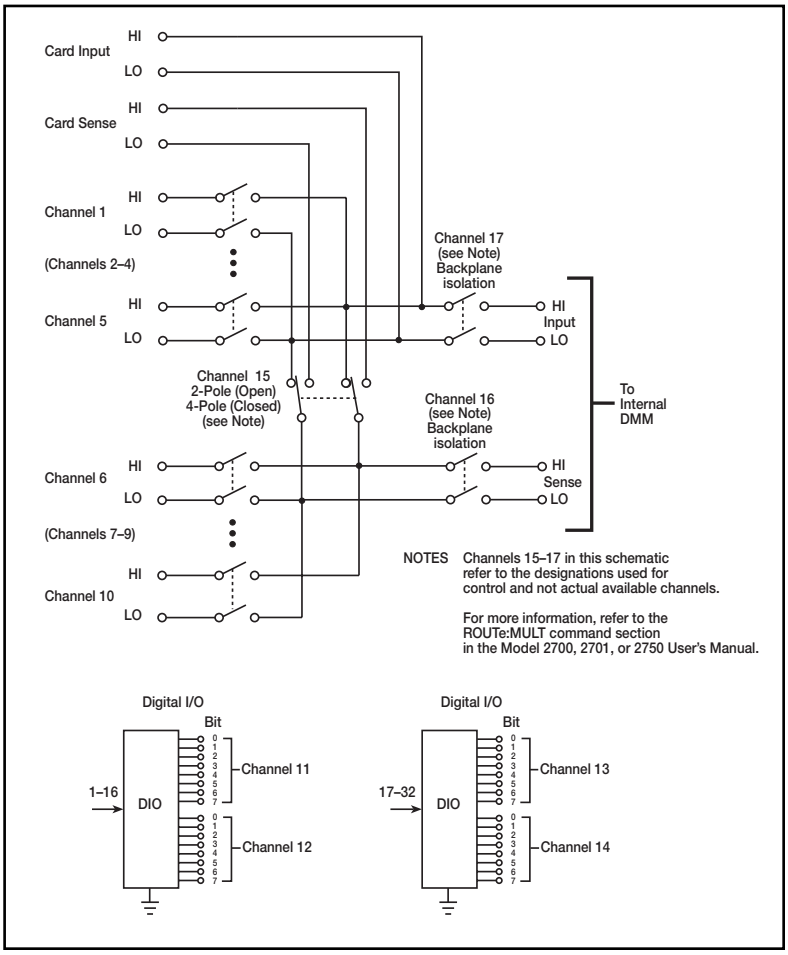

1.888.KEITHLEY (U.S. only)
www.keithley.com
KEITHLEY
A GREATER MEASURE OF CONFIDENCE

7708 40-CHANNEL DIFFERENTIAL MULTIPLEXER MODULE

FEATURES

- 40 differential channels for general-purpose measurements.
- 2- or 4-wire measurements.
- Oversize screw terminal connection blocks are standard for easier connection.
- 300V, 1A capacity for voltage channels; 60W, 125VA.
- Configurable as two independent banks of multiplexers.
- Built-in CJC sensors automatically linearize thermocouples.
- Relay closures stored in on-board memory.

GENERAL

40 CHANNELS: 40 channels of 2-pole relay input. All channels configurable to 4-pole.

RELAY TYPE: Latching electromechanical.

ACTUATION TIME: <3ms.

FIRMWARE: Specified for Model 2700 rev. B02, 2701 rev. A01, and 2750 rev. A01 or higher.

CAPABILITIES

CHANNELS 1–40: Multiplex one of 40 2-pole or one of 20 4-pole signals into DMM.

INPUTS

MAXIMUM SIGNAL LEVEL:

Channels (1–40): 300V DC or rms, 1A switched, 60W, 125VA maximum.

CONTACT LIFE (typ): $>10^5$ operations at max. signal level.
$>10^8$ operations cold switching.

CONTACT RESISTANCE: <1Ω at end of contact life.

CONTACT POTENTIAL: <±500nV typical per contact, 1μV max.
<±500nV typical per contact pair, 1μV max.

OFFSET CURRENT: <100pA.

CONNECTOR TYPE: Screw terminal, #20 AWG wire size.

ISOLATION BETWEEN ANY TWO TERMINALS: $>10^{10}$Ω, <100pF.

ISOLATION BETWEEN ANY TERMINAL AND EARTH: $>10^9$Ω, <200pF.

CROSS TALK (10MHz, 50Ω Load): <–40dB.

INSERTION LOSS (50Ω Source, 50Ω Load): <0.1dB below 1MHz.
<3dB below 2MHz.

COMMON MODE VOLTAGE: 300V between any terminal and chassis.

TEMPERATURE ACCURACY USING INTERNAL CJC: 1.0°C (see mainframe specification for details).

ENVIRONMENTAL:

OPERATING ENVIRONMENT: Specified for 0°C to 50°C.
Specified to 80% R.H. at 35°C.

STORAGE ENVIRONMENT: –25°C to 65°C.

WEIGHT: 0.52kg (1.16 lb).

ACCESSORIES AVAILABLE:
Model 7401 Type K Thermocouple Wire, 30.5m (100 ft).

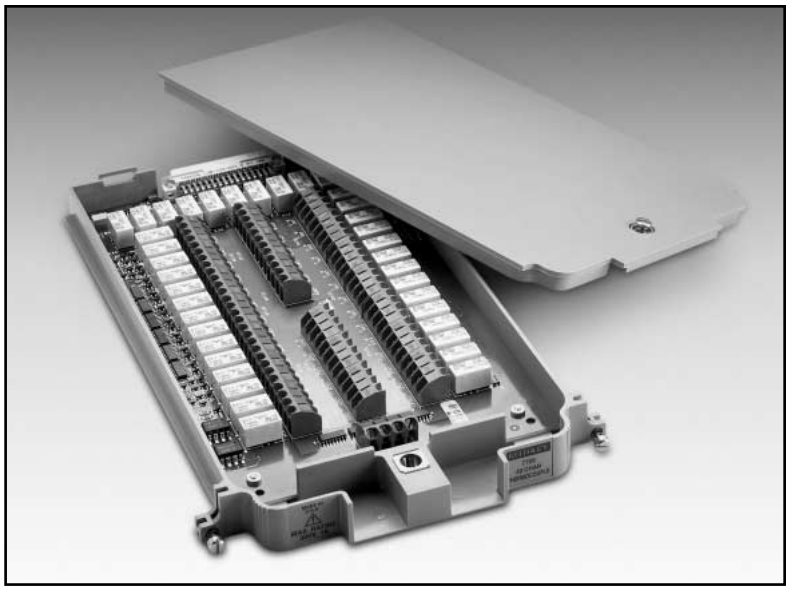

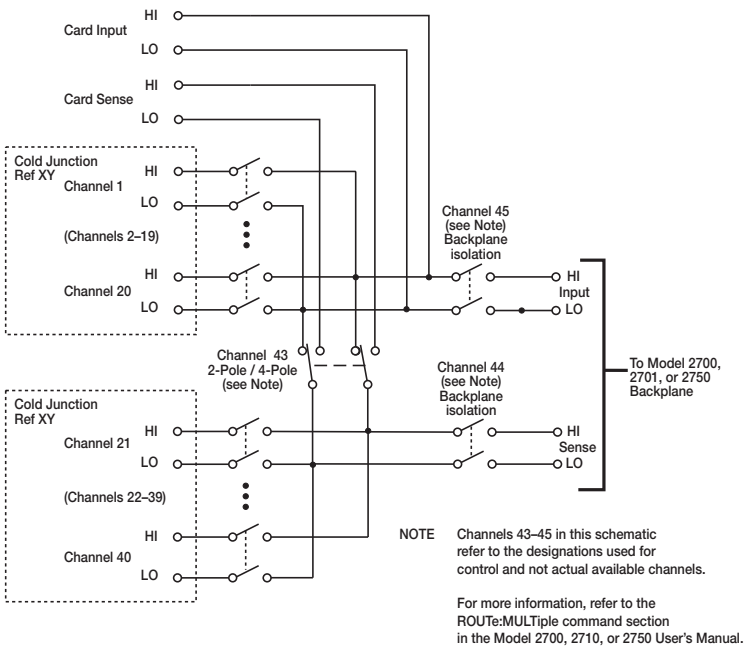

Integra Series Modules

Multimeter/Switch Systems

7709 6×8 MATRIX MODULE

FEATURES

- Automatic 2- or 4-wire connection to DMM
- 6 row×8 column matrix
- Two female "D-sub" connectors are standard for secure hook-up and quick teardown.
- 300V, 1A capacity.
- Two mating IDC connectors for ribbon cable are supplied.
- Relay closures stored in on-board memory.

GENERAL

MATRIX CONFIGURATION: 6 rows × 8 columns.

CONTACT CONFIGURATION: 2 pole Form A.

FIRMWARE: Specified for Model 2700 rev. B03, Model 2701 rev. A01, and Model 2750 rev. A01 or higher.

RELAY TYPE: Latching electromechanical.

ACTUATION TIME: <3ms.

CAPABILITIES

DMM CONNECTION:

2-Wire Functions

Row 1, channels 1–8, through channel 50.

4-Wire Functions

Row 1, channels 1–4 (Source) through channel 50 and Row 2, channels 13–16 (Sense), through channel 49.

CLOSE CHANNEL: CLOSE command connects channels 1–8 to DMM. For 4-wire, channels 1–4 are automatically paired with channels 13–16. ROUTe:MULTiple allows any combination of rows and columns to be connected at the same time.

INPUTS

MAXIMUM SIGNAL LEVEL: Any Channel to Any Channel (1–48): 300VDC or 300Vrms (425V peak) for AC waveforms, 1A switched, 60W, 125VA maximum.

SAFETY: Conforms to European Union Directive 73/23/EEC EN61010-1, CAT I.

CONTACT LIFE (typ): $>10^5$ operations at max signal level.
$>10^8$ operations cold switching.

CONTACT RESISTANCE: <1Ω any path and additional 1Ω at end of contact life.

CONTACT POTENTIAL: <3μV per contact pair.

OFFSET CURRENT: <100pA.

CONNECTOR TYPE: 50-pin female D-shell for rows and columns.
25-pin female D-shell for "daisy-chain" rows.
Supplied with male IDC ribbon cable connectors.

ISOLATION BETWEEN ANY TWO TERMINALS: $>10^9$Ω, <200pF.

ISOLATION BETWEEN ANY TERMINAL AND EARTH: $>10^9$Ω, <400pF.

CROSS TALK (1MHz, 50Ω Load): <–35dB.

INSERTION LOSS (50Ω Source, 50Ω Load): <0.35dB below 1MHz.
<3dB below 2MHz.

COMMON MODE VOLTAGE: 300VDC or 300Vrms (425V peak) for AC waveforms between any terminal and chassis.

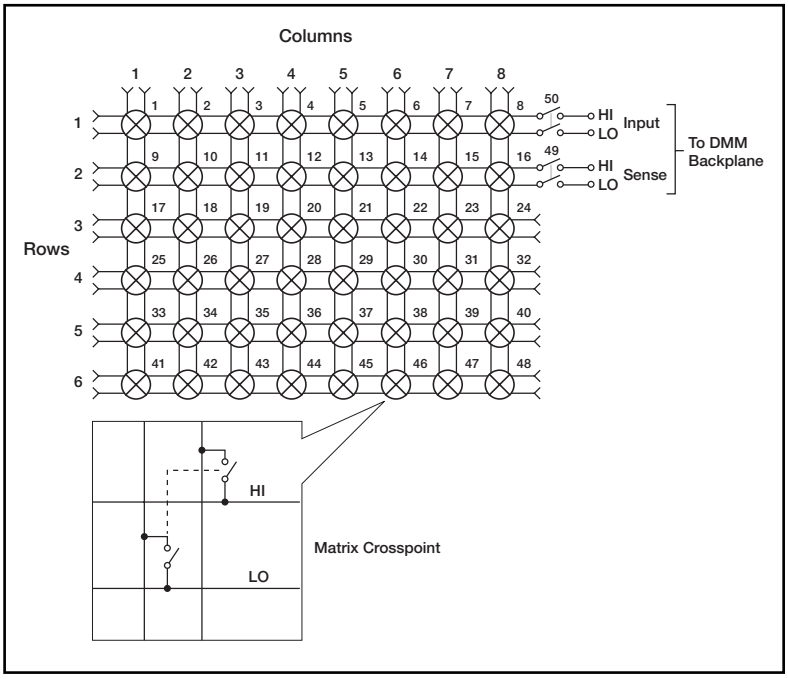

ENVIRONMENTAL:

OPERATING ENVIRONMENT: Specified for 0°C to 50°C.
Specified to 50% R.H. at 35°C.

STORAGE ENVIRONMENT: –25°C to 65°C.

WEIGHT: <0.52kg (1.16 lb).

ACCESSORIES AVAILABLE:

Model 7789	50/25 Pin Male D-Shell Solder Cup Connectors
Model 7790	50/50/25 Pin Female/Male D-Shell IDC Connectors
Model 7705-MTC-2	50 Pin Male to Female DSUB Cable, 2m (6.6 ft).
Model 7707-MTC-2	25 Pin Male to Female DSUB Cable, 2m (6.6 ft).

1.888.KEITHLEY (U.S. only)
www.keithley.com
KEITHLEY
A GREATER MEASURE OF CONFIDENCE

7710 20-CHANNEL SOLID STATE/LONG-LIFE DIFFERENTIAL MULTIPLEXER W/AUTOMATIC CJC

FEATURES

- Solid-state relays for long life and low maintenance (100 times longer life than mechanical relays)
- Higher scanning speeds of up to 500 channels per second
- Automatic CJC with no extra accessories required for thermocouple measurements
- Removable screw terminals offer simple, quick connections
- 20 channels for general purpose measurements
- Configurable as two independent banks of multiplexers

GENERAL

CHANNELS: 20 channels of 2-pole relay input. All channels configurable to 4-pole.

RELAY TYPE: Solid State Opto-Coupled FET.

ACTUATION TIME: <0.5ms (100mA load).

FIRMWARE: Specified for Model 2700 Rev. B05, Model 2750 Rev. A04, and Model 2701 Rev. A01.

CAPABILITIES

CHANNELS 1–20: Multiplex one of 20 2-pole or one of 10 4-pole signals into DMM.

INPUTS

MAXIMUM SIGNAL LEVEL: Any channel to any channel (1–20): 60VDC or 42V rms, 100mA switched, 6W, 4.2VA maximum.

COMMON MODE VOLTAGE: 300VDC or 300Vrms (425V peak) maximum between any terminal and chassis.

RELAY LIFE (TYP): $>10^5$ operational hours max. signal level or 10^{10} operations (guaranteed by design).

RELAY DRIVE CURRENT: 6mA per channel continuous, 25mA during initial pulse.

CHANNEL RESISTANCE (per conductor): <5Ω.

CONTACT POTENTIAL: <1μV per pair.

OFFSET CURRENT: <3nA @ 23°C (per channel); additional 0.13nA/°C >23°C.

CONNECTOR TYPE: 3.5mm removable screw terminals, #20 AWG wire size.

ISOLATION BETWEEN ANY TWO TERMINALS: $>10^9$Ω, <100pF.

ISOLATION BETWEEN ANY TERMINAL AND EARTH: $>10^9$Ω, <100pF.

CROSSTALK (CH-CH, 300kHz, 50Ω Load) : <–40dB.

INSERTION LOSS (50Ω Source, 50Ω Load): <0.5dB below 100kHz, <3dB below 2MHz.

TEMPERATURE ACCURACY USING INTERNAL CJC: 1°C (Type K) (see mainframe specifications for details).

SCANNING SPEEDS (see mainframe specifications for details)

Multiple Channels, Into Memory

	Channels/s		
	2700	2701	2750
7710 Scanning DCV	180/s	500/s	230/s
7710 Scanning DCV with Limits or Time Stamp On	170/s	500/s	230/s
7710 Scanning DCV alternating 2WΩ	45/s	130/s	60/s

Multiple Channels, Into and Out of Memory to GPIB or Ethernet

	Channels/s		
	2700	2701	2750
7710 Scanning DCV	145/s	440/s	210/s
7710 Scanning DCV with Limits or Time Stamp On	145/s	440/s	210/s
7710 Scanning DCV alternating 2WΩ	40/s	130/s	55/s

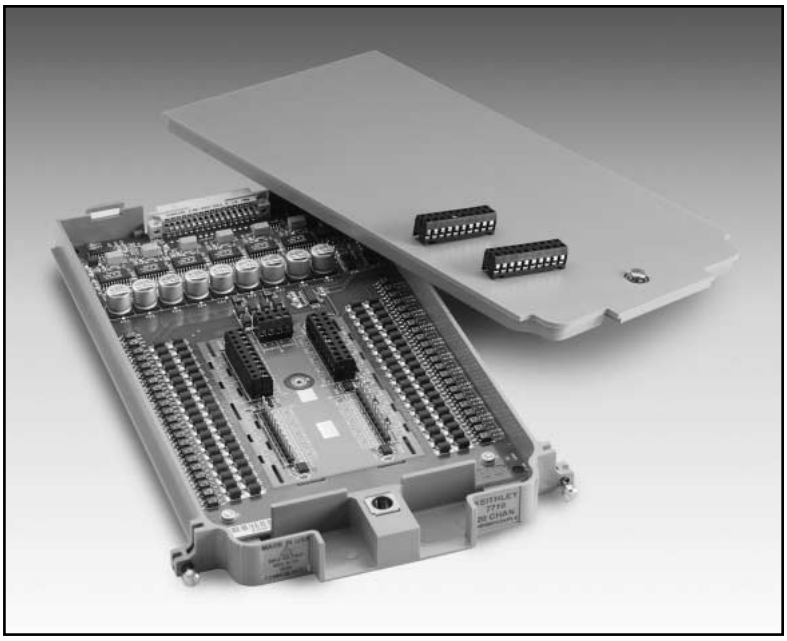

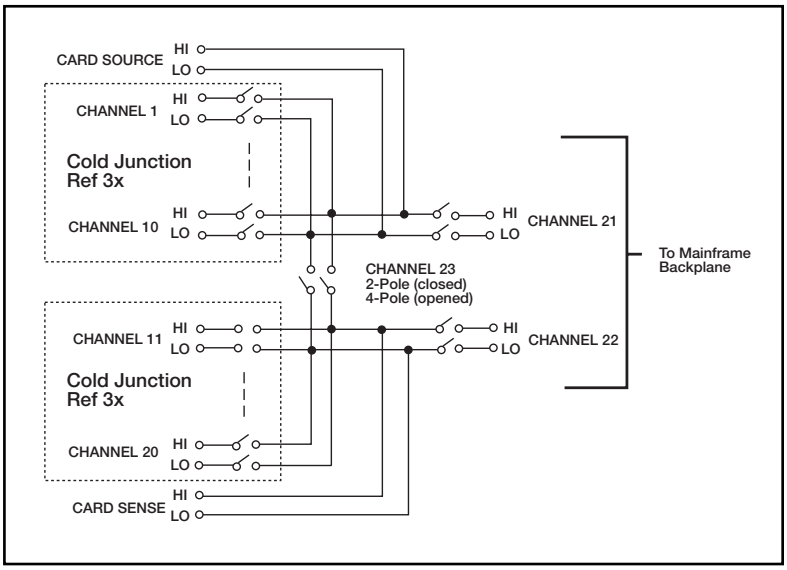

ENVIRONMENTAL

OPERATING ENVIRONMENT: Specified for 0°C to 50°C. Specified for 80% R.H. at 35°C.

STORAGE ENVIRONMENT: –25° to 65°C.

WEIGHT: 0.45kg (1 lb).

ACCESSORIES AVAILABLE: Model 7401 Type K Thermocouple Wire, 30.5m (100 ft).

Integra Series
Modules

Multimeter/Switch Systems

7711 2GHz 50Ω RF MODULE

FEATURES

- Outstanding signal routing performance to 2GHz
- Dual 1×4 configuration
- Rear panel connections
- On-board switch closure counter
- On-board S-parameter storage
- Switch up to 60VDC

AC PERFORMANCE (End of Life)

For $Z_{load} = Z_{source} = 50\Omega$

	<100 MHz	500 MHz	1 GHz	1.5 GHz	2 GHz
Insertion Loss Max.	<0.4 dB	<0.6 dB	<1.0 dB	<1.2 dB	<2.0 dB
VSWR Max.	<1.1	<1.2	<1.2	<1.3	<1.7 [2]
Ch-Ch Crosstalk[1] Max.	–85 dB	–65 dB	–55 dB	–45 dB	–35 dB

[1] Specification assumes 50Ω termination.
[2] Add 0.1VSWR after 5×10^5 closures (no load).

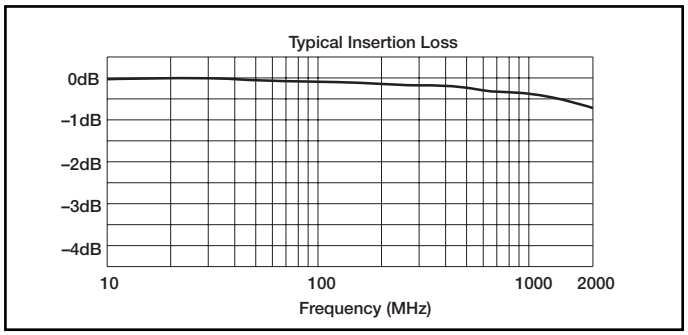

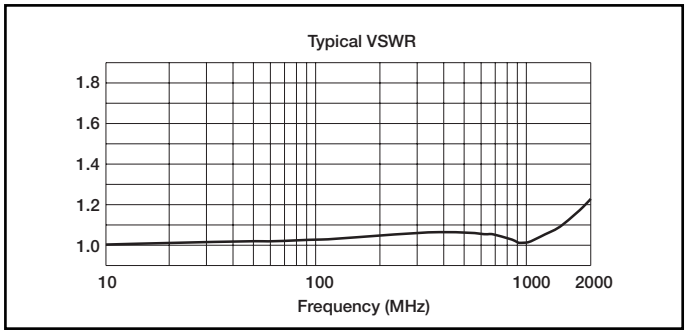

INPUTS (CHANNELS 1-8)

MAXIMUM SIGNAL LEVEL: Any channel to any channel or chassis (1–8): 30Vrms (42V peak for AC waveforms) or 60VDC, 0.5A.

MAXIMUM POWER: 20W per module, 10W per channel (refer to 7711/7712 Manual PA-818 for measurement considerations).

SAFETY: Conforms to European Union Directive 73/23/EEC EN61010-1, CAT I.

EMC: Conforms with European Union Directive 89/336/EEC; EN61326-1.

ISOLATION: **Multiplexer to Multiplexer:** >1GΩ.
Center to Shield: >1GΩ, <25pF.
Channel to Channel: >100MΩ.

CONTACT LIFE: 1×10^6 no load, 1×10^5 rated load (resistive load).

CONTACT POTENTIAL: <6μV.

CONTACT RESISTANCE: <0.5Ω (initial), <1Ω (end of life).

RISE TIME: <300ps (guaranteed by design).

SIGNAL DELAY: <3ns.

GENERAL

RELAY TYPE: High frequency electromechanical.

CONTACT CONFIGURATION: Dual 1×4 multiplexer, single pole four throw, Channels 1 and 5 are normally closed.

NOTES: One channel in each multiplex bank is always closed to the corresponding OUT connector.

CLOSE CHANNEL: ROUTe:CLOSe allows a single channel in a multiplex bank to be closed. ROUTe:MULTiple:CLOSe allows two channels (one in each bank) to be closed at one time.

OPEN CHANNEL: ROUTe:OPEN:ALL closes CH1 and CH5 to OUT A and OUT B respectively.

ACTUATION TIME: <10ms.

FIRMWARE: Specified for Model 2700 rev. B04, 2701 rev. A01, and 2750 rev. A03 or higher.

CONNECTOR TYPE: Ten external rear panel SMA connectors.

MATING TORQUE: 0.9 N·m (8 in-lb).

ENVIRONMENTAL

OPERATING ENVIRONMENT: Specified for 0°C to 50°C. Specified for 80% RH at 35°C.

STORAGE ENVIRONMENT: –25°C to 65°C.

WEIGHT: <0.5kg (1.1 lb).

ACCESSORIES AVAILABLE

7051-2	BNC Cable, male to male, 0.6m (2 ft.)
7051-5	BNC Cable, male to male, 1.5m (5 ft.)
7051-10	BNC Cable, male to male, 3.0m (10 ft.)
7711-BNC-SMA	Male SMA to female BNC Cables (5), 0.15m (0.5 ft)
7712-SMA-1	SMA Cable, male to male, 1m (3.3 ft)
7712-SMA-N	Female SMA to Male N-Type Adapter
S46-SMA-0.5	SMA Cable, male to male, 0.15m (0.5 ft.)
S46-SMA-1	SMA Cable, male to male, 0.3m (1 ft.)

1.888.KEITHLEY (U.S. only)
www.keithley.com

KEITHLEY
A GREATER MEASURE OF CONFIDENCE

7712 3.5GHz 50Ω RF MODULE

FEATURES

- 3.5GHz bandwidth
- Dual 1×4 configuration
- Rear panel SMA connections
- On-board switch closure counter
- On-board S-parameter storage

AC PERFORMANCE (End of Life)

For $Z_{load} = Z_{source} = 50\Omega$

	<500 MHz	1 GHz	2.4 GHz	3.5 GHz
Insertion Loss MAX	<0.5 dB	<0.65 dB	<1.1 dB	<1.3 dB
VSWR MAX	<1.15	<1.2	<1.45[2]	<1.45
Ch-Ch Crosstalk[1] MAX	–75 dB	–70 dB	–50 dB	–45 dB

[1] Specification assumes 50Ω termination.
[2] Add 0.1VSWR after 5×10^5 closures (no load).

INPUTS (CHANNELS 1-8)

MAXIMUM SIGNAL LEVEL: Any channel to any channel or chassis (1–8): 30Vrms (42V peak for AC waveforms) or 42VDC, 0.5A.

MAXIMUM POWER: 20W per module, 10W per channel (refer to 7711/7712 Manual PA-818 for measurement considerations).

SAFETY: Conforms to European Union Directive 73/23/EEC EN61010-1, CAT I.

EMC: Conforms with European Union Directive 89/336/EEC; EN61326-1.

ISOLATION: **Multiplexer to Multiplexer:** >1GΩ.
Center to Shield: >1GΩ, <20pF.
Channel to Channel: >100MΩ.

CONTACT LIFE: 5×10^6 no load, 1×10^5 rated load (resistive load).

CONTACT POTENTIAL: <12μV.

CONTACT RESISTANCE: <0.5Ω (initial), <1Ω (end of life).

RISE TIME: <200ps (guaranteed by design).

SIGNAL DELAY: <1.5ns.

GENERAL

RELAY TYPE: High frequency electromechanical.

CONTACT CONFIGURATION: Dual 1×4 multiplexer, single pole four throw, Channels 1 and 5 are normally closed.

NOTES: One channel in each multiplex bank is always closed to the corresponding OUT connector.

CLOSE CHANNEL: ROUTe:CLOSe allows a single channel in a multiplex bank to be closed. ROUTe:MULTiple:CLOSe allows two channels (one in each bank) to be closed at one time.

OPEN CHANNEL: ROUTe:OPEN:ALL closes CH1 and CH5 to OUT A and OUT B respectively.

ACTUATION TIME: <10ms.

FIRMWARE: Specified for Model 2700 rev. B04, 2701 rev. A01, and 2750 rev. A03 or higher.

CONNECTOR TYPE: Ten external rear panel SMA connectors.

MATING TORQUE: 0.9 N·m (8 in-lb).

ENVIRONMENTAL

OPERATING ENVIRONMENT: Specified for 0°C to 50°C. Specified for 80% RH at 35°C.

STORAGE ENVIRONMENT: –25°C to 65°C.

WEIGHT: <0.5kg (1.1 lb).

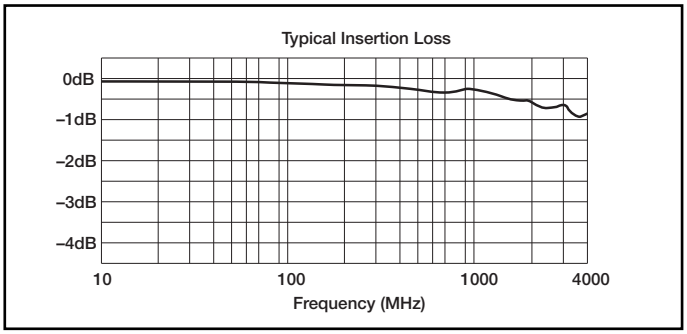

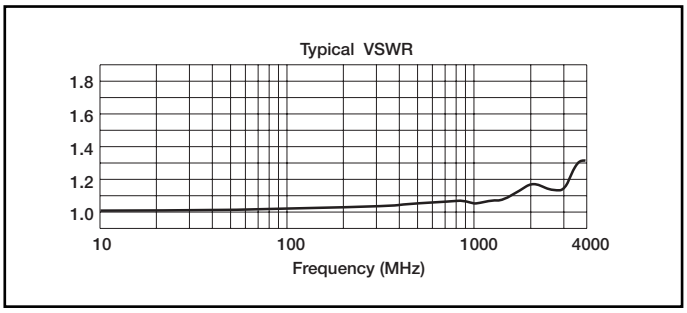

ACCESSORIES AVAILABLE

7712-SMA-1	SMA Cable, male to male, 1m (3.3 ft)
7712-SMA-N	Female SMA to Male N-Type Adapter
S46-SMA-0.5	SMA Cable, male to male, 0.15m (0.5 ft.)
S46-SMA-1	SMA Cable, male to male, 0.3m (1 ft.)

Integra Series Multimeter/Switch Systems

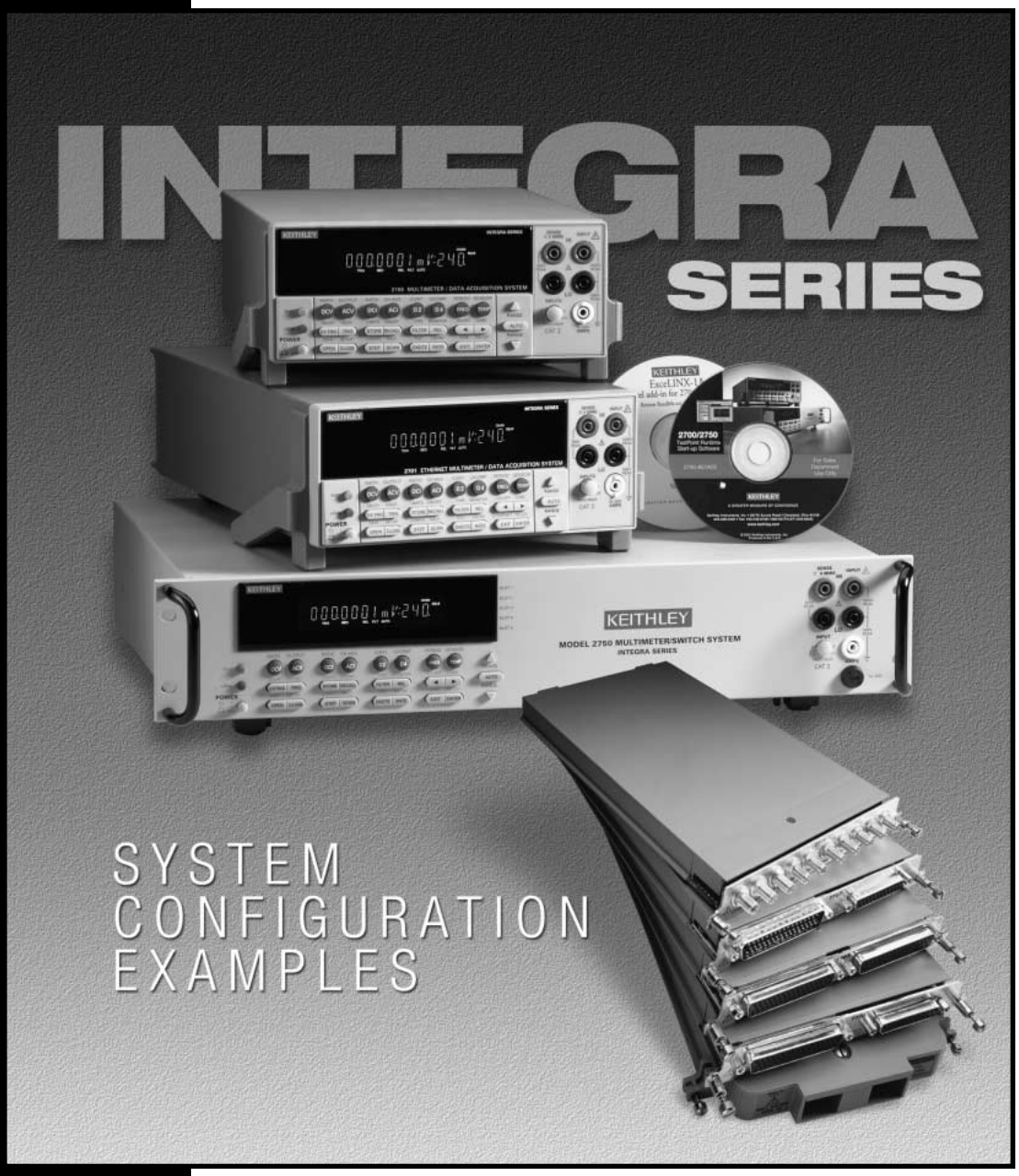

1.888.KEITHLEY (U.S. only)
www.keithley.com

KEITHLEY
A GREATER MEASURE OF CONFIDENCE

Simple Computer to Single Instrument Control

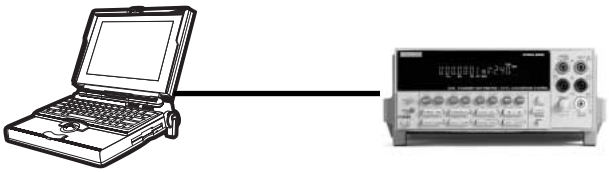

Interface	Maximum Distance	Maximum Speed	Cable Type
RS-232	~15 m†	115.2 kb/s (2701) 19.2 kb/s (2700, 2750)	Null modem cable Keithley Model 7009-5
GPIB	2 m	1 MB/s	Standard GPIB cable Keithley Model 7007-*
Ethernet	Hardwired: 100 m Wireless: >16 km	100 Mb/s	RJ-45 crossover cable

† RS-232 maximum distance is heavily dependent on the baud rate setting. Very slow baud rates can be operated at distances longer than 15m, while faster baud rates may require cables shorter than 15m.

Single Computer to Multiple Instruments

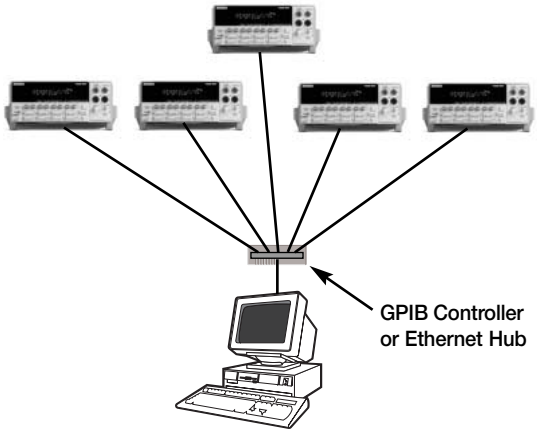

Interface	Maximum No. of Instruments	Maximum Distance	Maximum Speed	Cable Type
GPIB	14 per controller	2m per cable 20m per controller	1 MB/s	Standard GPIB cable Keithley Model 7007-*
Ethernet	∞	Hardwired: 100m per cable Wireless: >16 km	100 Mb/s	Standard RJ-45 straight-through cable

Multiple Computers to Multiple Instruments–Ethernet Only

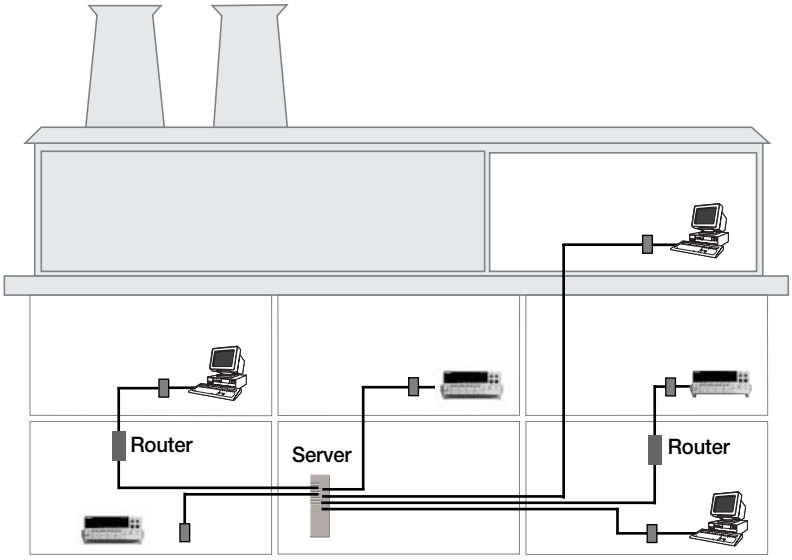

Call or visit www.keithley.com for Technical Note #2393, "Network Primer and Programming Tutorial for the Model 2701 Ethernet-Based DMM/Data Acquisition System." This document explains the basic principles for using instruments over a network and programming methods for Ethernet.

Thermocouple Configuration Example Using Internal CJC

Thermocouple connections

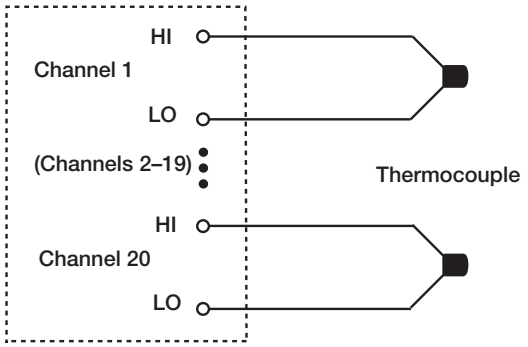

NOTE: The red lead is the LO signal on all thermocouples. This applies to U.S. standards.

Thermocouple Configuration Example Using External CJC

Thermocouple connections

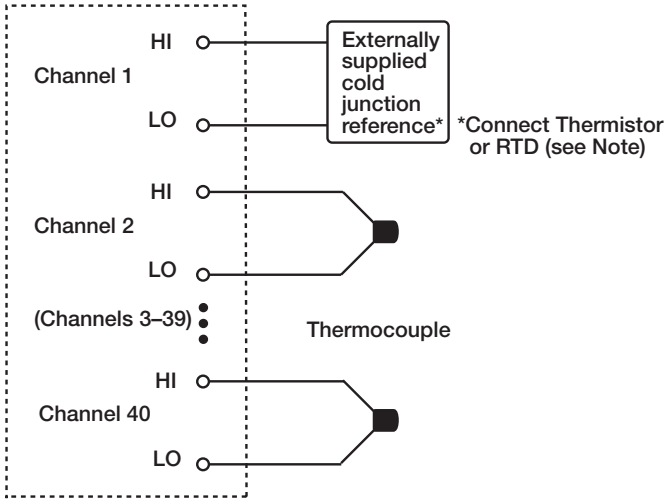

NOTE: If an RTD is connected as the cold junction reference, Channel 21 will be used for the sense leads of the RTD and is not available for connection of a thermocouple.

NOTE: The red lead is the LO signal on all thermocouples.

7708 Configuration Examples

Dual multiplexer mode example #1

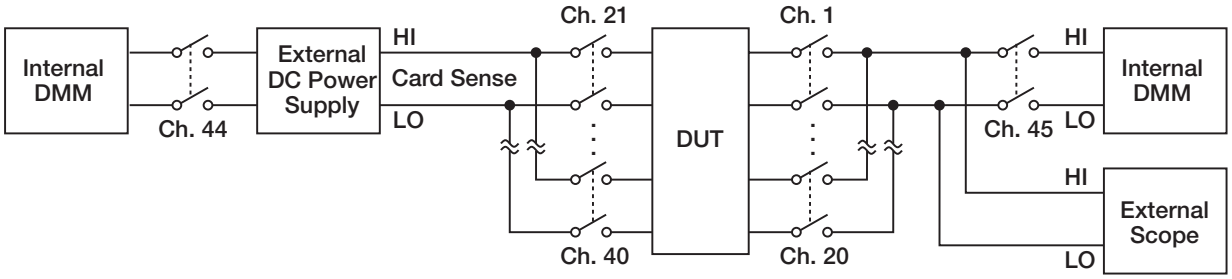

See Model 7708 specifications.

Channel 43 .....Closed
Channel 44 .....Open
Channel 45 .....Closed for DMM measure

NOTE: This configuration example can be duplicated with the 7700, 7701, 7702, 7703, 7706, 7707, and 7708 modules. See module specifications for their channel configurations.

1.888.KEITHLEY (U.S. only)
www.keithley.com
KEITHLEY
A GREATER MEASURE OF CONFIDENCE

7708 Configuration Examples (continued)

Using internal DMM and external instruments

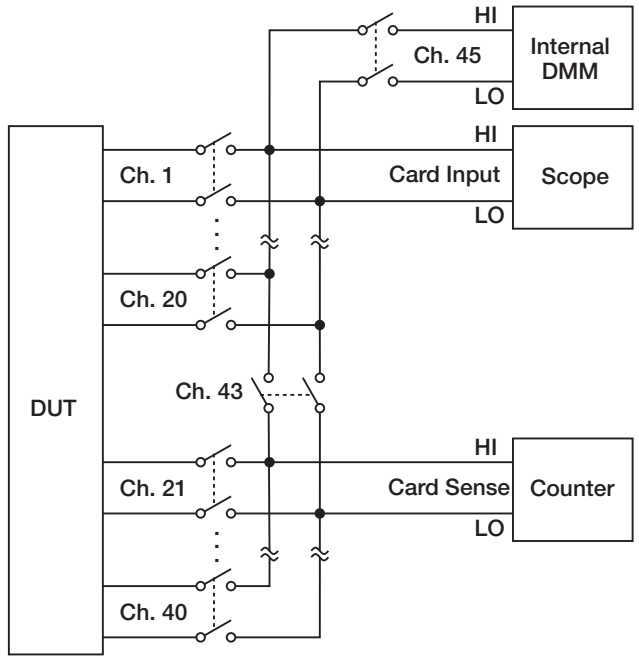

See Model 7708 specifications.

Channel 43 .....Open
Channel 44 .....Open
Channel 45 .....Closed

NOTE: This configuration example can be duplicated with the 7700, 7701, 7702, 7703, 7706, 7707, and 7708 modules. See module specifications for their channel configurations.

7705 Configuration Examples

Typical connections—indicator lamps, alarm, and relay

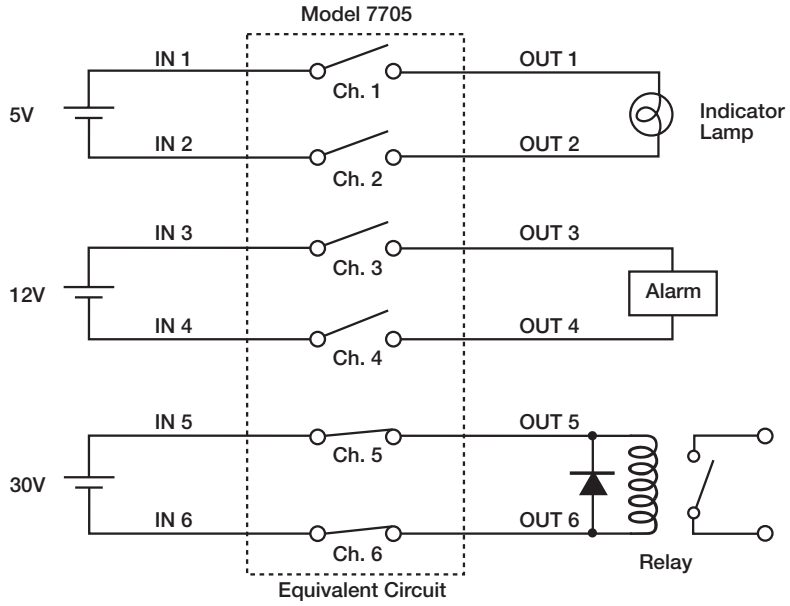

7705 Configuration Examples (continued)

Variable AC line/load test connections

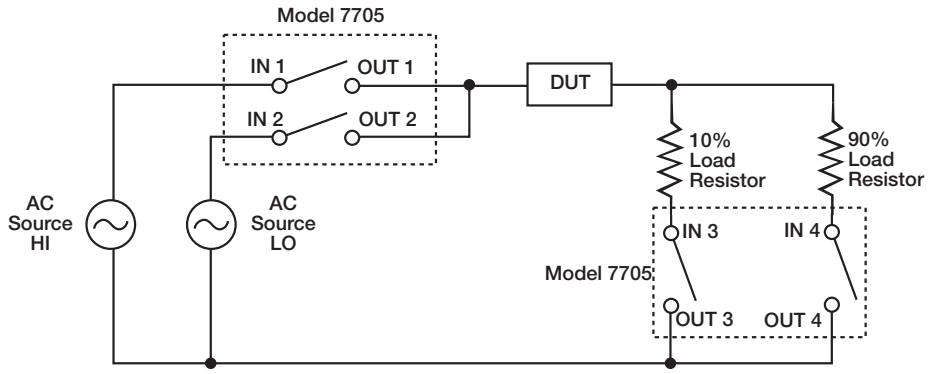

CAUTION: Maximum switch current is 2A.

Source is impedance limited from mains (Safety Category I signals).

Single Pole (Single Point Ground) Switching Example

Using the 7705 for independent switching and the 7701 to bring measurement of DUT to internal DMM of 2750

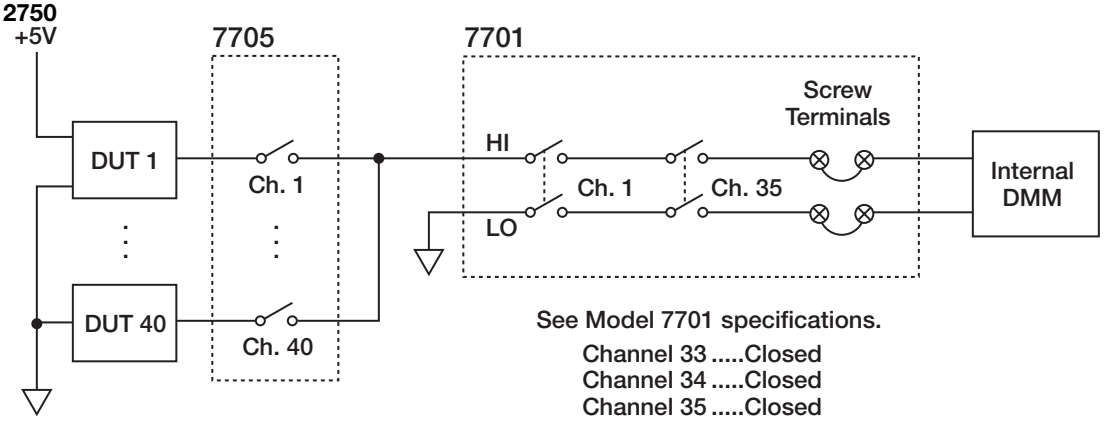

See Model 7701 specifications.

Channel 33 .....Closed
Channel 34 .....Closed
Channel 35 .....Closed

1.888.KEITHLEY (U.S. only)
www.keithley.com
KEITHLEY
A GREATER MEASURE OF CONFIDENCE

7705 Configuration Examples (continued)

7705 independent switch and 7701 multiplexer example

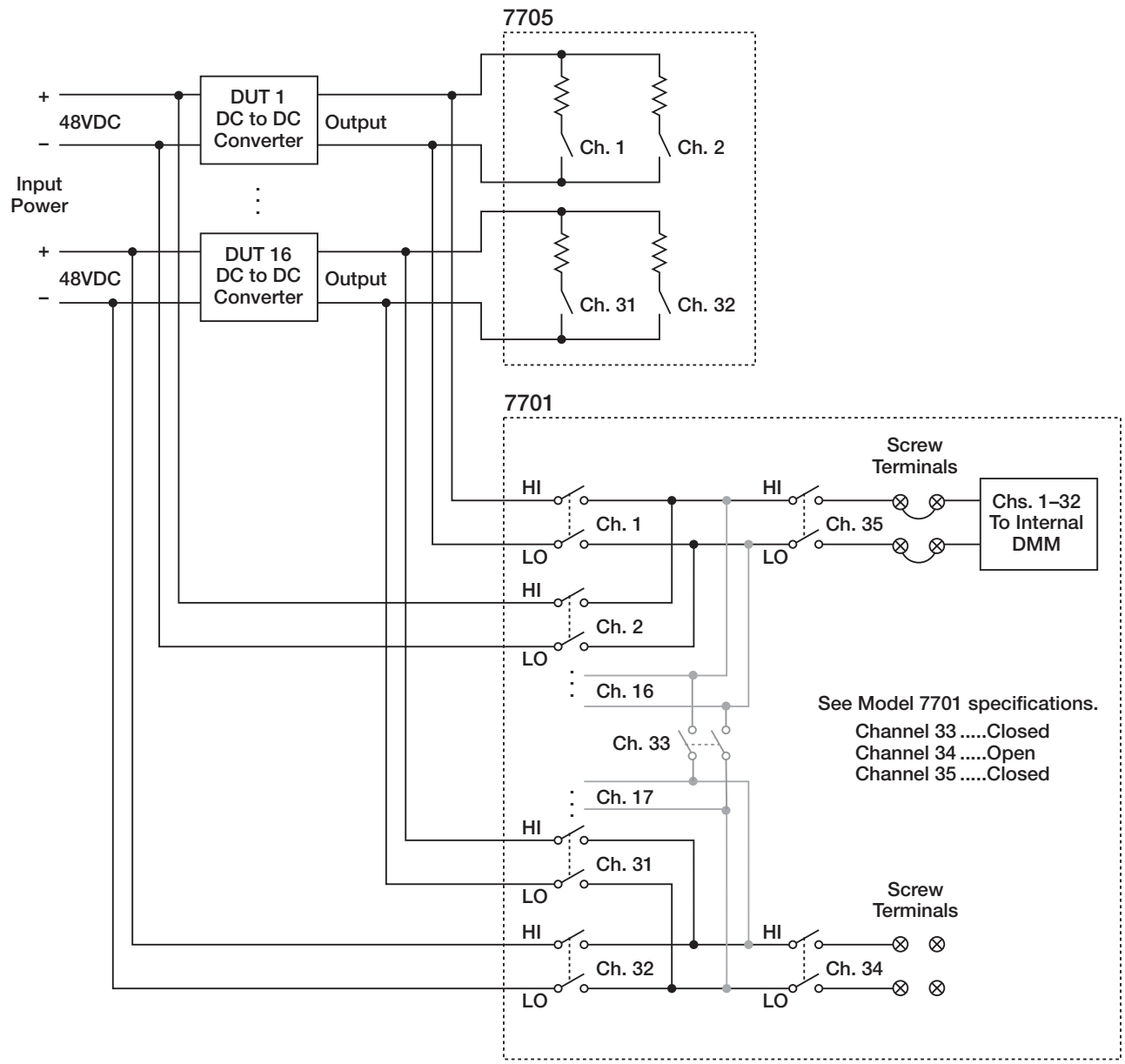

Analog Output and Digital I/O Examples

Typical digital output w/external power supply

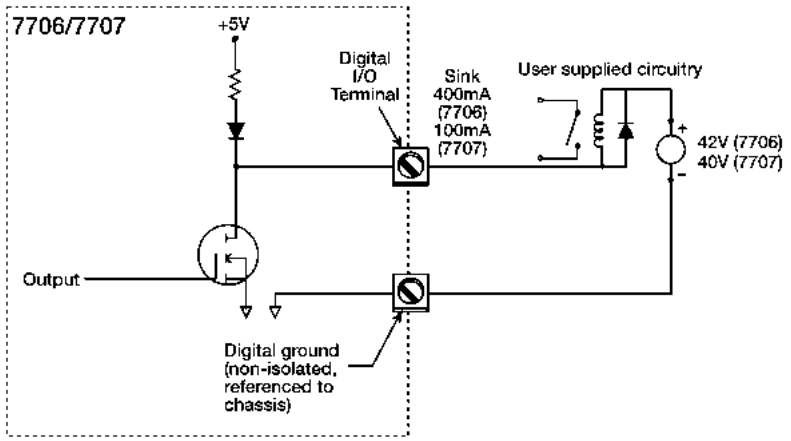

Digital Output

The 7706 module has two non-isolated 8-bit output ports that can be used for outputting digital patterns. The two ports can be combined to output a single 16-bit word or a dual 8-bit byte. A simplified diagram of a single output bit is shown here.

The 7707 module has four non-isolated 8-bit input/output ports that can be used for outputting digital patterns. The two ports can be combined to output a 16-bit word, or dual or quad 8-bit bytes.

The 7707 can also be configured (in blocks of 8) as digital inputs.

Typical digital output (no external power supply)

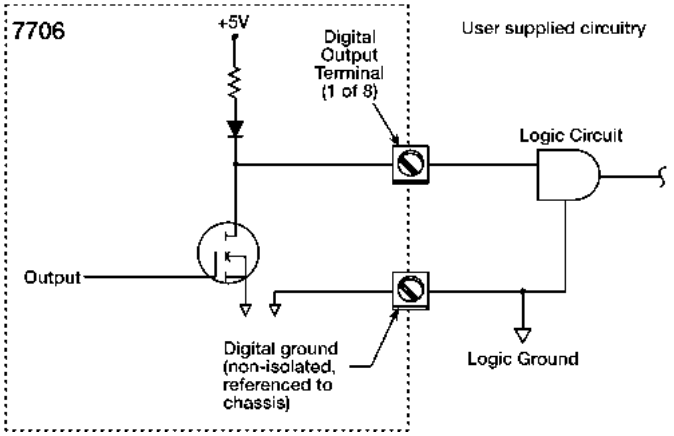

7706 analog output

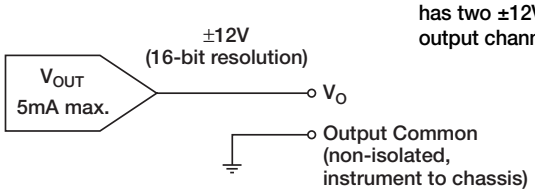

NOTE: The 7706 module has two ±12V analog output channels.

1.888.KEITHLEY (U.S. only)
www.keithley.com
KEITHLEY
A GREATER MEASURE OF CONFIDENCE

Analog Output and Digital I/O Examples (continued)

Connecting the Model 7707 Digital I/O module to industry standard solid-state relays (SSRs) to switch high VA (up to 980VA).

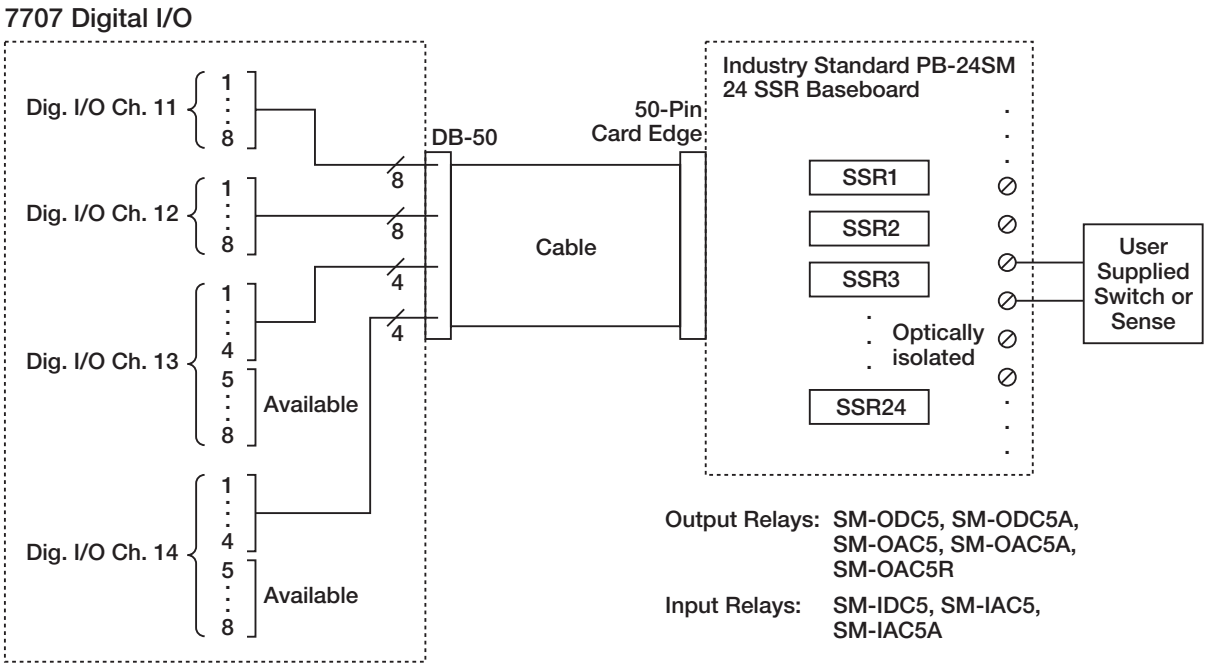

Output Relays: SM-ODC5, SM-ODC5A, SM-OAC5, SM-OAC5A, SM-OAC5R

Input Relays: SM-IDC5, SM-IAC5, SM-IAC5A

CAUTION: Adequate insulation barriers must be used on PB-24SM and cable for systems with >42V.

Matrix Configuration Example

7709 6x8 Matrix configuration example

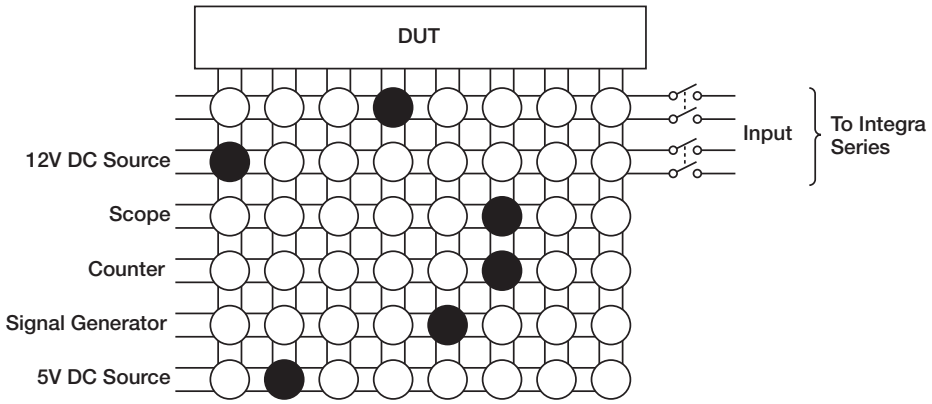

The 7709 Matrix Module can connect any combination of six differential channels of instrumentation to any combination of eight differential DUT channels. The instrumentation can be the Integra system's internal DMM or external equipment (AC and DC sources, internal or external meters, oscilloscopes, etc.) This matrix configuration allows wide flexibility for complex test systems.

7701 Configuration Example

7701 32-Channel common-side
4-wire Ohms configuration example

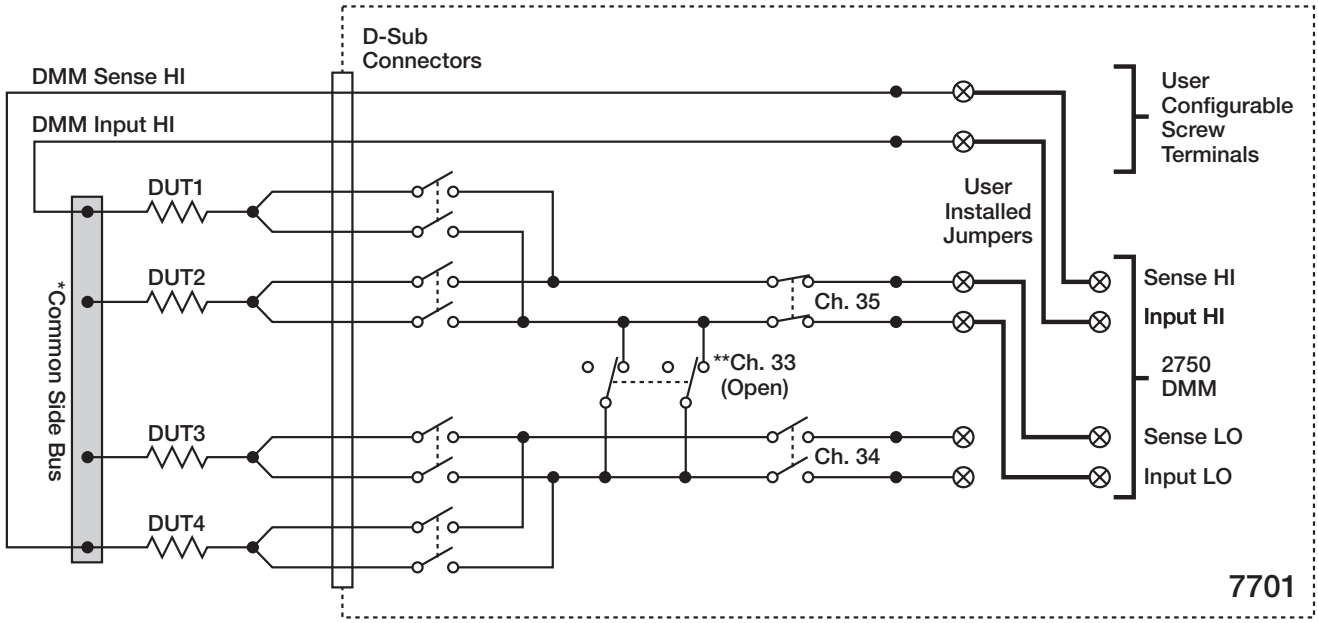

*NOTE: Common side connections must be made carefully to eliminate all lead resistance from the 4-wire ohms measurement. The common side bus should be a single wire or bus bar that connects the HI side of all the DUTs. DMM Input HI should be connected to one end of the common side bus and DMM Sense HI should be connected to the other end.

**NOTE: Refer to ROUTE:MULT section of the 2700, 2701, or 2750 manual for more information.

1.888.KEITHLEY (U.S. only)
www.keithley.com
KEITHLEY
A GREATER MEASURE OF CONFIDENCE

Specifications are subject to change without notice.

All Keithley trademarks and trade names are the property of Keithley Instruments, Inc.
All other trademarks and trade names are the property of their respective companies.

KEITHLEY

Keithley Instruments, Inc. 28775 Aurora Road • Cleveland, Ohio 44139 • 440-248-0400 • Fax: 440-248-6168
1-888-KEITHLEY (534-8453) • www.keithley.com

Sales Offices:

BELGIUM:	Bergensesteenweg 709 • B-1600 Sint-Pieters-Leeuw • 02-363 00 40 • Fax: 02/363 00 64
FINLAND:	Tietäjäntie 2 • 02130 Espoo • Phone: 09-54 75 08 10 • Fax: 09-25 10 51 00
FRANCE:	3, allée des Garays • 91127 Palaiseau Cédex • 01-64 53 20 20 • Fax: 01-60 11 77 26
GERMANY:	Landsberger Strasse 65 • 82110 Germering • 089/84 93 07-40 • Fax: 089/84 93 07-34
GREAT BRITAIN:	Unit 2 Commerce Park, Brunel Road • Theale • Berkshire RG7 4AB • 0118 929 7500 • Fax: 0118 929 7519
ITALY:	Viale San Gimignano, 38 • 20146 Milano • 02-48 39 16 01 • Fax: 02-48 30 22 74
NETHERLANDS:	Postbus 559 • 4200 AN Gorinchem • 0183-635333 • Fax: 0183-630821
SWEDEN:	c/o Regus Business Centre • Frosundaviks Allé 15, 4tr • 169 70 Solna • 08-509 04 600 • Fax: 08-655 26 10

© Copyright 2003 Keithley Instruments, Inc.
Printed in the U.S.A..

No. 2393
0103

SITRANS F M MAG 5100 W

Status: **Your configuration is complete**

Basic types **Options**

Configuration: Reset | Print | Download Change Quantity 1

Description	**Ex stock**
	[EUR]

Additional feature for pricing!

Total price for the marked (*) features

Label

0 .

Diameter

2D DN25, 1 Inch

Flange norm / Pressure rating

F EN 1092-1, PN 40

Flange material

4 Carbon steel flanges ASTM A 105, 300micron coating

Liner material

3 Liner Material: Hard NBR Rubber

Electrode material

2 Hastelloy C-276

Transmitter

L MAG 5000, IP67 / NEMA 4X/6, Polyamid enclosure, With display, 115-230VAC, 50/60 Hz

Communication

A No communication

Cable glands/terminal box

2 1/2 inch NPT Polyamid Terminal box or 6000 I compact.

Product number (MLFB) 7ME652 **0 2D F 4 3 2 L A 2**

B-row

Copy & Paste 7ME6520-2DF43-2LA2

Add to cart of Industry Mall

MOORE INDUSTRIES WORLDWIDE

TDY

PC-Programmable
Temperature Transmitter with Display

March 2015

Description

Moore Industries' universal TDY PC-Programmable Temperature Transmitter features a large integral display that shows real-time process status and valuable loop diagnostic information. Combining smart digital technology with advanced analog operation, the TDY delivers superior reliability, accuracy and ease of use.

The 2-wire (loop-powered) TDY programs in a minute or less to accept direct inputs from:

- **22 RTD Types**
  (2, 3, or 4-wire; Pt, Cu, or Ni; 10 to 1000 ohms)
- **9 Thermocouple Types**
  (J, K, E, T, R, S, B, N and C)
- **Direct Millivolt Sources**
  (-50 to 1000mV)
- **Resistance & Potentiometer Devices**
  (0 to 4000 ohms)

The TDY converts the input to an accurate 4-20mA output that is both linear and input scaleable-ready to interface to readout instruments, recorders, DCS units and other computer-based SCADA systems.

Figure 1. *Our ready-to-install TDY temperature assemblies include your choice of enclosure, sensor, thermowell and fittings in one easy-to-order package.*

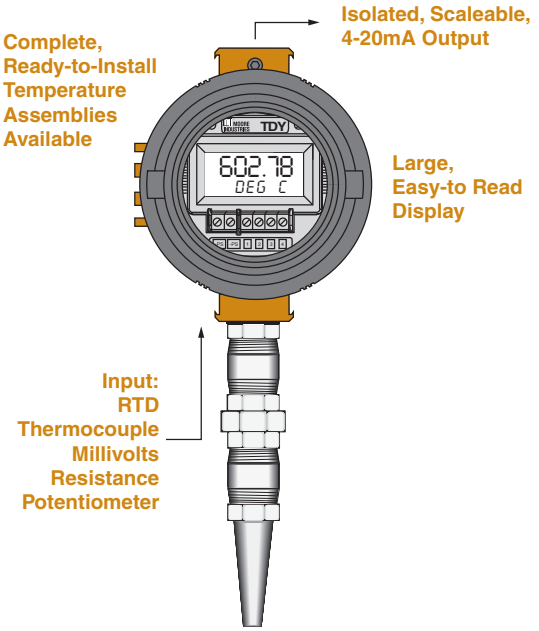

Available in a variety of mounting styles, *the TDY installs quickly and easily on a pipe or surface in the field, or on DIN rail and relay track in an multi-unit enclosure or cabinet.*

Features

- **Exceptional accuracy.** The TDY provides the highest accuracy (up to ±0.05°C) for your critical process applications.
- **Easy-to-read, customizable display.** The TDY's large display features alphanumeric characters that can be read easily in the field. It can be customized to display the input, output, or toggle between both.
- **Auto decimal point.** The TDY makes the most of its display area by automatically adjusting the decimal point in response to the number of digits required to represent the process variable being measured.
- **Sets up in a minute or less.** The ideal universal plant standard, our TDY offers dozens of input, output, and operation choices, and still configures fast from a single software window.
- **Fast measurement cycle.** Delivering output updates at least 8 times per second, these transmitters are twice as fast as comparable microprocessor-based instruments.

Certifications

FM APPROVED · CSA C US · ANZEx · Ex · CE · IECEx

© 2015 Moore Industries-International, Inc.

All product names are registered trademarks of their respective companies.

TDY

PC-Programmable
Temperature Transmitter with Display

Universal Solution

With the TDY, there's no need to specify and stock an array of single-function instruments:

- Simplify gathering information in the field or control room with its large, easy-to-read display.
- Convert RTD, T/C, mV, and Ohm signals to the linear 4-20mA needed by an indicator, recorder, PC, PLC, DCS, or similar SCADA system.
- Customize linearization to easily process inputs in non-linear, millivolt input applications.
- Stop ground loop problems with total isolation.
- Trim input readings directly from sensors to achieve maximum relative accuracy and match performance characteristics with your already-installed hardware.
- Convert signals from weak, low-level signals that allow inaccuracies from plant noise to stable, high-level signals that can withstand long-distance transmission through a noisy plant.
- Use true 4-wire RTD inputs to eliminate signal inaccuracies resulting from inevitable lead wire resistance imbalances.
- Increase DCS accuracy by using transmitters calibrated to a specific temperature range in place of direct DCS inputs that are only capable of measuring readings over the entire range of a sensor.
- Reduce installation costs by replacing expensive and fragile sensor wire runs and costly DCS input cards.
- Compensate for erratic input signals with programmable damping values.

Total Sensor Diagnostics

Our programmable transmitters perform continuous sensor diagnosis. This patented Moore Industries feature can save you from the costly problems of lost production time and hours of troubleshooting by identifying the type and location of the problem.

Monitors Sensor During Operation

If a RTD wire breaks or otherwise stops sending a signal during operation, the transmitter sends the output upscale or downscale (your choice) to warn of trouble.

The TDY instantly displays the type and location of the error. This helps you quickly diagnose the problem. If you do need additional help, our transmitters go even further! When the PC is connected to the TDY loop and an error occurs, the configuration software will display a detailed, plain-English error message.

Figure 2. *Total Sensor Diagnostics saves troubleshooting time.*

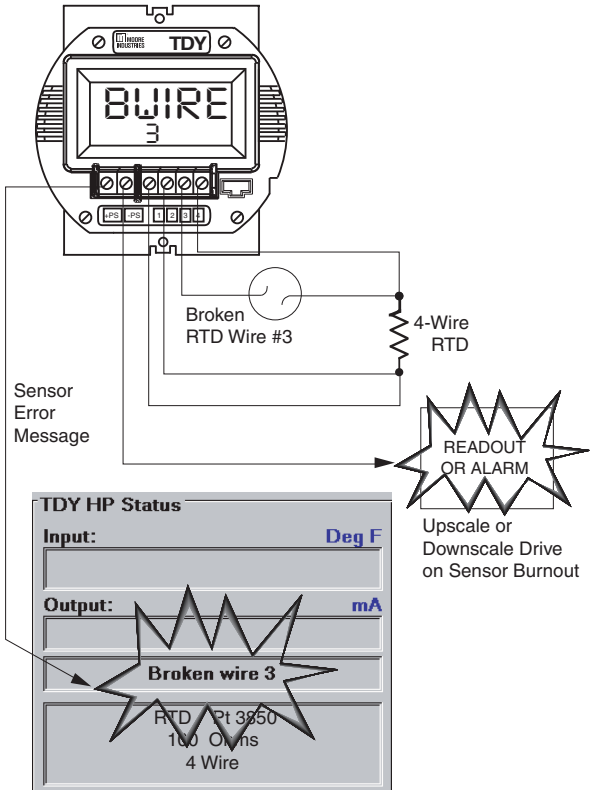

TDY Configuration
Software
(partial window shown)

Intelligent Configuration Software

Configuring the TDY is as simple as point-and-click. Custom linearization and trimming capabilities make it an even more valuable tool.

All you need is a PC running Windows®, our TDY Configuration Software and a Configuration Cable (software supplied with each order).

In minutes, you can begin configuring your transmitter's:

- Display type and range (zero and full scale; mV, %, ohms, ˚F, or ˚C)
- Input type and range (zero and full scale)
- 4-20mA output range (zero and full scale)
- Reference junction compensation or no reference junction compensation for T/C inputs
- Linearization or no linearization for T/C inputs
- Sensor type
- 50Hz or 60Hz noise rejection
- Broken wire detection ON or OFF for calibration
- Upscale or downscale on sensor burnout
- Custom instrument tag (up to 40 characters)
- Custom input linearization (up to 85 points)
- Custom input trimming to actual sensors
- Loop test fixed output for easy calibration of other instruments in the loop
- Damping time for erratic signal compensation (0-5 seconds)

Figure 3. All operating parameters can be set, and then viewed, on a single software screen.

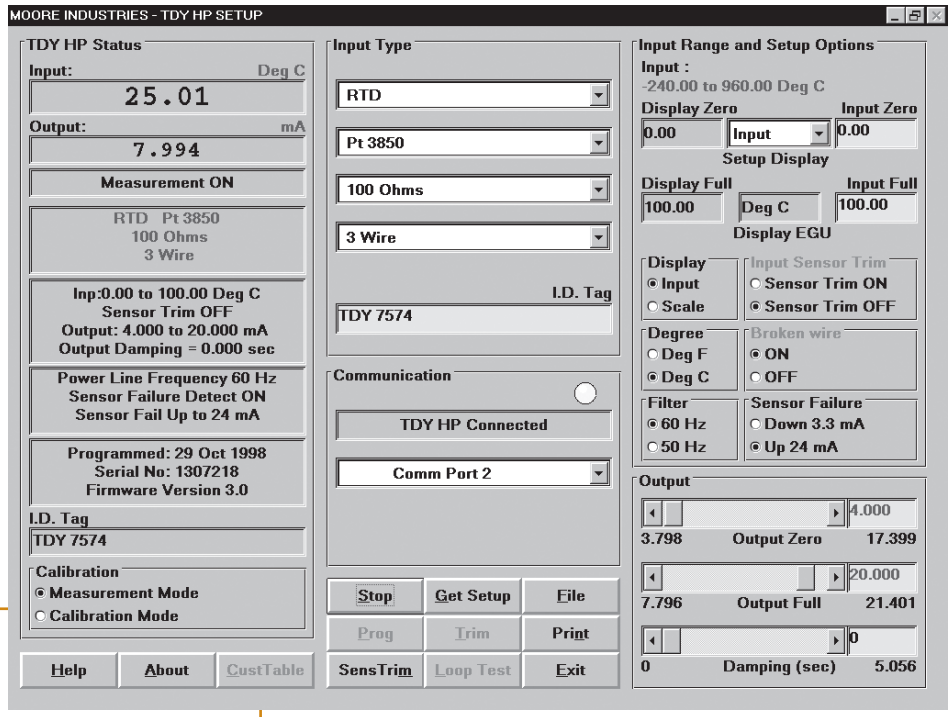

Digital Trimming Enhances Accuracy

A single click of the mouse "captures" the actual sensor input zero or full scale. Scaling values can be entered directly from the PC. Using the on-screen adjustments for output, Zero Scale can be set between 3.800 and 17.400mA. Full Scale can span from 7.800 to 21.400mA.

Precise Input Capturing

The TDY Configuration Software will capture the upper and lower range of the sensor with just a click of a mouse.

Custom Tables Ease Linearization Problems

Unusual inputs are no problem for the TDY. Not when it is so easy to use the Configuration Program's straight-forward interface to build a custom, 85-point linearization table (mV input type only).

Output Damping Ensures Stable Output

If your sensor is prone to step increments and decrements, use the TDY to lessen the impact on your process. Program a damping value from 0 to 5 seconds, averaging out sensor fluctuations over time and lessening the impact of step changes.

Specifications

Performance

Input Accuracy: Refer to Table 2 for standard accuracy specifications.
Output Accuracy: 4.8µA (±0.03% of 4-20mA span)
Overall Accuracy: Overall accuracy of the unit is the combined input and output accuracy. It includes the combined effects of linearity, hysteresis, repeatability and adjustment resolution. It does not include ambient temperature effect. Fir T/C input only, add the Reference Junction Compensation error.
Reference Junction Compensation Accuracy: ±0.45°C
Stability: Error is in % of conformance range.

Stability	Input to Output		
	1yr	3yrs	5yrs
T/C, mV	0.11	0.18	0.24
RTD Ohm Pot.	0.13	0.22	0.28

Isolation: 500Vac/1000Vdc input to output to case
Measurement Cycle: Output updates at least 8 times per second

Performance (Continued)

Output Response: 256msec, typical, 300msec, maximum, for output to change from 10% to 90% of its scale for an input step change of 0% to 100%.
Ripple: ≤10mVp-p, maximum
Power Supply and Load Effect: Negligible within power and load limits
Over-Voltage Protection: 4V maximum, on input; 48V maximum, on output; 48V reverse polarity protection on output
Output Current Limiting: 3.8mA and 21.4mA for input over/under range; 25mA maximum (hardware limit)
Load Capability: 583 ohms@24V, typical;

$$\frac{\text{Supply Voltage - 10V}}{0.024\text{A}} = \text{Ohms}$$

Burnout Protection: Total Sensor Diagnostics are user-selected via Windows®-based configuration software; Upscale to 23.6mA or Downscale to 3.6mA
T/C Input Impedance: 40 Mohms, nominal
RTD Excitation: 250 microamps, ±10%
RTD Lead Wire Resistance Maximum: RTD resistance + 2 times the lead wire resistance must be less than 4000 ohms; recommended <35 ohms per wire for 3-wire inputs; <5 ohms per wire for 10 ohm Cu inputs

Display

Type: LCD; Top Row, 10.16mm (0.4 in) high black digits on a reflective background; Bottom Row, 5.72mm (0.225 in) high black digits on a reflective background
Format: Two rows of five alphanumeric characters
Decimal Points: Automatically adjusting decimal point with a two decimal place maximum (Analog output display is always two decimal places)
Range: -99999 to 99999
Minimum Display Span: 1.00

Ambient Conditions

Operating and Storage Range: -40°C to 85°C (-40°F to 185°F)
Relative Humidity: 0-95%, non-condensing
Effect of Ambient Temperature on Accuracy: ±0.015% of span per °C change, maximum (+0.001% of resistance reading for RTD inputs)
Effect of Ambient Temperature on Reference Junction Compensation: ±0.015°C/°C change
RFI/EMI Immunity: 20V/m@80-1000MHz, 1kHz AM, when tested according to IEC 61326
Common Mode Rejection: 100dB min. @ 50/60Hz
Normal Mode Rejection: Refer to Table 1

Adjustments

All settings made using our Windows®-based configuration program, then stored in non-volatile memory

Weight

HP housing: 178g (6.3 oz)
BH housing: 1.5 kg (3.3 lbs)
D2LC housing: 688g (1 lb, 8.3 oz)

Table 1. *Normal Mode Rejection Ratio Table*

Sensor Type		Max. p-p Voltage Injection for 70dB at 50/60Hz
T/C: J, K, N, C, E		150mV
T/C: T, R, S, B		80mV
Pt RTD: 100, 200, 300 ohms		200mV
Pt RTD: 400, 500, 1000 ohms		800mV
Ni: 120 ohms		150mV
Cu: 9.03 ohms		100mV
Resistance	**mV**	
1-4kohms	250-1000	800mV
0.25-1kohms	62.5-250	200mV
0.125-0.25kohms	31.25-62.5	100mV

Specifications and information subject to change without notice. Printed in the U.S.A.

Ordering Information

Unit	Input	Output	Power	Options	Housings
TDY PC-Program-mable Temperature Transmitter with Display	**PRG** Programmable with supplied Configuration Software (see Table 1 for descriptions of available input types; factory configuration available)	**4-20MA** User scaleable with supplied software	**10-42DC** **10-30DC** for **-IS** option	**-IS Option** (cFMus, ATEX and IECEx Intrin-sically Safe approval)	**BH2NG** (*) or (‡) Aluminum 2-Hub, Explosion-Proof enclosure with glass cover **BH3NG** (*) or (‡) Aluminum 3-Hub, Explosion-Proof enclosure with glass cover **D1LC** 1-Hub, low base, clear cover, NEMA 4X (IP66) enclosure **D2LC** 2-Hub, low base, clear cover, NEMA 4X (IP66) enclosure **HP** Hockey-puck housing and spring clips **DN** Snap-in mounting for HP case on TS-32 DIN rail **FL** Mounting flanges on HP suitable for relay track or screw mounting **FLD** Mounting flanges on HP suitable for 3½" relay track or screw mounting **SB2NG** (*) or (‡) 316 Stainless Steel 2-Hub, Explosion-Proof enclosure with two ½-inch NPT entry ports and a glass cover **SB2MG** (*) or (‡) 316 Stainless Steel 2-Hub, Explosion-Proof enclosure with two M20 x 1.5 entry ports and a glass cover * Either **A** or **E** suffix (comes supplied with 2" pipe mount hardware) **A** suffix indicates ANZEx/TestSafe (Ex d) Flameproof approvals (i.e. BH2MG**A**) **E** suffix indicates ATEX (Ex d and tb) Flameproof approvals (i.e. BH2MG**E**) ‡ **P** suffix indicates enclosure comes equipped with base plate and U-bolts for mounting on a 2-inch pipe (i.e. BH2NG**P**) See BH, SB and D-BOX Datasheets for additional information.

To order, specify: Unit / Input / Output / Power / Option [Housing]
Model Number Example: TDY / PRG / 4-20MA / 10-42DC / -IS [BH2NG]

Complete Temperature Assemblies

Free yourself from the hassle of looking around for pieces and parts by ordering a complete assembly with just one order number. To complement our high-quality transmitters, we carry complete lines of RTDs, thermocouples, thermowells, connection heads and fittings. For accuracy as high as ±0.05°C, have your TDY and sensor calibrated together in our sensor-matching calibration bath.

Sensor-to-Transmitter Matching

The sensor matching process starts by immersing the temperature sensor into stabilized temperature baths. The TDY captures two points from the sensor and stores them in non-volatile memory. It then uses them to compensate for deviations between a sensor's stated linearization curve and its actual measurements. Sensor matching provides you with incredible accuracy at an affordable price. Accuracy varies with the sensor, so contact the factory for information on your sensor type.

Accessories

Each TDY order comes with one copy of our Configuration Software. Use the chart below to order additional parts.

Part Number	Part
750-75E05-01	**Intelligent PC Configuration Software**
803-039-26	**Isolated Configuration Cable**
803-040-26	**Non-Isolated Configuration Cable**
804-030-26	**Fuse Protected USB Communication Cable (required by IECEx and ATEX for products installed in Intrinsically-Safe areas)**

Certifications

TDY-HP

Factory Mutual Approvals:
Intrinsically-Safe
Class I, Division 1, Groups A, B, C & D
Class I, Zone 0, AEx ia IIC T4
Non-Incendive
Class I, Division 2, Groups A, B, C & D
Class I, Zone 2, AEx nA IIC T4

ATEX Directive 94/9/EC (FM Approvals):
Intrinsically-Safe and Type "n"
II 1 G Ex ia IIC T4 Ga
II 3 G Ex nA IIC T4 Gc

IECEx System (FM Approvals):
Intrinsically-Safe and Type "n"
Ex ia IIC T4 Ga
Ex nA IIC T4 Gc

CE Conformant – EMC Directive 2004/108/EC – EN 61326

Temperature Class T4, Tamb = -40°C to +85°C

TDY-HP in BH or SB2 Housing

Factory Mutual Approvals (FM Global Group):
Explosion-Proof & Dust-Ignition Proof
Class I, Division 1, Groups A*, B, C & D
Class II & III, Division 1, Groups E, F & G
Environmental Protection: NEMA 4X & IP66
T6 @ 60°C Maximum Operating Ambient
**For Group A applications, seal all conduits within 18"*

CSA Group (Canadian Standards Association):
Explosion-Proof
Class I, Division 1, Groups A*, B, C, & D
Class II, III, Groups E, F, & G
Type 4X, IP66
Ambient Temp. Range: -20°C to +60°C; T6
**For U.S. Group A applications, seal all conduits within 18"*

ATEX Directive 94/9/EC (ISSeP):
Explosion-Proof/Flameproof
II G Ex d IIC T6 Gb
II D Ex tb IIIC Db T85°C IP66

ANZEx (TestSafe):
Explosion-Proof/Flameproof
Ex d IIC T6 (Tamb 60°C)

Table 2. *TDY Input and Accuracy Table*

Input	Type	α*	Ohms	Conformance Range	Minimum Span	Input Accuracy	Maximum Range
RTD	**Platinum**	0.003750	1000	-50 to 500°C -58 to 932°F	15°C (27°F) for 100 ohms inputs 10°C (18°F) for 200 ohms inputs 7.5°C (13.5°F) for 500 and 1000 ohms inputs	±0.11°C ±0.2°F	-100 to 560°C -148 to 1040°F
		0.003850	100, 200, 300, 400, 500, 1000	-200 to 850°C -328 to 1562°F		±0.21°C ±0.38°F	-240 to 960°C -400 to 1760°F
		0.003902	100, 200, 400 500, 1000	-100 to 650°C -148 to 1202°F		±0.15°C ±0.27°F	-150 to 720°C -238 to 1328°F
		0.003911	100, 500	-200 to 630°C -328 to 1166°F		±0.17°C ±0.31°F	-235 to 710°C -391 to 1310°F
		0.003916	100	-200 to 510°C -328 to 950°F		±0.14°C ±0.25°F	-240 to 580°C -400 to 1076°F
		0.003923	98.129	-200 to 600°C -328 to 1112°F		±0.16°C ±0.29°F	-235 to 680°C -391 to 1256°F
		0.003926	100, 470, 500	-200 to 630°C -328 to 1166°F		±0.17°C ±0.31°F	-235 to 710°C -391 to 1310°F
		0.003928	100	-200 to 850°C -328 to 1562°F		±0.21°C ±0.38°F	-260 to 962°C -436 to 1763.6°F
	Nickel	0.000672	120	-80 to 320°C -112 to 608°F	10°C 18°F	±0.16°C ±0.29°F	-100 to 360°C -148 to 680°F
		0.000427	9.035	-50 to 250°C -58 to 482°F	100°C 180°F	±1.2°C ±2.16°F	-65 to 280°C -85 to 536°F
Ohms	**Direct resistance or Potentiometer**	n/a	n/a	0-4000 ohms	30 ohms	±0.4 ohms	n/a
T/C	**J**	n/a	n/a	-180 to 770°C -292 to 1418°F	35°C 63°F	±0.28°C ±0.5°F	-210 to 770°C -346 to 1418°F
	K	n/a	n/a	-150 to 1372°C -238 to 2501.6°F	40°C 72°F	±0.3°C ±0.54°F	-270 to 1390°C -454 to 2534°F
	E	n/a	n/a	-170 to 1000°C -274 to 1832°F	35°C 63°F	±0.26°C ±0.47°F	-270 to 1013°C -454 to 1855.4°F
	T	n/a	n/a	-200 to 400°C -328 to 752°F	20°C 36°F	±0.24°C ±0.43°F	-270 to 407°C -454 to 764.6°F
	R	n/a	n/a	0 to 1768°C 32 to 3214.4°F	50°C 90°F	±0.71°C ±1.28°F	-50 to 1786°C -58 to 3246.8°F
	S	n/a	n/a	0 to 1768°C 32 to 3214.4°F	50°C 90°F	±0.71°C ±1.28°F	-50 to 1786°C -58 to 3246.8°F
	B	n/a	n/a	400 to 1820°C 752 to 3308°F	75°C 135°F	±0.43°C ±0.77°F	200 to 1836°C 392 to 3336.8°F
	N	n/a	n/a	-130 to 1300°C -202 to 2372°F	45°C 81°F	±1.33°C ±2.39°F	-270 to 1316°C -454 to 2400.8°F
	C	n/a	n/a	0 to 2315°C 32 to 4199°F	100°C 180°F	±1.16°C ±2.09°F	0 to 2338°C
Millivolts	**DC**	n/a	n/a	-50 to 1000mV	4mV	±0.04mV	-50 to 1000mV

* α values with both 32 and 128-point linearization curves are available. (Lower resolution values provided for compatibility with older units.)

Figure 5. *Dimensions of the TDY HP housing with mounting flanges.*

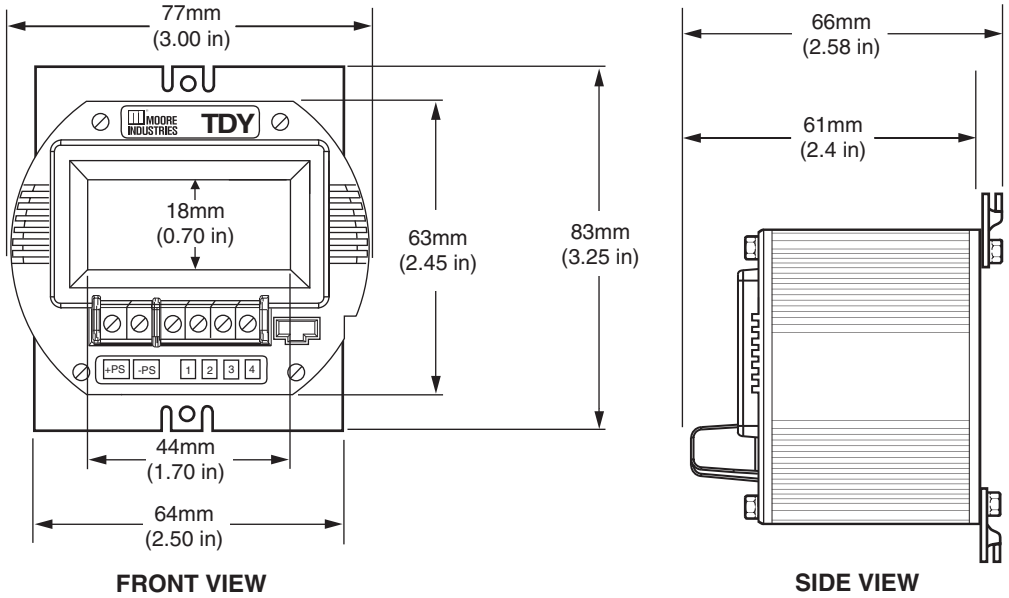

Figure 6. *Dimensions of the TDY with the BH explosion-proof enclosure.*

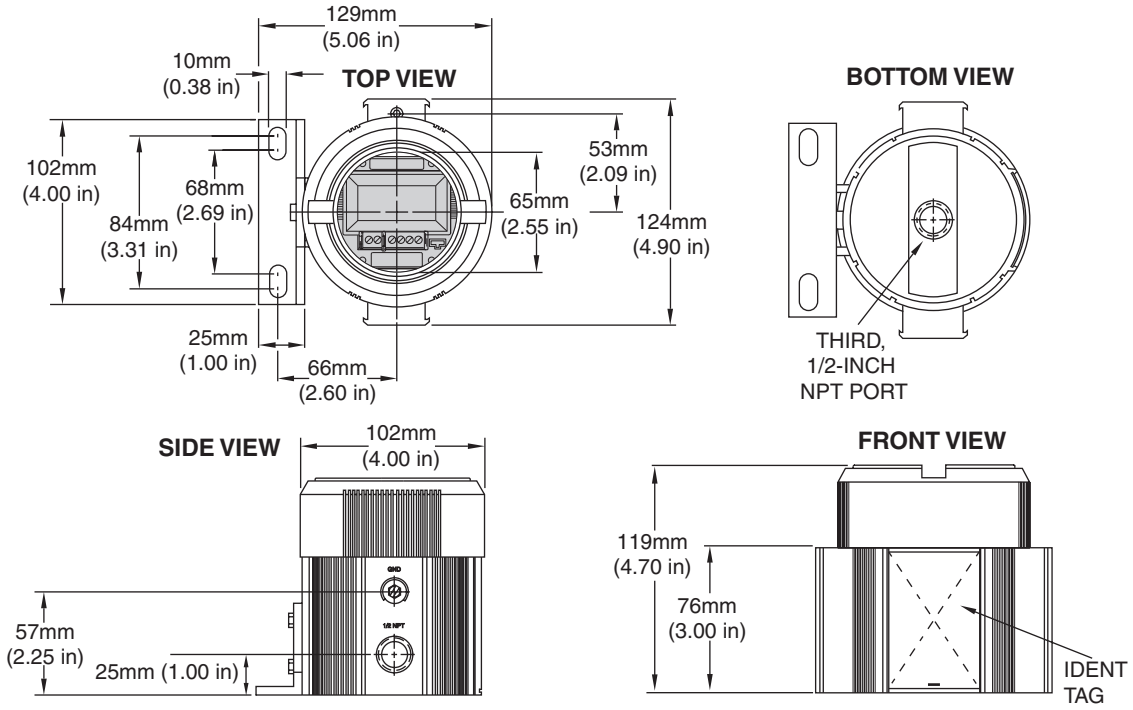

Figure 7. *Dimensions of the TDY D-Box housing.*

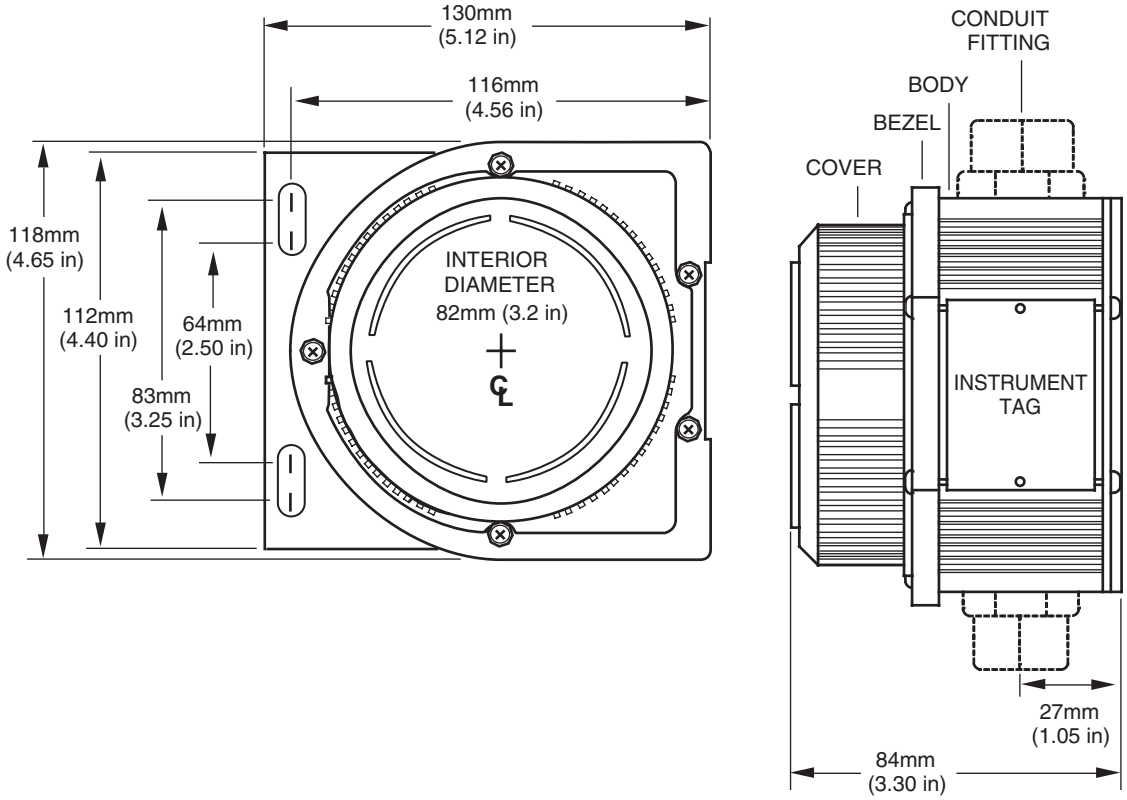

Figure 8. *Sensor connections for the TDY.*

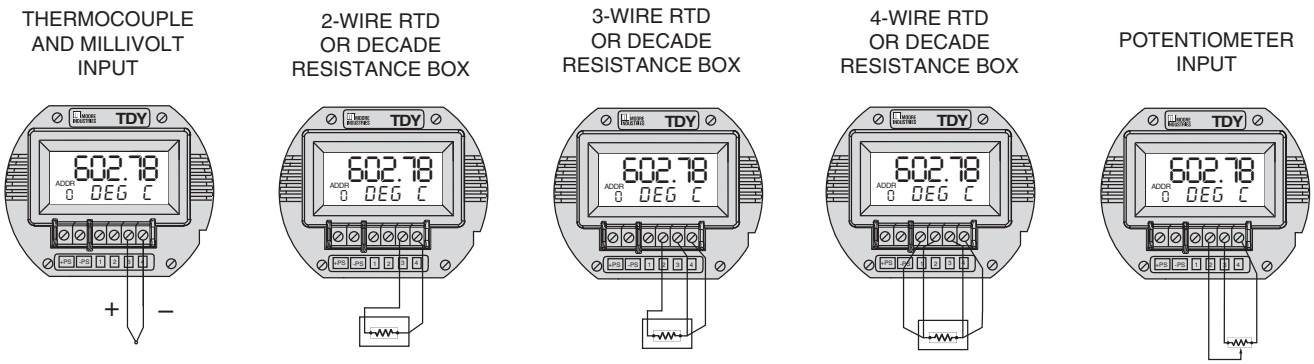

Cost effective, accurate, reliable

Inverse frequency shift capacitance continuous level measurement

SITRANS LC300

Answers for industry.

SIEMENS

Cost effective, accurate, reliable level measurement

SITRANS LC300 is an inverse frequency shift capacitance continuous level transmitter for liquids and solids applications. SITRANS LC300 is cost effective, reliable, low maintenance, and easy to install. It is ideal for standard and industrial applications in chemical, hydrocarbon processing, food and beverage, mining, aggregate and cement industries. Patented Active-Shield technology protects the measurement from the effects of moisture, vapors, foam, temperature or pressure variations, and material buildup.

- Accurate and reliable PFA-lined probes
- 2-wire (4 to 20 mA) current loop design
- Current signaling according to NAMUR NE 43
- Patented Active-Shield technology protects the measurement from the effects of moisture, vapors, foam, temperature, or pressure variations, and material build-up
- Integrated local LCD display
- Push-button calibration and programming
- Fully adjustable range: level, damping, diagnostics
- Corrosion-resistant construction and wetted parts
- Rugged, shear, and abrasion-resistant probe
- 25 m (82 ft) maximum insertion length

SITRANS LC300	
Power	
	12 to 30 V DC any polarity, 2-wire current loop circuit
Performance	
Range	1.66 to 3300 pF, minimum span 3.3 pF
Accuracy	<0.5% of actual measurement value
Temperature stability	0.25% of actual capacitance value
Non-linearity and reproducibility	<0.4% of full scale and actual measurement value
Current signaling	According to NAMUR NE 43, signal 3.8 to 20.5 mA, fault ≤ 3.6 or ≥21 mA (22 mA)
Wiring connections	max. 2.5 mm^2
Interface	
Output: loop current	4 to 20 mA/20 to 4 mA 2 wire current loop
Display (local)	LCD, 4 digit, each 0 to 9 and limited alpha characters
Mechanical	
Enclosure	• Aluminum, epoxy-coated • Ingress protect: Type 4/NEMA 4/IP65, IP68 • Cable inlet 2 x ½" NPT, 2 x M20x15
Sensor	AISI 316L / PFA
Process connection	• Threaded: ¾",1",1¼",1½" NPT/BSPP/BSPT/JIS-P • Flanges: 1 to 4" ASME, DIN DN 25 to 100
Probe diameter	• Rod version: 19 mm (0.75") with PFA jacket • Cable version: 9 mm (0.35") with PFA jacket, 6 mm (0.24") without PFA jacket
Probe lengths	• Rod version: min. 300 mm (12"), max. 5000 mm (197") • Cable version: min. 1000 mm (40"), max. 25000 mm (984")
Active shield length	• Rod version: 100 mm (3.94") • Cable version: 105 mm (4.13")
Process conditions	
Ambient temperature	-40 to 85 °C (-40 to 185 °F)
Process temperature	-40 to 200 °C (-40 to 392 °F)
Pressure	-1 to 35 bar g (-14.6 to 511 psi g)*
Approvals	
General	CE, CSA, FM,
Hazardous	CSA/FM, ATEX
Marine	Lloyd's Register of Shipping, categories ENV1, ENV2, ENV3, ENV5, and American Bureau of Shipping (ABS)
Pressure	PED 97/23/ EC, CSA B51
Other	C-TICK (Australia), Pattern Approved (China)

*Pressure rating of process seal is temperature dependent. Contact Siemens Milltronics for derating curves.
SITRANS is a registered trademark of Siemens AG. Specifications subject to change without notice.
© Siemens Milltronics Process Instruments Inc. 2008.

7ML1996-5KC03
Printed in Canada

7708

40-channel Differential Multiplexer Module

with Automatic CJC and Screw Terminals

- **40 differential channels for general-purpose measurements**
- **Two- or four-wire measurements**
- **300V, 1A capacity for voltage channels; 60W, 125VA**
- **Oversize screw terminal connection blocks are standard for easier connection**
- **Relay closures stored in onboard memory**

Ordering Information

7708 **40-channel Differential Multiplexer Module with Automatic CJC and Screw Terminals**

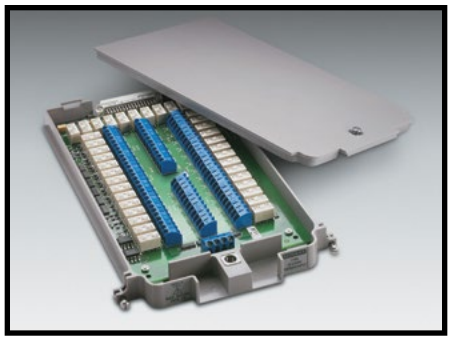

The Model 7708 plug-in module offers 40 channels of 2-pole or 20 channels of 4-pole multiplexer switching that can be configured as two independent banks of multiplexers. The built-in CJC sensors automatically linearize thermocouples, making the Model 7708 ideal for RTD, thermistor, and thermocouple temperature applications. It is also well suited for mixed-signal measurement applications that require multi-point monitoring, such as environmental stress screening.

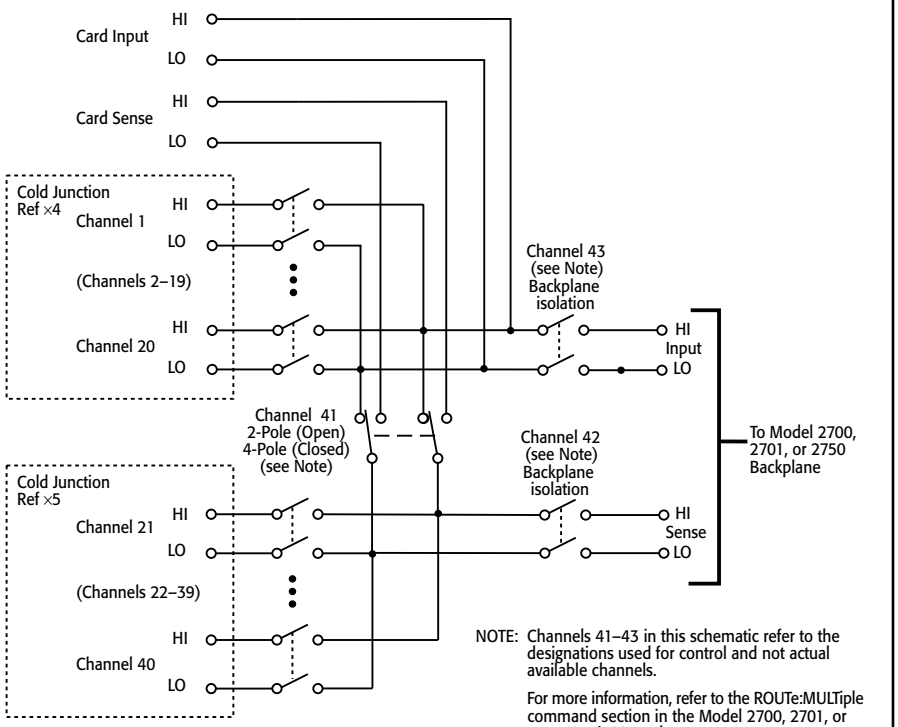

NOTE: Channels 41–43 in this schematic refer to the designations used for control and not actual available channels.

For more information, refer to the ROUTe:MULTiple command section in the Model 2700, 2701, or 2750 User's Manual.

Channels 42 and 43 can be individually controlled using ROUTe:MULTiple if the module is not to be connected to the internal DMM.

CAPABILITIES

CHANNELS 1–40: Multiplex one of 40 2-pole or one of 20 4-pole signals into DMM.

INPUTS

MAXIMUM SIGNAL LEVEL:

Channels (1–40): 300V DC or rms, 1A switched, 60W, 125VA maximum.

CONTACT LIFE (typ): $>10^5$ operations at max. signal level. $>10^8$ operations no load[1].

[1] Open thermocouple detector on during thermocouple measurements. Minimum signal level 10mV, 10μA.

CONTACT RESISTANCE: <1Ω at end of contact life.

CONTACT POTENTIAL:
<±500nV typical per contact, 1μV max.
<±500nV typical per contact pair, 1μV max.

OFFSET CURRENT: <100pA.

CONNECTOR TYPE: Screw terminal, #20 AWG wire size.

ISOLATION BETWEEN ANY TWO TERMINALS: $>10^{10}\Omega$, <100pF.

ISOLATION BETWEEN ANY TERMINAL AND EARTH: $>10^9\Omega$, <200pF.

CROSS TALK (10MHz, 50Ω Load): <–40dB.

INSERTION LOSS (50Ω Source, 50Ω Load): <0.1dB below 1MHz. <3dB below 2MHz.

COMMON MODE VOLTAGE: 300V between any terminal and chassis.

TEMPERATURE ACCURACY USING INTERNAL CJC: 1.0°C (see mainframe specification for details).

GENERAL

40 CHANNELS: 40 channels of 2-pole relay input. All channels configurable to 4-pole.

RELAY TYPE: Latching electromechanical.

ACTUATION TIME: <3ms.

FIRMWARE: Specified for Model 2700 rev. B02, 2701 rev. A01, and 2750 rev. A01 or higher.

ENVIRONMENTAL

OPERATING ENVIRONMENT: Specified for 0°C to 50°C. Specified to 80% R.H. at 35°C.

STORAGE ENVIRONMENT: –25°C to 65°C.

WEIGHT: 0.52kg (1.16 lb).

ACCESSORIES AVAILABLE

7401	Type K Thermocouple Wire, 30.5m (100 ft).

SERVICES AVAILABLE

7708-3Y-EW	1-year factory warranty extended to 3 years from date of shipment

Use with Integra Series mainframes: 2700, 2701, 2750

DIGITAL MULTIMETERS & SYSTEMS

KPCI-488LPA KUSB-488B

IEEE-488 (GPIB) Interface Solutions

- **PCI and USB bus versions**
- **IEEE-488.2 compatible for fast data transfer**
- **Windows® 7/Vista/XP/2000 drivers included**
- **LabVIEW® and LabWindows/CVI support**
- **Compatible with any standard GPIB instrument**

Ordering Information

KPCI-488LPA IEEE-488.2 Interface Board for the PCI Bus

KUSB-488B IEEE-488.2 USB-to-GPIB Interface Adapter for USB Port. Built in 2m (6.6 ft) cable

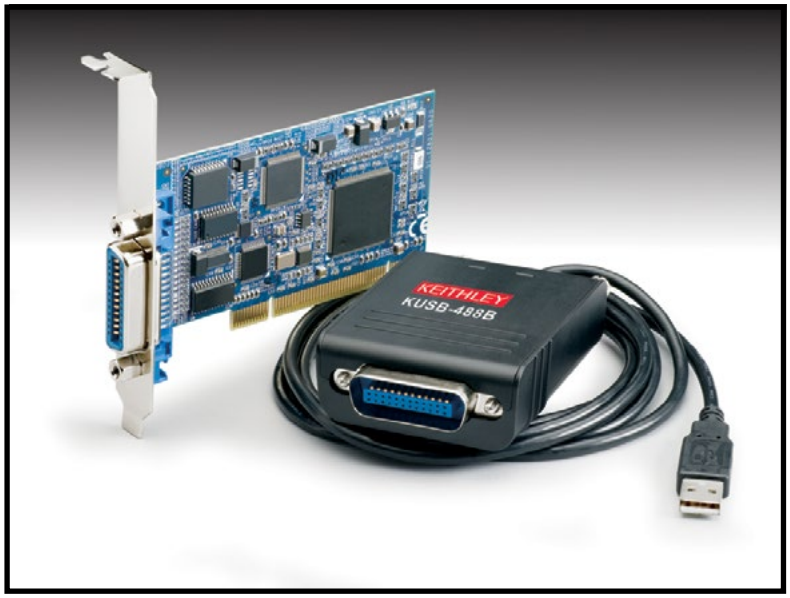

Keithley's GPIB interface solutions make it easy to add standard IEEE-488.2 bus control to any PC system. These high speed tools can control as many as 14 GPIB instruments or other devices over a distance of up to 20 meters. They are ideal for use with automated test equipment in laboratory and industrial applications.

The Keithley **Model KPCI-488LPA** is a low-profile, GPIB interface plug-in card that is 32-bit/33MHz PCI bus compatible. Its PCI interface supports both 3.3V and 5V PCI environments, making it suitable for most desktop computers and industrial PCs, including the new low-profile desktop systems. This low-cost solution supports Windows 7/Vista/XP/2000, and its driver library is command compatible with National Instruments™ and Capital Equipment Corporation™ command functions.

The Keithley **Model KUSB-488B** USB-to-GPIB interface turns any computer with a USB port into a fully functional GPIB controller. The KUSB-488B's small form factor makes it perfect for use with laptop computers in portable applications or for other applications in which the computer has no available PCI plug-in board slots. The product is USB 2.0 compliant and has an IEEE data transfer rate upwards of 1.5 MB/s through the USB port. No external power is required. KUSB-488B has a built-in 2-meter USB cable.

Software

The included utility software simplifies the setup and use of Keithley GPIB interface solutions and saves programming time. Every solution ships with 32-bit dynamic link libraries for Application Development Environments (ADEs) running under Windows 7/Vista/XP/2000 and drivers for the most current programming languages. This adds up to full compatibility with a full array of software, including:

- Microsoft Visual Studio 6.0 (Visual Basic, Visual C++)
- Microsoft Visual Studio .NET (Visual Basic .NET, C#)
- Microsoft Visual Studio 2005 and up
- Borland Delphi, Borland C Builder 6.0
- LabVIEW Version 7.0 and up (VISA and IEEE-488.2)
- LabWindows™/CVI Version 7.0 and up (VISA and IEEE-488.2)

Hardware Compatibility

These GPIB Interface solutions are fully compatible with all of Keithley's GPIB capable instruments. The Model 7010 adapter is required for the Model 428-PROG when used with the KUSB-488B.

	KPCI-488LPA	KUSB-488B
Bus/Form Factor	PCI	USB
Dimensions	4.7 × 2.5 in (120 × 64.5 mm)	3.2 × 2.6 × 1.1 in (81.7 × 66.1 × 27.8 mm)
Power (Current @ 5VDC)	400 mA typ., 750 mA max.	500 mA
Transfer Speed	1.5 Mbyte/s	1.5 Mbyte/s
EMC	European Directive 2004/108/EEC	European Directive 2004/108/EEC
Environmental	**Operating:** 0° to 55°C, 10% to 90% RH non-condensing **Storage:** –20° to 80°C, 5% to 90% RH non-condensing	**Operating:** 0° to 55°C, 10% to 90% RH non-condensing **Storage:** –20° to 80°C, 5% to 95% RH non-condensing

Vision™ OPLC™

Technical Specifications
V1040-T20B

V1040 OPLCs are programmable logic controllers that comprise a built-in operating panel containing a 10.4" Color Touchscreen. The V1040 offers function keys along with a virtual alpha-numeric keyboard which is automatically displayed when the application requires the operator to enter data. You can find additional documentation on the Unitronics' Setup CD and in the Technical Library at www.unitronics.com.

Technical Specifications

Power Supply	
Input voltage	12 or 24VDC
Permissible range	10.2-28.8VDC
Max. current consumption	840mA@12V 420mA@24V
Battery	
Back-up	7 years typical at 25°C, battery back-up for RTC and system data, including variable data.
Replaceable	Yes, without opening the controller.
Graphic Display Screen	See Note 1
LCD Type	TFT
Illumination backlight	White LED
Display resolution, pixels	800x600 (SVGA)
Viewing area	10.4"
Colors	65,536 (16-bit)
Touchscreen	Resistive, analog
'Touch' indication	Via buzzer
Screen brightness	Via software (Store value to SI 9).
Keypad	Displays virtual keyboard when the application requires data entry.

Notes:

1. Note that the LCD screen may have a single pixel that is permanently either black or white.

Keypad	
Number of keys	9 programmable function keys
Key type	Metal dome, sealed membrane switch

Program

Memory size: Application Logic – 2MB, Images – 80MB, Fonts – 1MB

Operand type	Quantity	Symbol	Value
Memory Bits	8192	MB	Bit (coil)
Memory Integers	4096	MI	16-bit
Long Integers	512	ML	32-bit
Double Word	256	DW	32-bit unsigned
Memory Floats	64	MF	32-bit
Timers	384	T	32-bit
Counters	32	C	16-bit

Data Tables	120K dynamic RAM data (recipe parameters, datalogs, etc.) Up tp 256K Flash data
HMI displays	Up to 1024
Program scan time	9 µsec per 1K of typical application

Removable Memory

Micro-SD card	Compatible with fast micro-SD cards; store datalogs, Alarms, Trends, Data Tables, backup Ladder, HMI, and OS. See Note 2

Notes:

2. User must format via Unitronics SD tools utility.

Communication

Serial ports	2. See Note 3
RS232	
Galvanic isolation	Yes
Voltage limits	±20VDC absolute maximum
Baud rate range	300 to 115200 bps
Cable length	Up to 15m (50')
RS485	
Galvanic isolation	Yes
Voltage limits	–7 to +12VDC differential maximum
Baud rate range	300 to 115200 bps
Nodes	Up to 32
Cable type	Shielded twisted pair, in compliance with EIA RS485
Cable length	1200m maximum (4000')
USB	See Note 4
Port type	Mini-B
Galvanic isolation	No
Specification	USB 2.0 compliant; full speed
Baud rate range	300 to 115200 bps
Cable	USB 2.0 compliant; up to 3m
CANbus port	1
Nodes	CANopen: 127; Unitronics' CANbus protocols: 60
Power requirements	24VDC (±4%), 40mA max. per unit. See Note 5

Galvanic isolation	Yes, between CANbus and controller		
Cable length/baud rate	25 m	1 Mbit/s	
See Note 5	100 m	500 Kbit/s	
	250 m	250 Kbit/s	
	500 m	125 Kbit/s	
	500 m	100 Kbit/s	
	1000 m*	50 Kbit/s	* If you require cable lengths over 500 meters, contact technical support.
	1000 m*	20 Kbit/s	
Optional port	User may install a single Ethernet port, or an RS232/RS485 port. Available by separate order.		

Notes:

3. The standard for each port is set to either RS232/RS485 according to DIP switch settings. Refer to the Installation Guide.
4. The USB port may be used for programming, OS download, and PC access. Note that COM port 1 function is suspended when this port is physically connected to a PC.
5. Supports both 12 and 24VDC CANbus power supply, (±4%), 40mA maximum per unit. Note that if 12 VDC is used, the maximum cable length is 150 meters.

I/Os

	Number of I/Os and types vary according to module. Supports up to 1024 digital, high-speed, and analog I/Os.
Snap-in I/O modules	Plugs into rear port to create self-contained PLC with up to 62 I/Os.
Expansion modules	Local adapter (P.N. EX-A1), via I/O Expansion Port. Integrate up to 8 I/O Expansion Modules comprising up to 128 additional I/Os.
	Remote adapter (P.N. EX-RC1), via CANbus port. Connect up to 60 adapters; connect up to 8 I/O expansion modules to each adapter.
Exp. port isolation	Galvanic

Dimensions

Size	289X244.5X59.1mm (11.37"X9.62"X2.32"). See Note 6
Weight	1.5kg (52.9 oz)

Notes:

6. For exact dimensions, refer to the product's Installation Guide.

Mounting

Panel-mounting	Via brackets

Environment

Inside cabinet	IP20 / NEMA1 (case)
Panel mounted	IP65 / NEMA4X (front panel)
Operational temperature	0 to 50ºC (32 to 122ºF)
Storage temperature	-20 to 60ºC (-4 to 140ºF)
Relative Humidity (RH)	5% to 95% (non-condensing)

The information in this document reflects products at the date of printing. Unitronics reserves the right, subject to all applicable laws, at any time, at its sole discretion, and without notice, to discontinue or change the features, designs, materials and other specifications of its products, and to either permanently or temporarily withdraw any of the forgoing from the market.

All information in this document is provided "as is" without warranty of any kind, either expressed or implied, including but not limited to any implied warranties of merchantability, fitness for a particular purpose, or non-infringement. Unitronics assumes no responsibility for errors or omissions in the information presented in this document. In no event shall Unitronics be liable for any special, incidental, indirect or consequential damages of any kind, or any damages whatsoever arising out of or in connection with the use or performance of this information.

The tradenames, trademarks, logos and service marks presented in this document, including their design, are the property of Unitronics (1989) (R"G) Ltd. or other third parties and you are not permitted to use them without the prior written consent of Unitronics or such third party as may own them.

V200-18-E3XB Snap-in I/O Module

The V200-18-E3XB plugs directly into the back of compatible Unitronics OPLCs, creating a self-contained PLC unit with a local I/O configuration.

Features

- 18 isolated digital inputs, includes 2 H.S.C inputs, type pnp/npn (source/sink)
- 15 isolated relay outputs
- 2 isolated pnp/npn (source/sink) transistor outputs, includes 2 H.S. outputs
- 4 isolated analog/PT100/TC inputs
- 4 isolated analog outputs

- Before using this product, it is the responsibility of the user to read and understand this document and any accompanying documentation.
- All examples and diagrams shown herein are intended to aid understanding, and do not guarantee operation. Unitronics accepts no responsibility for actual use of this product based on these examples.
- Please dispose of this product in accordance with local and national standards and regulations.
- Only qualified service personnel should open this device or carry out repairs.

User safety and equipment protection guidelines

This document is intended to aid trained and competent personnel in the installation of this equipment as defined by the European directives for machinery, low voltage, and EMC. Only a technician or engineer trained in the local and national electrical standards should perform tasks associated with the device's electrical wiring.

Symbols are used to highlight information relating to the user's personal safety and equipment protection throughout this document. When these symbols appear, the associated information must be read carefully and understood fully.

Symbol	Meaning	Description
	Danger	The identified danger causes physical and property damage.
	Warning	The identified danger can cause physical and property damage.
Caution	Caution	Use caution.

- Failure to comply with appropriate safety guidelines can result in severe personal injury or property damage. Always exercise proper caution when working with electrical equipment.

- Check the user program before running it.
- Do not attempt to use this device with parameters that exceed permissible levels.
- Install an external circuit breaker and take appropriate safety measures against short-circuiting in external wiring.
- To avoid damaging the system, do not connect / disconnect the device when the power is on.

Caution

- Ascertain that terminal blocks are properly secured in place.

Environmental Considerations

- Do not install in areas with: excessive or conductive dust, corrosive or flammable gas, moisture or rain, excessive heat, regular impact shocks or excessive vibration.

- Provide proper ventilation by leaving at least 10mm of space between the top and bottom edges of the device and the enclosure walls.
- Do not place in water or let water leak onto the unit.
- Do not allow debris to fall inside the unit during installation.

Wiring

⚡	■ Do not touch live wires.
⚠	■ Unused pins should not be connected. Ignoring this directive may damage the device. ■ Do not connect the 'Neutral' or 'Line' signal of the 110/220VAC to the device's 0V pin. ■ Double-check all wiring before turning on the power supply.

Wiring Procedures

Use crimp terminals for wiring; use 26-12 AWG wire (0.13 mm ^{2}–3.31 mm^2) for all wiring purposes.

1. Strip the wire to a length of 7±0.5mm (0.250–0.300 inches).
2. Unscrew the terminal to its widest position before inserting a wire.
3. Insert the wire completely into the terminal to ensure that a proper connection can be made.
4. Tighten enough to keep the wire from pulling free.

- To avoid damaging the wire, do not exceed a maximum torque of 0.5 N·m (5 kgf·cm).
- Do not use tin, solder, or any other substance on stripped wire that might cause the wire strand to break.
- Install at maximum distance from high-voltage cables and power equipment.

I/O Wiring—General

- Input or output cables should not be run through the same multi-core cable or share the same wire.
- Allow for voltage drop and noise interference with input lines used over an extended distance. Use wire that is properly sized for the load.

Digital Inputs

Each group of 9 inputs has a common signal. Each group can be used as either pnp (source) or npn (sink), when appropriately wired as shown in the following figures.

Inputs I0 and I2 can be used as normal digital inputs, as high-speed counters, or as part of a shaft encoder. Inputs I1 and I3 can be used as normal digital inputs, as high-speed counter resets, or as part of a shaft encoder.

npn (sink) digital input wiring

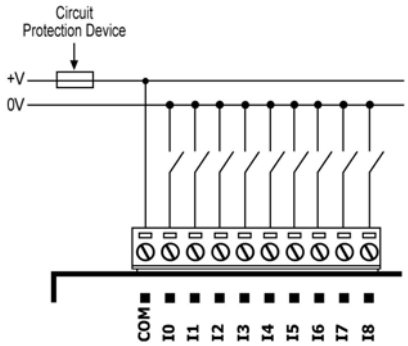

pnp (source) digital input wiring

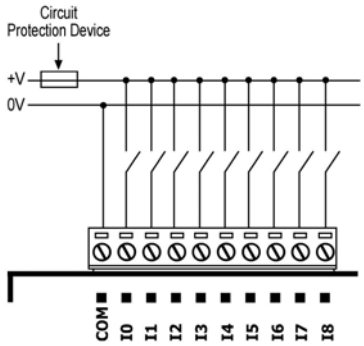

npn (sink) high-speed counter

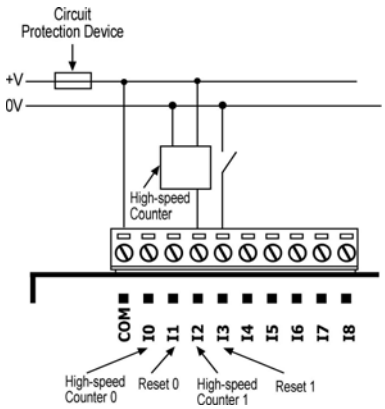

pnp (source) high-speed counter

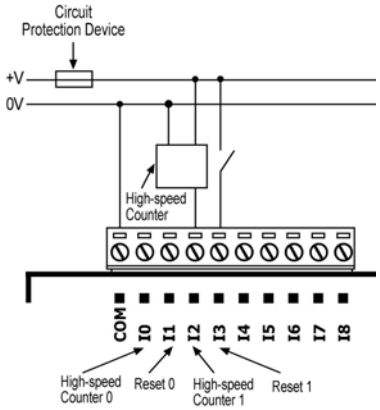

Inputs I0, I1, and I2, I3 can be used as shaft encoders as shown below.

npn (sink) shaft encoder wiring

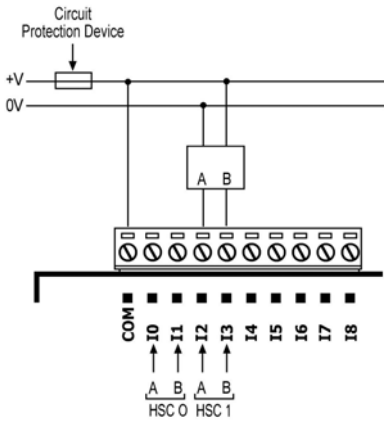

pnp (source) shaft encoder wiring

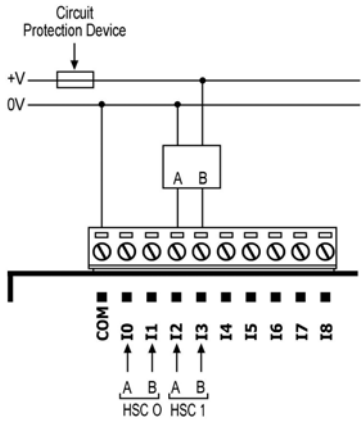

Digital Outputs

Wiring Power Supplies

Use a 24VDC power supply for both relay and transistor outputs.

1. Connect the "positive" lead to the "V1" terminal, and the “negative” lead to the "0V" terminal.

- In the event of voltage fluctuations or non-conformity to voltage power supply specifications, connect the device to a regulated power supply

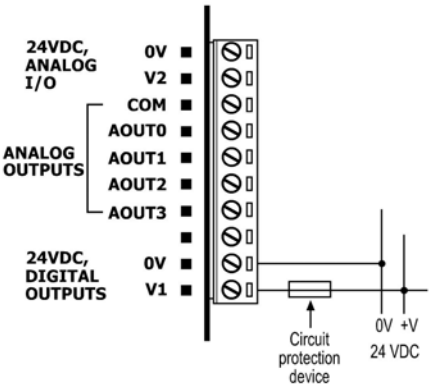

Relay Outputs

- Each output can be wired separately to either AC or DC as show below.
- The 0V signal of the relay outputs is isolated from the controller’s 0V signal.

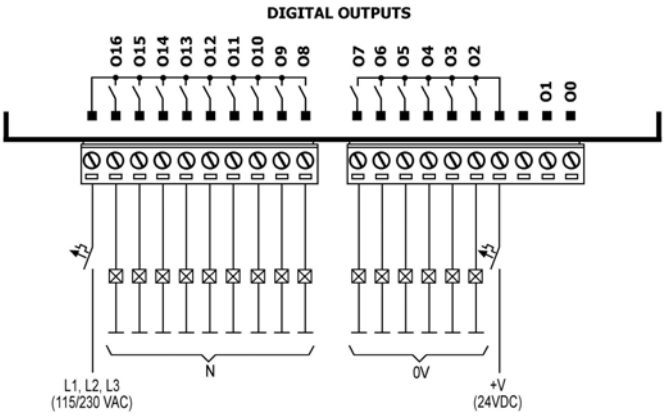

Increasing Contact Life Span

To increase the life span of the relay output contacts and protect the device from potential damage by reverse EMF, connect:

- a clamping diode in parallel with each inductive DC load,
- an RC snubber circuit in parallel with each inductive AC load.

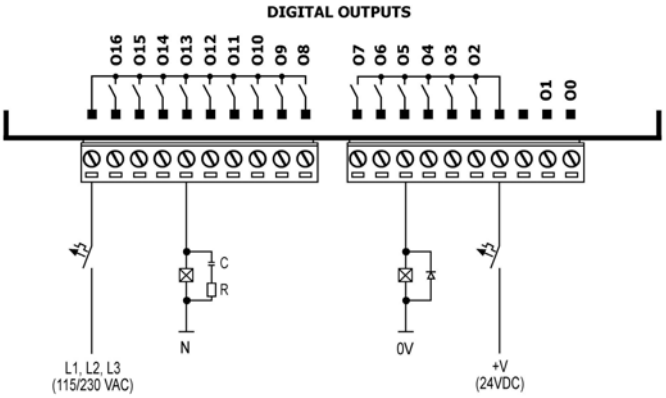

Transistor Outputs

- Each output can function as either npn or pnp, in accordance with jumper settings and wiring. Open the device and set the jumpers according to the instructions beginning on page 8.
- The 0V signal of the transistor outputs is isolated from the controller's 0V signal.

npn (sink)

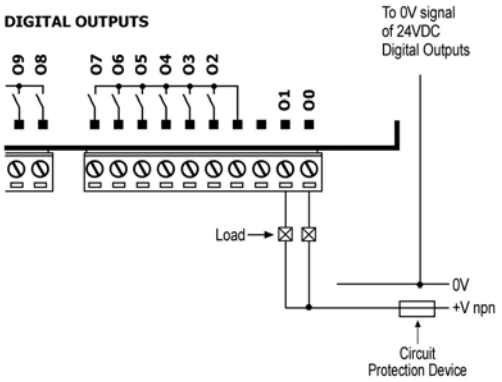

pnp (source)

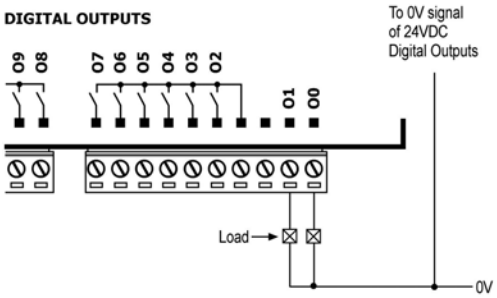

Analog I/O Power Supplies

Use a 24VDC power supply for all analog input and output modes.

1. Connect the "positive" cable to the "V2" terminal, and the "negative" to the "0V" terminal.

- In the event of voltage fluctuations or non-conformity to voltage power supply specifications, connect the device to a regulated power supply.
- Since the analog I/O power supply is isolated, the controller's 24VDC power supply may also be used to power the analog I/Os.

The 24VDC power supply must be turned on and off simultaneously with the controller's power supply.

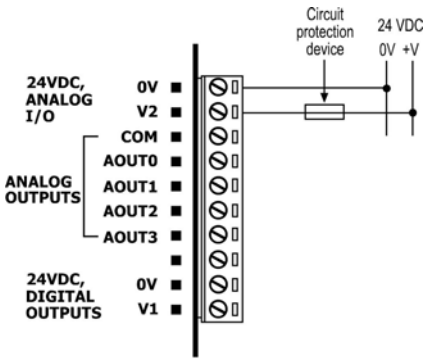

Analog / PT100 / TC Inputs

- Each input may be set as either analog, RTD, or thermocouple. To set an input:
  - Use the appropriate wiring as shown below.
  - Open the device and set the jumpers according to the instructions beginning on page 8.
- Shields should be connected at the signal source.
- In order to function correctly, the analog power supplies must be wired as shown on page 5.
- To ensure proper performance, a warm-up period of a half an hour is recommended.

Analog Inputs

- Inputs may be wired to work with either current or voltage.
- When set to current/voltage, all inputs share a common ACM signal.

current

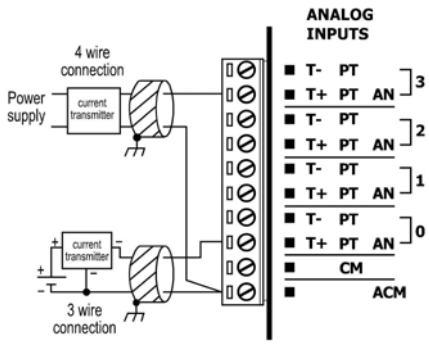

current/voltage

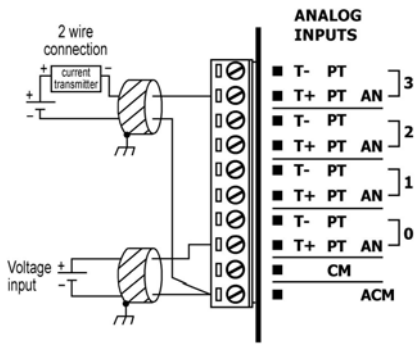

RTD Inputs

1. Wire one lead of each RTD input to the common signal (CM) as shown below.

- 4 wire PT100 can be used by leaving one of the sensor leads unconnected.

PT100

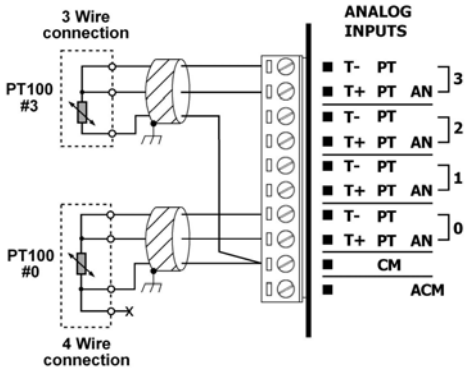

Thermocouple Inputs

- Supported thermocouple types include B, E, J, K, N, R, S, and T, in accordance with software and jumper settings. See table Thermocouple Input Ranges, on page 15.
- Inputs may be set to mV by software settings (Hardware Configuration); note that in order to set mV inputs, thermocouple jumper settings are used.

Thermocouple

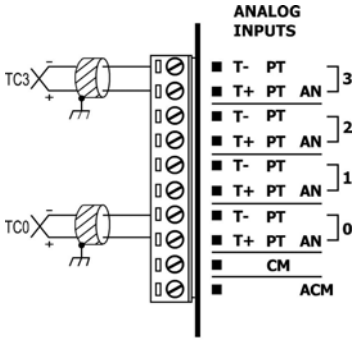

Analog Outputs

- Shields should be earthed, connected to the earth of the cabinet.
- An output can be wired to either current or voltage.
  - Use the appropriate wiring as shown below.
  - Open the device and set the jumpers according to the instructions beginning on page 8.
- To ensure proper performance, a warm-up period of a half an hour is recommended.

current/voltage

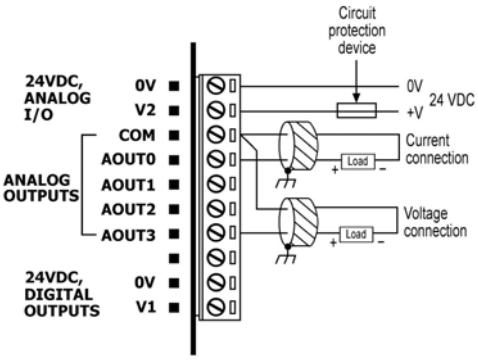

Changing Jumper Settings

To access the jumpers, you must remove the snap-in I/O module from the controller, and then remove the module's PCB board. Before you begin, turn off the power supply, disconnect and dismount the controller.

- Before performing these actions, touch a grounded object to discharge any electrostatic charge.
- Avoid touching the PCB board directly by holding the PCB board by its connectors.

Accessing the Jumpers

First, remove the snap-in module.

1. Locate the 4 buttons on the sides of the module, two on either side. Press the 2 buttons on either side of the module as shown, and hold them down to open the locking mechanism.
2. Gently rock the module from side to side, easing the module from the controller.

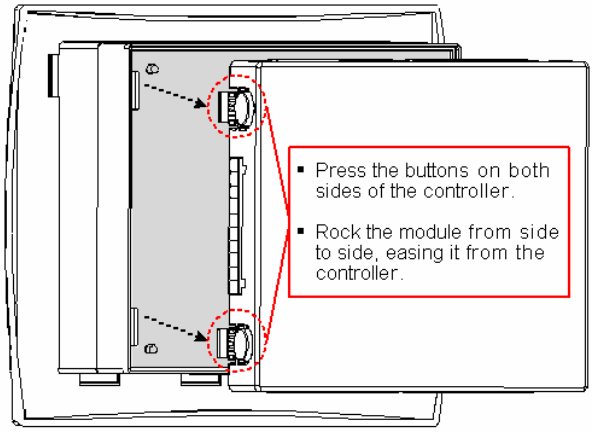

3. Using a Philips screwdriver, remove the center screw, shown in the figure below, from the module's upper PCB board. **Do not remove any other screws**.
4. Holding the PCB board by its edges, gently lift it out of the module.

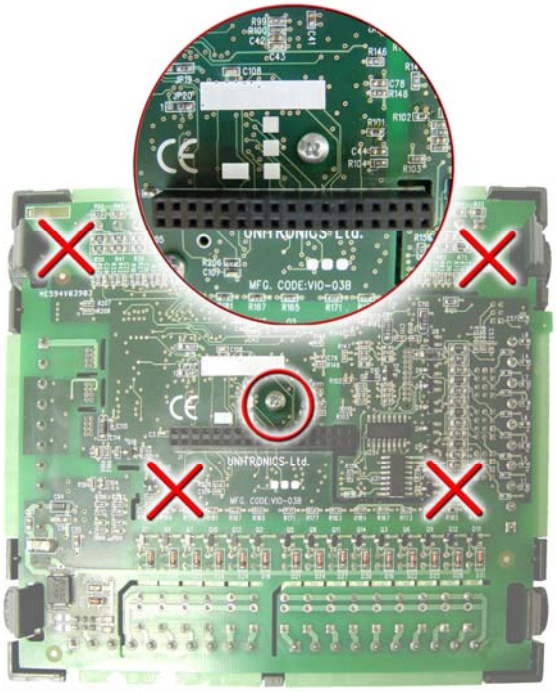

Select the desired function by changing the jumper settings according to the figure and tables shown below.

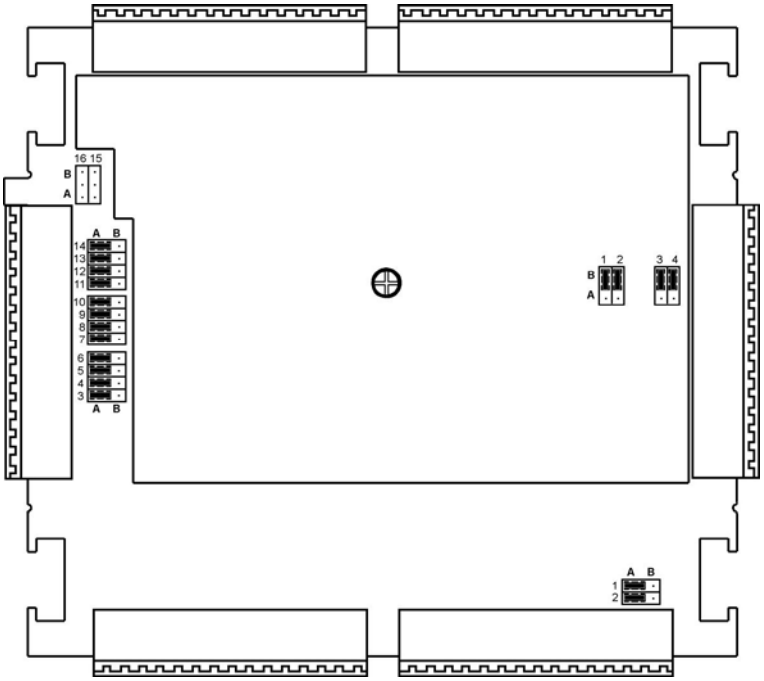

Analog Input Jumpers

Bottom PCB board

	Jumper #	Voltage*	Current	T/C or mV	PT100
Analog input 3	14	A	B	B	A
	13	A	B	B	A
	12	A	A	B	B
Analog input 2	11	A	B	B	A
	10	A	B	B	A
	9	A	A	B	B
Analog input 1	8	A	B	B	A
	7	A	B	B	A
	6	A	A	B	B
Analog input 0	5	A	B	B	A
	4	A	B	B	A
	3	A	A	B	B

Digital Output Jumpers

	Jumper #	PNP*	NPN
Digital Output 0	1	A	B
Digital Output 1	2	A	B

Note that Jumpers #15 & 16 are not used

Analog Output Jumpers

		Jumper #	Current	Voltage*
Top PCB board	**Analog Output 0**	1	A	B
	Analog Output 1	2	A	B
	Analog Output 2	3	A	B
	Analog Output 3	4	A	B

* Default factory setting

Reassembling the controller

1. Return the PCB board to the module and secure the center screw.
2. Next, reinstall the module. Line the circular guidelines on the controller up with the guidelines on the Snap-in I/O Module as shown below.
3. Apply even pressure on all 4 corners until you hear a distinct 'click'. The module is now installed. Check that all sides and corners are correctly aligned.

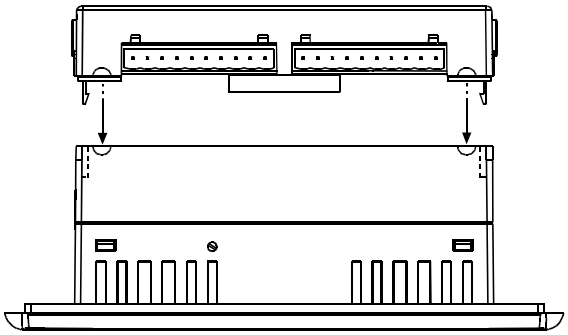

V200-18-E3XB Technical Specifications

Digital Inputs

Number of inputs	18 (in two groups)
Input type	pnp (source) or npn (sink)
Galvanic isolation	
Digital inputs to bus	Yes
Digital inputs to digital inputs in same group	No
Group to group, digital inputs	Yes
Nominal input voltage	24VDC
Input voltage	
pnp (source)	0-5VDC for Logic '0' 17-28.8VDC for Logic '1'
npn (sink)	17-28.8VDC for Logic '0' 0-5VDC for Logic '1'
Input current	6mA@24VDC for inputs #4 to #17 8.8mA@24VDC for inputs #0 to #3
Response time	10mSec typical
High speed inputs	Specifications below apply when these inputs are wired for use as a high-speed counter input/shaft encoder. See Notes 1 and 2.
Resolution	32-bit
Frequency	10kHz maximum
Minimum pulse width	40µs

Notes:

1. Inputs #0 and #2 can each function as either high-speed counter or as part of a shaft encoder. In each case, high-speed input specifications apply. When used as a normal digital input, normal input specifications apply.
2. Inputs #1 and #3 can each function as either counter reset, or as a normal digital input; in either case, its specifications are those of a normal digital input. These inputs may also be used as part of a shaft encoder. In this case, high-speed input specifications apply.

Digital Outputs

Digital Output's Power Supply

Nominal operating voltage	24VDC
Operating voltage	20.4 to 28.8VDC
Quiescent current	20mA@24VDC.
Max. current consumption	85mA@24VDC. See Note 3.
Galvanic isolation	
Digital power supply to bus	Yes
Digital power supply to relay outputs	Yes
Digital power supply to transistor outputs	No

Notes:

3. Maximum current consumption does not provide for PNP output requirements. The additional current requirement of PNP outputs must be added.

Relay Outputs

Number of outputs	15 relays (in two groups). See Note 4.
Output type	SPST-NO (Form A)
Isolation	By relay
Type of relay	Tyco PCN-124D3MHZ or compatible
Outputs' power supply	See Digital Output's Power Supply above
Galvanic isolation	
Relay outputs to bus	Yes
Group to group, relay outputs	Yes
Relay to transistor outputs	Yes
Output current	3A maximum per output (resistive load) 8A maximum total for common (resistive load)
Rate voltage	250VAC / 30VDC
Minimun load	1mA@5VDC
Life expectancy	100k operations at maximum load
Response time	10mS (typical)
Contact protection	External precautions required (see Increasing Contact Life Span, p.4)

Notes:

4. Outputs #2,3,4,5,6 and 7 share a common signal. Outputs #8,9,10,11,12,13,14,15 and 16 share a common signal

Transistor Outputs

Number of outputs	2, high-speed. Each can be individually set as pnp (source) or npn (sink) via wiring and jumper settings. See Note 5.
Output type	pnp: P-MOSFET (open drain) npn: N-MOSFET (open drain)
Galvanic isolation	
Transistor outputs to bus	Yes
Transistor outputs to transistor outputs	No
Transistor outputs to relay outputs	Yes
Output current	pnp: 0.5A maximum per output npn: 50mA maximum per output
Maximum frequency	Resistive load pnp: 2kHz npn: 50kHz Inductive load 0.5Hz
ON voltage drop	pnp: 0.5VDC maximum npn: 0.4VDC maximum
Short circuit protection	Yes (pnp only)
pnp (source) power supply	See Digital Output's Power Supply above
npn (sink) power supply	
operating voltage	3.5V to 28.8VDC, unrelated to the voltage of either the I/O module or the controller

Notes:

5. Both transistor outputs may be used as high-speed outputs.

Analog I/O's Power Supply	
Nominal operating voltage	24VDC
Operating voltage	20.4 to 28.8VDC
Quiescent current	70mA@24VDC
Max. current consumption	130mA@24VDC
Galvanic isolation	
Analog power supply to bus	Yes
Analog power supply to analog inputs	Yes
Analog power supply to analog outputs	Yes
Analog/ PT100/ TC Inputs	
Number of inputs	4
Type of input	Set via appropriate wiring and jumper settings.
Analog Inputs Power Supply	
Galvanic isolation	
Analog/PT/TC inputs to bus	Yes
Analog/PT/TC inputs to analog outputs	Yes
Analog /PT/TC inputs to Analog /PT/TC inputs	No
Analog inputs	
Input range	0-10V, 0-20mA , 4-20mA
Power supply	See Analog I/O's Power Supply above
Conversion method	Succesive approximation
Resolution at 0-10V, 0-20mA	14-bit (16384 units). See Note 6.
Resolution at 4-20mA	3277 to 16384 (13107 units). See Note 6.
Conversion time	Synchronized to cycle time
Input impedance	>1MΩ—voltage 121.5Ω—current
Absolute maximum rating	±20V—voltage ±40mA—current
Full-scale error	±0.4%
Linearity error	±0.04%
Status indication	Yes. See Note 7.

Notes:

6. 12 or 14-bit resolution may be selected via software.

7. The analog value can indicate faults as shown below:

Value	Possible Cause
16384	Input value deviates **slightly above** the input range
32767	-Input value deviates **greatly above** or **below** the input range -Power supply disconnected

PT100 inputs

Input range	-200 to 600°C/-328 to 1100°F. 1 to 320Ω. See Note 8.
Conversion method	Voltage to frequency
Resolution	0.1°C/0.1°F
Conversion time	200mS minimum per channel, depending on software filter type
Input impedance	>10MΩ
Auxillary current for PT100	150µA typical
Full-scale error	±0.4%
Linearity error	±0.04%
Status indication	Yes. See Note 9.

Notes:

8. The device can also measure resistance with the range of 1-320 Ω at a resolution of 0.1 Ω.
9. The analog value can indicate faults as shown below:

Value	Possible Cause
32767	- Sensor is not connected to input - Value exceeds permissible range - Power supply disconnected
-32767	Sensor is short-circuited

Thermocouple inputs

Input range	As shown in the table on page 15. See Note 10.
Conversion method	Voltage to frequency
Resolution	0.1°C/0.1°F maximum
Conversion time	100mS minimum per channel, depending on software filter type
Input impedance	>10MΩ
Cold junction compensation	Local, automatic
Cold junction compensation error	±1.5°C / ±2.7°F maximum
Absolute maximum rating	±0.6VDC
Full-scale error	±0.4%
Linearity error	±0.04%
Warm-up time	½ hour typically, ±1°C/±1.8°F repeatability
Status indication	Yes. See Note 11.

Notes:

10. The device can also measure voltage within the range of -5 to 56mV, at a resolution of 0.01mV.
    The device can also measure raw value frequency at a resolution of 14-bits(16384)
11. The analog value can indicate faults as shown below:

Value	Possible Cause
32767	- Sensor is not connected to input - Sensor value exceeds the maximum value - Power supply disconnected
-32767	Sensor value is under the minimum value

Table 1: Thermocouple input ranges

Type	Temperature range	Wire Color	
		ANSI (USA)	BS 1843 (UK)
mV	-5 to 56mV	-	-
B	200 to 1820°C (300 to 3276°F)	+Grey -Red	+None -Blue
E	-200 to 750°C (-328 to 1382°F)	+Violet -Red	+Brown -Blue
J	-200 to 760°C (-328 to 1400°F)	+White -Red	+Yellow -Blue
K	-200 to 1250°C (-328 to 2282°F)	+Yellow -Red	+Brown -Blue
N	-200 to 1300°C (-328 to 2372°F)	+Orange -Red	+Orange -Blue
R	0 to 1768°C (32 to 3214°F)	+Black -Red	+White -Blue
S	0 to 1768°C (32 to 3214°F)	+Black -Red	+White -Blue
T	-200 to 400°C (-328 to 752°F)	+Blue -Red	+White -Blue

Analog Outputs

Number of outputs	4 (single-ended)
Output range	0-10V, 4-20mA. See Note 12.
Resolution	12-bit (4096 units)
Conversion time	Synchronized to scan time.
Load impedance	1kΩ minimum—voltage 500Ω maximum—current
Galvanic isolation	
Analog outputs to bus	Yes
Analog outputs to Analog/PT/TC inputs	Yes
Analog outputs to analog outputs	No
Linearity error	±0.1%
Operational error limits	±0.2%

Notes:

12. Note that the range of each I/O is defined by wiring, jumper settings, and within the controller's software.

Environmental	IP20 / NEMA1
Operating temperature	0° to 45°C (32° to 113°F)
Storage temperature	-20° to 60° C (-4° to 140°F)
Relative Humidity (RH)	5% to 90% (non-condensing)
Dimensions (WxHxD)	138x23x123mm (5.43x0.9x4.84")
Weight	279g (9.87 oz)

About Unitronics

Unitronics has been producing PLCs, automation software and accessory devices since 1989.

Unitronics' OPLC controllers combine full-function PLCs and HMI operating panels into single, compact units. These HMI + PLC devices are programmed in a single, user-friendly environment. Our clients save I/O points, wiring, space, and programming time; elements that translate directly into cost-efficiency.

Unitronics supports a global network of distributors and sales representatives, as well as a U.S. subsidiary.

For more information regarding Unitronics products, contact your distributor or Unitronics headquarters via email: export@unitronics.com.

Under no circumstances will Unitronics be liable or responsible for any consequential damage that may arise as a result of installation or use of this equipment, and is not responsible for problems resulting from improper or irresponsible use of this device.

No part of this document may be used for any purpose other than for the purposes specifically indicated herein nor may it be reproduced or transmitted in any form or by any means, electronic or mechanical, including photocopying and/or recording, for any purpose without written permission from Unitronics.

The information appearing in this document is for general purposes only. Unitronics makes no warranty of any kind with regard to the information appearing in this document, including, but not limited to, implied warranties of merchantability and/or fitness for a particular use or purpose. Unitronics assumes no responsibility for the results, direct and/or indirect, of any misuse of the information appearing in this document nor for any use of the Unitronics products referred to herein in any manner deviating from the recommendations made in this document. Unitronics assumes no responsibility for the use of any parts, components, or other ancillary appliances including circuitry other than as recommended hereunder or other than that embodied in the Unitronics product.

Unitronics retains all rights to its proprietary assets including, but not limited to its software products which are copyrighted and shall remain the property of Unitronics. Copyright protection claimed includes all Forms and matters of copyrightable materials and information legally allowed including but not limited to material generated from the software programs which are displayed on the screen of the Unitronics products such as styles, templates, icons, screen displays, looks, etc. Duplication and/or any unauthorized use thereof are strictly prohibited without prior written permission from Unitronics.

All brand or product names are used for identification purpose only and may be trademarks or registered trademarks of their respective holders.

Unitronics reserves the right to revise this publication from time to time and to amend its contents and related hardware and software at any time. Technical updates (if any) may be included in subsequent editions (if any).

Unitronics product sold hereunder can be used with certain products of other manufacturers at the user's sole responsibility.

5410-1082-9

Back-UPS Pro

Power Saving Back-UPS XS 1500

More Images

APC Back-UPS Pro,865 Watts /1500 VA,Input 120V /Output 120V, Interface Port USB

Includes: USB cable, User Manual

Standard Lead Time: Usually in Stock

Average Customer Review 4

20 of **25** (80%) reviewers would recommend this product to a friend.

Read all reviews | Write a review

BX1500G

Contact Sales

Add Options

Email Technical Specifications

Printer Friendly

Locate a Partner

Product Category

Computer and Peripheral

> Back-UPS

> Back-UPS Pro

> Back-UPS Connect

Network and Server (3)

Data Center and Facility 3 Phase (9)

Special Applications (5)

UPS Management (7)

UPS Replacement Batteries (2)

Return to Uninterruptible Power Supply (UPS)

Technical Specifications | Product Overview | Documentation | Software & Firmware | Options | Ratings and Reviews

Output

Output Power Capacity	865 Watts / 1500 VA
Max Configurable Power	865 Watts / 1500 VA
Nominal Output Voltage	120V
Output Frequency (sync to mains)	50/60Hz +/- 3 Hz
Topology	Line Interactive
Waveform Type	Stepped approximation to a sinewave

Output Connections	(5) NEMA 5-15R (Battery Backup) (5) NEMA 5-15R (Surge Protection)

Input

Nominal Input Voltage	120V
Input Frequency	50/60 Hz +/- 3 Hz (auto sensing)
Input Connections	NEMA 5-15P
Cord Length	6 feet (1.83 meters)

Batteries & Runtime

Battery Type	Maintenance-free sealed Lead-Acid battery with suspended electrolyte : leakproof
Included Battery Modules	1
Typical recharge time	16 hour(s)
Replacement Battery	APCRBC124
RBC Quantity	1
Runtime Graph	

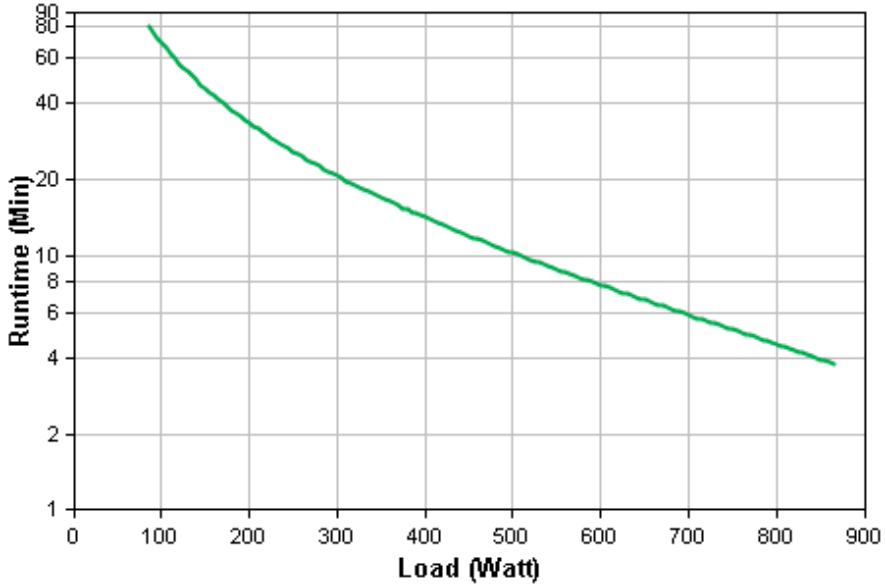

Hover over the line on the graph above to view the runtime at any desired load

Curve fit to measured runtime data. All measurements taken with new, fully charged batteries, at typical environmental conditions, with no electrical input and balanced resistive load (PF = 1.0) output.

View Enlarged Graph View Runtime Chart

Energy Use/Efficiency

Load	Efficiency
25%	97.7%
50%	98.5%
75%	98.6%
100%	98.5%

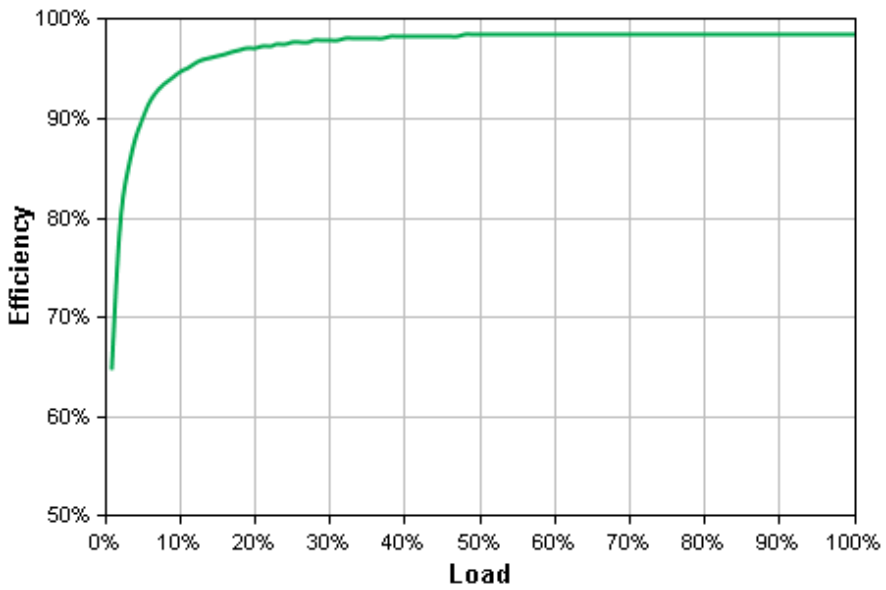

Hover over the line on the graph above to view the efficiency at any desired load

Curve fit of data measured in accordance with the ENERGY STAR Program Requirements Product Specification for Uninterruptible Power Supplies (UPSs) - Eligibility Criteria Version 1.0. All measurements taken in normal mode(s), at typical environmental conditions, with 120V/60Hz electrical input and balanced resistive load (PF = 1.0) output.

View Enlarged Graph

Communications & Management

Interface Port(s)	USB
Control panel	Multi-function LCD status and control console

Surge Protection and Filtering

Surge energy rating	354 Joules
Filtering	Full time multi-pole noise filtering : 5% IEEE surge let-through : zero clamping response time : meets UL 1449

Data Line Protection	RJ45 10/100 Base-T Ethernet protection, Cable modem / Video protection

Physical

Maximum Height	11.85 inches (301 mm)
Maximum Width	4.40 inches (112 mm)
Maximum Depth	15.04 inches (382 mm)
Net Weight	23.76 lbs. (10.80 kg)
Shipping Weight	26.40 lbs. (12.00 kg)
Shipping Height	15.24 inches (387 mm)
Shipping Width	9.37 inches (238 mm)
Shipping Depth	19.21 inches (488 mm)
Master Carton Units	1.00
Master Carton Dimensions (Length x Width x Height)	16 inches (405 mm)
Master Carton Weight	55.64 lbs. (25.29 kg)
Color	Black
SCC Codes	1073130426839 7
Units per Pallet	16.00

Environmental

Operating Environment	32 - 104 °F (0 - 40 °C)
Operating Relative Humidity	0 - 95%
Operating Elevation	0-30000 feet (0-9000 meters)
Storage Temperature	5 - 113 °F (-15 - 45 °C)
Storage Relative Humidity	0 - 95%
Storage Elevation	0-50000 feet (0-15000 meters)

Conformance

Approvals	California (CEC) Battery Charger, ENERGY STAR (USA), TUV
Standard warranty	3 years repair or replace
Equipment protection policy	Lifetime : $150000

Sustainable Offer Status

RoHS	Compliant
REACH	REACH: Contains No SVHCs
PEP	Available in Documentation tab
EOLI	Available in Documentation tab

*Except where noted, all prices are Estimated Resale Price (ERP) - Without Tax/VAT. Pricing in other locations and sites may vary.

**The time to recharge to 90% of full battery capacity following a discharge to shutdown using a load rated for 1/2 the full load rating of the UPS.

©APC by Schneider Electric

Appendix D

List of Scientific/Technical Publications

APPENDIX D
Publications

2013

- Lanas, V.A., Y. Ahn, and B.E. Logan. 2013. Effects of carbon brush anode size and loading on microbial fuel cell performance in batch and continuous mode. *J. Power Sources,* 247:228–234.
- Lanas, V.A. and B.E. Logan. 2013. Evaluation of multi-brush anode systems in microbial fuel cells. *Biores. Technol*., 148: 379–385.

2014

- Hoskins, D.L., X. Zhang, M.A. Hickner, and B.E. Logan. 2014. Spray-on polyvinyl alcohol separators and impact on power production in air-cathode microbial fuel cells with different solution conductivities. *Biores. Technol.,* 172:156–161.
- Yang, W., F. Zhang, W. He, J. Liu, M.A. Hickner, and B.E. Logan. 2014. Poly(vinylidene fluoride-co-hexafluoropropylene) phase inversion coating as a diffusion layer to enhance cathode performance in microbial fuel cells. *J. Power Sources,* 269:379–384.
- Yang, W. W. He, F. Zhang, M.A. Hickner, and B.E. Logan. 2014. Single step fabrication using a phase inversion method of poly (vinylidene fluoride)(PVDF) activated carbon air cathodes for microbial fuel cells. *Environ. Sci. Technol. Lett.,* 1:416–420.
- Zhang, X., Xia, X., Ivanov, I., Huang, X., Logan, B.E. 2014. Enhanced activated carbon cathode performance for microbial fuel cell by blending carbon black. *Environ. Sci. Technol.,* 48(3), 2075–2081.
- Zhang, X., D. Pant, F. Zhang, J. Liu, and B.E. Logan. 2014. Long-term performance of chemically and physically modified activated carbons in microbial fuel cell air-cathodes. *ChemElectroChem*, 1:1859–1866.

2015

- Logan, B.E., M.J. Wallack, K.-Y. Kim, W. He, Y. Feng, and P. Saikaly. 2015. Assessment of microbial fuel cell configurations and power densities. *Environ. Sci. Technol. Lett*., 2: 206-214
- Kim K.-Y., W. Yang, and B.E. Logan. 2015. Impact of Electrode Configurations on Retention Time and Domestic Wastewater Treatment Efficiency Using Microbial Fuel Cells. *Water Res.,* 80: 41–46
- Yang, W., K.-Y. Kim, and B.E. Logan. 2015. Development of carbon free diffusion layer for activated carbon air cathode of microbial fuel cells. *Biores. Technol.,* 197: 318-322
- Zhang, X., W. He, L. Ren, J. Stager, P.D. Evans, and B.E. Logan. 2015. COD removal characteristics of air-cathode microbial fuel cells. *Biores. Technol.,* 176:23–31.

2016

- He, W., X. Zhang, J. Liu, X. Zhu, Y. Feng and B.E. Logan. 2016. Microbial fuel cells with an integrated spacer and separate anode and cathode modules. *Environ. Sci.: Water Res. Technol.*, 2: 186–195.
- He, W., W. Yang, Y. Tian, X. Zhu, J. Liu, Y. Feng and B.E. Logan. 2016. Pressurized air cathodes for enhanced stability and power generation by microbial fuel cells. *J. Power Sources*, 332: 447–453.
- He, W., M.J. Wallack, K.-Y. Kim, X. Zhang, W. Yang, X. Zhu, Y. Feng and B.E. Logan. 2016. The effect of flow modes and electrode combinations on the performance of a multiple module microbial fuel cell installed at wastewater treatment plant. *Water Res*., 105: 351-360.

- Kim K.-Y., W. Yang, P.J. Evans and B.E. Logan. 2016. Continuous treatment of high strength wastewaters using air-cathode microbial fuel cells. *Biores. Technol*., 208: 58-63.
- Kim K.-Y., W. Yang, Y. Ye, N. LaBarge and B.E. Logan. 2016. Performance of anaerobic fluidized membrane bioreactors using effluents of microbial fuel cells treating domestic wastewater. *Biores. Technol.*, 208: 58-63.
- LaBarge, N., Y. Ye, K.-Y. Kim, Y.D. Yilmazel, P. Saikaly, P. Hong and B.E. Logan. 2016. Impact of acclimation methods on microbial communities and performance of anaerobic fluidized bed membrane bioreactors*. Environ. Sci.: Water Res. Technol.,* 2: 1041-1048.
- Ye, Y., N. LaBarge, H. Kashima, K.-Y. Kim, P. Hong, P.E. Saikaly, and B.E. Logan. 2016. An aerated and fluidized bed membrane bioreactor for effective wastewater treatment with low membrane fouling. *Environ. Sci.: Water Res. Technol.*, 2: 994-1003.
- Zhang, X., W. He, W. Yang, J. Liu, Q. Wang, P. Liang, X. Huang and B.E. Logan. 2016. Diffusion layer characteristics for increasing the performance of activated carbon air cathodes in microbial fuel cells. *Environ. Sci.: Water Res. Technol.*, 2: 266–273.